SEISMICALLY INDUCED LANDSLIDE HAZARD ANALYSES FOR LOWER INDIAN HIMALAYA

Ph.D. THESIS

by

RITU RAJ NATH

DEPARTMENT OF EARTHQUAKE ENGINEERING
INDIAN INSTITUTE OF TECHNOLOGY ROORKEE
ROORKEE – 247 667 (INDIA)
JUNE, 2019

SEISMICALLY INDUCED LANDSLIDE HAZARD ANALYSES FOR LOWER INDIAN HIMALAYA

A THESIS

Submitted in partial fulfilment of the
requirements for the award of the degree

of

DOCTOR OF PHILOSOPHY

in

EARTHQUAKE ENGINEERING

by

RITU RAJ NATH

DEPARTMENT OF EARTHQUAKE ENGINEERING
INDIAN INSTITUTE OF TECHNOLOGY ROORKEE
ROORKEE – 247 667 (INDIA)
JUNE, 2019

INDIAN INSTITUTE OF TECHNOLOGY ROORKEE
ROORKEE

CANDIDATE'S DECLARATION

I hereby certify that the work which is being presented in the thesis entitled **"SEISMICALLY INDUCED LANDSLIDE HAZARD ANALYSES FOR LOWER INDIAN HIMALAYA"** in partial fulfilment of the requirements for the award of the Degree of Doctor of Philosophy and submitted in the Department of Earthquake Engineering of the Indian Institute of Technology Roorkee, Roorkee is an authentic record of my own work carried out during a period from July, 2013 to June, 2019 under the supervision of Dr. M. L. Sharma, Professor, Department of Earthquake Engineering, Indian Institute of Technology Roorkee, Roorkee.

The matter presented in the thesis has not been submitted by me for the award of any other degree of this or any other Institute.

(RITU RAJ NATH)

This is to certify that the above statement made by the candidate is correct to the best of my knowledge.

(Prof. M. L. Sharma)
Supervisor

The Ph.D. Viva-Voce Examination of Mr. Ritu Raj Nath, Research Scholar, has been held on **21st September, 2019.**

Chairman, SRC

21/09/2019

Signature of External Examiner

This is to certify that the student has made all the corrections in the thesis.

Signature of Supervisor
Dated:

Head of the Department

ABSTRACT

The entire Himalayan arc is recognized as a global hotspot for landslide and seismic events; which may be ascribed to the orogeny processes that had formed the Himalaya. Every year landslides and related natural disaster events claim many lives and destroy property, infrastructure, and the environment of the Himalaya. It is estimated that Himalayan landslides kill 1 person/100 sq. km per year and average losses due to Himalayan landslides is more than USD 1 million/year. Given the great relief, high seismicity, active tectonism, high volume of precipitation, and wide variety of rock and sediment types; landslides seem ubiquitous in the Himalaya and is perhaps the major present-day process shaping the landscape. With ingress of roads and other heavy constructions like dams and hydro power plants in this fragile mountain chain, the overall risk of landslide hazard increases manifold. This necessitates an accurate and updated landslide hazard zonation (LHZ) for the Himalayan belt, based on which future land-use pattern can be envisaged. LHZ is a scientific practice of predicting the spatial distribution of landslides over a region which is determined as a function of landslide occurrence and various landslide related factors. Considering the high incidences of landslide disasters and their long term socio-economic impact, national guidelines are drafted to guide the activities envisaged for mitigating landslide risk through Landslide Hazard Zonation (LHZ) mapping.

The classical approach of LHZ mapping is based on examination of various static landslide causative factors with occasional inclusion of triggering factors like rainfall and earthquakes. As the positive correlation between seismicity and landslide occurrence had become more and more prominent, the classical approaches got changed; and a paradigm shift has been observed in LHZ studies of-late. More emphasis is now given on comprehending the occurrence and mechanism of seismically induced landslides due to the complexity and enormity of such events. There have been several earthquakes in the Himalayan region *viz.* Chamoli earthquake (M_w-6.8), Kashmir earthquake (M_w-7.6), Sikkim earthquake (M_w-6.9), Nepal earthquake (M_w-7.8), which caused widespread landslide events. In fact, in many cases, losses due to seismically induced landslides have been more than those caused directly due to shaking. Out of the all earthquake related casualties, which are not caused directly by ground shaking, approximately 70% may be attributed to landslides. In this context, LHZ studies considering earthquakes as main triggering factor is a time bound priority for the Himalayan region. However, a critical review of the existing literature reveals that there is a paucity of macro-scale, regional level studies quantifying the role of seismicity in LHZ mapping for the Himalayan arc in general, and the lower Himalayan belt in particular. An endeavour has been

made in this research work to carry out LHZ mapping under both static and seismic conditions for a part of lower Indian Himalaya. The research work has been carried out in three phases: (a) in the first phase, the study area's present scenario of landslide susceptibility under static conditions is assessed using statistical method of LHZ mapping; (b) in the second phase, suitable method for carrying out seismically induced LHZ mapping is formulated; and (c) in the third phase, LHZ maps of the study area are prepared under different seismic conditions to quantify the role of seismicity in landslide occurrence and spatial distribution in the study area.

The study area encompasses approximately 12,350 sq. km.; with estimated population of more than 15 lakhs as per the 2011 India census. Several important and thickly populated cities of Uttarakhand and Himachal Pradesh are located in the study area. Geologically, the study area exhibits a complex and heterogeneous amalgamation of fifteen formations from different ages'. The study area falls in Zone IV as per IS 1893(Part I): 2016, indicating that the whole study area is seismically very active. The area caters three major thrusting systems of the Himalayan arc: Main Frontal Thrust (MFT), Main Boundary Thrust (MBT) and a portion of Main Central Thrust (MCT), along with numerous transverse lineaments.

In the first phase, eight static landslide causative parameters are identified for the study area. A comprehensive landslide inventory has been prepared, which is the primary step in LHZ mapping and data has been extracted from various sources. The prepared landslide inventory is used for proximity analyses to establish correlation between landslide activities and various causative parameter. Information Value method, one of the widely used statistical methods of LHZ mapping, has been applied to prepare the initial LHZ map of the study are under static causative parameters. The prepared LHZ map has identified almost 37% of the total study area as the zones of high to very high landslide susceptibility.

Different statistical methods, which are widely used for landslide susceptibility assessment, generally lack in incorporating seismic indicators. This may be attributed to the paucity of sufficient earthquake induced landslide inventories, which is attributed to the rarity of an extreme earthquake event. Moreover, the conventional studies correlating earthquake magnitude and landslide distribution, types and coverage area drew criticism from researchers due to limitations of the dataset used and the regional and characteristic biasness associated with earthquake events. Such scenarios become exaggerated for the Himalayan region, where not until recently, much attention have been paid to seismically induced landslide hazard zonation. Most of the LHZ studies carried out for the Himalayan belt considered static landslide causative factors only; and the few studies that did consider earthquake scenarios, are concentrated around the Chamoli earthquake, Sikkim earthquake and Nepal earthquake. All
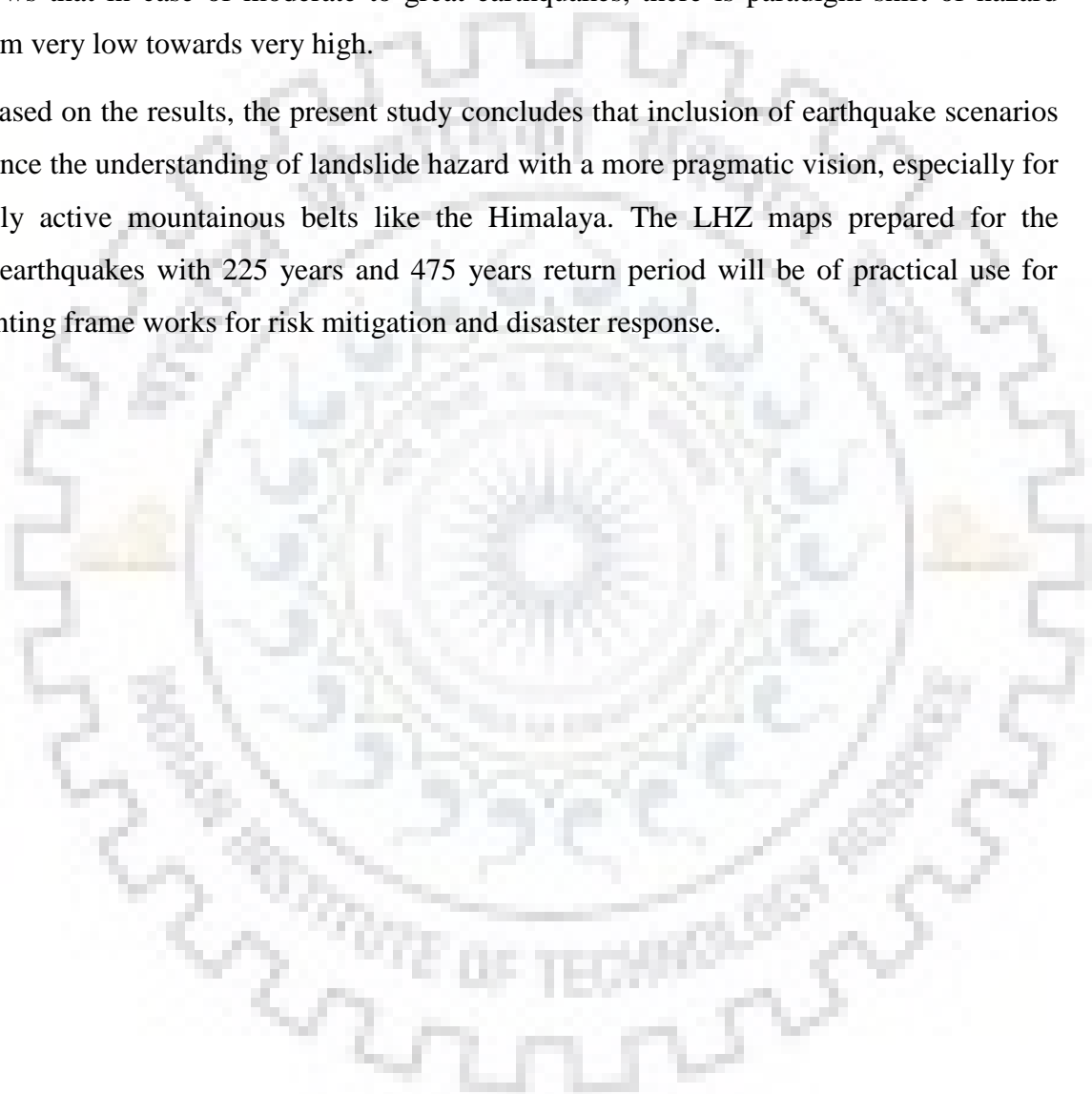
these earthquakes, in-spite-of having originated in the Himalaya only, differ significantly from one another in terms of their characteristics. Thus, it is understood that any statistical method derived from earthquake induced landslide inventory developed for a particular earthquake event may not be adequate enough for a different tectonic set up. Alternatively, Map combination method of LHZ mapping has been used in this research work where, probabilistically generated peak ground acceleration (PGA) is considered as landslide triggering seismic factor. The biggest advantage of this method is that various landslide causative parameters (static as well as triggering) can be incorporated as thematic layers, which are assigned a weight depending upon their perceived control on landslide occurrence. The weights of various thematic layers are numerically integrated to generate the LHZ map. However, the subjectivity in weight assignment procedure is the main limitation in this method. To address this issue, a landslide susceptibility scale is developed for the study area statistically, which is used to assign the weights of various thematic classes. Information Value method, Frequency Ratio method and Fuzzy Cosine Amplitude Methods are correlated to develop the susceptibility scale, which is further used for multi-hazard integration. The LSZ map prepared using the developed scale, is compared with other LSZ maps prepared using statistical methods for performance evaluation of the developed susceptibility scale. The developed susceptibility scale has produced better results for the study area.

Use of probabilistic PGA values as landslide triggering factor in LHZ mapping has a distinct advantage: it eliminated the regional and characteristic biasness associated with an single earthquake, which increases the applicability of the method. The predicted PGAs are not from a single event, but rather represents the stress deformation expected in the region. Moreover application of PSHA in LHZ allows incorporation of seismotectonic environment (in terms of faults and lineaments) of a bigger area (R~300 km) which would likely to produce earthquakes in the study area, and recorded past seismicity. A detailed PSHA study has been carried out for the study area. The results of PSHA is discussed in terms of expected PGA for five scenario earthquakes with return periods of 10, 50, 100, 225 and 475 years. Consideration of the entire range of earthquake sizes quantifies the impact and implications of seismicity in landslide hazard comprehensively.

Assignment of weights to different earthquake scenarios is a difficult task in LHZ mapping. There is no statistical correlation available to quantify the size of a scenario earthquake with landslide spatial distribution. Therefore a new method has been implemented in this research work to assign the weights objectively. The method, which is based on the normalized PGA values of different scenario earthquakes, could portray the relative importance

of different earthquake size on LHZ mapping effectively. Five LHZ maps of the study area are prepared under seismic conditions to understand the role and impact of seismicity in landslide occurrence and their spatial distribution in the lower Himalaya. It is observed that for an earthquake scenario with 475 years return period, almost 51% of the total area falls under very high landslide hazard. This is a significant outcome of the study, which highlights the consideration of seismicity in LHZ mapping for the Himalayan arc. The results of the research work shows that in case of moderate to great earthquakes, there is paradigm shift of hazard zones from very low towards very high.

Based on the results, the present study concludes that inclusion of earthquake scenarios will enhance the understanding of landslide hazard with a more pragmatic vision, especially for seismically active mountainous belts like the Himalaya. The LHZ maps prepared for the scenario earthquakes with 225 years and 475 years return period will be of practical use for implementing frame works for risk mitigation and disaster response.

ACKNOWLEDGEMENT

Dubey, Gautam Reddy, Govind Rathor, Kranthi Kumar, Manendra Yadav, Mitesh Surana, K. V. Naveen Kumar, Neeraj Lohchab, Nidhin S.P., Pradip Muley, Rajesh Shukla, Rajiv Sachdeva, Rana Pratap Singh, Rinalini Lahon, Ritu Naznin Begum, Shraboni Adhikari, Suruj Neog and Vijay Singh. I would like to take this opportunity to thank all of them here.

I would like to take a moment and remember my late mother here. It was beyond my capacity to express my indebtedness towards my parents and my extended family for their support throughout this journey. A special note of thanks must be extended to my fiancée Ms. Bhaswati Bora, who has been a never-ending source of strength and support.

I would also like to express my gratitude to all who have helped, guided and support me in one way or the other but have been inadvertently left out because all may not have been mentioned, but none has been forgotten.

Last but not the least, I would like to thank the Almighty for showing the light of this day in my life.

Dated: (Ritu Raj Nath)

CONTENTS

LIST OF FIGURES

LIST OF TABLES

1.1   Preamble

Landslides are one of the most catastrophic natural disasters. The term landslide is used to describe a wide variety of processes that result in the downward and outward movement of slope forming materials composed of rocks, soils, artificial fills, or a combination of these. The materials may move by falling, sliding, toppling, spreading or flowing (USGS, 1981). About 15% of the total landmass of India is susceptible to landslides and other flow related phenomena, exceeding 0.49 million sq. km. (NDMA, 2009). A quick examination of the landslides data from 1950 to 2013 will reveal that these regions have witnessed some of the worst landslides in history. For example some devastating landslides during this period had occurred in Guwahati (18th September, 1948), Darjeeling (3-5th October, 1968), Chamoli (28th March, 1999 after Chamoli Earthquake), Amboori (9th November, 2009), and Kedernath (16-17th June, 2013) (IMD, GSI, India Today). As the population of India continues to expand at a geometrical rate, unplanned urbanization and settlement of life-lines have alarmingly spread into mountainous areas, with inadequate or little consideration for the prevailing natural hazards. This has lead to a high exposure level along with higher degree of susceptibility, which in turn increases the overall risk of landslide hazard in India. It is observed that the menaces of landslide hazard are much greater than commonly recognized in many countries, and generate a yearly loss of property larger than that from any other natural disaster, including earthquakes, floods and windstorms (Schuster and Fleming, 1986; Alexander, 1989; Guzzetti et al., 1999). Recognizing the enormous risk associated with the landslide hazard, national guidelines on landslide hazard are drafted (BIS 1998, GSI 2005, NDMA 2009) to direct the activities envisaged for mitigating the risk emanating from landslides at all levels. The main objectives of these guidelines are to institutionalize the landslide hazard mitigation efforts, to make the society aware of the various aspects of landslide hazard and to prepare the society to take suitable action to reduce both risks and costs associated with landslide hazard. Landslides are powerful, sudden and devastating natural calamities, mitigation of which requires intrinsic plan of action involving civic authorities, academics, geoscientists and practicing engineers.

1.2   Definition and Causes of Landslides

The complex mechanism and the broad spectrum of landslide hazard make it very difficult to accept a single definition of the event with universal applicability. In general, any downward movement of earth's masses (eg. soil, rock, debris etc.) can be incorporated in the

definition of landslides. However there exists wide variations of landslide events in terms of rate, direction and types under different environmental conditions; and therefore it has not yet been possible to reach a consensus regarding a singular definition of landslides. The most widely accepted definition was proposed by Chorley et al. (1985), which defines the event as "*the detachment and down-slope transport of soil and rock materials under the influence of gravity. The sliding or flowing of these materials is due to their position and gravitational forces, but mass movement is accelerated by the presence of water, ice and/or air. This definition of mass movement permits consideration of the movement of earth materials at all scales and at all rates*". The definition implies that gravity is the sole important force and no transporting medium such as wind, flowing water, ice or molten lava is involved. Although flowing water is excluded from the process by definition, water nevertheless plays a very important role in the whole phenomena by over-steepening slopes through surface erosion at their bases and by generating seepage forces through groundwater flow (Bloom, 1978). The term *landslide* incorporates both the failed mass of a landslide deposit and historically active unstable slopes (Bosi, 1978; Cruden, 1991).

1.2.1 Landslide Causative Parameters

As suggested by Aleotti and Chowdhury (1999), demarcation of landslide susceptible areas is possible through identification and analysis of factors that had caused slope instability in the past. The landslide causative factors may broadly be classified into two classes (Crozier, 1986; Siddle et al., 1991; Dikau et al., 1996; Naithani, 1999; Kanungo et al., 2009): the internal or preparatory factors and the external or triggering factors. The internal factors generally constitute the most favourable set of conditions under which mass movement would occur, as well as when triggered by an external causative factor like an earthquake or incessant rainfall. The internal causative factors that incorporate the inherent geomorphological attributes, often exhibit temporal variation in their geometry and material properties (Kanungo et al., 2009). It is understood that slope failure ultimately implies to a prevailing set of ground conditions at that specified duration rather than the singular effect of one or more individual parameters.

Although, the landslide causative factors may exhibit spatial and temporal variations on regional basis, there are a definite set of parameters which are widely accepted by various researchers (Dikau et al., 1996; Naithani, 1999; Kanungo et al., 2009). The two major categories of landslide causative factors are given in Table 1.1 below:

Table 1.1: Landslide Causative factors

(I) Internal or Preparatory:	Lithology of the slope
	Morphology of the slope
	Relative relief of the slope
	Distance from Thrusts, faults and lineaments
	Drainage density of the basin
	Road density (Anthropogenic factor)
	Land Use Land Cover Pattern (Anthropogenic factor)
(II) External or Triggering:	Weather (Extreme hydrological conditions, snowfall etc.)
	Earthquakes
	Undercutting by river

It is to be noted here that the process of landslide occurrence and its spatial distribution over an area depends on various landslide causative factors and both these natural as well as anthropogenic factors diverge from region to region.

1.3   Current Scenario of Landslide Hazard in the Himalaya

Every year, especially during the summer monsoon period, landslides and related natural disaster events claim many lives and destroy property, infrastructure, and the environment of the Himalaya. The economic loss in landslide damage alone in this region is estimated at USD 1 billion per year. Li (1990) estimated that the loss of life due to landslides and related earth flow phenomena in the Himalayan region constitutes about 30% of the world's total landslide-related damage value. The Durham Landslide Fatality Database suggests that over 1,000 people were killed in landslide events in the Himalayas in 2007 alone, which represents almost 35% of the global total. Furthermore, Dunning et al. (2007) estimated that over 20,000 people were killed by landslides during the 2005 Kashmir Earthquake in Pakistan and India. The rugged topography, the complex geological structures, the fragile soil cover, the high intensity monsoon rainfall, the large temperature variations, and the occurrence of very large magnitude earthquake events, can be attributed to the frequent landsliding in the Himalayas (Shroder Jr., 1998). The main reasons of mass movement in the Himalayan belt may be grouped into four major categories (these categories are in fine concurrence with table 1.1):

- Geological

- Morphological

- Physical

- Anthropogenic

The Himalaya is the youngest and the highest mountain range on Earth, which extends over a length of about 2400 km. The whole mountain chain is very fragile and seismically hyper-active. Because of this, the transitory earth stresses are very high on the slopes of Himalayan Mountains. There exists a wide range of material contrast in the whole region. Along with this, the uneven spatial distribution of sheared materials, jointed and fissured materials, adversely oriented discontinuities and permeability contrasts make the Himalayas very susceptible to landslide hazard.

Thus, it is very important to recognize the risk of landslide hazard in the Himalaya and to reduce the impact of future landslide disasters. One of the key approach for this purpose is to identify areas with high potential of landslide occurrence and to follow a rational land use pattern. In this context, Landslide Hazard Zonation (LHZ) mapping of the Himalayan belt becomes an absolute necessity, considering the socio economic impact of landslide related disasters here. LHZ mapping is a scientific practice of predicting the spatial distribution of landslides over a region which is determined as a function of landslide occurrence and various landslide related factors (Varnes, 1984; Kanungo, 2009). The objective is to identify the places which are vulnerable to landslide hazard and ranked them according to their degree of susceptibility. The following section provides with a brief review of the present state of research on LHZ mapping for the Himalayan belt.

1.4 Landslide Hazard Zonation (LHZ) Mapping in the Himalaya: A Brief Review

The landslide susceptibility mapping in the Himalayan region gained momentum since the early part of the '90s decade, where most of the mapping was carried out as desktop based studies (Pachauri and Pant, 1992; Anbalagan, 1992; Anbalagan and Singh; 1996). The GIS and advanced remote sensing techniques then became popular from early 2000s (Gupta et al., 1999; Saha et al., 2002; Sarkar et al., 2004; Kanungo et al., 2006; Pareek, 2008 etc.). The last few years have seen a surge in research correlating the high seismicity and landslide occurrence in this region mainly through the studies from Pareek and Sharma (2010); Pareek et al. (2013); Bhattacharyya and Sharma (2012) and Nath and Sharma (2018). The following section summarizes the significant contribution of some of the prominent researchers in LSZ mapping for Garhwal Himalaya since 1990.

Pachauri and Pant (1992) proposed LHZ map using quantitative analysis of existing landslides with geological, geotechnical and topographical attributes for Aglar river catchment area and observed significant correlation between landslide activity and the distance from the fault. Anbalagan (1992) proposed the Landslide Hazard Evaluation Factor (LHEF) rating scheme in which weights were calculated based on empirical approach derived from both past

experience of landslide causative factor and their impact on landslide occurrence. A LSZ map was produced for Kathgodam area using LHEF rating scheme. Sarkar et al. (1994) carried out LHZ for Srinagar-Rudraprayag area where slope-angle, lithology, distance from major geological discontinuities, land cover, drainage and relative relief were considered as instability factor. Pachauri et al. (1998) used geological and geomorphological attributes for LSZ mapping and observed correlation between landslide distribution and rupture zones of some seismic activities of Kangra earthquake (1905). Gupta et al. (1999) successfully used an integrated remote sensing and GIS based approach for LHZ mapping in a part of Bhagirathi river valley. Pachauri (2001) generated a LHZ map for Chamoli region which showed that maximum landslide density occurred at the highest earthquake (Chamoli Earthquake, 1999) intensity zone. The study proves that earthquakes are one of the major causative factors for mass movement in this region. Arora et al. (2004) carried out LHZ for a part of Bhagirathi river valley using A.N.N. approach in which geological and anthropogenic factors were considered as neurons for A.N.N. Saha et al. (2005) proposed a Modified Nominal Landslide Hazard Factor (mNLHF) for LSZ mapping (bi-variate statistical based method) in Bhagirathi river valley area where the computed weight values were used directly to generate landslide hazard index map. Kanungo et al. (2006) developed a combined neural network and fuzzy approach to generate LSZ maps. Ray et al. (2007) used Fuzzy set based approach to prepare LSZ map for a part of Garhwal Himalaya, and concluded that seismic activities in the Garhwal Himalayan region influence the slope stability conditions which results in form of surface rupture and fractures that produce co-seismic landslides. Kanungo et al. (2009) reviewed the available methods of LSZ mapping and observed that a combination of two distribution-free approaches could effectively reduce the subjectivity of weight assignment process. Pareek et al. (2010) studied the impact of seismic factors on landslide susceptibility zonation for a part of Indian Himalayas. Bhattacharya et al. (2011) demonstrated that SBAS InSAR technique not only monitor the surface movement in the form of landslide but also it can be considered as an effective tool to recognize new landslides in complex steep mountain region. Sarkar et al. (2012) carried out rock mass classification and slope stability assessment of road cut slopes in Garhwal Himalaya. Das et al. (2012) presented Bayesian logistic regression (BLR) for landslide susceptibility assessment along road corridors. The methodology is tested in a landslide-prone area in the Bhagirathi river valley. Pareek et al. (2013) studied the effect of seismic displacements on landslide susceptibility zonation (LSZ) in Garhwal Himalayan region using GIS and remote sensing techniques. Pareek et al. (2014) used California's Division of Mines and Geology (DMG) procedure for estimating the slope failure mechanism under seismic conditions. Developed a displacement tool based on the DMG procedure in GIS

environment. Pain et al. (2014) Carried out finite element stability analysis for three rock slopes in Garhwal Himalayas using two dimensional plane strain element and concluded that numerical modelling of rock slides is a versatile approach to understand the failure mechanism and the dynamics of rock slopes. Anbalagan et al. (2016) did a comprehensive study for the identification of landslide susceptibility zones using landslide frequency ratio and fuzzy logic in GIS environment. Gupta et al. (2016) documented the spatial distribution of landslides and its consequences in the lower reaches of the Bhagirathi Valley between Bhatwari and Uttarkashi due to the June 15-17th flooding event in Bhagirathi River. Gupta et al. (2017) carried out finite element stability analysis for failed slope of the Surabhi Resort landslide located in the Mussoorie Township, Garhwal Himalaya using shear strength reduction technique. Bandooni et al. (2018) used geo-informatics technologies and numerical models to analyse the environmental vulnerability of the mid-Garhwal Himalayan region and observed that the anthropogenic activities and natural disasters had been the primary causes of such fragile geo-environment.

1.5 Research Motivation and Problem Statement

A critical review of the existing literature would point out that the majority of the LHZ studies carried out for the Himalayan regions consider internal or preparatory landslide causative parameters only. Most of the past studies did not incorporate earthquakes in LHZ mapping for the Himalaya, despite recognizing a strong correlation between Himalayan seismicity and the landslide activities. The few studies that had focused on seismically induced LHZ mapping were concentrated around Chamoli earthquake (1999); Sikkim earthquake (2011) and Nepal earthquake (2015) only. Moreover, there has been a paucity of macro-scale, regional level LHZ mapping for the Himalaya as a whole, and particularly for the lower Himalayan belt, where rapid population growth and urbanization have been observed in the preceding three decades.

It is imperative to discuss here the relevance of studying seismically induced LHZ mapping for the Himalaya. There have been several earthquakes in the Himalayan region (Pareek et al, 2012; Prakash, 2013; Collins and Jibson, 2015) *viz.* Chamoli earthquake (29 March 1999, M_w-6.8), Kashmir earthquake (8 October 2005, M_w-7.6), Sikkim earthquake (18 September 2011, Mw-6.9), Nepal earthquake (25 April 2015, M_w-7.8) and so forth; which caused widespread and damaging landslides. In fact, in many cases, losses due to seismically induced landslides have been more than those caused directly due to shaking (Bird and Bommer, 2004). Marano et al. (2010) reported that out of the all earthquake related casualties, which are not caused directly by ground shaking, approximately 70% may be attributed to

landslides. Tanyas et al. (2017) observed that from 2004 to 2010, a total of 47,736 earthquake-induced landslide casualties were reported by many researchers (Kennedy et al., 2015; Petley, 2012). Moreover, impacts of seismically induced landslides are of long term nature, which manifest their damage intensity in terms of indirect socio-economic losses (Marui and Nadim, 2009; Tang et al., 2016; Korup, 2006). Recognizing the enormous risk associated with earthquake induced landslides, the National Guidelines on Landslides and Snow Avalanches (NDMA, 2009) has accentuated on incorporating multi-hazard integration, especially coalescing seismic and landslide hazards. Such multi-hazard studies will assume paramount significance for seismically active belts like the Himalaya. An accurate LHZ mapping of the Himalayan region, considering earthquake scenarios as a main triggering factor would be of immense practical use for decision based future land-use planning.

1.5.1 Problem Statement

In this context, an endeavour has been made in this research work *"to quantify seismic factor using probabilistic seismic hazard assessment and its implication in LHZ mapping for a part of lower Himalayan belt."* The primary scope of the research work incorporates comprehending the role and implication of the seismotectonic environment of the Himalaya in spatial distribution of landslides in a holistic way. Probabilistic seismic hazard assessment is used to generate earthquake scenarios for different return periods, so as to include the effect of an entire range of earthquake sizes objectively. Finally a part of the lower Himalayan belt is chosen as the study area to bridge the identified research gaps.

1.6 Aim, Objectives and Scope of the Study

The main aim of this research work is to prepare LHZ maps of the study area under both static and seismic conditions to quantify the impact of earthquakes in landslide hazard. The main objectives of the study include:

- Preparation of a comprehensive landslide inventory to be used for landslide zonation mapping.
- Quantification of role of seismicity in terms of fault distance and spatial distribution of landslides in the study area.
- Preparation of LHZ maps for the study area under static conditions using different available techniques to ascertain the best suited LHZ map for the area, and integration of triggering factor (i.e. seismicity) with the same.
- Generation of different strong ground motion scenarios using Probabilistic Seismic Hazard Assessment (PSHA) technique to be used as triggering factor(s) for LHZ mapping.

- Quantification of effect of seismicity in terms of scenario earthquakes in Landslide Hazard Zonation (LHZ) mapping for the study area.

The research work is carried out in three phases. In the first phase, different available LHZ mapping techniques have been explored to ascertain the best suited method for the study area. In this phase only preparatory landslide causative parameters are considered. The second phase focuses on generation of seismic factors using probabilistic seismic hazard assessment. Finally, studies of both first and second phases are collated and LHZ maps under seismic conditions are prepared in the third phase. It is to be noted here that rainfall, although recognized as a main triggering factor of landslides in the Himalaya, has not been considered in the present study. There are two reasons for that: (i) it is assumed that two extreme landslide triggering factors will not act simultaneously and (ii) it is very difficult to generate the relevant dataset for huge study area considered. The research work has exclusively focused on understanding the effect of seismicity in LHZ mapping and therefore rainfall has been excluded.

1.7   Thesis Outline

The thesis comprises of eight chapters. In chapter 1, the relevance of carrying out seismically induced LHZ mapping in the Himalaya, a brief review of the current research work in LHZ studies for the Himalayan and research motivation are discussed. The research problem investigated, and the aim, scope and objectives of the research works are stated in this chapter.

Chapter 2 includes a review of the available literature on LHZ mapping. It incorporates detailed discussions on the basic assumptions of LHZ mapping, various methodology of LHZ mapping, role of seismicity in landslide occurrence and use of probabilistic seismic hazard assessment in LHZ mapping.

In chapter 3, preparation of a relevant dataset to carry out LHZ mapping is discussed. This chapter incorporates discussions on the study area, various landslide causative parameters, applicability of Geographical Information System (GIS) in LHZ studies, and data used for preparation of thematic maps.

Chapter 4 presents LHZ mapping of the study area under static landslide causative parameters. In this chapter, a statistical approach of LSZ mapping is included. Also incorporates a comprehensive assessment of the LSZ map in terms of effects of Tectonic features on landslide distribution for the lower Himalayan belt.

Chapter 5 discusses the challenges of LHZ mapping under seismic conditions, development of a LHZ scale for multi hazard integration and performance evaluation of different LHZ mapping techniques.

A detailed Seismic Hazard Assessment of the study area within Probabilistic framework is put forth in Chapter 6. This chapter includes discussions on the methodology of PSHA, compilation and treatment of earthquake catalogue, seismotectonic modeling, and estimation of seismic hazard parameter for the study area. A brief review of the present state of research on seismic hazard assessment in India has also been included in this chapter.

In chapter 7, LHZ mapping under seismic conditions is described. Detailed discussions on inclusion and implications of probabilistic peak ground acceleration (PGA) parameter in LHZ mapping, and impact of various scenario earthquakes in spatial distribution of hazard zones are incorporated in this chapter. Chapter 7 presents the results of the analyses to quantify the role and effect of seismicity in LHZ mapping.

Finally, chapter 8 discusses the main conclusions of the research work. The primary outputs of the study and scope for future works are included in chapter 8.

LITERATURE REVIEW

2.1   Preamble

A natural hazard may be defined either as the probability of sudden change in a reasonably stable condition to an unstable one (Scheidegger, 1994) or as the probability of occurrence of a potentially damaging phenomenon within a given area in a given time (Varnes et. al, 1984). The latter remains the most widely accepted definition as it incorporates the concepts of magnitude, geographical location and time recurrence. The first refers to the dimension or intensity of the natural phenomenon which in turn depicts its behaviour and destructive power; the second identifies the place where the phenomena will occur and the third signifies the temporal frequency of the event. For example earthquakes predictive models traditionally attempt to define the hazard in terms of energy released (magnitude), location (epicenter) and time recurrence (return period). Similarly flood hazard evaluation essentially consists of prediction of the temporal variation of an extreme hydrological event of a given magnitude (peak flow/ volume) and its location and spatial extent (extrapolated from past records and ground morphology). However, there exists both conceptual and operational confusion in using those terms strictly to define landslide hazard. The term landslide incorporates both the movement of the slope material or of an existing landslide mass and the landslide deposit (the failed mass). The regional predictive models which generally attempt to identify the location of a potential mass movement, are based on a set of relevant environmental characteristics and assume that a slope will be more likely to fail in the future under the same conditions which had led to past and present failures (Varnes et. al, 1984). They provide information on potentially unstable slopes. These models are generally limited to a single slope. On the other hand landslide inventories (maps of landslide deposit) give information on spatial extent of the deposition of failed mass which formed within generally unknown (or unspecified) period of time. But they do not incorporate time and magnitude, speed, kinetic energy or momentum of the failed mass. The limitations of both models can be easily understood as none can singularly define the spatial distribution and temporal variation of the event. Thus, there is no consensus in accepting a singular definition of landslide hazard. Also, there is ambiguity in use of the terms "Landslide Hazard Zonation" and "Landslide Susceptibility Zonation"; albeit the final goal of both the practice remains almost the same. Landslide Susceptibility Zonation (LSZ) involves the spatial distribution and rating of the terrain units according to their propensity to produce landslides (Fell et al., 2008).

Here various internal/preparatory landslide causative parameters are examined. On the other hand, when the temporal variation of an even is considered, the term "Landslide Hazard Zonation" (LHZ) should be used. Thus, LHZ mapping indicates consideration of one or more landslide triggering factors in the study.

As the present research work incorporates examination of landslide hazard under both preparatory and triggering factors, it is imperative to understand the advantages and limitations of different methods of LSZ mapping. This chapter focuses on that. Also, a brief discussion on the basic assumptions of LSZ mapping, role of seismicity in landslide occurrence and use of probabilistic seismic hazard assessment in LHZ mapping are included in this chapter.

2.2   Basic Assumptions of Landslide Susceptibility Zonation

It is very difficult to reach a consensus either on the method or on the scope of producing LSZ maps (Brabb, 1984; Carrara, 1989; Nieto, 1989; Guzzetti, 1999). There exists a variety of methods for LSZ mapping and each method has its own advantages as well as limitations. Yet, even with of the lack of consensus, all these methods are based on some basic assumptions which are widely accepted (Varnes et al., 1984; Carrara et al., 1991; Hutchinson and Chandler, 1991; Anbalagan, 1992; Hutchinson, 1995; Turner and Schuster, 1995; Guzzetti et al., 1999; Kanungo et al., 2009).

The basic assumptions of LSZ mapping are as follows:

i.   There exists distinct adjustments in the morphological features of a slope post failure, most of which could be identified, categorized and mapped both in the field and through remote sensing techniques (Rib and Liang, 1978; Varnes, 1978; Hutchinson, 1988; Dikau et al., 1996). This implies that post failure morphological features of a slope are discernible, which often form the skeleton of any LSZ mapping as inventories.

ii.   The set of conditions that had rendered slope failures in the past, would more likely to cause instability in the future as well (Varnes et al., 1984; Carrara et al., 1991; Hutchinson, 1995). In other words, to predict the future occurrence, the past and present landslides in an area are the key. The assumption which follows the principle of uniformitarianism, implies that the landslides are resulted from actions of continuous and uniform processes.

iii. Predictive models of landslide occurrence could be established by identifying and mapping the inherent causative factors that control the initiation as well as propagation of mass movement (Dietrich et al., 1995). The assumption justifies the application of

predictive models used for LSZ mapping and formulates the mathematical framework within which the various landslide causative factors would correlate.

Ideally, any method of LSZ mapping should accommodate all these assumptions together, failure to which the applicability of the method would be severely challenged irrespective of its scope or the goal of the investigation. Yet, a number of factors act as hindrance to the satisfactory application of all these principles. As suggested by Aleotti and Choudhury (1999), the spatial discontinuity of landslide distribution, paucity of historical data and subjectivity of the whole process are some of the major concerns in any LSZ mapping practice.

2.3 Methods of Landslide Susceptibility Zonation

LSZ mapping approaches can be either *qualitative or quantitative* and *direct or indirect*. Kanungo et al. in 2009 proposed a comprehensive taxonomy of LSZ mapping, where two main classes have been identified with various subclasses allotted to each class. Table 2.1 illustrates the classification scheme.

Table 2.1: Taxonomy of LSZ methods (Kanungo, 2009)

Category I- Qualitative Approach

    1. Distribution Analysis

    2. Geomorphic Analysis

    3. Map Combination Method

Category II- Quantitative Approach

1. Statistical Analysis

    a) Bi-variate Analysis

    b) Multi-variate Analysis

2. Probabilistic Approach

3. Distribution-free Approach

    a) Fuzzy set based analysis

    b) A.N.N. based analysis

2.3.1 Qualitative Approach

This approach depends on the individual perception about the impact of different causative parameters which are responsible for landslide occurrence. The inputs are generally derived by field surveys, aerial photographs and integration of remote sensing data. This approach for landslide susceptibility zonation includes distribution analysis, geomorphic analysis and map combination method.

A. Distribution Analysis

This method is also referred to as landslide inventory and is a relatively simpler one. Here, spatial distribution of landslides over an area is presented using remote sensing techniques like satellite imagery or aerial photographs, field surveys and/or available historical data (Wright and Nilsen, 1974; Canuti et al. 1979; Wieczorek, 1984; Espizua and Bengochea 2002). The catalogue is represented in a map either as a polygon or as a point event or may be used to develop a landslide density map for the area. The method, though fails to establish a correlation between landslide occurrence and the causative factors, is a quantitative representation of landslide distribution which often forms the backbone of other methods of hazard analysis. The main disadvantages of the approach are its incapability to portray the degree of susceptibility for future landslides and it does not provide information on temporal variations of the landslide distribution.

B. Geomorphic Analysis

In this method, LSZ maps are directly derived from in-situ geomorphological studies. The method is direct and qualitative, where LSZ is carried out in the field itself by the investigators (Meneroud and Calvino, 1976; Humbert, 1977; Landry; 1979; Hearn, 1995). Professional experience and first-hand knowledge about the terrain and different causative factors are a pre-requisite. French ZERMOS maps (Humbert, 1977) are one of the most comprehensive maps produced using geomorphic analysis. However, the main limitations of the method are that it cannot be updated with time and are indeed subjective.

C. Map Combination Method

This is one of the more widely used methods for LSZ mapping due to its relative simplicity and accuracy. Soeters and van Westen (1996) had proposed the following steps involved in this methods:

✓ Selection and mapping of the causative factors

✓ Thematic data layer preparation with relevant categories of the factors

✓ Assignment of weights and ratings to factors and their categories respectively

✓ Integration of thematic data layers

✓ Preparation of LSZ map showing different zones

The wide range of applications of the GIS platform has made is possible to prepare and integrate different thematic data layers for various landslide causative factors (Gupta and Joshi, 1990; McKean et al., 1991; Champati Ray, 2005; Sarkar and Kanungo, 2004; Pareek et al., 2012 etc.). However, the process of assignment of ranks and weights to different instability factors and their subsequent sub-classes still involves a lot of subjectivity. Moreover, it is very difficult to avoid the region-specific biasness associated with the LSZ maps produced using this method (Kanungo, 2009).

2.3.2 Quantitative Approach

In quantitative approach, the relative importance of various landslide causative factors are ascertained objectively to reduce subjectivity. There are different methods available in the literature which is summarized as follows

A. Statistical Analysis

This method evaluates the practical relationships between different causative factors and the past and present landslide distribution over a region. Some of the widely used methods are discriminant analysis, linear and logistic regression etc. (Carrara, 1983; Carrara et al., 1991; Carrara et al., 1995; Roth, 1983; Yin and Yan, 1988; Neeley and Rice, 1990; Mark, 1992; van Westen, 1993, 1994). This may be either bi-variate or multi-variate.

Bi-variate Analysis

Here, thematic layers are prepared for each landslide causative factor which is then superimposed on the landslide distribution layer to calculate the landslide density. Based on that, weight is assigned to individual factor. Some of the methods are frequency analysis approach (Pachauri and Pant, 1992, Sarkar et al., 1995; Mehrotra et al., 1996); information value (InfoVal) approach (Yin and Yan, 1988; Jade and Sarkar, 1993; van Westen, 1997; Lin and Tung, 2003; Saha et al., 2005) and landslide nominal risk factor (LNRF) approach (Gupta and Joshi, 1990). The bi-variate analysis, although considered quantitative, still incorporates a certain degree of susceptibility.

Multi-variate Analysis

In multi-variate analysis (Aleotti and Choudhury, 1999), first the percentage of landslide affected areas in each grid cell is calculated and they are classified into stable/unstable zones.

Then an absence/presence matrix of a given category of a given thematic layer is prepared, for which multivariate analysis is carried out. Finally, reclassification of the area based on the results and their classification into susceptibility zones are done. The method itself is cumbersome and complex, and often external statistical tools has to be used along with GIS. The most commonly used analyses are discriminant analysis and regression analysis (Yin and Yan, 1988; Jade and Sarkar, 1993; Wieczorek et al., 1996; Atkinson and Massari, 1998; Chung and Fabbri, 1999; Clerici et al., 2002).

The main disadvantages of statistical method (Kanungo et al., 2009) are its requirement of large dataset for desired precision level, and amalgamation of continuous and categorical thematic data layers. Sometimes, it may produce weak physical relationship between some factors and landslide distribution, which will reduce the credibility of the LSZ map generated.

B. *Probabilistic Approach*

In this method, the relationships of different causative factors with spatial distribution of landslide occurrence in an area is evaluated within a probabilistic framework. This reduces the subjectivity in the weight assignment process. Some of the widely used methods are conditional probability model, weight of evidence method (Bayesian model), certainty factor method (favourability mapping model) etc. The conditional probability model proposed by Chung and Fabri (1999) compares five different procedures viz. direct estimation, regression model, modified regression model, Bayesian estimation under conditional independence, and modified Bayesian model to estimate the conditional probability of landslide susceptibility. They had observed that multivariate regression analysis was better suited than the other probability models. Bayesian probability model (weight of evidence method) was adopted by Lee et al (2002) to calculate the Landslide Susceptibility Index (LSI) based on which different zones of landslide susceptibility were assigned. van Westen et al. (2003) also used the weight of evidence method to derive the ranks of all thematic data layers statistically. Lee and Min (2001) adopted probabilistic prediction model based on likelihood ratio to prepare a LSZ map. The main advantage of this method is that both continuous and categorical thematic data can be transformed into continuous thematic data and hence would provide with a more quantitative adaptation.

C. *Distribution-Free Approach*

Distribution-free approaches viz. Fuzzy logic and A.N.N. tend to diminish the drawback of statistical methods associated with data quality (mostly size and reliability of the input dataset). Gorsevski et al. (2003) had combined together GIS, Fuzzy k-mean and Bayesian modelling

approach to generate a LSZ map. Ercanoglu and Gokceoglu (2004) developed a model based on fuzzy relation concept for preparation of LSZ map. Arora et al. (2004) proposed an ANN black box approach for LSZ mapping. A combined neural and fuzzy approach was developed by Kanungo et al. (2006) for the Himalayan belt, and reported that distribution-free approaches are the best objective way to determine the weights to various causative factors. Moreover, they can also manage both continuous and categorical data efficiently. In recent years, with availability of different data mining tools, machine learning methods of landslide hazard assessment are getting popular amongst researchers. Many machine learning algorithms have been developed and applied for landslide susceptibility mapping studies in various parts of the world. Lee et al. (2004), Yesilnacar and Topal (2005), Pradhan and Lee (2010), Yilmaz (2010), Zare et al. (2013), Thai Pham et al., (2015), Arnone et al. (2016) utilized Artificial Neural Network (ANN) for spatial prediction of landslide distribution. Neuro-fuzzy have been used by Vahidnia et al., 2010; Oh and Pradhan, 2011; Akgun et al., 2012; Lee et al., 2015; Chen et al., 2017). In addition to these other machine learning algorithms used in landslide studies are Decision tree (DT) (Saito et al., 2009; Nefeslioglu et al., 2010; Pradhan, 2013; Tien Bui et al., 2016; Kavzoglu et al., 2014a, 2014b; Wu et al., 2014), Random forest (RF) (Trigila et al., 2015; Pourghasemi and Kerle, 2016; Hong et al., 2016; Youssef et al., 2016) Boosted regression tree (BRT) (Dickson and Perry, 2016; Youssef et al., 2016), Maximum entropy (Felicísimo et al., 2013; Park, 2015; Hong et al., 2016; Kornejady et al., 2017), Naive Bayes (NB) (Tien Bui et al., 2012; Thai Pham et al., 2015; Tsangaratos and Ilia, 2016), Support vector machine (SVM) (Yao et al., 2008; Yilmaz, 2010; Marjanović et al., 2011; Micheletti, 2011; Tien Bui et al., 2012; Pourghasemi et al.; 2013; Hong et al., 2015).

The different methods of LSZ mapping have their own advantages and limitations. The choice of a method is governed by many criteria viz. aim and scope of the investigation, scale of the investigation, expected level of precision, professional expertise associated and quality of the data available. Use of two or more methods are generally recommended for a better susceptibility zonation map.

2.4   Role of Seismicity in Landslide Occurrence

The study of seismicity and landslide hazard may be traced back to as early as 1783, post the Calabrian Earthquake, Italy, 1783 (Keefer, 2002). These studies have ever since tried to correlate earthquake magnitude and distance to landslide distribution in a region. With the increasing availability of various resources like aerial photographs, satellite imagery, digital elevation models and progress of new computational tools like the GIS, these studies have

become more detailed and comprehensive. Many researchers have tried to compile comprehensive reports on historical development of post-earthquake field investigations on earthquake-induced landslides; and documented the chronological development of studies pertaining to this topic (Keefer, 1984, 2002; Rodriguez et al., 1999 etc.). Keefer (1984) carried out an extensive study to correlate seismicity and landslide hazard where data from 40 historical world-wide earthquakes were studied to examine the characteristics, geologic environments, and hazards of landslides caused by seismic events. The study identified 14 types of seismically induced landslides and concluded that each type of these landslides occurs in a particular set of geologic environments. This implies that the study of earthquake induced landslide susceptibility should be region specific and must take the geological set-up into account for a better assessment of the prevailing hazard. In an another study, Keefer (2000) examined the pattern of landslide distribution post the 1989, Loma Prieta earthquake using statistical methods and observed a strong inverse correlation of landslide concentration with distance from the earthquake source and a strong positive correlation with slope steepness. The study also suggested a more complex relationship between landslide occurrence and rock properties for the California region. Jibson (1993) observed that prediction of earthquake induced landslide displacement becomes very important for many seismic analysis and design of engineered slopes. He proposed the usage of Newmark's sliding block method as a workable tool of estimating approximate landslide displacements. In this method the landslide is modelled as a rigid-plastic block sliding on an inclined plane and deems to have provided better results than pseudostatic analysis. The study used a simplified Newmark method, which estimated the displacements as a function of landslide critical acceleration and earthquake shaking intensity. Harp and Jibson (1996) mapped 11,000 co-seismic landslides triggered by the 1994 Northridge earthquake and observed that the most common types of landslides were highly disrupted, shallow falls and slides of rock or debris, with only a fraction of landslides belonged to deeper, more coherent slumps and block slides classes. Wang et al. (2002) and Chigira et al. (2003) published research works on landslides induced by the 1999 Chi-Chi earthquake and identified approximately 10,000 distributed landslides. The study revealed that the aerial rate of landslides decreases from the epicenter and the effect of rock type on the landslide rate is also significant. The Japan Geographical Institute (2004) published a detailed landslide distribution map post the 2004 Mid Niigta prefecture earthquake and identified 1353 landslides induced by the event. The map, published at a scale of 1:30,000 greatly contributed to the post disaster relief and recovery strategy. Chigira and Yagi (2006) discussed the basic causes and mechanisms of the deep landslides triggered by the same event. Wang et al. (2007) observed that the co-seismic landslides induced by the 2004 Mid Niigta prefecture earthquake,

were more frequent in a range of slope angles between 15^0 and 40^0. Yin et al. (2009) examined the severity of the landslide hazards triggered by the 2008 Wenchuan earthquake in China and observed that the earthquake had directly caused more than 15,000 geo-hazards in the form of landslides, rockfalls, and debris flows. The study identified more than 10,000 potential geohazard sites, especially for rockfalls, reflecting the susceptibility of high and steep slopes in mountainous areas affected by the earthquake. Yagi et al. (2009) reported the distribution and characteristics of landslides induced by the Iwate–Miyagi Nairiku Earthquake in 2008 in Japan. In the study co-seismic landslides were morphologically classified into five types, *viz.* deep-seated slide, debris slide, shallow debris slide, secondary shallow debris slide, and debris flow. It is observed that the most destructive and predominant landslides in the earthquake-affected area were shallow debris slides. Chakraborty et al. (2011) assessed the damage caused by the co-seismic landslides of the 2011 Sikkim earthquake, India. The study observed that a large number of fresh landslides (mostly rockslides) were triggered in the steep and rocky Saffo-Tung mountain area of Sikkim due to the event and the number of reactivated landslides is quite lower than the number of new landslides. Xu et al. (2012) prepared earthquake induced landslide hazard map using GIS and Weight of Evidence method for Yushu County, China after the 2010 Yushu earthquake. The study identified 2038 co-seismic landslides and considered twelve earthquake triggered landslide associated controlling parameters *viz.* elevation, slope gradient, slope aspect, slope curvature, topographic position, distance from main surface ruptures, peak ground acceleration, distance from roads, normalized difference vegetation index, distance from drainages, lithology, and distance from all faults. Tang et al. (2015) reported landslides triggered by the 2013 Lushan earthquake in China and observed that largest landslide density occurred at a distance between 5 and 10 km from the epicentre of the event. The study found that the landslide concentration increased with increasing slope angle until a maximum for the slope class 45°–55°, and slopes consisting of deeply weathered and fractured sandstones and mudstones were the most susceptible to co-seismic landslides. Tanyas et al. (2017) prepared a worldwide digital database on earthquake induced landslide inventory and examined the underlying characteristics of landslide size, topographic slope, roughness, local relief, distance to streams, peak ground acceleration, peak ground velocity, and Modified Mercalli Intensity. The study discussed the quality, completeness, and representation of earthquake induced landslide inventories and proposed a scoring method for an overall evaluation of earthquake induced landslide inventories. Jing et al. (2018) investigated the mechanics of the earthquake-induced Hongshiyan landslide in China and concluded that the marginal pre-earthquake stability of the Hongshiyan slope, coupled with the strongest seismic loading were the main reasons for the large-scale catastrophic rock slope failure induced by the

moderate event of 2014. Roback et al. (2018) discussed the size, distribution, and mobility of landslides caused by the 2015 Gorkha earthquake in Nepal and mapped approximately 25,000 landslides induced by the event.

In this context, a critical review of the studies pertaining to seismically induced landslides in the Garhwal Himalayas will assume a very important connotation. The works of many researchers have highlighted the significance of establishing a relationship between Himalayan seismicity and landslide susceptibility for this region. Pachauri and Pant (1992) proposed a LSZ map for Aglar river catchment area using quantitative analysis of existing landslides with geological, geotechnical and topographical attributes. A positive relationship between the Aglar fault and landslide activity of the area had been observed where maximum landslide distribution was reported in the proximity of the fault. In another study for Dehradun district (situated at the foothill of the Himalayan belt), Pachauri et al. (1998) had observed that the rupture zone for some of the seismic activities in this region were associated with the 1905 Kangra Earthquake and found out that the critical aspects of the nearby landslides with the faults and lineaments trend in NW-SE direction conforming to the strike of the rupture zone. The same researcher in 2001 again established the correlation between major earthquake events and landslide occurrence after the 1999 Chamoli Earthquake, where maximum landslide density was observed at the highest earthquake intensity zone (Pachauri et al., 2001). Ray et al. (2007) used a fuzzy set based approach for LSZ mapping in parts of Garhwal Himalayas and concluded that seismic activities in the Garhwal Himalayan region have influenced the slope stability conditions that resulted in the form of surface ruptures and fractures. The study also revealed that the long term slope stability is largely controlled by the seismic activities in this area. In a similar study with Pachauri (2001), Pareek and Sharma (2010) assessed quantitatively the impact of seismic factors in LSZ mapping for Chamoli region. They have used GIS and remote sensing techniques and concluded that any major seismic event not only reactivated the old landslide, but would also render new slope instabilities (Pareek et al,. 2013). Using California's Division of Mine and Geology (DMG) procedure, they have developed a GIS based tool to examine the slope failure mechanism under seismic conditions (Pareek et al., 2014). Bhattacharya et al. (2012) have carried out an extensive study to estimate the surface displacement of the Delhi-Haridwar-Ridge (DHR) [Mansadevi landslide is situated at the S-E of DHR] using Differential SAR interferometry and observed a displacement rate of 8–10 mm per year in $N15^0E$ direction of the Indian plate. This convergence rate estimated in the study was relatively low in comparison with those obtained from previous classical studies and it was attributed to occurrence of silent/quite earthquakes, aseismic slip, differential movement of the

DHR, etc. In another study Bhattacharya et al. (2011) have also noticed slow surface movements of the Mansadevi landslide relative to neighboring area during 1992 to 1998 and concluded that the present landslide is a cumulative effect of those slow surface movements. All these works have clearly indicated that it is impossible to neglect the impact of the hyper-active seismicity in the Himalayan belt in landslide distribution and recurrence in this area.

Although the correlation between Himalayan seismicity and landslide susceptibility has been well established, one may still figure out that generally these studies are of deterministic nature (considering a single earthquake event). Seldom, the whole tectonic environment is considered as a landslide causative parameter. Because of this, the effects of various earthquake sizes have been excluded from these studies. The smaller microseism having very low stress drops (Sharma and Wason, 1994), which are a product of high transitory stresses have seemed to cause perennial slope instability especially in loose weathered material. Mansadevi landslide is a prime example, where the material yielding is commonly observed as breaking off, toppling and/or sliding of mudstone or sandstone (Nath et al., 2018). On the other hand, strong ground motion like the 1999 Chamoli earthquake would not only reactivate the older landslides, but would generate fresh mass movements as well (Pareek et al., 2012). Thus, it may be concluded that while landslides produced by moderate to large earthquakes are of catastrophic nature, one should not neglect the effect of microseisms that prevents the slopes from natural arresting of the instability. In other words, various earthquake events with different magnitude range will have different effects on landslide occurrence and distribution.

In the current practice of LSZ mapping, often a single earthquake event is considered as a triggering or external causative factor; whereas it is now understood that the tectonic set up of the whole environment plays a major role in controlling the occurrence and distribution of landslides in this region. However, this would itself be very challenging as demarcation and subsequent delineation of the whole tectonic environment in an area is qualitative and requires robust analyses. Alternatively, the scenarios for strong ground motion due to damaging earthquakes may be used as a more qualitative parameter in preparing the LSZ maps. For that purpose probabilistic seismic hazard analysis (PSHA) may be used as a very effective tool.

2.5   Use of Probabilistic Seismic Hazard Analysis in Landslide Susceptibility Zonation

During the early part of the last decade, probabilistic assessment of landslide susceptibility gained worldwide popularity. The earlier deterministic studies (considering a single earthquake event) are still popular, although researchers now try to incorporate the prospect of temporal variation of seismic events in landslide susceptibility assessment (Nadim et al., 2006; Saygili and Rathje, 2009; Yin et al., 2009; Abou-Jaoude and Wartman, 2017 etc.).

This is due to the fact that the generation of earthquake induced landslide hazard maps for new or scenario events is complicated as each earthquake has specific characteristics, and existing earthquake induced landslide inventories considering a particular event only reflect the characteristics of that single earthquake (Tanyas et al., 2017). Nadim et al. (2006) has conducted a study to identify global landslide and avalanche hotspot using five layers of input data. The landslide hazard is estimated considering the lithology and morphometry of the slope, moisture content, precipitation received and the expected level of ground shaking. Using Global Seismic Hazard Program (GSHAP), 10 classes of expected Peak Ground Acceleration (PGA) for a 475-year return period earthquake have been considered as a seismic triggering factor for landslides. The study has identified India as one of the 4 major regions with highest risk to landslide hazard. Saygili and Rathje (2009) produced probabilistically based seismic landslide susceptibility maps for the southern California region. The study incorporated a scalar approach, which uses PGA and earthquake magnitude and a vector approach, which uses PGA and PGV (Peak ground Velocity) to estimate earthquake induced sliding displacements. The displacement level with a 10% probability of exceedance in 50 years was used in that study to identify landslide hazard zones. Abou-Jaoude and Wartman (2017) presented a framework to assess earthquake-induced and rainfall induced landslide hazards for Labanon based on the geological maps, digital elevation model (DEM), earthquake peak ground acceleration (PGA) maps, rainfall data, and a preliminary landslide inventory database. For the 475-year return period PSHA ground motions, the study had identified highly susceptible areas where high disrupted soil slides and rock-slope failure hazards were identified. These studies have confirmed that PGA values derived from Probabilistic Seismic Hazard Analysis (PSHA) could effectively be used as a representative of the expected ground shaking which would induce any future mass movement. PSHA is a platform, where the probabilistic distribution functions of geometry of the source and size distribution are convolved with the rate of seismicity to predict future strong ground motion. Therefore, the PGAs predicted are not used here as from single events but are representatives of the expected deformations and stress releases in future in a finite time period. Consideration of this finite time for exceedance probabilities of strong ground motion would provide an opportunity to examine the probabilities in next finite time period. Most of the studies consider the scenario for 475 years return period (10% probability of exceedance in 50 years) as a conservative approach. But to appreciate the role of seismicity in a more holistic way, the implication of different scenarios of strong ground motion on potential landslide susceptibility should also be examined. PSHA provides with such opportunities to coalesce the different scenarios of strong ground motion with the spatial distribution of landslide occurrence in an area. This in turn would help to quantify the role of

seismicity on future mass movement expected in that area where PGA is used to quantify the seismicity rather than the actual ground motion. Also, PSHA could sufficiently capture the expected strength reduction of the rock mass due to repetitive dynamic forces since the different scenario earthquakes are calculated considering various seismogenic source zones and the recorded past seismicity.

2.6   Summary

A critical examination of the available literature reveals that quantification of landslide hazard is a complex process and there exists a variety of methods for landslide susceptibility zonation mapping. Before preparing a LSZ map for an area, various landslide causative factors should be comprehensively assessed as they are the key in evaluating the prevailing hazard and estimating the potential susceptibility from any future events. The scope and scale of the investigation greatly influence the selection of hazard modeling techniques along with the quality of the dataset available. The methods of LSZ mapping can be either qualitative or quantitative, and combination of two or more methods generally reduce the subjectivity involved in the process. The common set of guidelines in landslide susceptibility analysis considers two sets of landslide causative factors: the internal and the external factors. The internal factors are of static nature and comprise of various geo-morphological features of the slope and different anthropological conditions. These factors are attributed to the preparatory causes of the prevailing landslides. In most of the cases, rainfall and earthquakes (generally a single event) are considered as the external causative factors. But they often neglect the dynamic environments *i.e.* tectonics of the area, which seem to be a major disadvantage of the current practice. In this regard, an alternate approach is to use PSHA to generate peak ground acceleration (PGA) maps for various strong motion scenarios and to incorporate the PGA parameter as a landslide triggering factor. Thus the approach would effectively capture the effect of an entire range of earthquake sizes within a finite time period, as well as the contributions of major tectonic features would be implied. Thus, consideration of seismicity as a landslide triggering factor will enhance the understanding of landslide hazards with a more pragmatic vision, especially for seismically hyperactive mountainous belts, like the Himalaya.

DATA PREPARATION

3.1 Preamble

The first step of any Landslide Hazard Zonation (LHZ) study is the collection and collation of relevant information on different landslide causative parameters of that particular area. In general, occurrence of landslide is a complex process, which depends on many geo-environmental and anthropogenic parameters. Each parameter varies significantly from one another in physical and morphological attributes. Moreover, their degree of control on landslide occurrence also vary considerably. Thus the task of information collation is difficult, time consuming and requires robust analysis. As an alternative, thematic maps of various landslide causative factors are prepared at a common scale, resolution and coordinate system. The thematic maps are used to explore qualitative and quantitative information on various themes (causative parameters) and their attributes on the ground surface. This chapter incorporates discussion on the study area, various landslide causative parameters, applicability of Geographical Information System (GIS) in LHZ studies, and data used for preparation of thematic maps.

3.2 Study Area

For implementing a macro-scale, regional basis LHZ study, a stretch of lower Himalayan belt has been chosen as the study area of the present research work. The study area spreads over Uttarakhand and Himachal Pradesh States of India (Figure 3.1) and encompasses approximately 12,350 sq. km.; with estimated population of more than 15 lakhs as per the 2011 India census. Several important and thickly populated cities of Uttarakhand and Himachal Pradesh such as Dehradun (administrative capital of Uttarakhand state), Shimla (administrative capital of Himachal Pradesh state), Haridwar, Rishikesh, Paonta Sahib, Devprayag (places with religious importance) and Mussoorie, Lansdown, Chakrata, Nahan, Vikas Nagar (popular tourist attractions) are located in the study area. Table 3.1 shows the population and area of the major cities of the study area.

Table 3.1: Population and Area of Major Cities

Major Cities	Population* (2011 Census)	Area ** (sq.km)
Dehradun	6,00,000	300
Shimla	2,50,000	40
Haridwar	2,30,000	25
Rishikesh	1,20,000	22

Solan	40,000	33
Kotdwar	30,000	80
Mussoorie	30,000	15
Lansdwone	8000	6
Chakrata	5000	8

source: Office of the Registrar General & Census Commissioner, India (censusindia.gov.in)

** source: National Portal of India (india.gov.in)*

There are three National Highways (NH no. 58, 22, 72 and 707(A)) and several State Highways along with various auxiliary roads. Parts of Jim Corbett National Park and Rajaji National Park, two bio-diverse green forests of national importance are also situated within the study area.
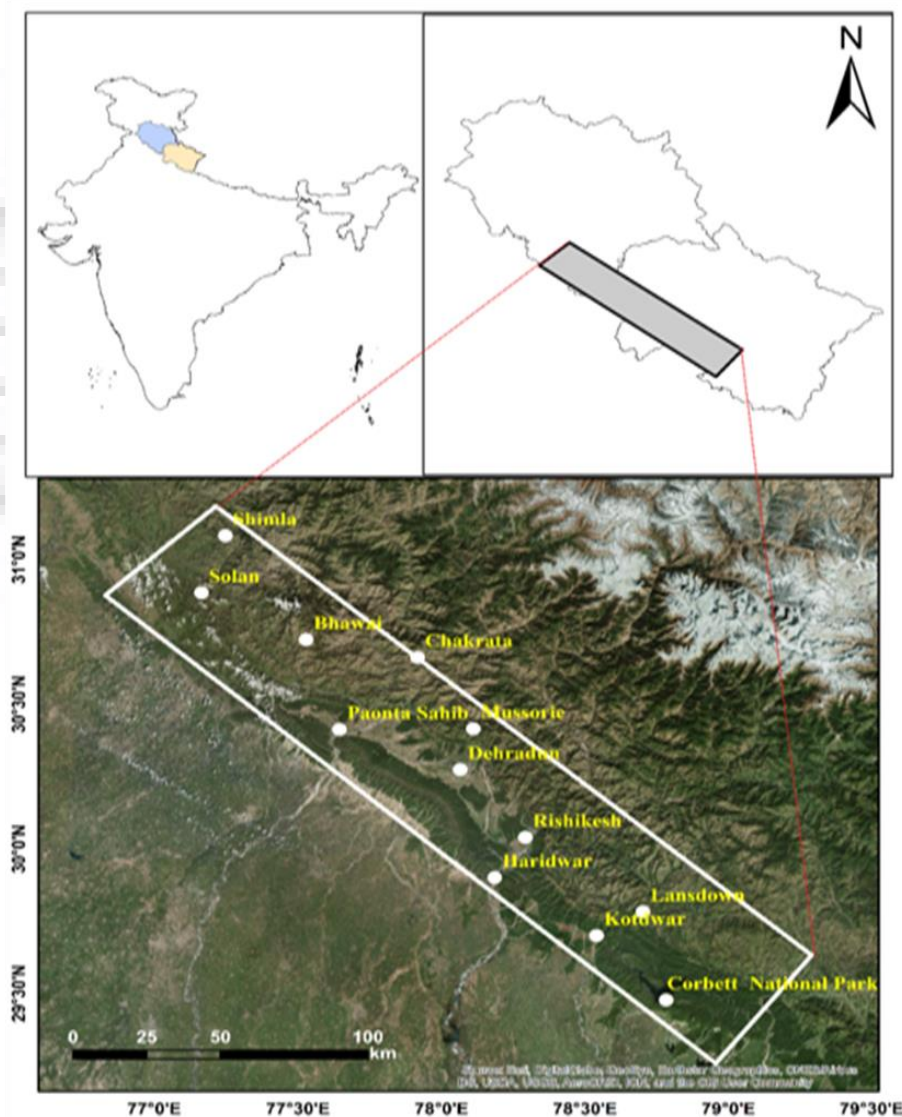
Fig. 3.1: The Study Area

3.2.1   Geology and Tectonics of the Study Area

The composition and types of slope forming materials determine the physio-chemical and engineering behaviours *viz.* texture, degree of weathering, shear strength, and permeability

etc. of the rock and soil; which in turn control the degree of landslide susceptibility. The geological discontinuities like joints, fissures, fractures, beddings, folds etc. and the orientation of the discontinuities also governs the potential of failure. Special attention should be paid to bedrock and its structural features in assessing the landslide potential, especially for rock slopes so as to understand the mechanism of failure. Thus, an updated Geological map of the study area becomes a necessity for LHZ mapping. In the present study, geological map has been derived from existing published map at 1: 326,000 scale from Valdiya (1980); which again updated through field investigations. It is shown in Figure 3.2.

Geologically, the study area exhibits a complex and heterogeneous amalgamation of fifteen formations from different ages' *viz.* Lower Siwalik Group, Middle Siwalik Group, Krol, Infra-krol and Blaini Formation, Tal Formation, Almora Crystalline Formation, Amri Formation, Jonsar Formation, Subathu Formation *etc*. The most commonly available rock types are Sandstones, Limestones, Carbonaceous Shales, Slate, Dolomite, and Conglomerate, with locally available Quarzite, Gneiss, Amphibolite and Mudstones. Owing to such an assorted matrix of lithology, the form and orientation of structural discontinuities (in terms of joints, fractures, fissures *etc.*) also vary to a great extend in this area. Table 3.2 shows the different geological formations with the rock types available in the study area.
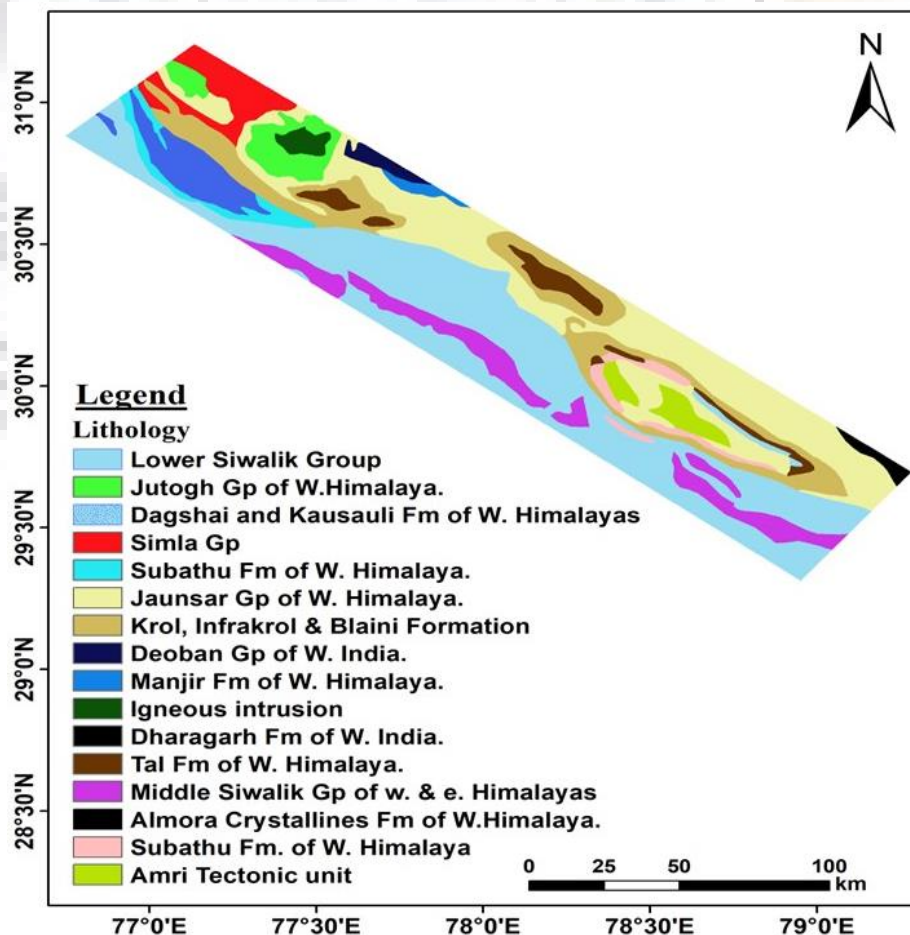
Fig. 3.2: Geological Map of the Study Area

Table 3.2: Geological Units of the Study Area

Sl. No.	Geological Units	Available Rock Types	Perceived level of landslide susceptibility
1	Lower Siwalik Group	Sandstones, Siltstone, Shales and locally available Mudstone and Conglomerate	L
2	Jutogh Group of Western Himalaya	Mica Schist, Quartzite, Marbles	L-M
3	Dagshai & Kausauli Formation of Western Himalaya	Green Sandstone, Purple Clay, Micaceous Sandstone	H
4	Simla Group	Carbonates	M-H
5	Subathu Formation of Western Himalaya	Impure Limestone, Red Shale, Sandstone	H-VH
6	Jaunsar Group of Western Himalaya	Limestone, Slates, Quartzite and Volcanic Rocks (Rhyolite, Diorite *etc.*)	H
7	Krol, Infrakrol & Blaini Formation	Limestone, Carboneous Shales, Slate	VH
8	Deoban Group of Western India	Dolomitic Limestone	L
9	Manjir Formation of Western Himalaya	Dark Grey to Black Shales/ Slate	H-VH
10	Igneous Intrusion	Granite	VL
11	Dharagarh Formation of Western Himalaya	Diorite	VL
12	Tal Formation of Western Himalaya	Limestone, Sandstone, Dolomite, Mudstone	H
13	Middle Siwalik Group of Western and Eastern Himalaya	Sandstones	L-M
14	Almora Crystalline Formation of Western Himalaya	Quartize, Gneiss, Amphibolite	M
15	Amri Tectonic unit	Gneiss, Schist	L

* VL- Very Low, L- Low, M- Moderate, H- High, VH- Very High

The study area falls in Zone IV as per IS 1893(Part I): 2016. The maximum peak ground acceleration expected in this region is 0.24g corresponding to an earthquake with 2475 years return period. This indicates that the whole study area is seismically very active as is the case with the whole Himalayan belt. The study area caters three major thrusting systems of the Himalayan arc. The most prominent tectonic features of the study area are the Main Boundary Thrust (MBT) and the Main Frontal Thrust (MFT) along with a portion of Main Central Thrust (MCT). Also numerous transverse lineaments have criss-crossed the area. Figure 3.3 shows the major faults and lineaments of the study area.
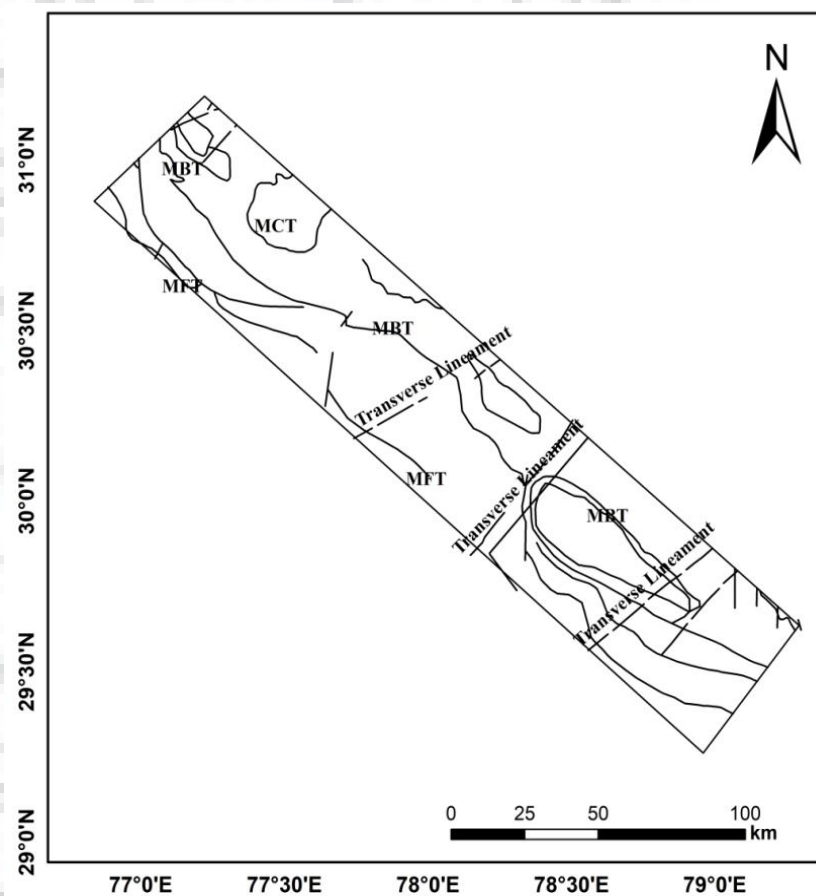
Fig. 3.3: Major Faults and Lineaments of the Study Area

It is important to understand the role and implications of the three major thrusting systems (MCT, MBT and MFT) of the Himalaya on overall seismic hazard. The Main Central thrust (MCT) which marks the southern edge of the High Himalayas is generally considered inactive as it has not yet disturbed the Quaternary sequences. The Main Boundary Thrust (MBT) has been locally observed to displace Quaternary deposits. MBT lies at the southern edge of the Lesser Himalaya, and is perceivable as the bedrock along the arc. There have been ample evidences to suggest that the Main Frontal Thrust (MFT), which is expressed by uplift and folding of late Holocene deposits (Kumar et al. 2001), dislodges Tertiary and Quaternary sequences of the Siwalik Group over the Indo-Gangetic plain. Molnar et al. (1985) suggested

that all three major earthquakes of the last century (1905-Kangra, 1934-Bihar, and 1950-Assam earthquakes) had occurred due to slip in the MFT. The large co-seismic displacements observable at different places across the MFT, when vetted against the radiocarbon dating from trench exposures have suggested that the last great earthquake had occurred between 1402 to 1422 A.D. (Sharma and Lindholm, 2012). During the last two decades, extensive research work have been carried out on seismicity of the whole Himalayan arc and the general consensus is that the next big earthquake will be produced by the Main Frontal Thrust (Kumar et al. 2001, Sharma and Lindholm 2012, Bhattacharya et al. 2012). Thus, consideration of the effects of these three major tectonic features on landslide occurrence and their spatial distribution is absolutely vital for the present research work.

3.3 Identification of Landslide Causative factors in the Study Area

As discussed in Chapter 1, four major categories of landslide causative parameters are identified for the Himalayan belt, which are geological causes, morphological causes, physical causes and anthropogenic causes. Based on these categories, nine landslide causative parameters are considered for the study area. The identified parameters also satisfy the classification system given in table 1.1, which is presented in section 1.2.1. Out of the nine parameters, eight are identified as the internal or preparatory parameters. Seismicity, which is considered as an external or triggering parameter, is also included as a main causative factor. The parameters are given in table 3.3 below.

Table 3.3: Landslide Causative Parameters for the Study Area

Sl. No	Landslide Causative Parameter	Category/Class	Remarks
1	Lithology/Geological Units	Geological/ Preparatory	There exists a wide range of material contrast in the whole Himalayan region. The uneven spatial distribution of sheared materials, jointed and fissured materials, adversely oriented discontinuities and permeability contrasts make the Himalaya very susceptible to landslide hazard.
2	Slope Angle	Morphological/ Preparatory	The slope angles in this region range between 30^0- 45^0 leading to the formation of near vertical slip surfaces.
3	Distance from Major Tectonic Features	Physical/ Preparatory	The effect of uplift and rebound, especially at plate terrene boundaries, where different

			lithologies are juxtaposed, can be reasoned with the repetitive slope failures in the Himalaya.
4	Elevation	Morphological/ Preparatory	The Himalaya is the tallest mountain in the world, and therefore, the available relief through which slope failure can act is the greatest.
5	Distance from Drainage	Physical/ Preparatory	The high rate and volume of discharge throughout the Himalaya, especially high velocity downstream flow cause a great deal of fluvial erosion in the mountains.
6	Distance from Road	Anthropogenic/ both Preparatory and Triggering	A rapid rise in infrastructures including roads, hydropower stations and dams etc. with inadequate or little consideration for the natural hazards has considerably contributed to triggering of landslides in the mountains of the Himalaya.
7	Land-Use-Land-Cover (LULC)	Anthropogenic/ Preparatory	
8	Slope Aspect	Morphological/ Preparatory	Aspects of the slope more or less implicate a local effect and are generally considered on region-specific basis.
9	Seismicity	Physical/ Triggering	Earthquakes are recognized as a major landslide triggering factor worldwide. The effect of seismicity is more prominent in loose, weathered materials in steeper slopes.

As discussed in section 1.6, rainfall has not been considered in the study as the main aim of this research is focused on seismically induced landslide hazard. It is also worth mentioning that other parameters such as distance from anticline and syncline folds, slope curvatures etc have been considered for LHZ mapping in the Himalaya (Kayastha et al., 2013). However, these studies are of micro-scale nature carried out for smaller areas. Considering the scope of the present study, and the size of the study area (> 12000 sq. km.), the present research work includes the most prominent landslide causative parameters only. The eight preparatory parameters given in Table 3.1 (Sl. No. 1 to 8) are considered by almost all the LHZ studies carried out for the Himalayan region exclusively.

3.4   Use of Geographical Information System (GIS) in Landslide Hazard Zonation

Once the landslide causative parameters are finalized, the next step is to extract relevant information for LHZ mapping. As the study area is located in the quintessentially rugged terrain of the Himalaya, only a fraction of it has been physically accessible. Invariably, remote sensing techniques have to be used to mine data on different causative parameters. Use of remotely sensed data has been an effective and popular choice for LHZ mapping in the Himalayan region. The main advantage of using remotely sensed data is that from a single high resolution image in digital format, with multi-spectral information, a range of ground surface features can be identified, classified and mapped directly. With technological proliferation, it is now possible to store, manage, collate and analyze large amount of multiple data sets effectively. Geographical Information System (GIS) has been an excellent platform for such purpose. GIS may be defined as a *"powerful set of tools for collecting, storing, retrieving at will, transforming, and displaying spatial data from the real world for particular set of purposes"* (Burrough, 1986). GIS has been used in LHZ studies to store spatial and non-spatial data in digital format, and also to manipulate and analyze different data layers to produce results in presentable form (Gupta et al., 1999; Saha et al., 2002; Sarkar et al., 2004; Kanungo et al., 2006; Pareek, 2010; Kayastha et al. 2013; Gupta et al., 2016; Bandooni et al., 2018; Peethanbaran et al., 2018). It is important to carry out proximity analysis for identifying the effects of different causative parameters on landslide activities, which can be performed using GIS at great speed. In the present research work, the GIS platform developed by *Economic and Social Research Institute, California* (Arc-GIS, V.10.6) has been used.

3.5   Preparation of Thematic Data Layers

3.5.1   Landslide Distribution Layer

Identification and mapping of the existing landslides in an area is the first and most important task for landslide hazard analysis. In the present research work, a three steps procedure has been followed to finalize the landslide inventory for the study area. The prepared inventory is then used for identification of high risk areas and it also forms the frame work for all statistical analyses of LHZ mapping. In the first step, high resolution LISS IV images of the year 2016 [spatial resolution of 5.8m] from RESOURCESAT 2 (ISRO, 2011) satellite have been used for initial identification of the existing landslides. Seven '*scenes'* of LISS IV have been used to cover up the complete study area. Table 3.4 presents the specifications of a particular '*scene'* for illustrative purpose. Figure 3.4 shows some of the identified landslides in the study area using LISS IV image.

Table 3.4: Specification of the remote sensing images used in the study

Specifications	Resourcesat 2 LISS IV images
Path/Row	97/50
Spectral Bands	3
Spectral Ranges	B2: 0.52–0.59 μm
	B3: 0.62–0.68 μm
	B4:0.77–0.86 μm
Spatial Resolution	5.8 meters
Swath	70 km
Quantization	10 bit
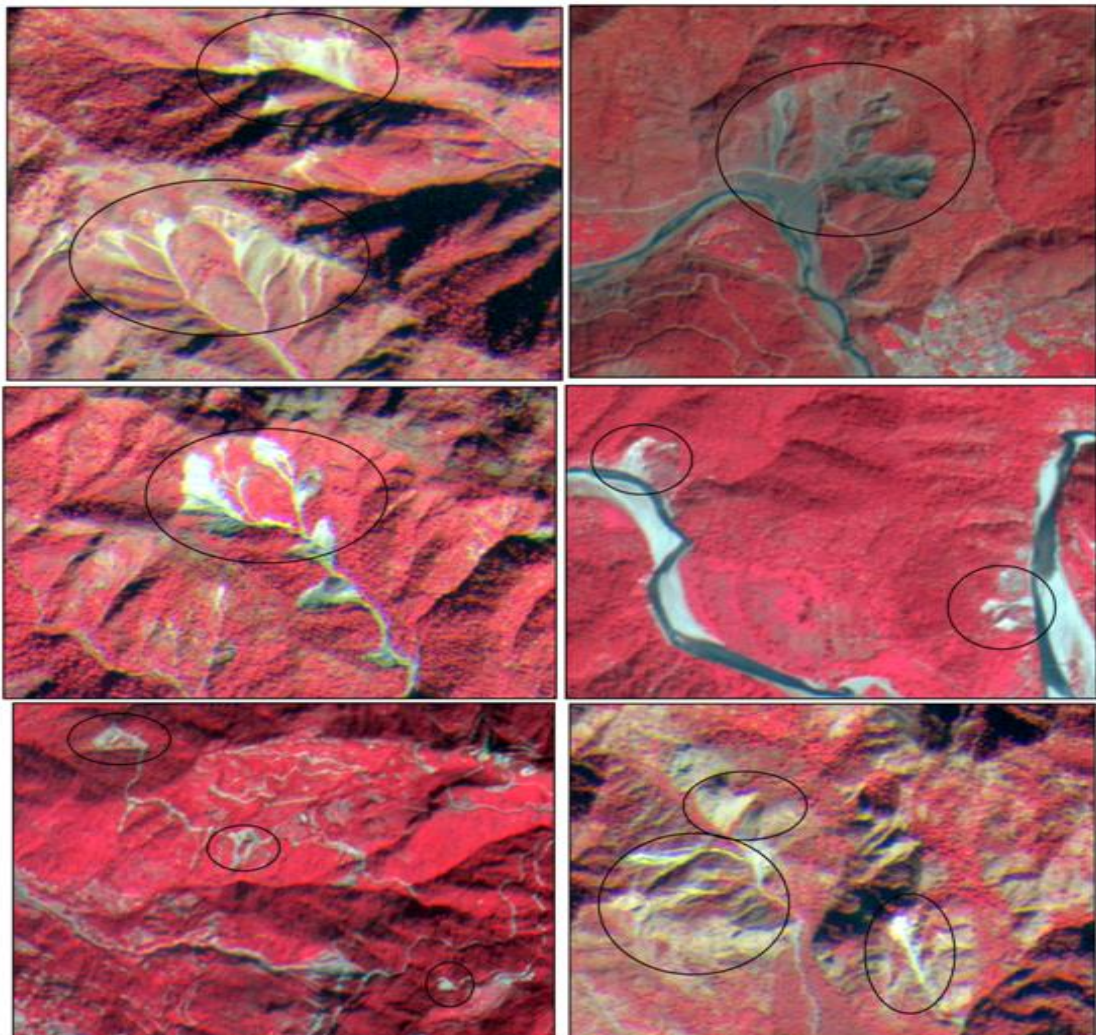
Fig. 3.4: Identification of Existing Landslides using LISS IV Imagery

In the second step, the prepared landslide inventory is further validated using Google earth platform. Google earth platform amalgamate and superimpose a range of satellite imagery from various sources to render a 3-D, synoptic view of the ground surface. For the study area,

Google earth platform presents images from *DigitalGlobe* [Airbus] and *Landsat* [Copernicus] satellites, with a historical time scale from 2003 onwards. This helps in identifying older landslides, and also any ambiguity in demarcation of potential landslides in LISS IV was reduced. Figure 3.5 shows some of the identified landslides using Google earth platform.

Lat   30°15'49.97"N   Lat   30°31'18.13"N   Lat   30°27'44.38"N
Long 78°11'55.18"E   Long 78°07'01.44"E   Long 78°03'02.49"E
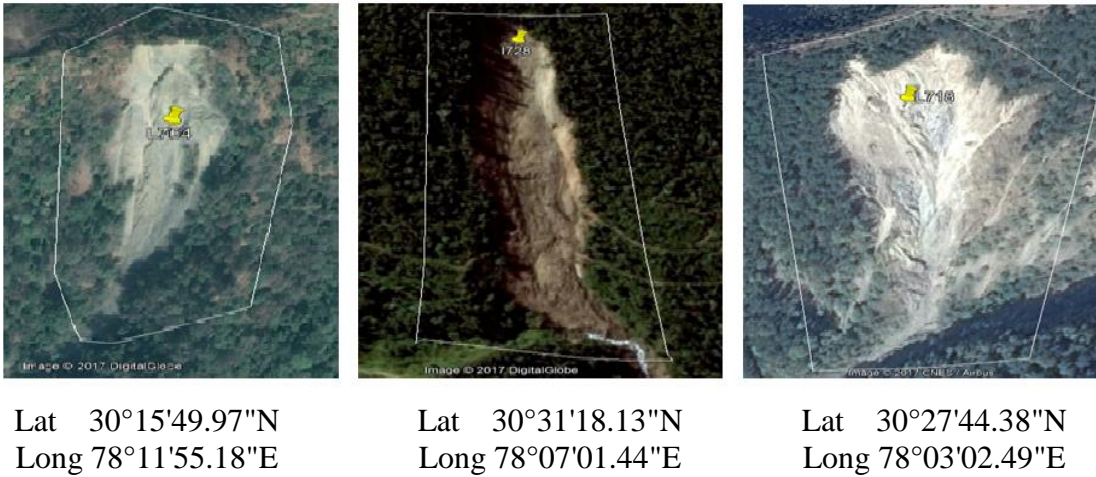
Fig. 3.5: Identification of Existing Landslides using Google Earth Platform

In the third phase, field reconnaissance survey has been done at selected few location for ground-truthing. Figure 3.6 below shows the field photographs of selected landslides in the study area.

Lat   30°32.369' N   Lat $30^0$57.683' N   Lat $30^0$49.815' N
Long $77^0$49.896' E   Long $76^0$57.326' E   Long $76^0$56.924' E
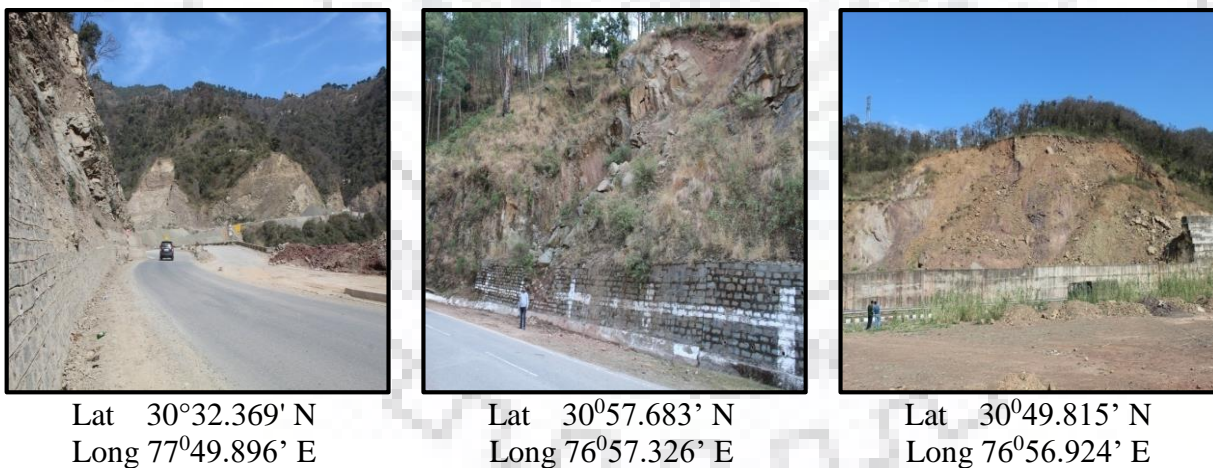
Fig. 3.6: Field Photographs of Selected Landslides

Preparation of an accurate and comprehensive landslide inventory is the most important task in any LHZ study. In the present research work, a three steps procedure has been followed for accurate mapping of the exiting landslides. For that purpose, geo-referenced LISS IV images, Google Earth platform and Field survey has been used. It is illustrated in Figure 3.7, which shows (a) Field Photographs, (b) LISS IV image and (c) Digital Globe [Google Earth platform] image of Mansadevi Landslide in Haridwar, Uttarakhand [$29^0$57'23"N, $78^0$09'44"E].
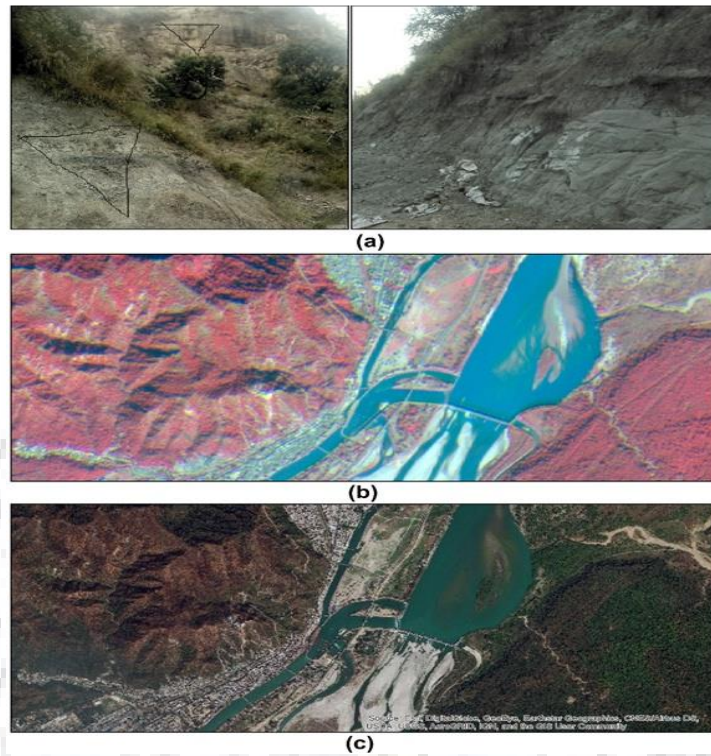
Fig. 3.7: Mansadevi Landslide, Haridwar

The identified landslides are exported to Arc-GIS 10.6 to prepare the landslide distribution layer for the study area. A total of 1062 landslides have been identified, demarcated and mapped in the present study. Details of the landslide inventory is given in Appendix A-1. Figure 3.8 shows the landslide distribution layer prepared for the research work.
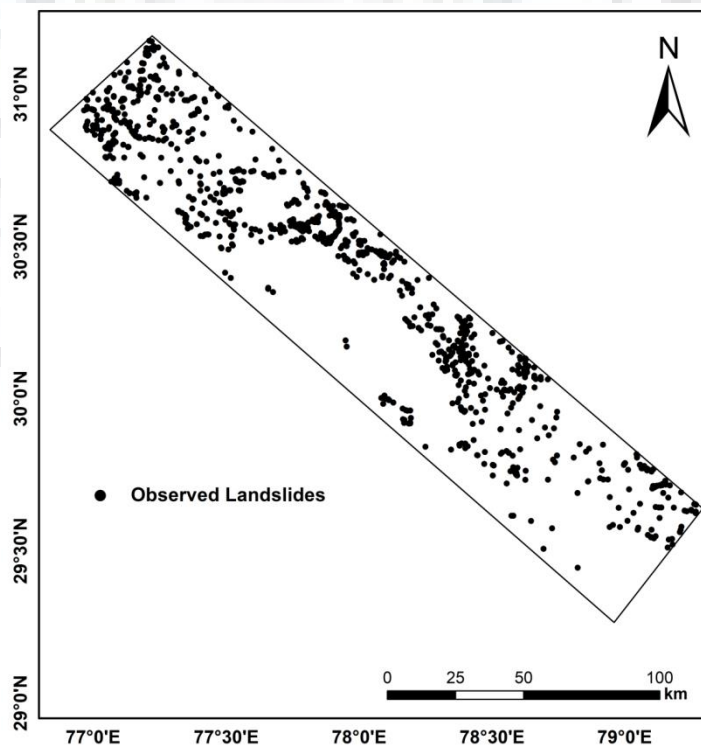
Fig. 3.8: Landslide Distribution Layer of the Study Area

3.5.2   Digital Elevation Model (DEM) and its Derivatives

The topography of the land surface is of fundamental importance for LHZ studies, as it controls flow source and direction, soil moisture and solar energy distribution. This in turn affects the local climate and vegetation which are important factors that limits the density and spatial extent of landslides (Ayalew and Yamagishi, 2005). The surface topography of an area can be derived in the form of Digital Elevation Model (DEM). DEM represents the spatial variation of elevation of an area digitally, which is an important landslide controlling factor. In the present study, the DEM of the study area is extracted from ASTER GDEM V2.

Advanced Spaceborne Thermal Emission and Reflection Radiometer (ASTER) Global Digital Elevation Model Version 2 (GDEM V2) was released jointly by the Ministry of Economy, Trade, and Industry (METI) of Japan and the United States National Aeronautics and Space Administration (NASA) on October 17, 2011. It has a spatial resolution of 30 meters, with 1^0 x 1^0 tiles that covers almost 99% of the total landmass of earth. Considering the scope of the study and the size of the study area, 30m resolution is found adequate for the present research work. The study area has the minimum and maximum elevations of 201m and 3638m above mean sea level respectively, which is shown in Figure 3.9. The DEM is categorized into five (5) classes at an interval of 500 m. It is observed that maximum landslide density corresponds to an elevation class of [500-1000]m, followed by the class of [1000-1500]m. The least landslide density is observed at elevations less than 500m.

The DEM has been used to derive various terrain attributes like slope angle, slope aspect and the drainage density of the study area, which are used as input data layers for LHZ mapping. The drainage density map is further validated using SoI (Survey of India) toposheets at a scale of 1:50,000.

3.5.3   Slope Angle Map

Slope angle is the most influencing parameter for GIS-based LHZ mapping (Guzzetti et al., 1999; Kanungo et al., 2009) as gravitational forces increases with steeper slopes. At regional level, it also controls the hydraulic continuity. In the study area, slope angles range from 6^0 to 72^0. The slope map of the study area is given in Fig. 3.10, which is classified into 5 classes. Slopes greater than 35^0 have been observed to be more susceptible to landslides in the study area.

3.5.4   Slope Aspect Map

Slope aspect provides with information on solar and insolation soil moisture conditions over that sloping surface, which further affects the distribution of vegetation and hydrological

conditions and thus the landslide activity. It more or less implicate a local effect and are generally considered on region-specific basis. A slope aspect map of the study area is shown in Fig. 3.11. It is categorized into nine (9) classes. It is observed that slopes with East, West and North-West directions have the highest concentration of landslides in the study area.

3.5.5 Drainage Euclidian Distance Map

Drainage density in a basin might provide with important information on erosion rates in that area. Undercutting of the toe by rivers and drains are two of the major contributing factors of landslides and could be directly linked with landslide susceptibility. Low surface drainage generally induces high infiltration rate which in turn will cause more pore water pressure and thus will increase the overall landslide susceptibility. In this research work, proximity analysis of Euclidian distance of the existing landslides from the drainage network have been carried out. Euclidian distance is a raster based spatial analyst tool in GIS. It provides with the perpendicular (minimum) distance between *source* and *cell*. The drainage Euclidian distance map of the study area is shown in Fig. 3.12. It is categorized into 5 classes at an interval of 250m. Maximum landslide activities have been observed at a distance of less than 250m. The effect of drainage is observed to get minimized at a distance more than 1000m.
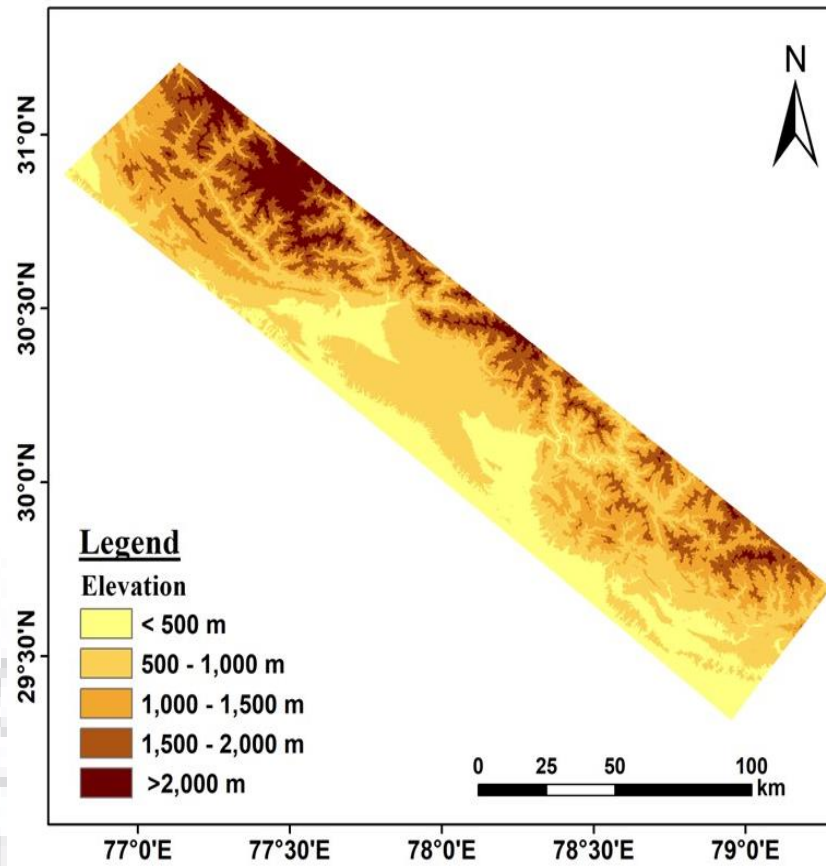
Fig. 3.9: DEM of the Study Area
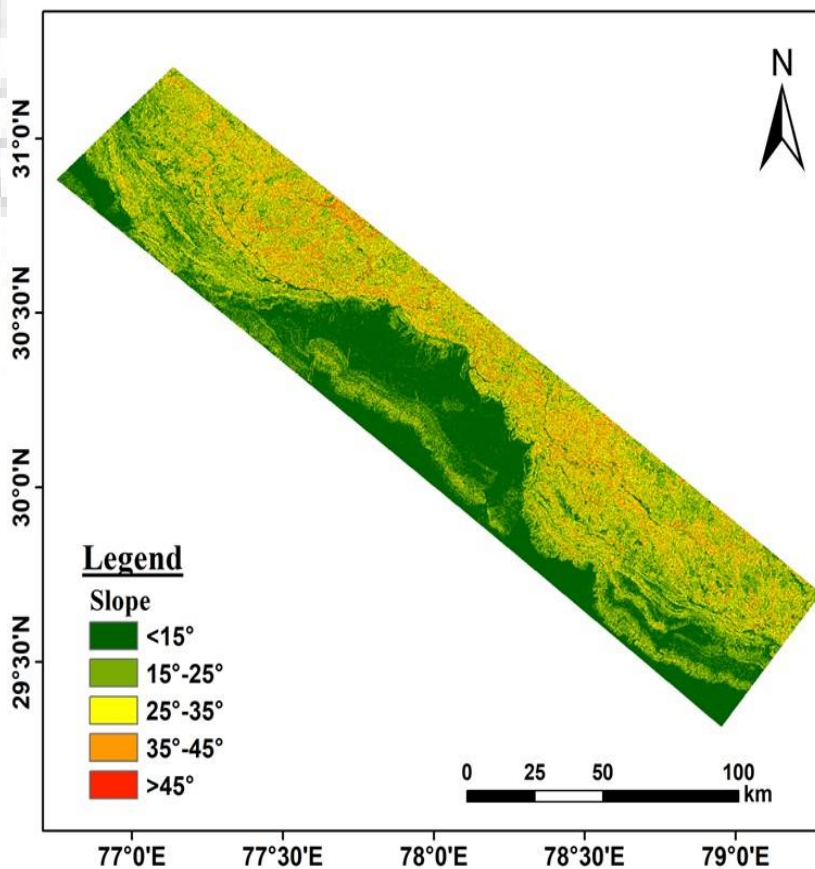
Fig. 3.10: Slope Angle Map of the Study Area
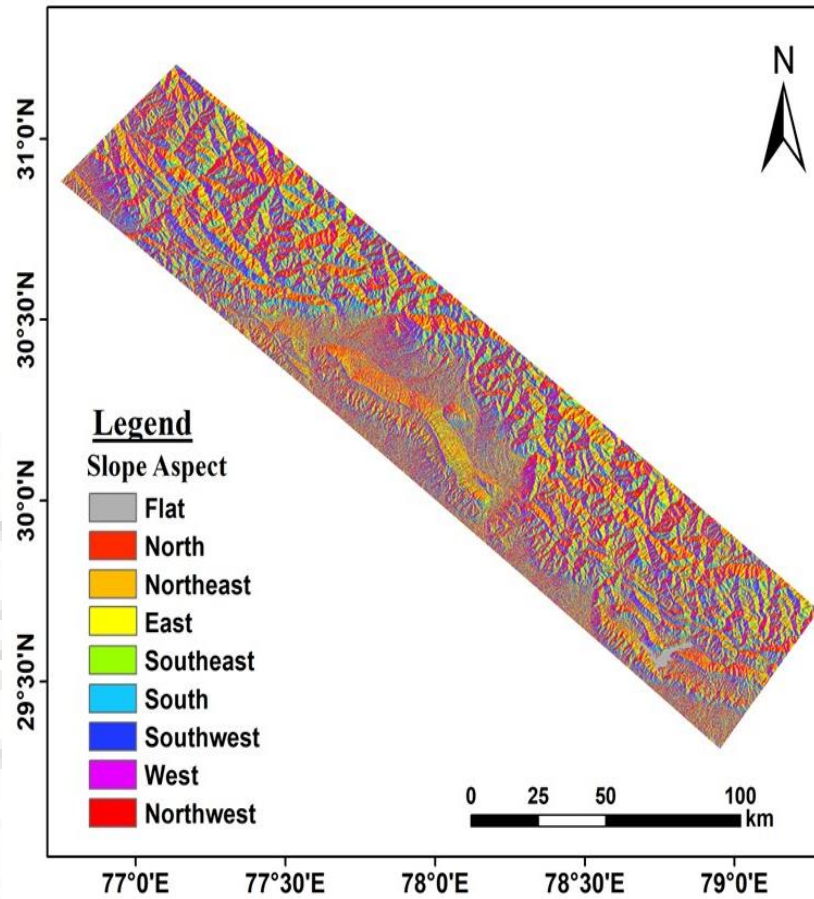
Fig. 3.11: Slope Aspect Map of the Study Area
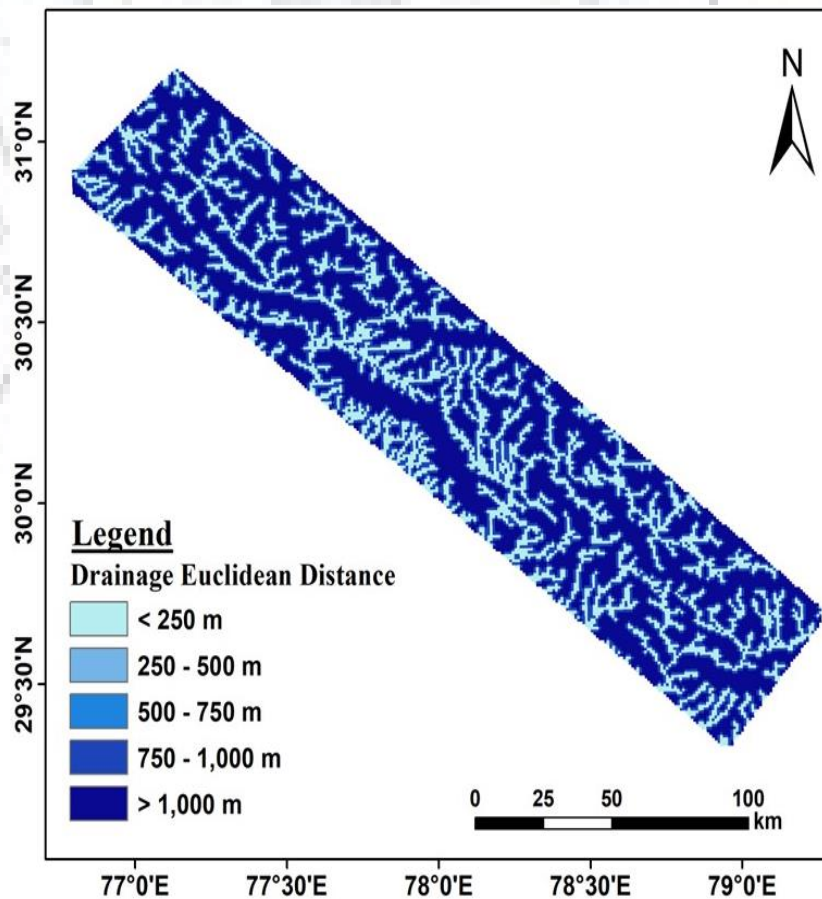
Fig. 3.12: Drainage Euclidian Distance Map of the Study Area

3.5.6   Fault Euclidian Distance Map

The study area is traversed by three major thrusting systems of the Himalaya *viz.* MCT, MBT and MFT. Also, there exist number of transverse lineaments as well. Any major geological discontinuity will have prominent effect on landslide occurrence and distribution in an area. Susceptibility of a slope to failure increases manifold if active tectonic features like thrust, faults, and lineaments are located in close proximity. The transitory earth stresses will be much higher beneath such landslides which in turn would cause recurrent slope instability. The presence of shear zones and crushed zones in the bedrocks, which is a result of plate tectonic activities, should be considered in assessing the landslide potential in an area.

The tectonic map of the study area is presented in Fig. 3.3. The seismotectonic atlas of India (GSI) has been extensively referred to in preparing the tectonic map. Additionally, different auxiliary data (*https://data.gov.in/catalog/digital-seismotectonic-atlas-india-and-its-environs; http://bhukosh.gsi.gov.in; published literatures*) are also used for corroboration. The digitized fault contours are exported in Arc GIS 10.6 to calculate the Euclidian distance of the existing landslides from the nearest *source* (fault/thrust/lineaments). The fault Euclidian distance map of the study area is shown in Fig. 3.13. The minimum and the maximum distances have been observed to be 0 km (i.e. landslides observed at the fault wall itself) to 14.9 km. The map is categorized into 5 classes at an interval of 3km. The highest landslide density has been observed at a distance of less than 3 km from a major discontinuity.

3.5.7   Road Euclidian Distance Map

Construction of roads in the fragile mountain chains of the Himalaya has increased the landslide risk manifold. With higher road density, the overall instability of the slope will increase due to under-cutting of the hill toe. It may be considered as both landslide preparatory as well as triggering parameter, depending upon the slope geometry. Thus consideration of road distance becomes a very important parameter in LHZ mapping.

There is a sporadic distribution of road networks throughout the study area. It caters three National Highways (NH no. 58, 22, 72 and 707(A)) and several State Highways along with various auxiliary roads. While the urban centers of the area have a high concentration of road networks, the overall density of road is moderate due to large forest areas. The road network map is derived from various available sources (*www.mapsofindia.com, www.gismaps.in, www.ucost.in*). From the road network map, Euclidian distance from existing roads has been calculated, which ranges from a minimum of 15m to a maximum of 750m. A map of the road Euclidian distance is shown in Fig. 3.14. It is categorized into 5 classes. While

the highest landslide density is observed at a distance of less than 100m, at distance greater than 500m, minimal effects of roads on landslide activities have been observed.
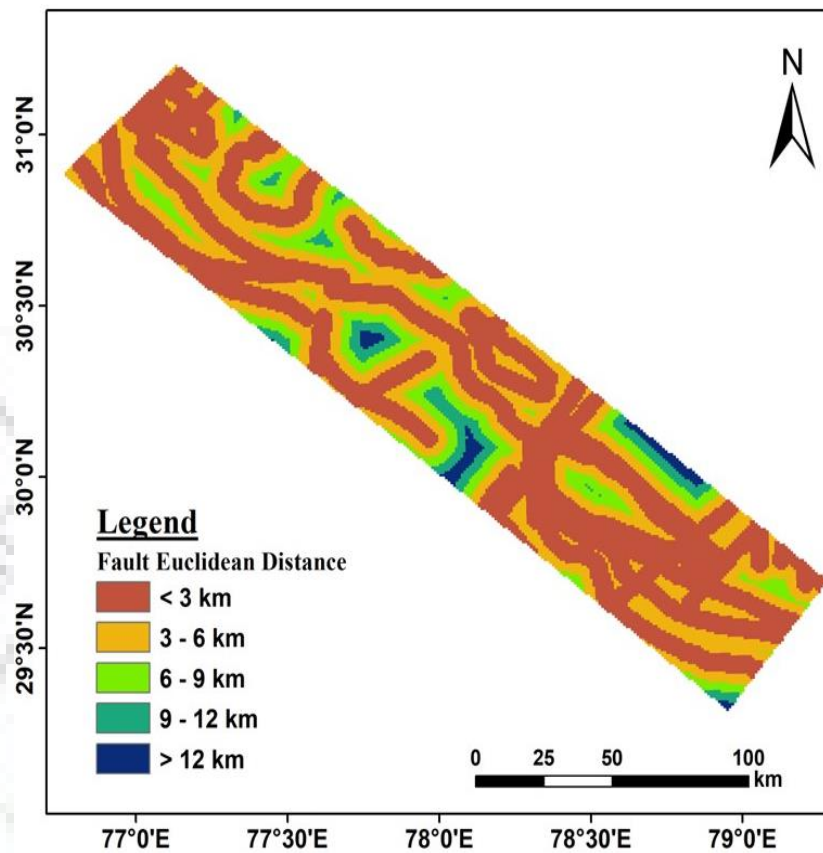
Fig. 3.13: Fault Euclidian Distance Map of the Study Area
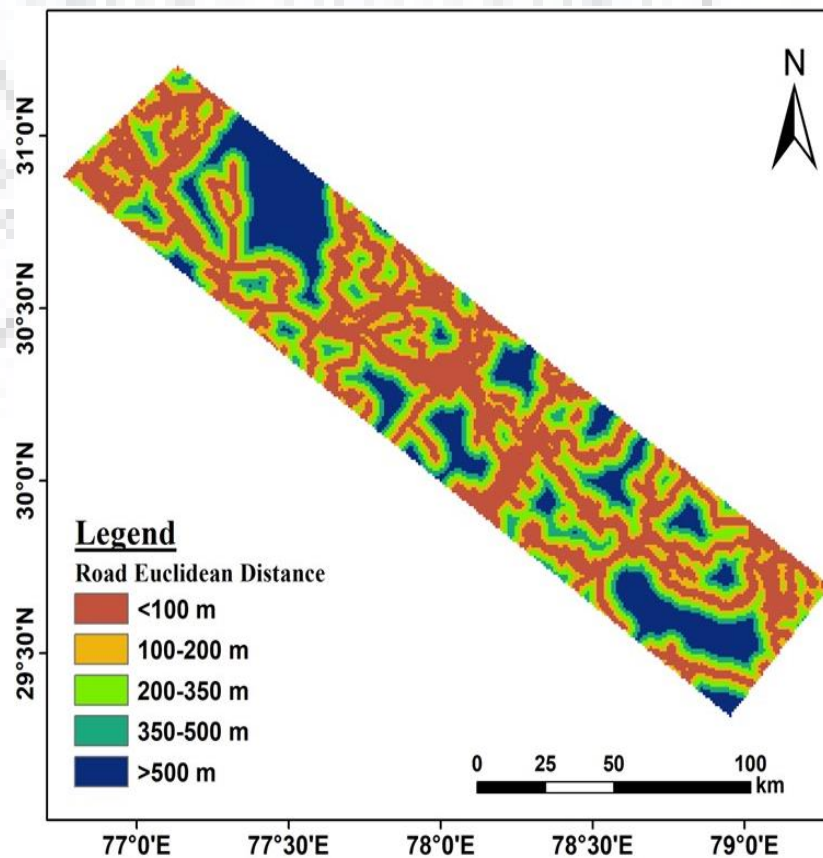
Fig. 3.14: Road Euclidian Distance Map of the Study Area

3.5.7 Land-Use-Land-Cover (LULC) Map

LULC pattern is an important parameter for LHZ mapping, although it has been observed that the effects of LULC pattern are secondary and generally, rather than inducing any new slope failure, more often than not, they dictate the degree of landslide susceptibility. In the present study, Maximum Likelihood algorithm, which is one of the most popular methods, has been adopted to classify the different LULC types. It is a supervised classification system. Landsat 8 satellite imagery with 30m spatial resolution have been used in this research work for LULC classification considering its obvious advantage over LISS IV image (Landsat 8 is a true colour composite image, whereas LISS IV is a false colour composite image). The LULC map of the study area is shown in Fig. 3.15. It is categorized into seven (7) distinct classes of land cover types. Table 3.5 below gives the percentage area of each LULC types and the percentage of the observed landslide area in each class.

Table 3.5: LULC Patterns in the Study Area

Sl. No.	LULC Type	Percentage of the Total Study Area	Percentage of the Observed Landslide Area
1	Sparsely Vegetated Area	57.2	63.5
2	Deciduous Forest Area	12.2	9.8
3	Evergreen Forest Area	15.6	12
4	Shrub Land Area	12.2	11.5
5	Built-up Area	1.2	1
6	Barren Land	1.2	2.2
7	Water Body	0.4	0
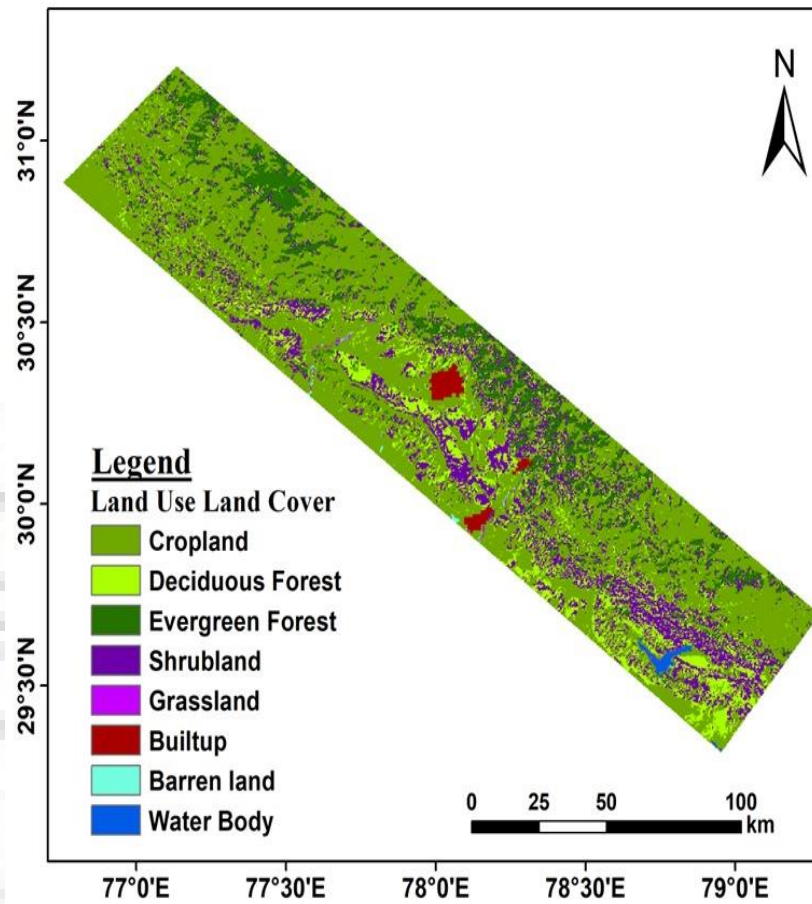
Fig. 3.15: LULC Map of the Study Area

3.6   Summary

The chapter incorporates detailed discussions on the study area and its geological as well as tectonic environments. Various landslide causative parameters identified for the study area are discussed at length. A brief discussion on the use of GIS in LHZ mapping is included here. The chapter discusses in details the method and data used for preparation of thematic maps, which will be used as input parameters for LHZ mapping. DEM has been used to prepare thematic layers for slope angle, slope aspect and drainage density in the study area. Preparation of a comprehensive landslide inventory is the first and the most fundamental step in LHZ studies. In this research work, a three steps procedure has been followed for that purpose. The landslide inventory shows that there are significant concentration of landslide events near major tectonic features. The prepared landslide distribution map has been used for proximity analyses to establish correlation between landslide activities and various causative parameter.

LANDSLIDE SUSCEPTIBILITY ZONATION (LSZ) UNDER STATIC CAUSATIVE PARAMETERS

4.1 Preamble

In the present research work, a part of the lower Indian Himalaya has been selected to understand the role and effect of seismicity in landslide occurrence and their distribution. For this study area, eight (8) internal or preparatory landslide causative parameters have been identified; and seismicity has been considered as a main external or landslide triggering factors. The internal factors are fundamentally of static nature, i.e. there is little or no temporal variations expected in their attributes. Thematic maps of the eight parameters have been generated (as discussed in Chapter 3), which is analyzed with respect to the landslide distribution layer to establish correlation between landslide activity and various classes of thematic layers.

In the next phase, the present susceptibility level of the study area has been assessed under the condition of static landslide causative parameters. This is of particular importance as the generated Landslide Susceptibility Map (LSZ) map will be used to understand the intrinsic effects of various causative parameters, before incorporation of seismicity in landslide hazard assessment. In this chapter, a statistical approach of LSZ mapping is included. An accurate LSZ map of the study area has been produced, which shows the current scenario of landslide susceptibility for different important sites of the study area. The prepared LSZ map is validated statistically and the success of the predictive map is calculated. The chapter also incorporates a comprehensive assessment of the LSZ map in terms of effects of Tectonic features on landslide distribution for the lower Himalayan belt. It is worth mentioning here that the term *'landslide susceptibility'* has been used deliberately in this chapter instead of *'landslide hazard'*, as only static landslide causative parameters are considered in this phase.

4.2 Statistical Approach of LSZ Mapping: Information Value Method

For all LSZ mapping approaches, it is imperative to understand the influence of each landslide causative parameter (thematic class) on landslide occurrence and to calculate their relative importance. This relative importance is generally referred to as the *"weight"* of a parameter, which signifies its perceived degree of control on landslide activities. A thorough knowledge of the study terrain is essential for identifying the relative importance of landslide causative factors. In qualitative approach of LSZ mapping, weights are determined based on

such terrain knowledge of the investigator, and thus it incorporates a certain degree of subjectivity.

On the other hand, statistical approach of LSZ mapping evaluates the practical relationships between different landslide causative parameters and the spatial distribution of the existing landslides over a region. Here, the relative importance of each thematic class of a causative parameter is determined statistically. Therefore, the subjectivity of weight assignment procedure is reduced in this approach. The most important step in statistical approach is to determine the landslide density in each thematic class and then weight of that class is defined. In the present study, one of the most widely used and globally recognized statistical approach: Information Value (Info Val) method has been used to prepare the initial LSZ map of the study area. Info Val method (van Westen, 1997) is based on the probability of landslide occurrence within each class of thematic data layers, where the weight of a particular class is determined as

$$W_i = \left[\frac{Densclas}{Densmap}\right] = \ln \frac{N_{Pix}(S_i)/N_{Pix}(N_i)}{\sum_{i=1}^{n} N_{Pix}(S_i)/\sum_{i=1}^{n} N_{Pix}(N_i)} \tag{4.1}$$

where, W_i denotes the calculated weight of the ith class of a particular thematic data layer (e.g. barren land class in LULC thematic layer) containing n numbers of classes; *Densclas* denotes the landslide density within that particular class; *Densmap* denotes the landslide density within that particular thematic data layer, $N_{pix}(S_i)$ denotes the number of pixels that contain landslides in the ith class of a particular thematic data layer; and $N_{pix}(N_i)$ denotes the number of pixels in that i^{th} class. Weights are calculated for all the n number of classes of a particular thematic data layer. The calculated weights are added in the form of Info Val to all thematic data layers, which are then arithmetically overlaid in GIS environment to prepare a Landslide Susceptibility Index (LSI) map. Further, the LSI map is categorized into different susceptibility classes (generally 5 classes) to produce the LSZ map of an area. A schematic diagram of the working principle is given in Fig. 4.1 below.
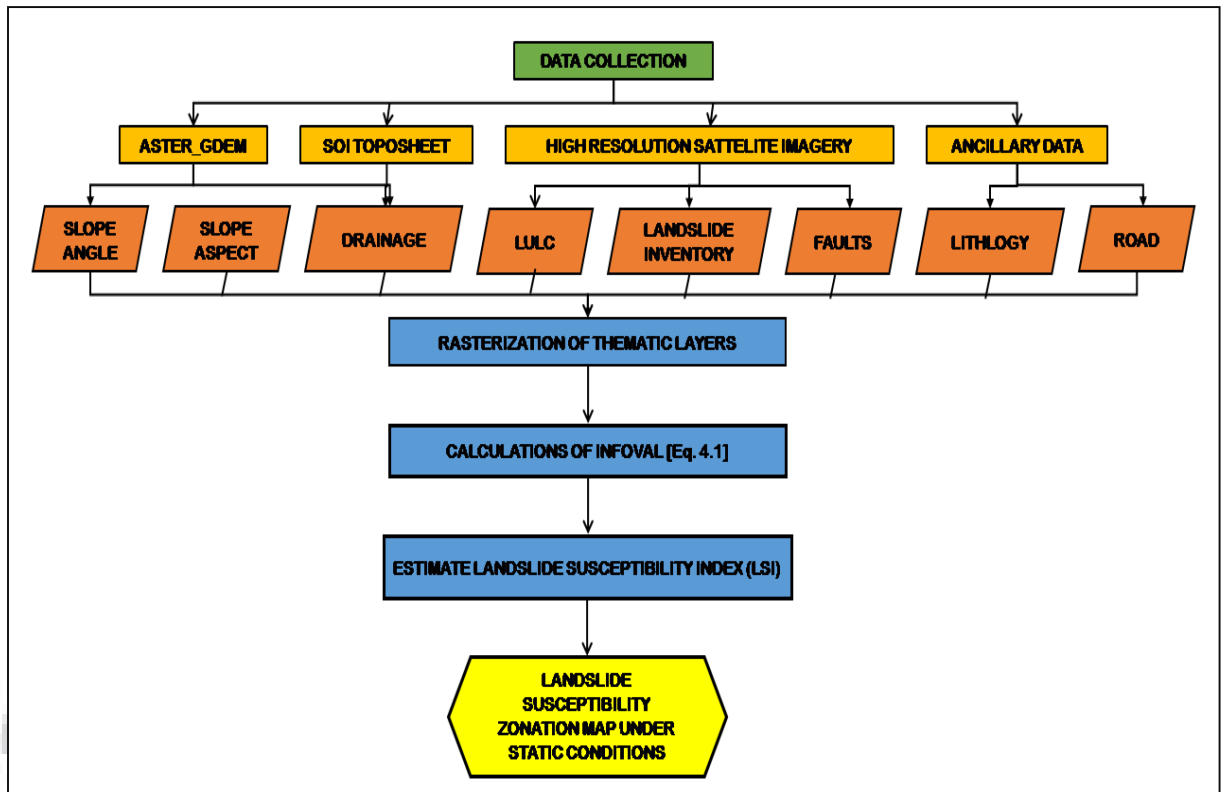
Fig. 4.1: Schematic Diagram of InfoVal Method Working Principle

4.3   Results: Landslide Susceptibility Zonation Map of the Study Area

Table 4.1 shows the calculated Information Values (Info Val) of different landslide thematic layer classes for the study area.

Table 4.1: Information Value of Different Landslide Thematic Layer Classes

Landslide Causative Factor Class	Number of Total Pixels $N_{pix}(N_i)$	Number of Landslide Pixels $N_{pix}(S_i)$	Info Val (W_i)
Slope Angle			
$<15^0$	5403279	2092	-0.710
15^0-25^0	3520086	5163	-0.132
25^0-35^0	3073718	9300	0.183
35^0-45^0	1394610	7856	0.453
$>45^0$	209626	2558	0.789
Geological Units			
Krol, Infrakrol & Blaini Fm	1691691	7754	0.363
Subathu Fm of W. Himalaya	286108	1142	0.303
Manjir Fm of W. Himalaya	69478	260	0.275
Subathu Fm. of W. Himalaya	241667	726	0.180
JaunsarGp of W. Himalaya	3131804	8886	0.155
Tal Fm of W. Himalaya	417349	1046	0.101

SimlaGp	528344	1316	0.098
Almora Crystalline Fm of W. Himalaya	81679	186	0.059
Dagshai and Kausauli Fm of W. Himalayas	560550	953	-0.067
Jutogh Gp of W. Himalaya	475571	592	-0.203
Middle Siwalik Gp	1024292	863	-0.372
Lower Siwalik Gp	4601763	3003	-0.483
Amri Tectonic unit	273470	176	-0.489
Deoban Gp of W. India	105946	66	-0.503
Dharagarh Fm of W. India	946	0	-2.274
Igneous intrusion	110664	0	-4.342
Fault Euclidian Distance			
0-3 km	7193388	15136	0.025
3-6 km	4068248	8002	-0.004
6-9 km	1577930	2762	-0.055
9-12 km	565676	809	-0.143
>12 km	196077	260	-0.175
Elevation			
< 500 m	2720775	1076	-0.701
500-1000 m	4535294	13451	0.174
1000-1500 m	3515152	9334	0.126
1500-2000 m	2115842	2894	-0.162
> 2000 m	714256	214	-0.821
Drainage Euclidian Distance			
< 250 m	2165236	6795	0.057
250-500 m	1598154	4089	-0.032
500-750 m	931472	2081	-0.030
750-1000 m	319620	466	-0.119
> 1000 m	26326	47	-0.561
Road Euclidian Distance			
< 100 m	720633	2043	0.181
100-200 m	735637	2000	0.162

200-350 m	857568	1992	0.094
350-500 m	935429	1923	0.041
> 500 m	10352052	17482	-0.044
LULC Patterns			
Sparsely Vegetated	7783545	18015	0.067
Deciduous Forest	1708949	2100	-0.208
Evergreen Forest	1710523	3200	-0.025
Shrub Land	2199289	3143	-0.142
Built-up	130394	151	-0.234
Barren Land	16350	339	1.019
Water Body	52269	21	-0.693
Slope Aspect			
Flat	45962	0	-4.728
N	1946651	2191	1.612
NE	1886506	2796	1.718
E	1665650	4886	1.960
SE	1731584	1727	1.509
S	1629473	1798	1.526
SW	1571058	2785	1.716
W	1577831	4837	1.956
NW	1497886	5903	2.042

The calculated InfoVal signify the relative importance of a particular thematic class in landslide susceptibility. A positive Information Value denotes a positive correlation between landslide activities and that particular class. On the other hand, a negative Information Value indicates a weak correlation. Higher the InfoVal, stronger is the correlation. For example, in the slope angle thematic layer, classes of slope angle less than 15^0 and 15^0-25^0, negative InfoVal were obtained meaning that very little landslide activities have been observed in these two thematic class. On the contrary, the positive InfoVal calculated for classes of slope angle 25^0-35^0 and 35^0-45^0 imply that there exist a strong positive correlation between landslide activities and the thematic classes. The InfoVal is significantly higher (closer to 1) for the class of slope angle greater than 45^0, which means that that maximum landslide activities have been observed for this particular class. Similarly, for geological unit thematic layer, the highest landslide activities have been observed for Krol, Infrakrol & Blaini Formation, followed by Subathu

Formation. On the other hand, igneous intrusion class, that consists of intact rocks like granite and diorite, is negligibly susceptible to slope failure and same is denoted by the largest negative InfoVal calculated for that particular class. For thematic layer of fault Euclidian distance, the strongest and the weakest correlation between landslide activity and thematic class have been observed at a distance of less than 3 km and greater than 12 km respectively. Similarly, for the thematic layers of drainage Euclidian distance and road Euclidian distance, the highest landslide activities have been observed at a distance of less than 250 m and 100 m respectively. The weakest correlations corresponding to the same data layers have been observed at a distance of more than 1000 m and 500 m respectively. In the LULC pattern data layer, the highest Info Val has been obtained for barren areas, followed by sparsely vegetated land covers. Build up areas have the lowest Info Val, although the smaller pixel counts (only 1% of the total area falls under build up area approximately) might have played a role here. Expectedly, evergreen forest areas and deciduous forest areas are less susceptible to landslide events. Interestingly, landslide activities have been well distributed for all most all slope directions (aspects).

Once the Info Val of various thematic classes are obtained, they are appended to the thematic data layers; which are then reclassified based on their Information Value. The reclassified thematic layers are overlaid arithmetically in Arc-GIS 10.6 to calculate Landslide Susceptibility Index (LSI) of each pixel. The LSI values are then segregated using '*Natural Breaks'* to categorize the LSI map into five classes of Landslide Susceptibility. Natural breaks in Arc-GIS 10.6 provides with an optimal classification scheme that finds class breaks, which (for a given number of classes) will minimize within-class variance and maximize between-class differences. The susceptibility classes are based on linguistic variables of perceived susceptibility level. In this study, five classes of landslide susceptibility i.e. Very Low (VLS), Low (LS), Moderate (MS), High (HS) and (VHS) have been considered. The final LSZ map of the study area is shown in Fig. 4.2 below.
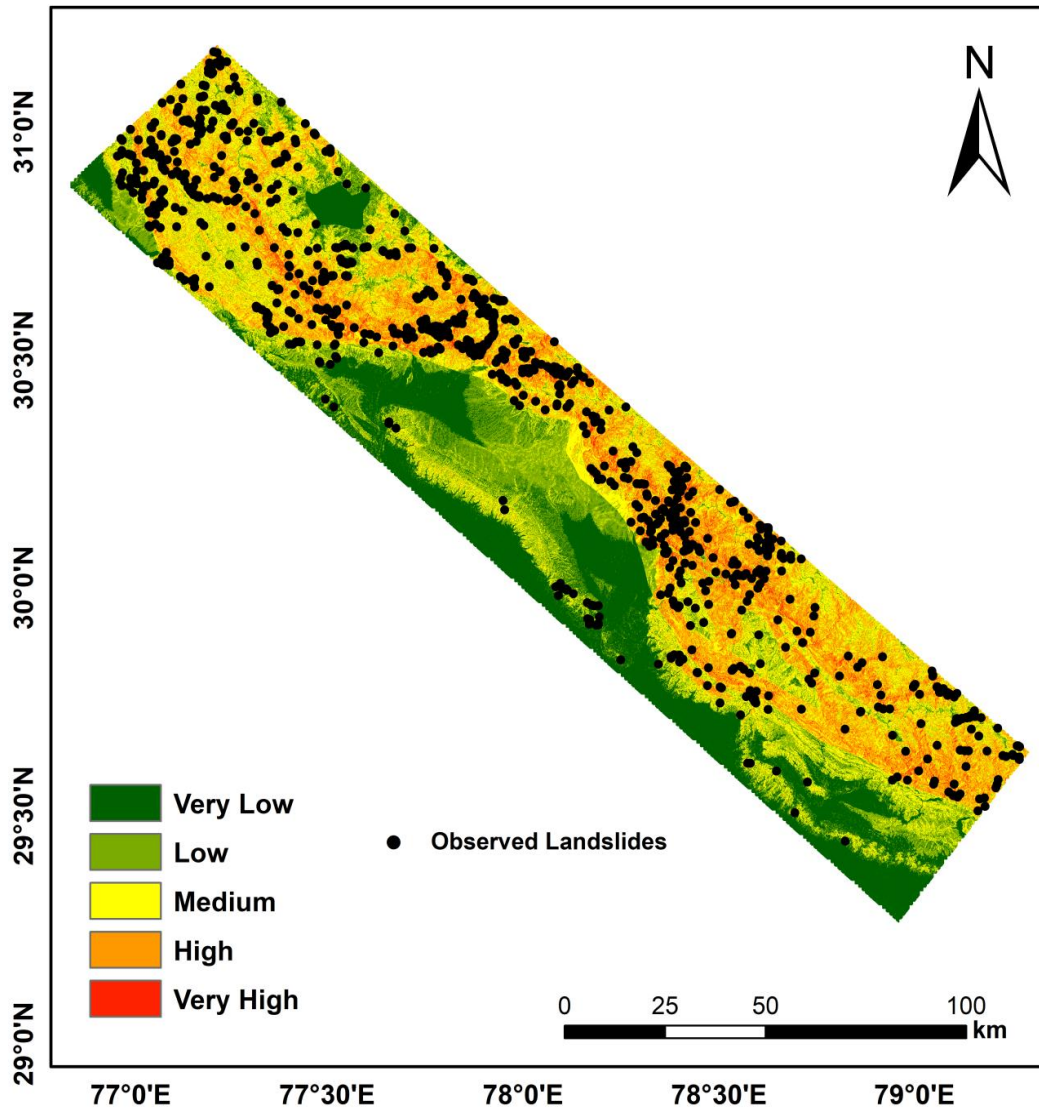
Fig. 4.2: Landslide Susceptibility Zonation Map of the Study Area using Info Val Method

The prepared LSZ map of the study area shows the current landslide susceptibility level for various important cities of Uttarakhand and Himachal Pradesh states of India. Shimla, Mussoorie and Lansdowne, three very popular tourist attraction sites are observed to have very high to high level of landslide risk. Dehradun, the administrative capital of Uttarakhand state is low to moderately susceptible to landslide hazard. Nahan, Ponta Sahib, Kotdwar some thickly populated cities in the study, are observed to have low landslide susceptibility. Two other important religious centres Haridwar and Rishikesh lie in the zone of moderate susceptibility. The case of Haridwar is an interesting one: despite being a relatively plainer site with gently favouring landslide causative parameters, it falls under moderately susceptible zone. This is due to its proximity to MFT, which is believed to have governed the current susceptibility level of landslide hazard in Haridwar. This point is well augmented by the presence of very prominent *Mansadevi* landslide in this area.

The prepared LSZ map is further analyzed both spatially and statistically to validate the reliability of the predictive model. The spatial analysis provides with the information on the the distribution pattern of susceptibility zones in correlation with observed landslide incidences, whereas statistical methods shows the accuracy of the predictive map. Also, the success rate of the predictive map is estimated using Success Rate Curve (Chung and Fabbri, 1999).

4.3.1 Map Validation

For spatial validation of the LSZ map, the existing landslides of the study area are superimposed on the prepared map (Fig. 4.2). It is observed that the maximum landslide distribution confines to the zones of HS and VHS, where zone of MS contains fewer landslides than HS and VHS. Only few landslides are distributed sporadically in the zones of LS and VLS. Table 4.2 shows the landslide distribution patterns across the LSZ map.

Table 4.2: Spatial Analysis of the LSZ map

LSZ Class	Area (sq. km)	% of Total Area	No. of Observed LS	LS Frequency per sq. km
Very Low (VLS)	114.50	0.009	0	0
Low (LS)	4058.97	0.311	45	0.01
Moderate (MS)	4083.08	0.312	207	0.05
High (HS)	3884.99	0.297	525	0.14
Very High (VHS)	929.24	0.071	285	0.31

From Table 4.2 it is observed that although the zone of very high landslide susceptibility constitutes the lowest percentage of the total area (~7%), it contains the highest frequency of observed landslides per sq. km (31%). On the other hand, no landslide incidence was observed in the very low susceptibility zone. For the zone of low landslide susceptibility, frequency of landslide incidence per sq. km is only 1%. Also, there is a gradual decrease in frequency of observed landslide per sq. km from the very high to the very low susceptible zones, with considerable class separation. Hence, from the spatial analysis of the prepared LSZ map it can be concluded that the calculated and classified susceptibility zones are in good agreement with occurrences of pre-existing landslides.

In the present study, the Frequency Ratio (FR) analysis of LSZ classes is used as the statistical validation method. In this method, the similarity between susceptibility zones and landslide inventory is compared. In FR method, the ratio of the landslide pixels in a particular thematic class to the total landslide pixels is correlated with the ratio of the area of that particular thematic class to the total study area (in terms of pixel counts). It is mathematically expressed as

$$FR = \frac{\text{LS Pixels in Factor Class}\big/\text{Total LS Pixels}}{\text{Total Pixels in Factor Class}\big/\text{Total Pixels in the Area}} \qquad (4.2)$$

Figure 4.3 shows the calculated FR of the LSZ classes. The highest value (3.78) of FR is calculated for VHS zone. This implies that despite having a smaller area, the class of VHS surrounds a very good portion of the existing landslides (27%). Similarly, the class of HS zone has a high value of FR indicating a positive correlation between the prepared LSZ map and landslide inventory.
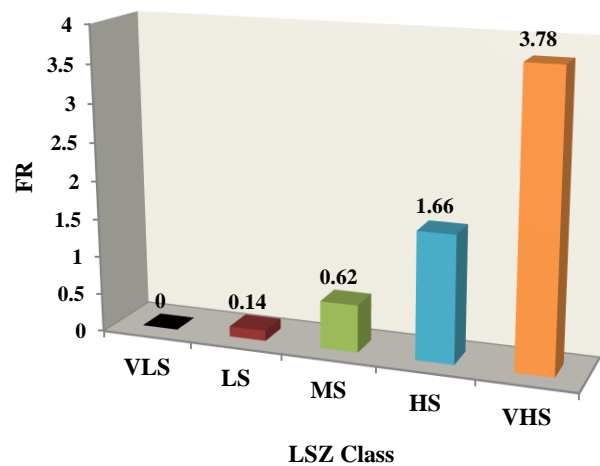
Fig. 4.3: Statistical Analysis of the LSZ Map

The analysis of success rate curve is also used as an effective method for validating a LSZ map (Chung and Fabbri, 1999). The area under the curve is often considered to measure the prediction accuracy qualitatively. The success rate curve is obtained by plotting the cumulative percentage of observed landslide occurrence against the cumulative percentage of LSZ area, as shown in Fig. 4.4.
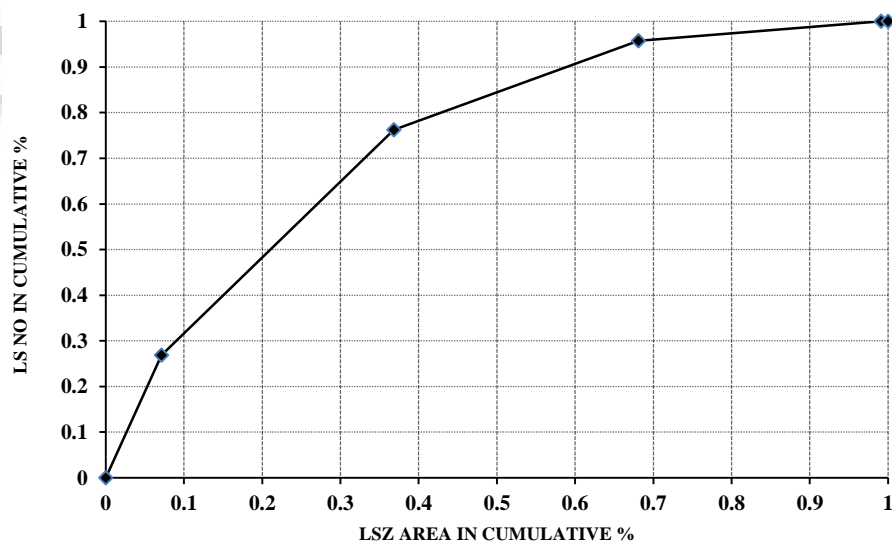
Fig. 4.4: Success Rate Curve of the LSZ Map

Both spatial and statistical analyses imply that the prepared LSZ map as shown in Fig. 4.2 depicts a realistic scenario where maximum number (~75%) of observed landslides falls in VHS and HS zones. The area under the success rate curve in Fig. 4.4 is computed to be 0.797. This denotes that the overall success rate of the prepared LSZ map is appox. 79.7%, which is in accord with the acceptable norm used for LSZ studies (Kayastha *et al.*, 2013).

4.4   Assessment of the LSZ Map in terms of Tectonic Features

An interesting pattern of landslide incidence has been observed in the study area: there is a high concentration of observed landslides near all tectonic features (Fig. 4.5), especially where all the three major thrusting systems viz. MCT, MBT and MFT merge.

In general any major geological discontinuity should be considered as an important causative parameter (internal/preparatory) in LSZ mapping (Kanungo, 2006; Kayastha et al., 2013). And, when such discontinuities are seismically active, like the MCT, MBT and MFT in the Himalaya, their implications in the occurrence and spatial distribution of landslides turn out to be far reaching. Literature survey indicated that major tectonic features play important role for landslide occurrences (Keefer, 1984; Rodriguez et al, 1999; Liao and Lee, 1999; Chigira et al., 2010; Xu et al., 2012). Apart from the earthquakes generated due to the slip in an active fault or lineament, the aseismic fault motions also control the rate and occurrence of landslides near major tectonic features (Bhattacharya et al., 2015). In the Himalayan belt, a strong correlation between fault activities and landslide distribution has been suggested in the past. Pachauri and Pant (1992) observed a positive relationship between the Aglar fault and landslide activities of the area, where maximum landslide distribution was reported in the proximity of the fault. Bhattacharya et al. (2015) noticed slow surface movements of the Mansadevi landslide relative to neighboring area during 1992 to 1998; and concluded that the present landslide is a cumulative effect of those slow surface movements. Thus, consideration of active tectonic features is a vital part in LSZ studies, especially for seismically active Himalayan regions. Yet, most of the past studies mainly focused on smaller scale local LSZ mapping (Anbalagan, 1992; Pain et al., 2014; Kumar et al., 2017; Pandey et al., 2018) and thus lacked an adequate database to correlate quantitatively tectonic activities and landslide distribution in the Himalaya. To quantify the role of tectonic features on landslide distribution, there are two prerequisites: (i) it requires presence of adequate number of active tectonic features in terms of faults and lineaments and (ii) there should be substantial number of observed landslides in the vicinity of tectonic features to be statistically significant. Thus, for a quantitative comprehension of the effect of tectonic features on landslide occurrence and their distribution pattern, regional LSZ studies are required. These challenges precisely underline the difficulty in

quantifying the role of tectonic features in the Himalaya for micro/ meso-scale LSZ studies at local level.
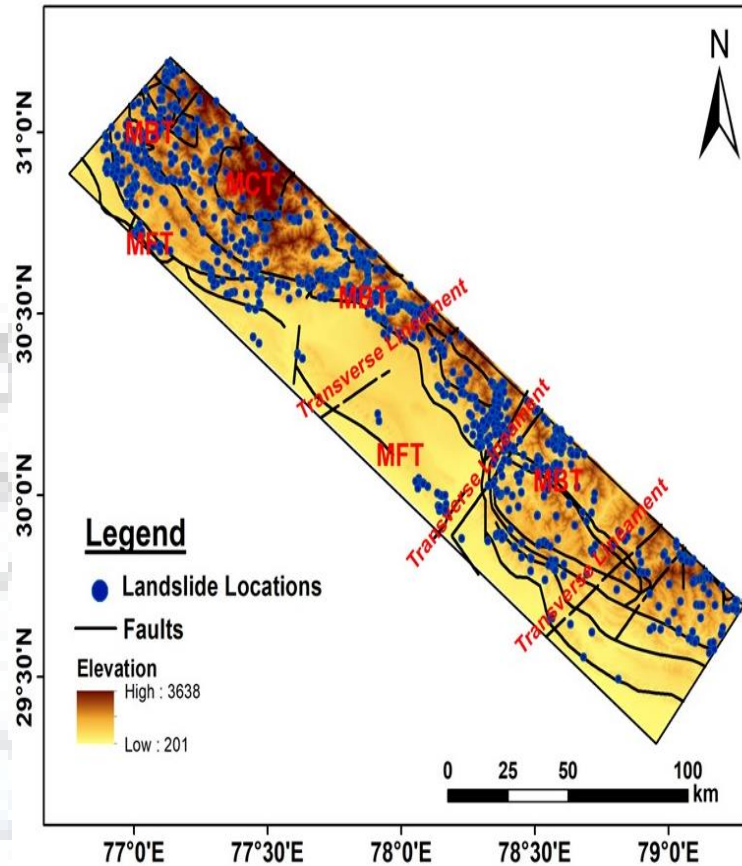
Fig. 4.5: Landslide Distribution Pattern near Major Tectonic Features

An attempt has been made in this research work to examine quantitatively the effect of tectonic features on landslide distribution in the study area. The study area encompasses around 12,350 sq. km area and is traversed by three active faults *viz.* MCT, MBT and MFT, along with many transverse lineaments. The number of observed landslides in the whole study area is 1062. Therefore, it provides with a perfect platform to carry out the study in a holistic way. The results of this study would be of particular importance for other micro/meso-scale city specific landslide studies in the Himalayan region, where it is difficult to create a relevant dataset correlating fault distance and landslide distribution.

4.4.1 Methodology

To quantify the role of tectonic features on landslide occurrence and their spatial distribution, the study area is divided into two parts: around 2/3rd part of the study area is considered as the training area from which data has been extracted, and the remaining 1/3rd part is considered as testing area for result validation (Fig. 4.6). The training part and testing part has almost similar numbers of observed landslides (583 in the training area and 479 in the testing area). Along with MBT and MCT (both traverse throughout the study area) a portion of

MCT is also present in the testing area. The selection of training and testing area is based on the near-homogeneity of other landslide causative parameters in these areas. The river Yamuna demarcates the boundary between the training and testing areas. The term *fault* is used here to denote all tectonic features (i.e. thrusts and transverse lineaments).
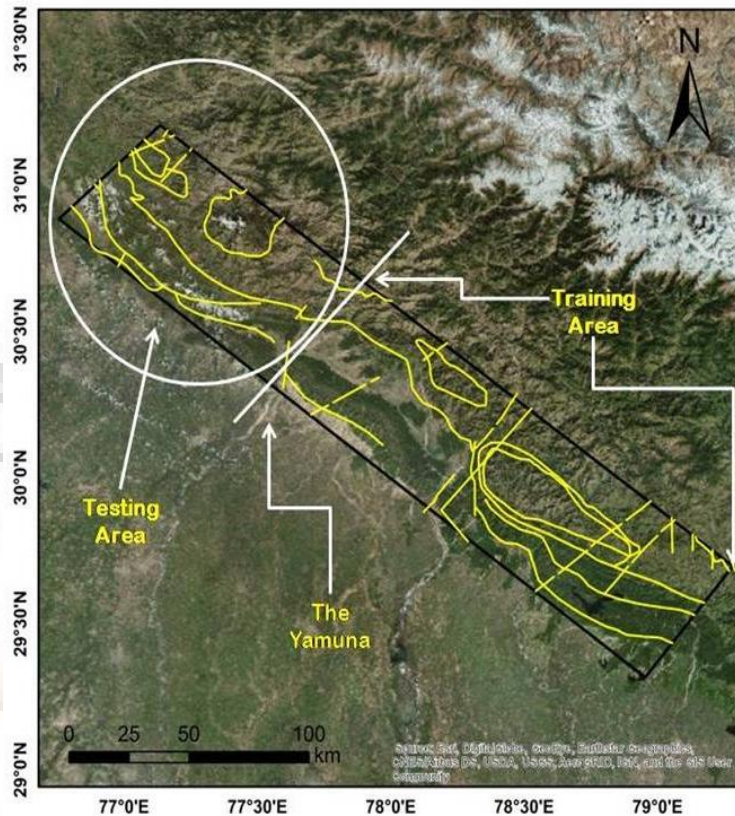
Fig. 4.6: Demarcation of Training and Testing Areas

Two thematic data layers: the landslide distribution map and the fault Euclidian distance map have been prepared for the training area following the same procedure as given in sections 3.5.1 and 3.5.6 respectively (Chapter 3). In the next step, these two thematic layers are collated to create a database on the Euclidian distance of the existing landslides from the nearest fault. It is followed by the extraction of relevant data (*i.e.* number of observed landslides *vs.* fault Euclidian distance) for every 100m class interval. Finally, regression analysis has been performed with number of observed landslides as a dependent variable and fault distance as an independent variable to quantify the effect of fault distance on probability of landslide occurrence. An equation has been derived to best fit the regression model and coefficient of determination is calculated. An schematic diagram of the working methodology is shown in Fig. 4.7.

4.4.2 The Proposed Equation: Effect of Fault Distance on Probability of Landslide Occurrence

For the training area, data on the number of observed landslides against fault Euclidian distance have been extracted using the spatial analyst tool in Arc-GIS 10.6. The prepared database is given as Appendix A-2. From the database it is observed that the distance of observed landslide events from faults vary from 0 (i.e. landslides observed at the fault wall itself) to 14.90 km for the training area. The number of observed landslides against fault Euclidian distance have been plotted as shown in Fig. 4.8.
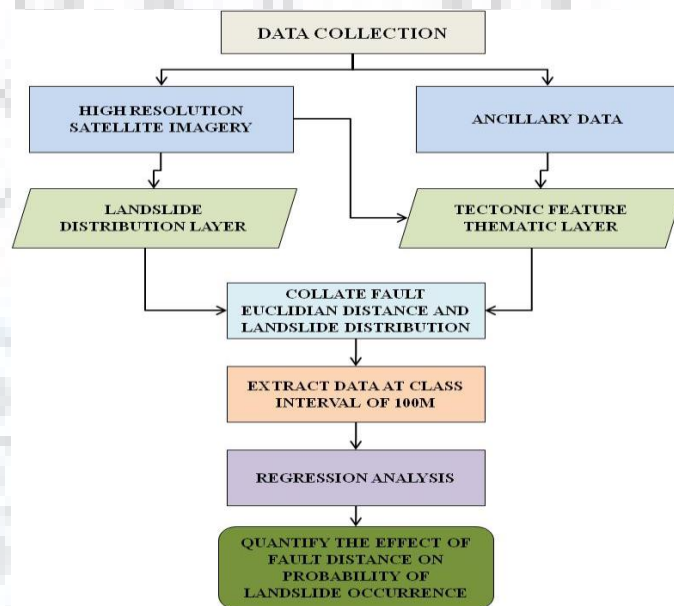
Fig. 4.7: Schematic Diagram for Quantifying the Effect of Fault Distance on Landslide Activities
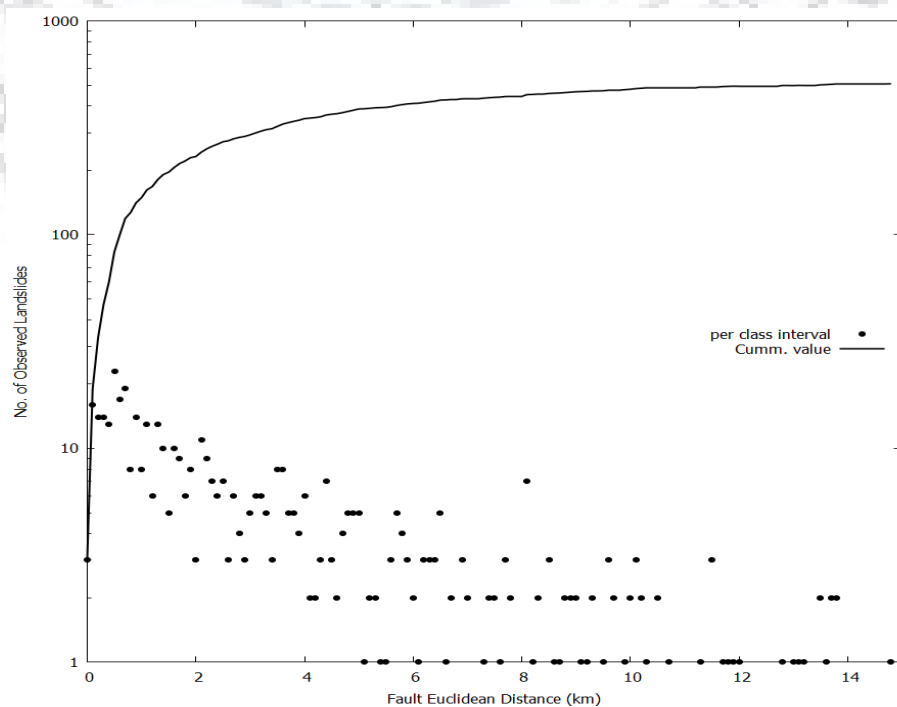
Fig. 4.8: Landslide Distribution *vs.* Fault Euclidian Distance

The points in Fig. 4.8 indicate the observed landslide number per class interval (i.e. for each 100m distance bin) and the continuous line represents the corresponding cumulative value. It is evident that the number of observed landslides decreases exponentially with increasing distance from the faults and thus confirms a strong inverse correlation between fault distance and landslide distribution for the training area. To have a better perspective and illustration, the number of observed landslides for each thematic class of fault Euclidian distance data layer (refer to table 4.1) is extracted for the training area. It is given in table 4.3.

Table 4.3: Observed Landslide Frequency in Different Thematic Classes

Fault Distance	Observed Number of Landslides Per Class	Cumulative Number of Landslides Per Class	Ratio of Observed Landslide
0-3 km	332	332	0.57
3-6 km	138	470	0.24
6-9 km	68	538	0.12
9-12 km	33	571	0.06
12-15 km	12	583	0.02

Table 4.3 shows that 57% of the total observed landslides occurs at a distance of less than 3 km from any major tectonic feature. Frequency of the observed landslides decreases to 24% and 12% respectively as the distance from faults increases to 6 km and 9 km. For the class interval of 12-15 km this frequency becomes a negligible 0.02, implying that the effect of fault distance practically gets nullified at a distance of more than 12 kms. Based on these observations, a statistical correlation between probability of landslide distribution and distance from faults is derived using regression analysis of the training data. This is given by equation (4.3), which quantifies the effect of fault distance on landslide distribution in the study area.

$$f\{Y\} = 0.322e^{-0.28047x} \tag{4.3}$$

Where, *Y* represents the probability of landslide occurrence for *x* km fault distance in the training area.

4.4.3 Validation of the Proposed Equation

For the testing area, data on number of observed landslides has been extracted at per km fault Euclidian distance to calculate the actual landslide probability (frequency) per km (the independent variable, *x* in Eq. 4.3 is derived for km unit). Then probability of landslide incidence per km fault Euclidian distance is calculated using Eq. 4.3. The observed and the

calculated probabilities are compared to estimate the error. Table 4.4 shows the validation of the proposed method for the testing area.

Table 4.4: Observed and Calculated Landslide Probabilities for Fault Distance

Fault Distance (km)	Calculated LS Frequency	Observed LS Frequency
1	0.24	0.26
2	0.18	0.18
3	0.14	0.17
4	0.10	0.12
5	0.08	0.08
6	0.06	0.10
7	0.05	0.03
8	0.03	0.04
9	0.03	0.00
10	0.02	0.01
11	0.01	0.00
12	0.01	0.00

In the testing area, maximum fault Euclidian distance is observed as 11.4 km. Table 4.4 indicates that the calculated and observed probabilities finely concur. For this dataset, the estimated standard error (ε_0) is 1.596%. A graph of probability of landslide incidence *vs.* fault Euclidian distance is plotted (Fig. 4.9) and the coefficient of determination (R^2) is calculated.
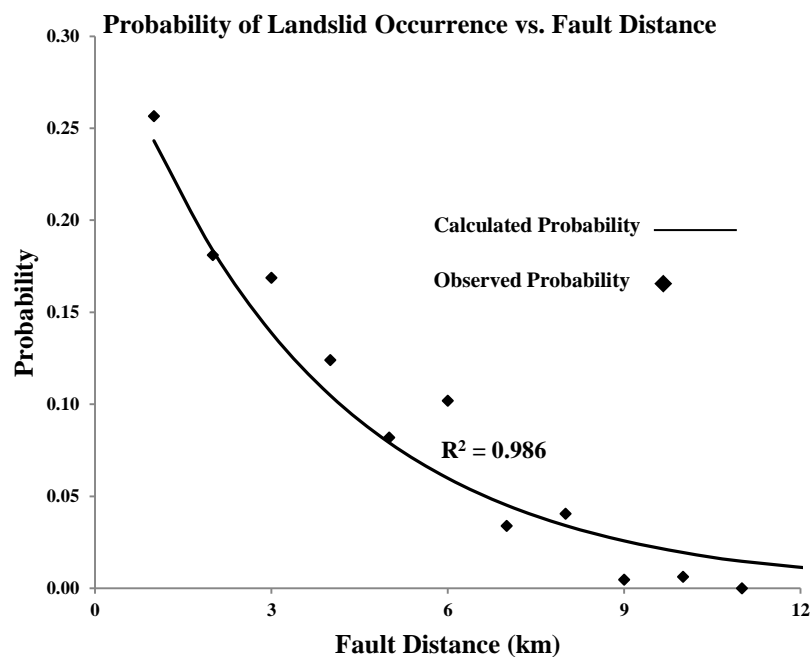
Fig. 4.9: Probability of Landslide Incidence *vs.* Fault Distance

From Fig. 4.9, it is understood that for the study area, there exists a strong inverse correlation between landslide activities and distance from tectonic features. It is observed more than 4/5th of the observed landslides in the training area (~81%) occurred at a distance of less than 6 km from any major tectonic features. As the distance from the fault increases, landslide incidence decreases. This effect of tectonic features on landslide activities has been quantified in the form of Eq. 4.3. The high value of coefficient of determination (R^2) indicates the proposed equation can depict this scenario realistically.

It is to be noted that slope failure ultimately implies to a prevailing set of ground conditions at that specified duration, rather than the singular effect of one or more individual parameters. This makes it more difficult to quantify the effect of a singular causative factor on occurrence of landslides. Therefore, one must understand that the calculated probabilities given by Eq. 4.3, do not physically represent the overall probability of slope failure, but quantifies the effect of fault distance on landslide incidence. In absence of relevant data on faults, these results will be of practical importance to comprehend the implication of tectonic environment on landslide events of the lower Himalayan belt for future studies.

4.5   Contribution of Tectonic Features on Landslide Susceptibility

As discussed in the previous section, the occurrence and spatial distribution of landslides in an area are governed by many important parameters. For the study area, eight such causative parameters have been identified. Having established the strong correlation between fault distance and landslide activities, it will be interesting to examine the relative contribution of tectonic features on landslide susceptibility for the study area. Landslide Relative Frequency (LRF), a statistical approach of LSZ mapping has been used to calculate the relative importance of various landslide causative parameters. Once again, the testing area (Fig. 4.6), which has a uniform fault density throughout, is selected for this purpose. Also, due to the size of the total study area, there are significance variations in the spatial attributes of all causative parameters. This acts as a major hindrance in comprehending their effects in a holistic way. For example, there is a sporadic distribution of road networks in the study area, whereas for the testing area, the distribution is near homogenous. Similarly drainage density and fault density of the total study area are non-uniform and vary considerably throughout. Therefore, a smaller area has been selected to maximize the near-homogeneity of landslide causative parameters.

Landslide Relative Frequency (LRF) is derived from the frequency ratio (FR) of the factor classes. It is a standard method which has been adopted by many researchers successfully (Lee et al., 2008; Ozdemir and Altural, 2013; Kumar and Anbalagan, 2016, Sangeeta and Maheshwari, 2018). As discussed in section 4.3.1, the FR of particular thematic

class is calculated using Eq. 4.2. In the next step, LRF is calculated as the ratio of FR of that class to the total FR of the data layer. Mathematically,

$$LRF = \frac{Factor\ Class\ FR}{\sum Factor\ Class\ FR} \tag{4.4}$$

Each causative parameter has different degree of control on landslide occurrence. The relative importance or contribution of each parameter is determined by a predictor rating (R_i) which is calculated as

$$R_i = \frac{(LRF_{max} - LRF_{min})_i}{(LRF_{max} - LRF_{min})_{min}} \tag{4.5}$$

Generally, value of R_i is normalized to indicate the statistical contribution of a particular parameter in landslide susceptibility. Table 4.5 shows the calculation of FR and LRF of different causative parameters for the testing area.

Table 4.5: Calculation of FR and LRF for the Testing Area

Landslide Causative Factor Class	Number of Total Pixels $N_{pix}(N_i)$	Number of Landslide Pixels $N_{pix}(S_i)$	FR	LRF
Slope Angle				
$<15^0$	1475010	946	0.240	0.028
15^0-25^0	1484429	2511	0.632	0.075
25^0-35^0	1336703	4781	1.336	0.159
35^0-45^0	613696	3957	2.409	0.286
$>45^0$	126025	1282	3.801	0.452
Geological Units				
Krol, Infrakrol & Blaini Fm	999777	1312	0.489	0.049
Subathu Fm of W. Himalaya	484046	592	0.455	0.045
Manjir Fm of W. Himalaya	569025	953	0.624	0.062
Subathu Fm. of W. Himalaya	536819	1316	0.913	0.091
Jaunsar Gp of W. Himalaya	294583	1092	1.380	0.138
Tal Fm of W. Himalaya	831321	3989	1.787	0.178
Simla Gp	705775	3555	1.875	0.187
Almora Crystalline Fm of W. Himalaya	114421	47	0.153	0.015
Dagshai and Kausauli Fm of W. Himalayas	77144	260	1.255	0.125
Jutogh Gp of W. Himalaya	119139	0	0.000	0.000
Middle Siwalik Gp	946	0	0.000	0.000
Lower Siwalik Gp	108825	265	0.907	0.090

Amri Tectonic unit	174444	92	0.196	0.020
Deoban Gp of W. India	999777	1312	0.489	0.049
Dharagarh Fm of W. India	484046	592	0.455	0.045
Igneous intrusion	569025	953	0.624	0.062
Fault Euclidian Distance				
0-3 km	2607306	7726	1.092	0.349
3-6 km	1655367	4526	1.008	0.322
6-9 km	610036	1129	0.682	0.218
9-12 km	89081	84	0.348	0.111
>12 km	702	0	1.092	0.349
Elevation				
< 500 m	489508	88	0.066	0.017
500-1000 m	1133185	6013	1.953	0.291
1000-1500 m	1595136	5024	1.159	0.291
1500-2000 m	1148645	2151	0.689	0.173
> 2000 m	585335	179	0.113	0.028
Drainage Euclidian Distance				
< 250 m	2165236	6795	1.174	0.281
250-500 m	1598154	4089	0.957	0.229
500-750 m	931472	2081	0.836	0.200
750-1000 m	319620	466	0.545	0.130
> 1000 m	26326	47	0.668	0.160
Road Euclidian Distance				
< 100 m	232597	2462	3.914	0.448
100-200 m	193071	883	1.691	0.194
200-350 m	255120	774	1.122	0.128
350-500 m	230526	763	1.224	0.140
> 500 m	4063798	8574	0.780	0.089
Slope Aspect				
Flat	781	0	0	0
N	588066	971	0.617	0.079
NE	602808	1468	0.910	0.116

E	540434	1439	0.995	0.127
SE	601157	2269	1.410	0.180
S	711447	3120	1.639	0.209
SW	749950	2457	1.224	0.156
W	638440	1175	0.688	0.088
NW	602780	578	0.358	0.046

After calculating the LRF values of each thematic class, the maximum and the minimum LRF values of a particular causative parameter are obtained. Then Ri is calculated using Eq. 4.5. Table 4.6 shows the calculated Normalized Ri value of each causative parameter.

Table 4.6: Calculation of Normalized Predictor Rating of Causative Parameters

Parameter	LRF_{max}	LRF_{min}	LRF_{max} - LRF_{min}	R_i	Normalized R_i
Slope	0.450	0.020	0.430	3.308	0.21
Fault Euclidian Distance	0.440	0.080	0.360	2.769	0.17
Road Euclidian Distance	0.340	0.000	0.340	2.615	0.16
Elevation	0.290	0.017	0.273	2.100	0.13
Aspect	0.200	0.000	0.200	1.538	0.10
Geological units	0.180	0.000	0.180	1.385	0.09
Drainage Euclidian Distance	0.280	0.130	0.150	1.154	0.07
LULC	0.210	0.080	0.130	1.000	0.06

The calculated Normalized R_i values indicate the relative importance of various causative parameters for the testing area. Slope angle parameter is expectedly recognized as the highest contributor of landslide susceptibility with a normalized R_i value of 0.21. For fault Euclidian distance data layer, the value of normalized R_i is computed as 0.17, which means it has an contribution of 17% to landslide susceptibility. This statistically demonstrates the impact of tectonic features on landslide activities in this particular area. The testing area has a high density of road networks, and therefore, their contribution is estimated as a high 16%. However, there exist some ambiguity in the presented results, especially for the geological units and drainage Euclidian data layers. The importance of lithology in landslide susceptibility is universally recognized and it is considered as a main causative parameter. Similarly, for the Himalayan belt, drainage density is considered as a very important causative parameter. The explanation for lower values of R_i for these two parameters lie in the even distribution of observed landslides over all the thematic classes of these two data layers. Hence the LRF

method could not portray their effects efficiently, which may be considered as a kernel disadvantage of the method.

It is to be noted here that these calculated values of R_i imply the relative importance of various parameters for testing area only, corresponding to the particular dataset used. For different terrain conditions, the relative importance will invariably vary from the calculated values. As with the case of any statistical technique of LSZ mapping, the accuracy of these results are region specific and data dependent.

4.6   Summary

This chapter includes the results of a statistical approach of landslide susceptibility zonation (LSZ) mapping for the study area. The prepared LSZ map has categorized the study area into five distinct zones of landslide susceptibility *viz.* very low, low, moderate, high and very high. The zone of very high and high landslide susceptibility comprises 37% part of the total study area and covers almost 76% of the total observed landslides. The analysis of the success rate curve predicts an overall success rate of 79.7% for the LSZ map produced. It also shows the current landslide susceptibility level for various important cities of Uttarakhand and Himachal Pradesh states of India.

In the study area, it is observed that approximately 57% of the existing landslides occurs at a distance of less than 3 km from tectonic features, out of which 28% landslide activities take place within a distance of 1 km from tectonic features. The occurrence of observed landslides decreases to 24% and 11% respectively as the distance from faults increases to 6 km and 9 km. For fault distance greater than 12 km, this percentage reduces to a negligible 2%, implying that the effect of fault distance practically gets nullified at a distance of more than 12 km. The results of the study quantify a strong inverse relationship between landslide distribution and fault distance in lower Himalayan arc which is presented in the form of an equation. The equation will be useful for other micro/mesoscale city specific landslide studies in the Himalayan region, where it is difficult to create a relevant dataset correlating fault distance and landslide distribution.

The chapter also incorporates a statistical analysis to assess the relative importance of various landslide causative parameters for a part of the study area. It is observed that slope angle is the most influencing landslide causative parameter in the study area. Distance from major tectonic features is observed to be another important parameter in the study area. The results of this chapter will be further used to develop a LSZ scale for the study area for multi-hazard integration.

DEVELOPMENT OF LANDSLIDE SUSCEPTIBILITY ZONATION (LSZ) SCALE

5.1 Preamble

The present research work aims to understand the impact of earthquakes in landslide occurrence and distribution for a part of lower Himalayan belt. For this purpose, eight landslide causative parameters have been identified for the study area and seismicity is considered as a landslide triggering factor. A landslide susceptibility zonation map of the study area has been prepared (Fig. 4.1 in chapter 4) to assess the current susceptibility scenario for the study area. It is observed that under static landslide causative factors, around 37% of the total study area falls under high (HS) and very high (VHS) susceptibility zones. In the next phase, seismicity has been incorporated in landslide hazard zonation (LHZ) mapping. This chapter includes discussion on the challenges of LHZ mapping under seismic conditions, development of a LHZ scale for multi hazard integration and performance evaluation of different LHZ mapping techniques.

5.2 LHZ Mapping under Seismic Conditions: Challenges

There have been several earthquakes in the Himalayan region (Pareek et al, 2012; Prakash, 2013; Collins and Jibson, 2015) *viz.* Chamoli earthquake (29 March 1999, M_w-6.8), Kashmir earthquake (8 October 2005, M_w-7.6), Sikkim earthquake (18 September 2011, Mw-6.9), Nepal earthquake (25 April 2015, M_w-7.8), which caused widespread landslide events. In fact, in many cases, losses due to seismically induced landslides have been more than those caused directly due to shaking (Bird and Bommer, 2004). Marano *et al.* (2010) reported that out of the all earthquake related casualties, which are not caused directly by ground shaking, approximately 70% may be attributed to landslides. Impacts of seismically induced landslides are of long term nature, which manifest their damage intensity in terms of indirect socio-economic losses (Marui and Nadim, 2009; Tang et al., 2016; Korup, 2006). In this context, Landslide Hazard Zonation (LHZ) mapping for the Himalayan region under seismic condition becomes very important considering its active seismicity and the volume of landslide incidences. The works of many researchers have highlighted the significance of establishing a relationship between Himalayan seismicity and landslide hazard for this region. Yet, only a small amount of studies have included seismicity in LHZ mapping for the Himalaya (Champati ray et al., 2007; Pareek et al., 2010, 2012; Bhattacharya et al., 2013; Chakravorty et al., 2015).

The main challenge in preparing earthquake induced LHZ map is the selection and applicability of a well-recognized method. Although, various methods (Kanungo et al., 2009) are available for assessing the landslide susceptibility of a region, it is difficult to figure out a better suited method for earthquake induced LHZ mapping. Different statistical methods, which are widely used for landslide susceptibility assessment, generally lack in incorporating seismic indicators (Tanyas et al., 2017). This may be attributed to the paucity of sufficient earthquake induced landslide inventories, which is further ascribed to the rarity of an extreme earthquake event. Moreover, the conventional studies correlating earthquake magnitude and landslide distribution, types and coverage area (Keefer, 1984; Rodriguez et al., 1999; Papadopoulos and Plessa, 2000) drew criticism from researchers due to limitations of the dataset used (Hancox et al., 2002) and the regional and characteristic biasness associated with earthquake events (Jibson and Harp, 2012; Gorum et al., 2014). Such scenarios become exaggerated for the Himalayan region, where not until recently, much attention have been paid to seismically induced landslide hazard zonation. As observed by Pareek et al. (2012), most of the landslide susceptibility studies carried out for the Himalayan belt (Anbalagan 1992; Sarkar et al. 1995; Arora et al. 2004; Saha et al. 2005; Kanungo et al. 2009; Pain et al. 2014; Kumar and Anbalagan, 2015) considered static landslide causative factors only. Moreover, the few studies that did consider earthquake scenarios, are concentrated around the Chamoli earthquake (Pachauri, 2001; Pareeket al., 2010, Sangeeta and Maheswari, 2018); Sikkim earthquake (Chakravorty et al., 2011) and Nepal earthquake (Collins and Jibson, 2015). All these earthquakes, in-spite-of having originated in the Himalaya only, differ significantly from one another in terms of their characteristics (amplitude, frequency content and duration). Thus, it is understood that any statistical method derived from earthquake induced landslide inventory developed for a particular earthquake event may not be adequate enough for a different tectonic set up. These points rather indicate the challenges in seismically induced LHZ studies precisely.

5.2.1 LHZ Mapping under Seismic Conditions: An Alternative Approach

As discussed in the previous section, there are two main issues in carrying out seismically induced LHZ mapping: (i) selection of an appropriate hazard zonation technique and (ii) selection of earthquake ground motion for which the regional and characteristic biasness should be eliminated. To address both these issues, an alternative approach has been adopted in this research work.

The selection of any statistical LHZ technique is governed by the availability of relevant dataset and its quality. Since there has not been any major earthquakes reported for the lower Himalaya in recent past, it is very difficult to prepare an earthquake induced landslide

inventory targeting the study area exclusively. Therefore, Map combination method, a qualitative approach, has been selected as the suitable LHZ mapping technique for the study area. Map combination method (Soeters and ven Westen, 1996) is a simple and straight forward method, where different landslide causative parameters are incorporated as thematic layers. Then the thematic layers are assigned a weightage based on their perceived influence on landslide occurrence. Generally, the weightage of landslide causative parameters are decided by the investigator based on previous terrain knowledge. Hence, there is subjectivity in weight assignment process, which is the biggest limitation of this method. By adopting this approach, seismicity can be added as a thematic layer, which will be assigned an appropriate weightage. Details discussion on the weightage assignment procedure is presented in the subsequent sections.

The other challenge is the selection of earthquake scenarios for LHZ studies. It is extremely difficult to adopt any particular process for the selection of earthquake scenarios. Consideration of recorded past seismicity will invariably incorporate its characteristic biasness and the prepared landslide inventory will be applicable to that particular region only. Also, there are different attributes through which an earthquake can be described. The fundamental attributes are the amplitude, frequency content and duration of an earthquake. Selection of a particular attribute to represent a strong ground motion is another important criterion. Considering all these aspect, the present research work have selected Peak Ground Acceleration (PGA) parameters generated through Probabilistic Seismic Hazard Assessment (PSHA) to describe the seismicity parameter to be considered for LHZ mapping. Elaborate discussions on the selection criteria are presented in chapter 6. The PGA parameters are incorporated as thematic data layers to generate seismically induced LHZ maps of the study area.

5.3   Methodology

The steps involved in Map Combination method (Soeters and van Westen, 1997) are: collection of input data on various landslide causative factors, preparation of thematic data layers, assignment of weights to different thematic data layers, numerical integration of thematic data, and generation of LSZ map. The numerical integration of weights of different thematic layers in a GIS environment will produce a numerical value know as Landslide Potential Index (LPI) for each pixel. The term LPI is used instead of LSI/LHI (Landslide Susceptibility/Hazard Index) to allow scope for both susceptibility and hazard. LPI (Sarkar and Kanungo, 2004) indicates the likelihood of landslide occurrence based on the prevailing

causative factors in an area. Higher value of LPI indicates greater susceptibility to landslide hazard and vice-versa. Mathematically, it may be defined as,

$$LPI = \sum_{i=1}^{n} \sum_{j=1}^{m} R_i \times W_{i,j} \tag{5.1}$$

Where, R_i and W_{ij} denote the rank of ith data layer of landslide causative factor and weight of jth thematic class of ith layer respectively.

As discussed in the previous section, assignment of ranks and weights to different data layers and their thematic classes is a subjective procedure. It varies from one investigator to another. While the ranks (R_i) are assigned to indicate the relative importance of a particular parameter within the selected set of causative parameters, the weights ($W_{i,j}$) are assigned based on the perceived degree of susceptibility of a particular thematic class within a causative data layer. The perceived susceptibility implies correlation between a particular thematic class and landslide activities within a data layer. This correlation can be obtained by different statistical analyses available for LSZ mapping, which will in turn denote the degree of susceptibility for different thematic classes objectively. Based on this, a methodology has been developed for the study area, where the perceived degree of susceptibility of various thematic classes of different landslide causative factors are determined statistically; which is then used to assign the corresponding weight ($W_{i,j}$). Moreover, to further reduce any ambiguity of statistical data, more than one statistical analyses were performed and concurrency have been checked. Based on the concurrency, linguistic variables of perceived susceptibility level (very low to very high) are decided which are used to finalize the value of $W_{i,j}$ for thematic classes. In this research work, three statistical methods viz. InfoVal, FR and Fuzzy Cosine Amplitude (r_{ij}) have been used. The methodology for InfoVal and FR have already been discussed in Chapter 4 (section 4.2 and 4.3.1). Here, methodology for Fuzzy Cosine Amplitude is discussed.

Fuzzy Cosine Amplitude (Kanungo et al., 2006; Peethambaran et al., 2019) is a similarity method, where pair-wise comparisons are made between member functions (data layers of landslide distribution and causative parameters). The strength of the relationship is denoted by Fuzzy ratings (r_{ij}). The value of r_{ij} lies from 0 to 1. Value of r_{ij} close to 1 denotes a strong relationship, whereas value close to 0 gives weak relation. r_{ij} is calculated as the ratio of total number of landslide pixels in the category to the square root of the multiplication of total number of pixels in that category and the total number of landslide pixels in the area (Kanungo, 2006).

Let n be the number of categories of a thematic layer represented as an array $X = \{x_1, x_2, …,x_n\}$, each of its element, x_i, is a vector of pixel p (image size) and can be represented as

$$x_i = \{x_{i1}, x_{i2}, ..., x_{ip}\} \tag{5.2}$$

If, x_i and x_j respectively represent the thematic class of a landslide causative parameter layer containing element x_{ik} ; and landslide distribution layer containing element x_{jk}, then, strength of relation (membership grade) is defined using Fuzzy Rating (r_{ij}) between x_{ik} and x_{jk} as

$$r_{ij} = \frac{|\Sigma_{k=1}^{p} x_{ik} x_{jk}|}{\sqrt{(\Sigma_{k=1}^{p} x_{ik}^2)(\Sigma_{k=1}^{p} x_{jk}^2)}} \tag{5.3}$$

It is to be noted here that all statistical methods i.e. InfoVal, FR and Fuzzy cosine amplitudes are fundamentally different from one another in their nature, description and treatment of data. However, the main objective of all these methods remains the same, which is establishing a correlation between landslide activity and a particular thematic class. Therefore, concurrency of the results of these statistical analyses will be a good parameter to determine the linguistic variable of perceived susceptibility, based on which final weights are assigned.

Determination of Ranks (R_i) of different causative parameters is a more difficult task as there are not many statistical methods available for this purpose. One of the statistical methods on hand is Landslide Relative Frequency (LRF) analysis, but it has some major limitations as discussed in chapter 4 (section 4.5). So a semi-qualitative method: Analytical Hierarchy Process (AHP) has been used in this research work to assign the ranks (R_i) of various landslide causative parameters. AHP has been used in LSZ mapping to avoid inconsistency of the weightage assignment process (Long and De Smedt, 2012; Kayastha et al., 2013; Papadakis and Karimalis; 2017). The consistency of the decision matrix (Saaty, 2000) is examined using Consistency Ratio (*CR*), which is defined as the ratio of Consistency Index (*CI*) and Random Consistency Index (*RI*). Mathematically, CI is defined as

$$CI = \frac{\lambda_{max} - N}{N-1} \tag{5.4}$$

$$CR = CI/RI \tag{5.5}$$

Where, λ_{max} is the largest Normalized Principle Eigen Vector and N is order of the decision matrix. The value of RI is predefined for different values of N (Table 5.1). If CR ≤ 10%, the decisions made (*i.e.* the ranks assigned) are consistent. If not, the process should be repeated.

Table 5.1: Random Consistency Index (Saaty, 1980, 2000)

N (order of the matrix)	1	2	3	4	5	6	7	8	9	10	11	12	13	14	15
RI	0	0	0.58	0.90	1.12	1.24	1.32	1.41	1.45	1.49	1.51	1.53	1.56	1.57	1.59

Once, the rank and weights of various landslide causative parameters are finalized, they form an integrated landslide susceptibility scale for the study area. The final rank and weights are added to the thematic data layers, which are then arithmetically overlaid in GIS environment to prepare a Landslide Potential Index (LPI) map. The LPI map is used to generate LSZ map of the study area. This LSZ map is compared to LSZ maps produced using (i) InfoVal method and (ii) Fuzzy operators to assess its performance. Ensuring a satisfactory performance assessment, this LSZ map will be used for multi hazard integration to generate seismically induced LHZ map for the study area. A schematic diagram of the working principle is shown in Fig. 5.1 below.
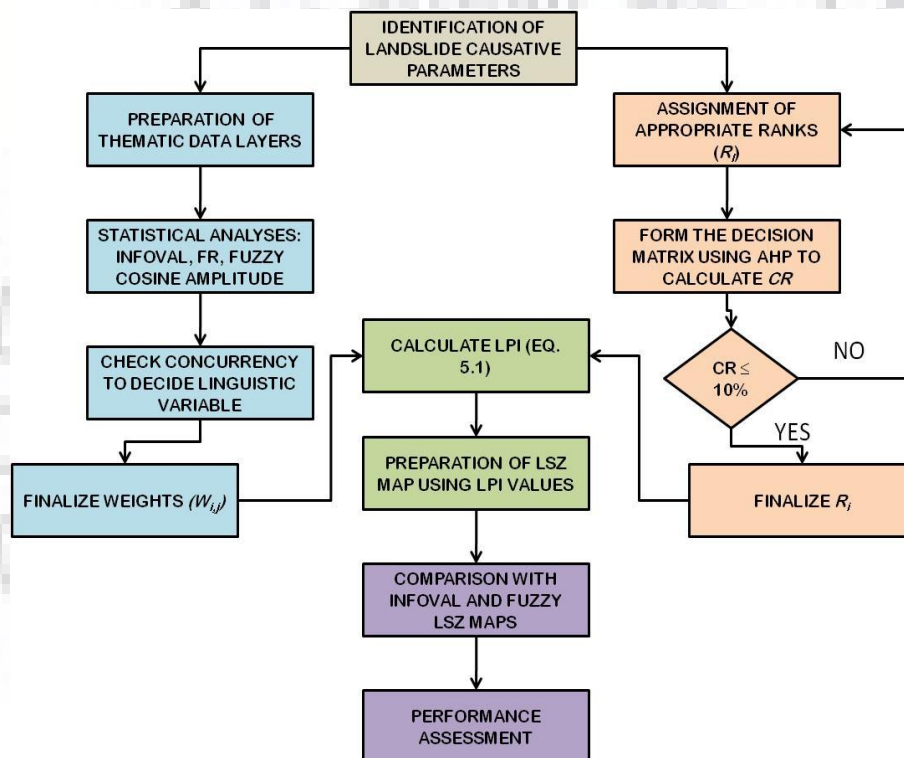
Fig. 5.1: Schematic Diagram for Development of Integrated LSZ Scale

5.4 Development of an Integrated LSZ Scale for the Study Area

5.4.1 Assignment of Weights ($W_{i,j}$)

Table 5.2 shows InfoVal, FR, Fuzzy ratings ($r_{i,j}$), perceived susceptibility levels and final weights ($W_{i,j}$) of different thematic classes.

Table 5.2: Assignment of Weights to different Thematic Classes

Parameter	InfoVal	FR	r_{ij}	Perceived Susceptibility Level (Linguistic Variables)	W_{ij}
Slope Angle					
$<15^0$	-0.710	0.195	0.005	Very Low (VL)	**1**
15^0-25^0	-0.132	0.740	0.017	Low (L)	**3**
25^0-35^0	0.183	1.526	0.032	Moderate (M)	**5**
35^0-45^0	0.453	2.841	0.041	High (H)	**7**
$>45^0$	0.789	6.154	0.034	Very High (VH)	**9**
Geological Units					
Krol, Infrakrol & Blaini Formation	0.363	2.322	0.036	VH	**9**
Subathu Fm of W. Himalaya	0.303	1.973	0.013	H-VH	**8**
Manjir Fm of W. Himalaya	0.275	1.698	0.006	H-VH	**8**
Subathu Fm. of W. Himalaya	0.180	1.477	0.009	H	**7**
Jaunsar Gp of W. Himalaya	0.155	1.440	0.031	H	**7**
Tal Fm of W. Himalaya	0.101	1.250	0.010	H	**7**
Simla Gp	0.098	1.248	0.011	H	**7**
Almora Crystalline Fm of W. Himalaya	0.059	1.050	0.007	M	**5**
Dagshai and Kausauli Fm of W. Himalayas	-0.067	0.853	0.008	H	**7**
Jutogh Gp of W. Himalaya	-0.203	0.623	0.005	M	**5**
Middle Siwalik Gp	-0.372	0.425	0.005	L	**3**
Lower Siwalik Gp	-0.483	0.332	0.004	L-VL	**2**
Amri Tectonic unit	-0.489	0.318	0.002	VL	**1**
Deoban Gp of W. India	-0.503	0.294	0.001	VL	**1**
Dharagarh Fm of W. India	-2.274	0.000	0.000	---	**---**
Igneous intrusion	-4.342	0.000	0.000	---	**---**
Fault Euclidian Distance					

0-3 km	0.025	1.061	0.034	VH	**9**
3-6 km	-0.004	0.992	0.024	H	**7**
6-9 km	-0.055	0.883	0.013	M	**5**
9-12 km	-0.143	0.721	0.007	L	**3**
>12 km	-0.175	0.669	0.004	VL	**1**
Elevation					
< 500 m	0.025	0.199	0.004	L	**3**
500-1000 m	-0.004	1.496	0.038	VH	**9**
1000-1500 m	-0.055	1.339	0.030	H	**7**
1500-2000 m	-0.143	0.690	0.012	M	**5**
> 2000 m	-0.175	0.151	0.002	VL	**1**
Drainage Euclidian Distance					
< 250 m	0.057	1.140	0.033	VH	**9**
250-500 m	-0.032	0.929	0.023	H	**7**
500-750 m	-0.030	0.934	0.017	M	**5**
750-1000 m	-0.119	0.761	0.008	L	**3**
> 1000 m	-0.561	0.275	0.002	VL	**1**
Road Euclidian Distance					
< 100 m	0.181	2.500	0.026	VH	**9**
100-200 m	0.162	1.371	0.014	H	**7**
200-350 m	0.094	1.171	0.013	M	**5**
350-500 m	0.041	1.037	0.012	L	**3**
> 500 m	-0.044	0.852	0.033	VL	**1**
LULC Pattern					
Sparsely Vegetated	0.067	1.167	0.039	H	**7**
Deciduous Forest	-0.208	0.620	0.010	L	**3**
Evergreen Forest	-0.025	0.943	0.015	M	**5**
Shrub Land	-0.142	0.721	0.013	M	**3**
Built-up	-0.234	0.584	0.003	VL	**1**
Barren Land	1.019	2.305	0.016	VH	**9**
Water Body	-0.693	0.203	0.001	VL	**1**

Slope Aspect					
Flat	0	0	0	---	**---**
N	1.612	0.567	0.010	L	2
NE	1.718	0.746	0.012	L	2
E	1.960	1.477	0.023	M	5
SE	1.509	0.502	0.008	L	2
S	1.526	0.555	0.009	L	2
SW	1.716	0.892	0.014	L	2
W	1.956	1.543	0.023	M	5
NW	2.042	1.984	0.029	M	5

Table 5.3 shows the assigned weights of various thematic classes. The weight values are distributed on a scale of 1 to 9. Five discrete values of 1, 3, 5, 7 and 9 are used to denote VL, L, M, H and VH levels of perceived susceptibility. Also, intermediate values like 8 and 2 are used to denote H-VH and L-VL susceptibility levels where deemed necessary. As discussed earlier, the weights are allocated based on perceived susceptibility level, which has been decided based on the concurrency of the results of three statistical analyses. For example, in slope angle data layer, strongest correlation has been observed for the thematic class of $[35^0 - 45^0]$ when Fuzzy cosine amplitude method was used. However, both InfoVal and FR methods show that this correlation is stronger for slope angles greater than 45^0. Since the results of two out of three analyses concur, it is considered for deciding the perceived susceptibility levels. Therefore, it is assumed that in the study area, slopes greater than 45^0 are highest susceptible to landslides and so weight of 9 is assigned to that thematic class. For most thematic classes, results of all the analyses concur as expected.

5.4.2 Assignment of Ranks (R_i)

Assignment of ranks to different causative data layer is a difficult task. It requires a thorough knowledge of the terrain. For this study area, it is observed that parameters slope angle and geological units have the most prominent effect on landslide activities. Similarly, the distance from the faults is considered to be a major landslide causative factor due to the presence of three major thrusting system *viz.* MCT, MBT and MFT and numerous transverse lineaments in the study area. The influence of drainage density and ground elevation on landslide distribution has also been observed to be prominent. Although road construction seems to be a major landslide causative factor in this area, owing to a sporadically distributed road network, its effect has been limited to only a fraction of the study area. LULC patterns and

slope aspect are observed to have low control on landslide susceptibility. Based on these observations, the following ranks (R_i) have been assigned to different landslide causative factors:

Table 5.3: Assignment of ranks (R_i) to landslide causative factors

Sl. No.	Landslide Causative Factor	Perceived Susceptibility Level	Rank (R_i)
1	Slope Angle	VH	**9**
2	Geological Units	VH	**8**
3	Fault Euclidian Distance	H	**7**
4	Elevation	M-H	**6**
5	Drainage Euclidian Distance	M-H	**6**
6	Road Euclidian Distance	M	**5**
7	LULC	L	**3**
8	Slope Aspect	VL	**2**

The consistency of this decision is checked using AHP. Table 5.4 shows the decision matrix formed.

Table 5.4: Decision Matrix to evaluate consistency of assignment of R_i

Parameters	1	2	3	4	5	6	7	8	Principle Eigen Vector
1. Slope Angle	1								0.323
2. Geological Units	1/2	1							0.221
3. Fault Euclidian Distance	1/3	1/2	1						0.146
4. Elevation	1/4	1/3	1/2	1					0.088
5. Drainage Euclidian Distance	1/4	1/3	1/2	1	1				0.088
6. Road Euclidian Distance	1/5	1/4	1/3	1/2	1/2	1			0.067
7. LULC	1/6	1/5	1/4	1/3	1/3	1/2	1		0.039
8. Slope Aspect	1/7	1/6	1/5	1/4	1/4	1/3	1/2	1	0.027

For the above decision matrix, 28 pair-wise comparisons are made. Solution of the decision matrix yields the following parameters:

Largest Principle Eigen Value, $\lambda_{max} = 8.276$ Consistency Index, $CI = 0.0394$

Random Consistency Index, $RI = 1.41$ for N = 8   Consistency Ratio, $CR = 0.028$ (2.8%)

Since CR < 10%, the decisions made (i.e. ranks assigned) are consistent.

5.4.3 Generation of LSZ Map using Map Combination Method

After finalization of ranks (R_i) and weights ($W_{i,j}$) of data layers and thematic classes, the next step is to prepare a Landslide Susceptibility Zonation (LSZ) map using map combination method. The final ranks and weights are then numerically integrated using Eq. 5.1 in Arc-GIS 10.6 to generate the LPI map of the study area. The LPI values are segregated using 'natural breaks' to categorize the LPI map into five classes of landslide susceptibility. The prepared LSZ map is shown in Fig. 5.2 below. To assess the performance of this prepared LSZ map, it is compared with the LSZ map produced using (i) InfoVal method (Chapter 4) and (ii) Fuzzy operators. Preparation of LSZ map using InfoVal method has already been discussed in chapter 4. Generation of LSZ map using Fuzzy operators will be discussed in the next section.
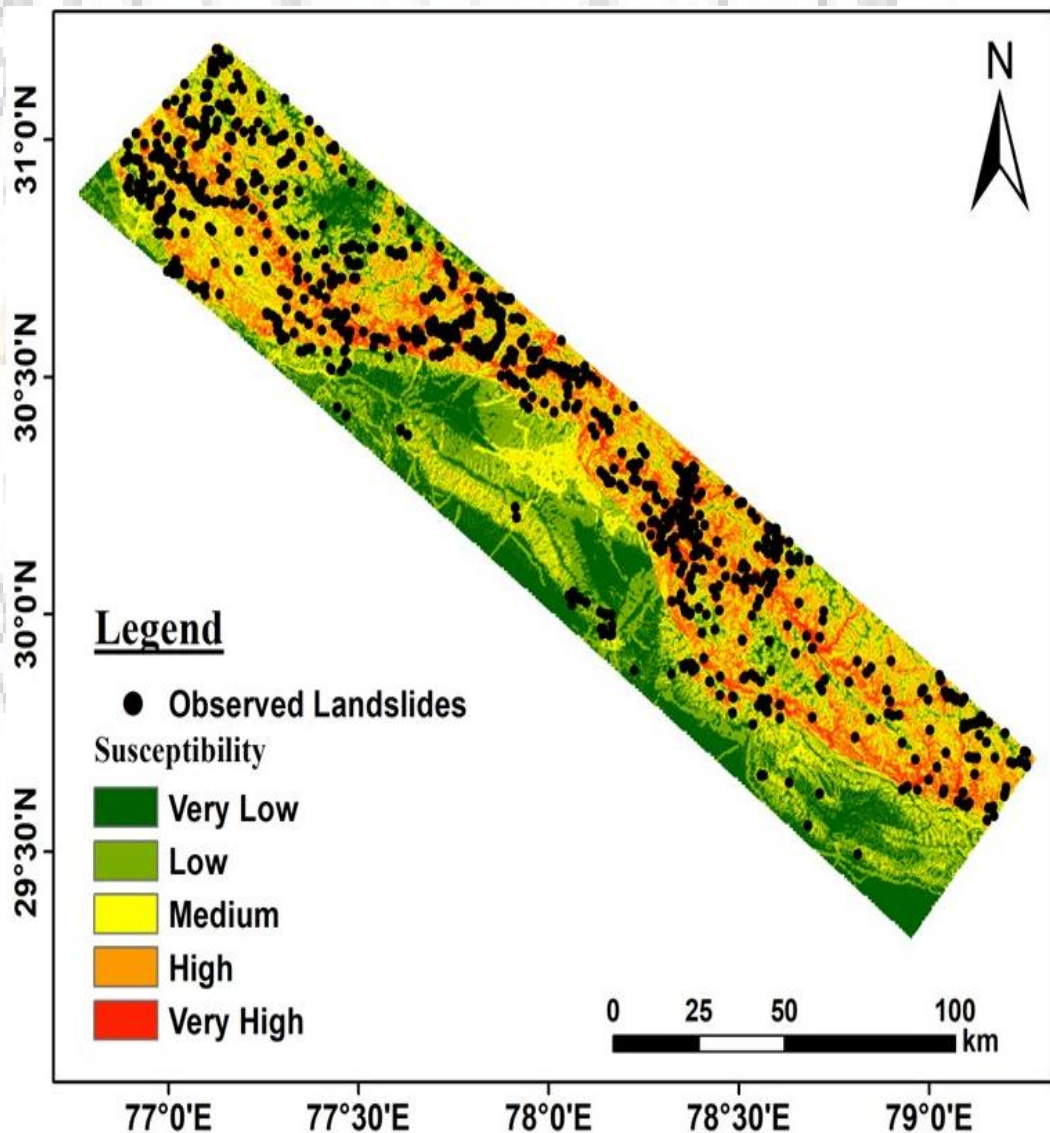
Fig 5.2: Landslide Susceptibility Zonation Map of the Study Area using Map Combination Method

5.5 Generation of LSZ Map using Fuzzy Operators

Fuzzy set theory based LSZ mapping is a statistical approach, where the weights of thematic classes are determined using Fuzzy cosine amplitude method (section 5.3). The weights are generated in the form of Fuzzy ratings ($r_{i,j}$) as given by Eq. 5.3. To incorporate Fuzzyness in LSZ mapping, different Fuzzy operators have been used (Kanungo et al., 2006; Peethambaran et al., 2019). Use of Fuzzy operators is an alternative to widely used arithmetic overlay approach, although it does not guarantee a more successful map (Kanungo et al. 2006). In this research work, three Fuzzy operators Fuzzy AND, Fuzzy OR and Fuzzy Gamma have been used. Fuzzy Gamma operator could also be used as Fuzzy SUM and Fuzzy PRODUCT operators by substituting the value of Gamma to 1 and 0 respectively.

If X is the universe of discourse and elements of X are denoted by x, then a fuzzy set A in X can be defined as a set of ordered pairs.

$$A = \{x, \mu_A(x) | x \in X\} \tag{5.6}$$

Where, $\mu_A(x)$ is the membership value of x in A, in the range [0, 1] with 0 representing non-membership and 1 representing the full membership. This membership value has been calculated as Fuzzy ratings ($r_{i,j}$) in this study.

Let $\mu_i(x), [i = 1, 2, \ldots, n]$ be the membership value of the fuzzy system having n variables, the combination of maps for a fuzzy set using different fuzzy operators can be written as:

Fuzzy AND

$$\mu_{AND}(x) = \text{MIN} [\mu_1(x), \mu_2(x), \ldots, \mu_n(x)] \tag{5.7}$$

Fuzzy OR

$$\mu_{OR}(x) = \text{MAX} [\mu_1(x), \mu_2(x), \ldots, \mu_n(x)] \tag{5.8}$$

Fuzzy GAMMA

$$\mu_\gamma(x) = [\mu_{SUM}(x)]^\gamma \times [\mu_{PRODUCT}(x)]^{1-\gamma} \tag{5.9}$$

Fuzzy SUM

$$\mu_{SUM}(x) = 1 - \prod_{i=1}^{n}(1 - \mu_i(x)) \tag{5.10}$$

Fuzzy PRODUCT

$$\mu_{PRODUCT}(x) = \prod_{i=1}^{n} 1\mu_i(x) \tag{5.11}$$

When the AND and OR operators used, only one membership value contribute to the result. LSZ maps using Fuzzy AND and OR operators are shown in Fig 5.3 and 5.4 respectively.
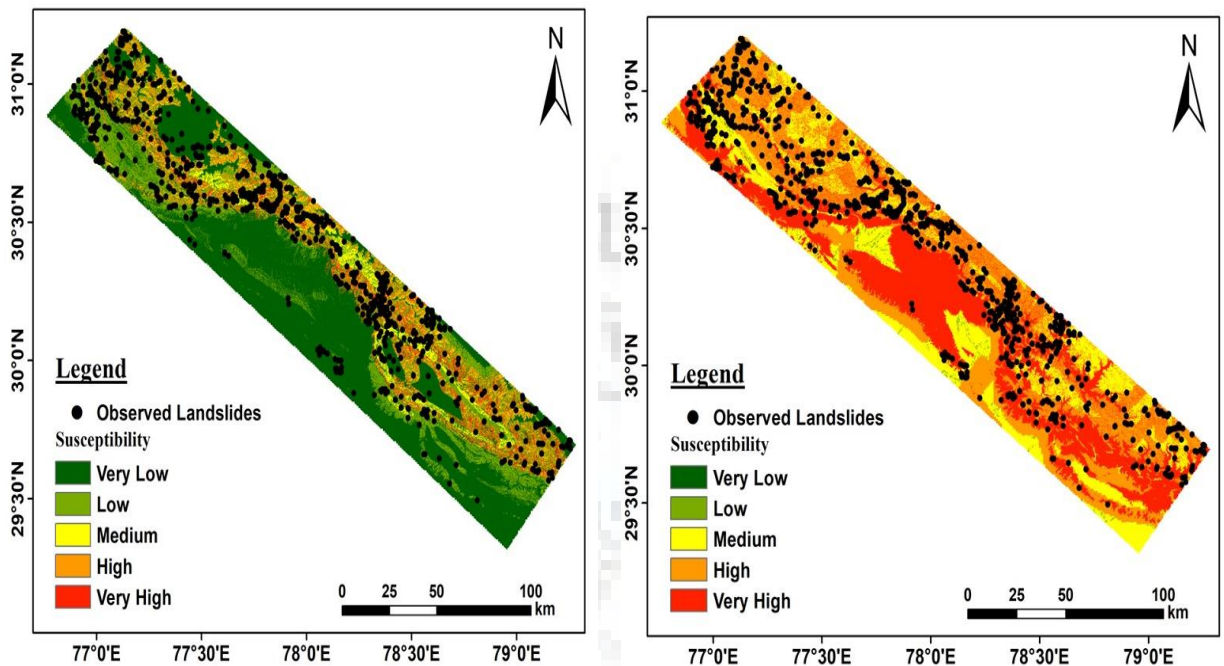
Fig. 5.3: LSZ map using Fuzzy AND Operator   Fig. 5.4: LSZ map using Fuzzy OR Operator

As can be observed from Fig 5.3 and 5.4, none of the Fuzzy operators AND/OR can portray the realistic scenario of current susceptibility levels for the study area. The LSZ map prepared using Fuzzy AND operator tends to underestimate the actual susceptibility level (most of the study area falls under low and very low susceptibility zones). On the other hand, the LSZ map prepared using Fuzzy OR operator tends to overestimate the actual susceptibility level (most of the study area falls under high and very high susceptibility zones).

The SUM operator make resultant fuzzy set larger than, or equal to the maximum value. On the other hand, the PRODUCT operator make resultant fuzzy set smaller than, or equal to the minimum value. This implies that the LSZ map prepared using SUM operator will be more or less similar to LSZ map prepared using OR operator; and the LSZ map prepared using PRODUCT operator will be more or less similar to LSZ map prepared using AND operator. Therefore, their results have been discarded.

The resultant set integrated with the Gamma operator has the value between that of Sum and Product operators. The value of Gamma is closely associated with the degree of compensation between the extreme confidence levels (Peethambaram et al., 2019). Kanungo et al. (2006) suggested that the optimal value of Gamma operator should be decided on the basis of trail and exigency. A range of Gamma values from 0.6 to 1.30 have been selected in this

research work, for which LSZ maps are prepared. The prepared maps are then compared in terms of their success rate curves (section 4.3.1). Generally, a Gamma value in the range of [0.9-1.0] has been observed to yield the best results. For the study area, Gamma value equals to 0.95 produces the best LSZ map. The prepared LSZ map is shown in Fig. 5.5 below. The prepared LSZ map seems to depict a reasonable scenario of the current susceptibility level for the study area.
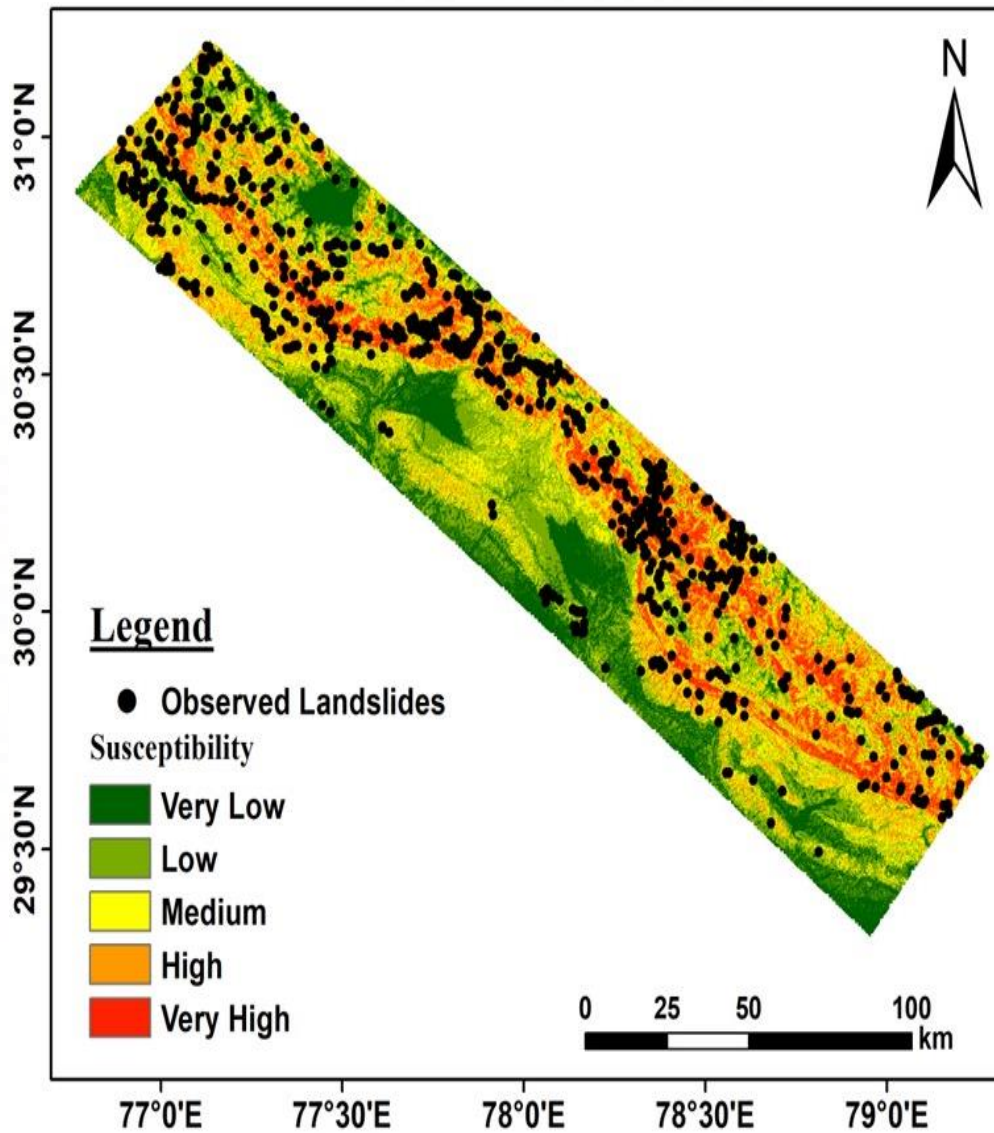
Fig. 5.5: LSZ map of the Study Area using Fuzzy Gamma Operator (γ=0.95)

5.6   **Performance Assessment of LSZ maps**

The prepared LSZ maps using InfoVal (Fig. 4.2), Map Combination (Fig. 5.2) and Fuzzy Gamma operator (Fig 5.5) are compared statistically to assess the performance of the Landslide Susceptibility Scale for the study area. The performance of the LSZ maps are assessed based on two parameters: (i) Area under ROC curve and (ii) FR of the susceptibility zones. The first parameter i.e. Area under ROC (Receiver Operating Characteristic) curve

(AUC) is used to assess the quality of pre-categorized images (Fig. 5.6). AUC is a measure of the success of the predictive model. Receiver Operating Characteristic (ROC) Curve is a graphical plot that illustrates the diagnostic ability of a binary classifier system as its discrimination threshold is varied. It is created by plotting the true positive rate (TPR) against the false positive rate (FPR) at various threshold settings. ROC analysis provides tools to select possibly *optimal* models and to discard *suboptimal* ones. The second parameter i.e. FR of the Susceptibility zones is computed for the categorized LSZ maps, where natural break is used to categorize each map into five distinct zones of landslide susceptibility (Fig. 5.7).
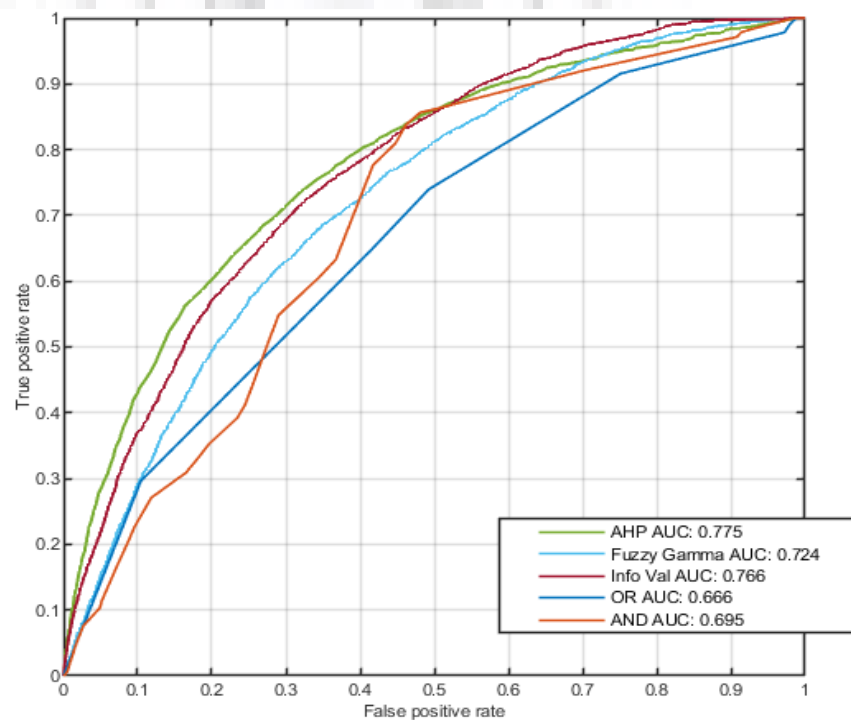
Fig. 5.6: ROC for Prepared LSZ Maps
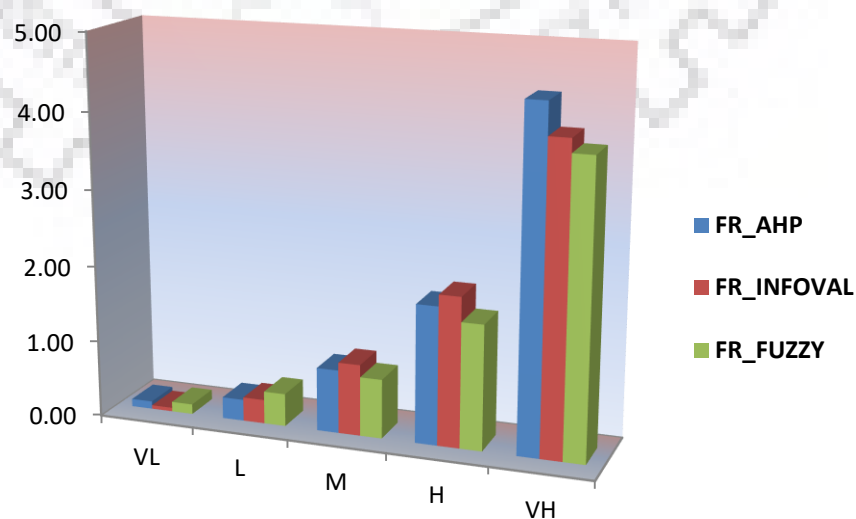
Fig 5.7: FR of Landslide Susceptibility Zones for Prepared LSZ Maps

Analysis of the ROC curves reveals that pre-categorized LSZ map prepared with the developed susceptibility scale (shown by the green line in Fig. 5.6 and denoted by AHP for demarcation) yields the highest AUC compared with other maps. Considering AUC as a direct measure of the success rate for that predictive model, it is assumed that the pre-categorized LSZ map using the developed landslide susceptibility scale is almost 77.5% accurate. This accuracy will be further improved upon appropriate segmentation of LPI values.

FR analysis of the landslide susceptibility zones is a statistical validation of LSZ maps (section 4.3.1). It is also used as an comparative parameter to assess the performance of LSZ maps prepared using different techniques. It is reported that the map, for which highest FR value is obtained for the zone of Very High Susceptibility (VH), yields the best result (Kanungo et al., 2006; Pareek et al., 2010, Peethambaran et al., 2019). It is observed that the categorized LSZ map prepared with the developed susceptibility scale (shown by the green column in Fig. 5.7 and denoted by AHP for demarcation) yields the highest FR value for VH susceptibility zone as compared with other maps.

Thus it can be inferred that the LSZ map prepared with the developed susceptibility scale, could portray a realistic scenario of the current level of landslide susceptibility efficiently. Also, the LSZ map prepared with the developed susceptibility scale has been assessed to perform better than two statistical approaches.

5.7 Segmentation of LPI Values: A Statistical Approach

In conventional LSZ studies, demarcation of different susceptibility class boundaries are done by segmenting the LPI values subjectively. One of the popular way of segmenting the LPI values is to apply 'natural breaks' to somewhat reduce the subjectivity. However, as the present research work envisages to quantify the impact of earthquake scenarios in landslide hazard, it is important to quantitatively fix the class boundaries of the final LSZ map prepared under static parameters. This necessitates a robust classification scheme of LPI values to demarcate different susceptibility class boundaries. For this purpose, probabilistic approach of LPI segmentation (Saha et al., 2005) has been adopted in this study.

This approach provides with a mathematical framework for segmenting the LPI values based on their probability distribution pattern. The LPI value of the LSZ map (Fig. 5.2) ranges from 80 to 336. The probability distribution of LPI value classes are shown in Fig. 5.8, which shows that the probability distribution follows normal distribution with zero skewness. For this distribution, the observed mean (μ_0) and observed standard error (σ_0) are computed to be 206.53 and 34.22 respectively. Based on this distribution pattern, class boundaries are fixed at

$(\mu_0-1.5m\sigma_0)$, $(\mu_0-0.5m\sigma_0)$, $(\mu_0+0.5m\sigma_0)$ and $(\mu_0+1.5m\sigma_0)$, where m is a positive non-zero value. The value of m is determined by the process of trial and exigency (Saha et al., 2005).
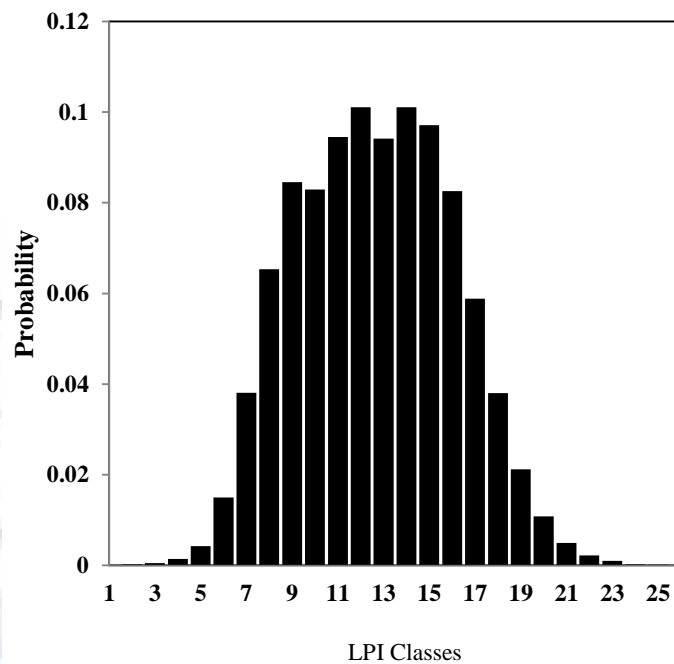
Fig. 5.8: Probability Distribution of LPI Class

With this probabilistic framework of LPI segmentation, the prepared LSZ map (Fig. 5.2) has been categorized several times for m = (0.7, 0.8, 0.9, 1.0, 1.1, 1.2, 1.3) and the corresponding success rate curves are prepared (Fig. 5.9). Saha et al. (2005) suggested that success of any LSZ operation can be judged by the measure that more number of landslides should fall in the very high LSZ as compared to other zones. Assuming that the first 10% of the success rate curve show the VHS zone, the value of m is fixed in such a way that it yields the highest success rate for the first 10% LSZ area. For the prepared LSZ map (Fig. 5.2), the highest success rate for the first 10% LSZ area has been observed for m = 0.8. Therefore, for the prepared LSZ map, value of m is decided as 0.8, for which class boundaries are fixed. Table 5.5 shows the segmentation of LPI values and the class boundaries for the LSZ map prepared using the developed landslide susceptibility scale.

Table 5.5: Segmentation of LPI Values

LSZ Class	LPI Boundary	Percentage of Total Area	Percentage of Observed Landslide
Very Low	80-165	17	2
Low	165-193	25	7
Moderate	193-220	28	20
High	220-248	23	32
Very High	248-336	7	38
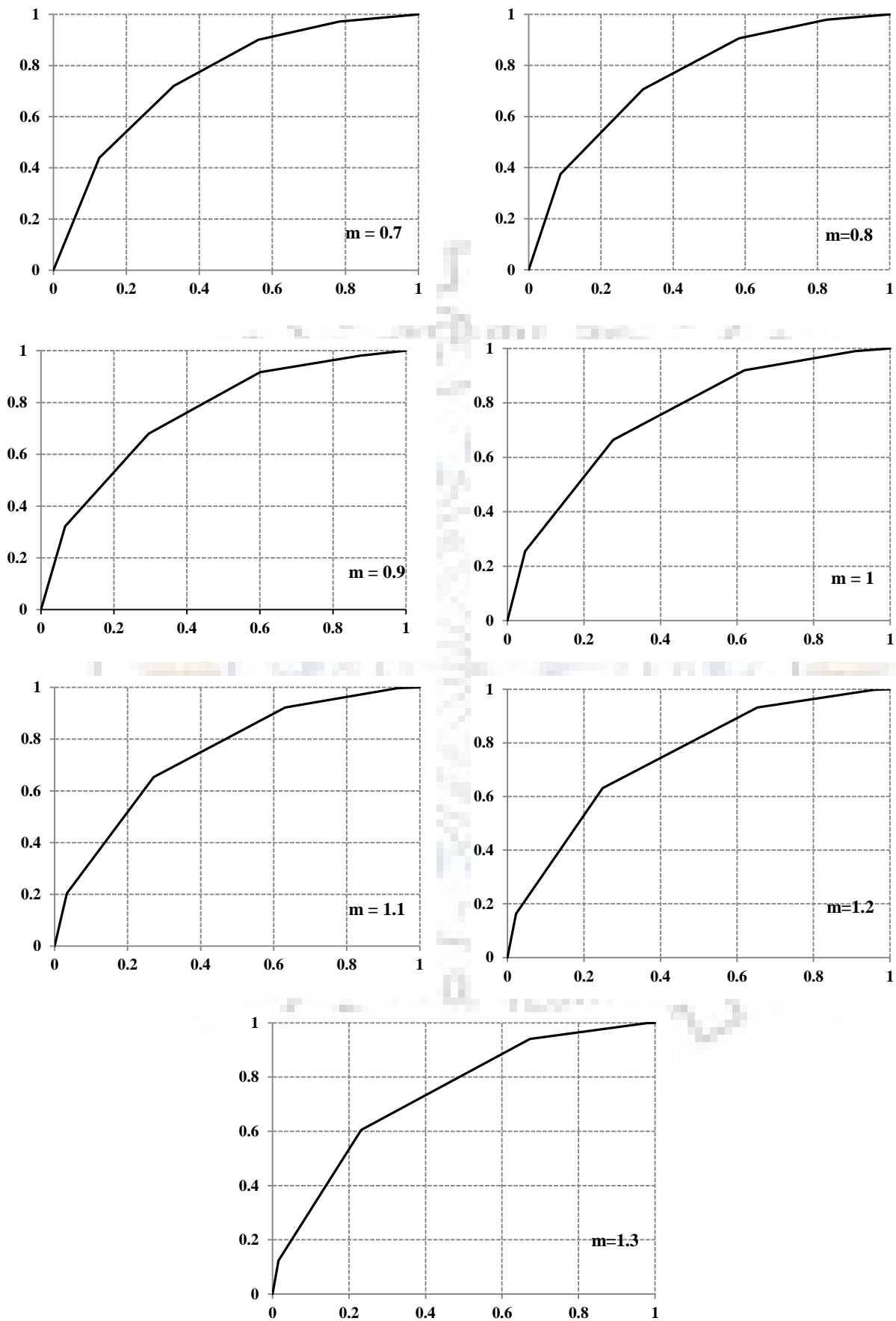
Fig. 5.9: Success Rate Curves of the LSZ Map for Different *'m'* Values

Analysis of the success rate curve corresponding to m = 0.8 reveals that area under the curve is 0.849. It implies that the final LSZ map of the study area, prepared with the developed landslide susceptibility scale has an accuracy of ~85%, which is a marked improvement of the LSZ map prepared using InfoVal method (79.7%). This prepared map (Fig. 5.2) will be denoted as LSZ_Static henceforth.

The prepared LSZ_Static is physically further validated through field surveys. Generally the presence of large landslides in very high and high susceptibility zones is indicative of the success of the predictive map. Fig. 5.10 (a, b) shows two enormous landslides identified in the very high susceptibility zones for the study area.

Fig. 5.10 (a): Landslide Observed at $30^0 33.817$' N, $77^0 51.081$' E
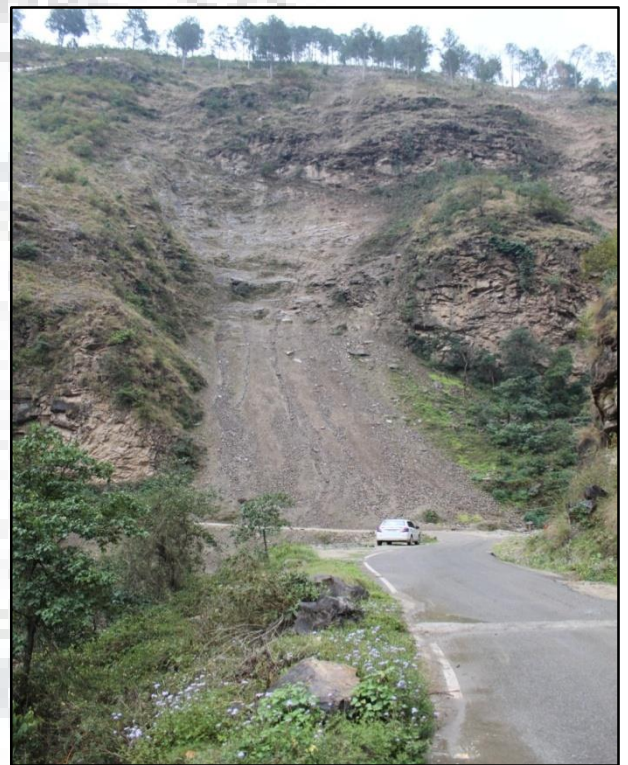
Fig. 5.10 (b): Landslide Observed at $30^0 10.762$' N, $78^0 35.375$' E

5.8   Summary

This chapter includes discussion on seismically induced landslide hazard zonation, the importance of undertaking such studies and the challenges faced. It is understood that there are two main challenges in preparing seismically induced LHZ maps: (i) selection of an appropriate mapping technique and (ii) selection of scenario earthquakes to be used as an input parameter. This chapter address the first issue in details, where an alternative approach has been suggested.

A landslide susceptibility scale has been developed for the study area coalescing three

statistical techniques of LSZ mapping. The developed scale is then applied to generate a LSZ map for the study area using Map combination method. The developed scale is devoid of subjectivity and hence can be used for other Himalayan regions as well. The performance of the LSZ_Static map, prepared with the developed landslide susceptibility scale is assessed by comparing it with LSZ maps produced using InfoVal and Fuzzy Operators. The performance of the LSZ_Static map is found to be satisfactory, and it yields the best results for the study area. Thus it is inferred that the developed landslide susceptibility scale can be used for multi hazard integration for the study area.

PROBABILISTIC SEISMIC HAZARD ASSESSMENT (PSHA)

6.1   Preamble

The present research work aims to quantify the impact of earthquakes in landslide hazard analysis for a part of lower Himalayan belt. As discussed in the previous chapter, one of the key challenges is the selection of an appropriate earthquake motion, for which seismically induced landslide hazard zonation (LHZ) is carried out. In most of the seismically induced LHZ studies, the primary focus has been to associate earthquake magnitude and spatial distribution of landslides in an area. The methodology adopted for such studies incorporates mapping and analysis of earthquake induced landslide inventory prepared post major events to establish correlation between EQ characteristics and landslide distribution (Keefer, 1984; Jibson, 1993; Rodriguez et al., 1999; Pachauri et al., 2001; Yin et al., 2009; Pareek et al. 2010, 2012; Xu et al., 2013; Tang et al., 2015; Roback et al. 2018). However, such studies have both conceptual and operational limitations owing to the regional and characteristic biasness (section 5.2) associated with an earthquake event. It is understood that any statistical method, that considers a single earthquake event, may be applicable for seismically induced LHZ mapping in other regions. Also, selection of a particular attribute (amplitude/ frequency content/ duration/ response spectra/ PGA *etc.*) to describe an earthquake is another important criterion for carrying out seismically induced LHZ mapping. Amplitude, frequency content and duration are fundamental attributes of an earthquake event and therefore, any of these three parameter could be selected for post event inventory analysis. But as discussed earlier, this will invariably incorporate characteristic biasness of an earthquake motion.

In this context, Peak Ground Acceleration (PGA) parameter generated through Probabilistic Seismic Hazard Assessment (PSHA) is considered to describe the seismicity parameter in the present study. Use of PSHA to generate PGA parameter has far reaching implications and advantages. PSHA is a platform, where the probabilistic distribution functions of geometry of the source and size distribution are convolved with the rate of seismicity to predict future strong ground motion. This means the PGAs predicted are not generated from single events but are representatives of the expected deformations and stress releases in future in a finite time period. Consideration of this finite time for exceedance probabilities of strong ground motion would provide an opportunity to examine the probabilities in next finite time period. This essentially eliminates the characteristic biasness of a single event and allows scope for incorporating an entire range of earthquake sizes. The effects of an entire range of earthquake sizes helps in understanding the impact of earthquake motion on LHZ mapping in a

holistic way. Moreover, use of PGA values generated through PSHA have enabled us to consider two major parameters: (i) seismotectonic environment (in terms of faults and lineaments) of a bigger area (R~300 km) which would likely to produce earthquakes in the study area, and (ii) recorded past earthquake events of a bigger area. The recorded past earthquake events are used to quantify the rate of seismicity in an area in PSHA method. Owing to the consideration of this recorded past seismicity, PSHA is assumed to have indicated efficiently the expected strength reduction of the rock mass due to repetitive dynamic forces as well. PGA parameter is also indicative of the expected force imparted by a particular earthquake size, and thus its use in seismically induced LHZ studies is well recognized (Nadim et al., 2006; Saygili and Rathje, 2009; Yin et al., 2009; Abou-Jaoude and Wartman, 2017). Use of probabilistic PGA parameter in seismically induced LHZ mapping has increased the applicability of the method.

This chapter includes discussions on the methodology of PSHA, compilation and treatment of earthquake catalogue, seismotectonic modeling, and estimation of seismic hazard parameter for the study area. A brief review of the present state of research on seismic hazard assessment in India has also been included in this chapter.

6.2   Seismic Hazard Assessment in India: A Brief Review

India has been devastated by many damaging earthquakes in the past (Pande, 2000). The first seismic hazard studies carried out for the Indian peninsula dated back to 1898, post the great Shillong earthquake (June 12th, 1897; M$_w$ 8.1) by Geological Survey of India (GSI). Since then, many researchers have contributed significantly in these field and considerable progress have been made. In the post-independence era, the first credible research work on the Himalayan seismicity was carried out by Tondon (1956) and Krishna (1959), followed by the micro-seismic intensity works of Guha (1962) and Gubin (1968). In the preceding decades, Bureau of Indian Standards, erstwhile Indian Standards Institution (ISI), published seismic hazard maps for India with six seismic zones in 1962 (ISI, 1962), seven zones in 1966 (ISI, 1966), five zones in 1970, 1975 and 1984 (ISI, 1970, 1975, 1984), and with four zones in 2002 and 2016 (BIS 2002, 2016),but none of those maps have been based on the frame work of either deterministic or probabilistic seismic hazard assessment. Presently, the country is divided into four seismic zones – Zones II with MSK intensity VI, Zone III with MSK intensity VII, Zone IV with MSK VIII and Zone V with MSK intensity IX or more. Each zone is associated with a seismic zoning factor which represents the expected PGA based on anticipated intensity of shaking. The zone factors (PGA) for Zone II, III, IV and V are 0.10g, 0.16g, 0.24g and 0.36g respectively.

The initial PSHA studies in India focused on preparing maps for the entire country in terms of PGA for the return period of 100 years (Basu and Nigam, 1977; Kalia and Rao, 1979). Khattri et al. (1984) generated probabilistic seismic hazard zonation maps for India in terms of PGA for a return period of 475 years and characterized the seismicity of the country with the help of 24 broad seismic source zones. They prepared the map for the entire country using a single site-to-source earthquake attenuation relationship and obtained a maximum hazard of 0.7g for the Himalayas. Bhatia et al. (1999) provided zonation maps in terms of PGA for a return period of 475 years for the entire India considering 86 seismic sources, which were later included in Global Seismic Hazard Assessment Program (GHSAP). Sharma (2003) conducted extensive studies on seismic hazard for northern India, and followed it up for northeast India (Sharma and Malik, 2006). Das et al. (2006) estimated uniform hazard spectra for pseudo spectral velocity for Northeast India and observed that a single zone factor as given by BIS (2002) for entire northeast of India is not sufficient. Jaiswal and Sinha (2007) reported that seismic hazard in some parts of peninsular India is higher than that given by BIS, 2002. Mahajan et al. (2010) carried out PSHA for the north-western Himalayas. Joshi and Sharma (2011) estimated of probabilistic PGA and its uncertainty for Northern Indian Region. Kumar and Sharma (2011) estimated the conditional probabilities of occurrence of moderate earthquakes in India using non-Poissonian distributions. Sharma and Lindolhm (2012) assessed the current level of seismic hazard for Dehradun using characteristic earthquake recurrence model. Nath and Thingbaijam (2012) conducted PSHA studies for entire India under Global Earthquake Model (GEM). The study indicated that the hazard distribution in the country is significantly higher than that specified previously by GSHAP and BIS, 2000. Patil et al. (2014) prepared PGA-based hazard maps for the 475-year and 2475-year return periods for the state of Himachal Pradesh and adjoining regions. Mridula et al. (2014) prepared the hazard maps for the region in the vicinity of Main Boundary Thrust (MBT) and Main Central Thrust (MCT) in the western Himalayas. Choudhury (2015) carried out seismic hazard assessment of Goa and reported maximum PGA of 0.15g in the state. Kolathayar et al (2015) included latest seismicity data and reported higher PGA values for north and northeast India than that of BIS, 2002. Choudhary and Sharma (2017) estimated the occurrence of large earthquakes in Himalayas region using Pareto Distribution. Choudhary and Sharma (2018) carried out the SHA for Himalaya region using constant moment rate and model.

National Disaster Management Authority, Government of India (NDMA, 2010) has also prepared seismic hazard maps for the entire country in terms of PGA and spectral acceleration (SA) at different natural periods for different return periods. This study is more comprehensive compared to the earlier studies as this has defined finer seismic source zones to characterize the

seismicity and has developed source-specific attenuation relations based primarily on the synthetic data. Department of Earthquake Engineering, Indian Institute of Technology Roorkee, has been actively involved in various research projects on site specific seismic hazard analysis for dams, reservoirs, bridges and National Thermal Power Plants. These studies are being used by the construction authorities for earthquake resistant design of engineering projects.

6.3   PSHA Methodology

The frame work of PSHA involves 4 basic steps (Krammer, 1996) as follows:

(i) Identification of seismically active source (seismogenic source) using heterogeneity in their physical, geological and seismological attributes;

(ii) Estimation of occurrence rate of all earthquake magnitude range using an appropriate earthquake recurrence model for each seismogenic source;

(iii) Selection of an appropriate Ground Motion Prediction Equation (GMPE) to compute target ground motion parameters

(iv) Determination of associated hazard level in terms of probability of exceedance of ground motion intensity parameter (IM).

The PSHA approach describes a combined probability distribution function for any intensity measure (IM) parameter due to the total expected seismicity in a particular site. Suppose, υ (M_j, R_i) defines the annual rate of occurrence of earthquake(s) for a set of magnitude (M_j) and distance (R_i), and λ ($Z > z$) defines the rate of occurrence of IM parameter Z exceeding a value z (a value fixed for Z based on engineering judgement); then λ ($Z > z$) can be mathematically expressed as the linear combination of υ (M_j, R_i) for n number of seismogenic sources considered for that particular site.

$$\lambda(Z > z) = \sum_{n=1}^{n} \sum_{i=1}^{i} \sum_{j=1}^{j} q(Z > z | M_j, R_i) \times \upsilon_n (M_j, R_i) \tag{6.1}$$

Where, q defines the probability of IM parameter Z exceeding the value z for an earthquake of magnitude M_j at a distance R_i.

So the probability of IM parameter Z exceeding the value z, due to all the earthquakes in all the source zones during an exposure period of T years can be defined by Poissonian distribution and expressed as:

$$P(Z > z | T) = 1 - \exp(-\lambda(Z > z) \times T) \tag{6.2}$$

It is to be noted here that the IM parameters represent different ground motion aspects (viz. PGA, PGV, PGD, Spectral acceleration, response spectra *etc.*). A plot of the probability P (Z >z|T) *vs.* z is known as the "hazard curve". The hazard curves are sometimes also plotted as Y (Z >z|T) versus z, where Y is the return period of Z. Generally the PSHA may be expressed by

any of the quantities: λ (Z>z), Y (Z >z|T) or P (Z >z|T); which are interrelated by simple relations. However, equation (2) provides a direct physical interpretation of the results of PSHA.

6.3.1 Poisson Probability Distributions for Inter Arrival Time

The G-R magnitude recurrence relations provide the annual occurrence rate of magnitude M_w, which is the reciprocal of the rate provide the return period of magnitude M_w. To convert the recurrence rate into the probability of earthquake occurrence, it is necessary to define the probability distributions for the earthquake recurrence time or inter arrival time (IAT). Most probabilistic seismic hazard analyses are based on the assumption that the probability of an earthquake occurring in a given future time does not depend on the time elapsed since the previous earthquake. This assumption is typically made by defining the occurrence of earthquakes as a Poisson process. For a Poisson process, the probability of having exactly n number of earthquakes of a given magnitude range in a time interval t are defined,

$$p(n, \lambda) = \frac{e^{-\lambda t} (\lambda t)^n}{!n} \tag{6.3}$$

The probability of no event ($n=0$) in time t is obtained as, from equation (6.3),

$$p(n = 0) = e^{-\lambda t} \tag{6.4}$$

Here, λ is annual occurrence rate of greater than equal to a particular magnitude from G-R magnitude recurrence relationship. The probability of no occurrence in time t given by Eq. 6.4 can equivalently be interpreted as the probability that the time for occurrence of the next event in the given magnitude range is greater than t. Thus, the probability of having a time less than or equal to t between two consecutive events can be written as

$$F(t) = 1 - e^{-\lambda t} \tag{6.5}$$

This by definition is the probability distribution of the recurrence time with the corresponding density function given by

$$f(t) = \frac{dF(t)}{dt} = \lambda e^{-\lambda t} \tag{6.6}$$

The probability distribution function of recurrence times can be used to define the conditional probability of occurrence in a small future time interval dt, given that a time interval t has elapsed since the occurrence of the previous event as

$$P(dt/t) = \frac{F(t+dt) - F(t)}{1 - F(t)} \tag{6.7}$$

From this, the probability of occurrence per unit time at time *t*, known as hazard function $h(t)$, can be obtained as

$$h(t) = \frac{f(t)}{1-F(t)} \tag{6.8}$$

As the probability per unit time represents the inverse of the recurrence time, the hazard function can be considered to represent the occurrence rate at time *t*. This is therefore also called the hazard rate function. Using the distribution and density functions of eqns. (4.36) and (4.37), the hazard function for the Poisson process is obtained as

$$h(t) = \frac{\lambda e^{-\lambda t}}{1-(1-e^{-\lambda t})} = \lambda \tag{6.9}$$

Thus the hazard function represents the constant occurrence rate for the Poissonian occurrence of earthquakes, exhibiting its memory less nature.

6.4 Compilation and Treatment of Earthquake Catalogue

The first step of a PSHA study is the preparation of a comprehensive earthquake catalogue, which is further subjected to different tests and treatments. Compilation of earthquake catalogue is a time consuming and delicate process, for which data from different sources are extracted. There are three major categories of data sources for compilation of earthquake catalogue: instrumental data, historical data and paleoseismic data. The instrumental earthquake data sources have started for the period since 1964 after the establishment of World-Wide Standard Seismographic Network (WWSSN). The early instrumental data are generally defined for the period from 1900 to 1963 AD, historical for the period from 1500 to 1899 AD, and paleoseismic for the period before 1500. The instrumental catalogue is compiled mainly from United States Geological Survey (USGS), International Seismological Centre (ISC) and India Meteorological Department (IMD). Additional data for recent earthquakes have been collected from the National Geophysical Research Institute (NGRI), Wadia Institute of Himalayan Geology (WIHG) and Institute of Seismological Research (ISR). For historical and paleoseismic catalogues, different published literature have been consulted. Many researchers (Nath et al., 2010; Raghukanth, 2010) also have compiled a unified catalogues for Indian region, which have greatly helped out in this research work. Figure 6.1 shows the observed earthquakes for various seismogenic source zones considered for this study. The earthquake catalogue compiled for the study is given in Annexure A-3.

6.4.1 Treatment of Earthquake Catalogue

Owing to extraction of data from several sources with widely differing accuracy and quality, an earthquake catalogue suffers from problems of heterogeneity in the types of

magnitude and spatial and temporal coverage area. It is therefore necessary to subject an available earthquake catalogue to several tests and treatments to extract the most reliable information for hazard analysis applications. The commonly used catalogue treatments are: homogenization (assignment of the same type of magnitude to all listed earthquakes), declustering (identification and removal of the dependent events) and completeness analysis (classification of the completeness period for all size of earthquakes).

Homogenization

The compiled earthquake events from various sources initially define the magnitudes with various magnitude scales; viz. Local Magnitude M_L, Surface wave Magnitude M_S, Body wave Magnitude m_B, and Moment Magnitude M_w etc. However, in real practice these magnitude scales do not represent equal value for same earthquake event. Homogenization refers to converting different types of magnitudes recorded in an earthquake catalogue to one type of magnitude using suitable empirical conversion relations. For hazard analysis applications, the type of magnitude used for homogenization is normally governed by the magnitude used in the selected ground motion attenuation relationship. Generally, most of the modern attenuation relationships are defined in terms of the Moment Magnitude (M_w) to ignore the saturation effects. All magnitude scales have been converted to the moment magnitude in the present study.

Many studies have proposed inter-relationship among different types of old and new types of magnitudes. For example, Gutenberg and Richter (1956) has given the following conversion relations from M_L and older M_S to m_B

$$m_B = 0.63\,M_S + 2.5 \tag{6.10}$$

$$m_B = 1.7 + 0.8\,M_L - 0.01M_L{}^2 \tag{6.11}$$

Abe (1981) has given a relationship between m_B and the new body wave magnitude m_b in ISC bulletins, whereas Chung and Bernreuter (1981) have given a relation between M_L and m_b as follows:

$$m_B = 1.5\,m_b + 2.2 \tag{6.12}$$

$$M_L = 0.88\,m_b + 0.54 \tag{6.13}$$

For the period prior to 1964, conversion relations are required from M_L, older M_S and longer period body wave magnitude m_B to M_W. For this purpose, M_W may be taken equal to the older M_S in the magnitude range of 6.5 to 8.5. If M_S is not available directly, m_B be converted

into M_S using the relationship of eqn. (6.10) which can be approximated as M_W. For magnitudes smaller than 6.5, it is obtained as

$$M_W = 0.887M_L + 0.67; 0 \leq M_L \leq 6.5 \tag{6.14}$$

Considering huge worldwide database of catalogues for the period 1965 to 2003, Scordilis (2006) has developed the conversion relations from new M_S and m_b to M_W, as:

$$M_W = 0.85m_b + 1.03; 3.5 \leq m_b \leq 6.2; n = 39,784 \tag{6.15}$$

$$M_W = \begin{cases} 0.67M_S + 2.07, 3.0 \leq M_S \leq 6.1; n = 23,921 \\ 0.99M_S + 0.08, 6.2 \leq M_S \leq 8.2; n = 2,382 \end{cases} \tag{6.16}$$

In this study above procedure of magnitude conversion has been followed. If the M_W magnitude is not reported directly, M_s was used as M_w for $M_s \geq 6.5$. If M_s not available, M_w can be obtained from m_B using eqn. (6.10). For smaller magnitudes, M_W can be obtained from M_L using eqn. (6.14). For the new magnitude types, if M_s is reported then the conversion relation of eqn. (6.15) and (6.16) have been used to convert to M_w scale.

Declustering

Since Poissonian distribution has been used in this study, it is important to include only the statistically independent main shocks in the catalogue. The process of identification and removal of fore and after-shocks of a main earthquake event is known as declustering, which is performed by adopting window method (Uhrhammer, 1986). Window method is very simple procedure for identification of fore-shocks and after-shocks. In this method, space and time windows are defined for the occurrence of dependent events according to size of the independent event i.e. the main-shock. For any earthquake of magnitude M_w in the catalogue, the space and time windows are defined by Eq. (6.17) and (6.18) respectively:

$$L(M_W) = e^{0.804M_W - 1.024} \tag{6.17}$$

$$T(M_W) = e^{1.235M_W - 2.87} \tag{6.18}$$

Fore-shocks and after-shocks are identified as the events which occur within this space window ($L(M_w)$) and time widow ($T(M_w)$).

Magnitude Completeness

There are various methods to estimate the lowest magnitude of completeness, M_c, for given time and space intervals, which are based on the deviation from the linearity of the G-R relationship. In this study, the Entire Magnitude Range (EMR) method by by Woessner and Wiemer (2005) has been used.

EMR method uses the data over the entire magnitude range, both below and above M_c. The data above M_c are described by the G-R relationship with parameters *a,* and *b* and these parameters are obtained by the Maximum Likelihood Method (MLM) (Utsa, 1965). The incomplete part below M_c is described by a Normal Cumulative Distribution Function as

$$q(M/\mu, \sigma) = \frac{C}{\sqrt{2\pi\sigma}} \int_0^M exp\left\{\frac{-1}{2}\left(\frac{x-\mu}{\sigma}\right)^2\right\} dx \qquad (6.19)$$

Where C is a normalization constant whose value is fixed such that $q(M/\mu, \sigma)$ is 1.0. Thus, $q(M/\mu, \sigma)$ represents the probability of detection of various magnitudes below M_c. Parameters μ and σ are determined by Maximum Likelihood Estimator (MLE) method. In the EMR method, the best selection of M_c value is based on the Log–Likelihood Function with three parameters μ, σ and β. The most appropriate value of M_c is the one that maximizes the Log–Likelihood Function given by Eq. 6.20.

$$logL(\mu, \sigma, \beta) = \sum_i \log f(M_i | \mu, \sigma, \beta) \qquad (6.20)$$

In an earthquake catalogue, listed earthquake events of different magnitudes are not complete for equal time periods. In general, the smaller magnitude earthquakes are not complete for the older times, because the recording instruments started to record small earthquakes very late. Also, the completeness years for different magnitude range varies with space and time. For accurate estimation of seismic hazard, number of earthquake of specific magnitude should be used with corresponding completeness periods. Stepp (1972) proposed simple statistical criterion to identify the most recent period of completeness for a magnitude class, characterized by a constant occurrence rate of earthquakes. The method is based on the deviation of the rate of decrease of the variance in occurrence rate with increase in time from the expected behaviour. In the Stepp's method, for the compiled catalogue of earthquakes magnitude bins of size 0.5-1.0 unit have been prepared. Each magnitude interval is further grouped into time intervals of about 5 to 10 years. Then the annual occurrence rate, $R(M)$, has been estimated for each magnitude bins with increasing time length and start with the utmost present time. The first time window consists 10 years, then next time window will 20 years, and so on. The completeness period, $R(M)$, becomes constant for each time window for a given magnitude bins. To identify the interval of completeness for a particular magnitude class, Stepp (1972) assumes $R(M)$ as the mean of a Poisson process. Thus, the variance of $R(M)$ for T time interval is defined as;

$$S_R{}^2 = \frac{R(M)}{T} \qquad (6.21)$$

Thus, the standard deviation S_R of the mean occurrence rate $R(M)$ varies as $1/\sqrt{T}$ with time for achieving the stationarity of $R(M)$. The plot of S_R and T, known as Stepp's completeness plot, should show this expected behaviour for the period of completeness. The period of completeness for a magnitude class has to include minimum number of of events. The interval which are not reported completely, is not included. Time interval bin should also be long enough to establish a stable mean rate of occurrence. The Stepp's method requires a certain degree of personal judgment, especially at the extreme lower and upper magnitudes due to the statistical variability of the occurrence rates. The magnitude-completeness by EMR method for identified seismogenic source zones is shown in Fig. 6.2.

6.5 Seismotectonic Modelling

6.5.1 Identification of Seismogenic Sources

The study area shares high seismicity of the north-western Himalayan region. It is falling in between the seismic gap of 1934 Bihar–Nepal earthquake and 1905 Kangra earthquake in the central Himalaya active region. After plotting the earthquake data with the tectonic map, the region is divided into seven seismogenic source zones based on geologic conditions, tectonic features and seismicity. Each seismogenic source zones along with seismicity and tectonic features are shown in Fig. 6.1.
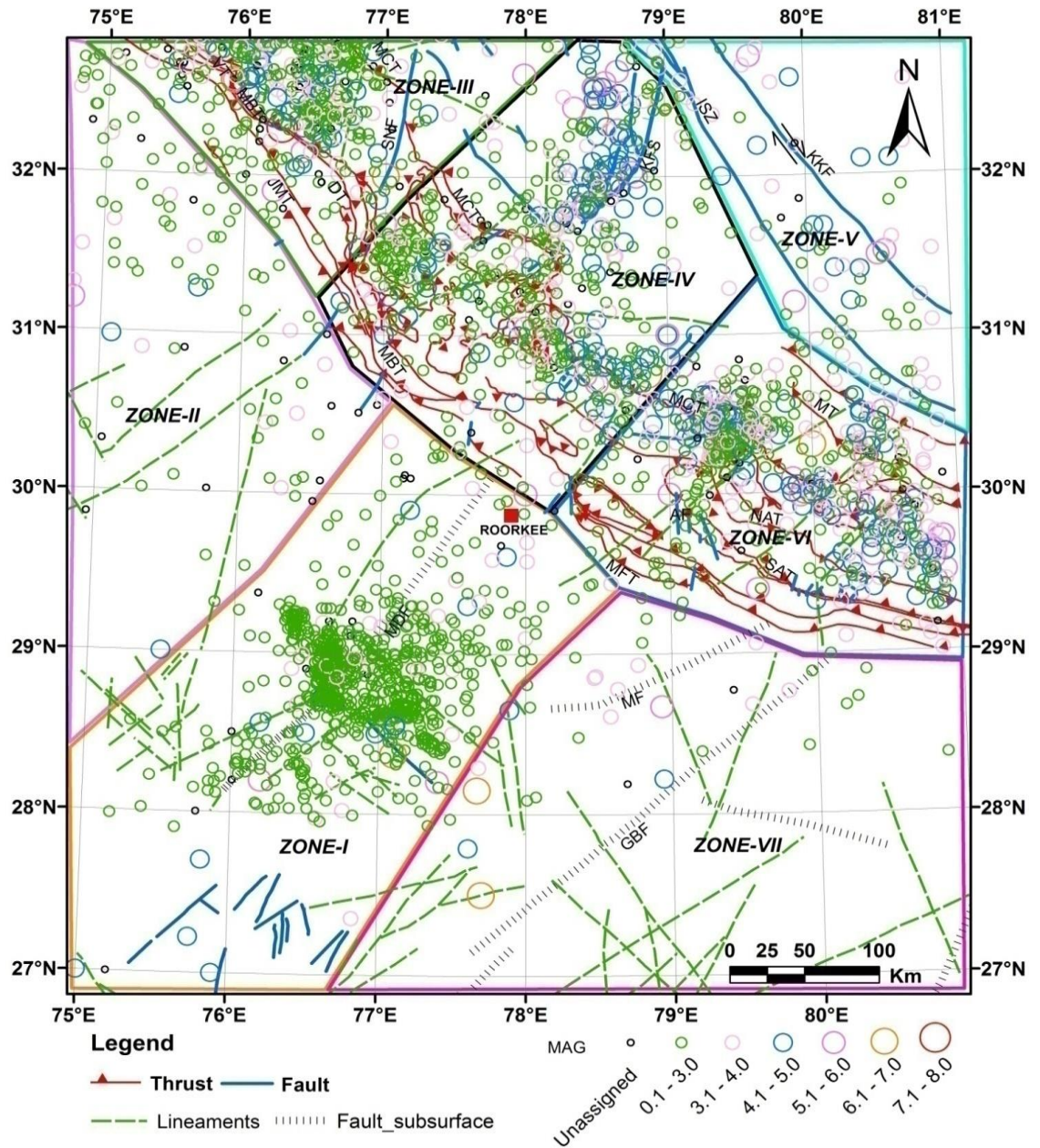
Fig. 6.1: Seismogenic Sources with Seismo-Tectonic Features

In this section, each seismogenic source is discussed briefly.

Seismogenic Zone-I

The seismogenic zone-I which is comprised of prominent tectonic feature the NNE trending subsurface Mahendragarh Dehradun Fault (MDF) which extends northeast ward up to the Himalayan foothills. The Delhi-Hardwar ridge is aligned with the MDF and is considered to be prolongation of the NNE-SSW directed Peninsular rock (Aravalli) as a horst delimited by faults. Further, in Delhi-Moradabad province the Neogene sediments directly overlie the Delhi basement. The Moradabad fault zone forms the eastern boundary of the Delhi-Moradabad

tectonic province. This NE-SW trending tectonic feature is traceable on to the shield area as a tectonic boundary between the Delhi folded belt and the Vindhyans.

Seismogenic Zone-II

This zone forms western most part Indo-Gangetic basin covering parts of Punjab and Haryana. This zone is filled with alluvium and marked by a few NE-SW and NW-SE trending lineaments.

Seismogenic Zone-III

The seismogenic zone-III constitutes north-western part of Himalayan structural belt. In this part the structural trend of the Himalaya is mostly NW-SE and is affected by transverse faults on the east by Sundernagar. Prominent tectonic features of this zone are Main Central Thrust (MCT), Main Boundary Thrust (MBT), Main Frontal Thrust (MFT) and Sundernagar Fault (SNF). SNF displaces MCT transversely for considerable distance. In the area northwest of SNF and north of MBT very high concentration of earthquake occurrence is reported indicating intense tectonic activity in the region. The 1905 Kangra earthquake of magnitude 8 has occurred in this zone only.

Seismogenic Zone-IV

The seismogenic zone-IV is comprised of the Himalayan belt of eastern and western parts of Himachal Pradesh and Uttarakhand respectively. In this area the structural trend of the Himalaya is mostly NW-SE. Prominent tectonic features of this zone are Main Central Thrust (MCT), southward dipping North Almora Thrust (NAT), Main Boundary Thrust (MBT) and Main Frontal Thrust (MFT). This structural belt has undergone different stages of crustal evolution and has been subjected to orogenic movements of varying intensity from time to time. Many significant earthquake clusters occur in this zone between MBT and MCT and also spread across the MCT making the region tectonically active. The 6.6 magnitude Uttarkashi earthquake of 1991 is located in this zone only. The zone also consists of neotectonic Kaurik Fault System (KFS) defined by number of half-graben faults occurring NE to the site and is active as it is considered that rupturing along the fault system had triggered Kinnaur earthquake of 1975 (GSI, 2000).

Seismogenic Zone-V

The seismogenic zone-V forms trans-Himalayan region north of the central crystalline belt. This zone is marked by Indus Suture Zone (ISZ) and extensive Karakoram Fault (KKF). ISZ marks the boundary between the Indian and Tibetan plates and south of this, litho-units of the main Himalayan belt are exposed and traverse across the study area from west to east. This

zone is represented by the obducted materials of the Neotethyan oceanic crust together with deep marine Triassic to Eocene sediments. KKF is the most extensive tectonic feature present in the region, which has affected the region with a huge dextral offset and is traceable towards northwest through the Shyok Suture to the Pamir. This fault extends for almost 1000 km from Central Pamir to Kumaon Himalayas.

Seismogenic Zone- VI

The seismogenic zone-VI is comprised of the Himalayan belt of eastern Uttarakhand and westernmost part of Nepal. In this part the structural trend of the Himalaya is mostly WNW-ESE. This part is affected by minor transverse faults and longitudinal E-W trending Alaknanda fault. Prominent tectonic features of this zone are Martoli Thrust (MT), Main Central Thrust (MCT), southward dipping North Almora Thrust (NAT), South Almora Thrust (SAT), Ramgarh Thrust (RT), Main Boundary Thrust (MBT), Main Frontal Thrust (MFT). This structural belt has undergone different stages of crustal evolution and has been subjected to orogenic movements of varying intensity from time to time. Many significant earthquake clusters occur in this zone. Earthquake clusters are located north and MBT and spread across the MCT indicating the area between MBT and MCT and north of MCT is active. The 1999 Chamoli earthquake of magnitude 6.8 has occurred in this zone.

Seismogenic Zone-VII

This seismogenic zone is marked by subsurface faults namely Moradabad Fault (MF) and Great Boundary Fault (GBF) and a few lineaments. These faults have NE-SW trends and have configures the basement tectonics. The Moradabad fault zone forms the boundary between Neogene and the Delhi basement in Delhi-Moradabad province.

Table 6.1 presents some salient tectonic features of each source zone.

Table 6.1: Important Tectonic Features of Seismogenic Sources

SSZ	Prominent tectonic features
SSZ I	MDF
SSZ II	Few NE-SW and NW-SE trending lineaments
SSZ III	MCT, MBT, MFT, SNF
SSZ IV	MCT, MBT, MFT, NAT
SSZ V	ISZ, KKF
SSZ VI	MCT, MBT, MFT, MT, NAT, SAT, RT
SSZ VII	MF, GBF

6.5.2 Computation of Seismicity Parameters

To comprehend the overall seismicity of a seismogenic source, seismicity parameters are correlated to a particular earthquake recurrence model. The choice of the recurrence model is often dictated by the seismotectonic characteristics of the source and the availability of data. The Gutenberg-Richter's (1954) relation, which is one of the most widely used earthquake recurrence models, relates the rate of occurrence of an earthquake and its magnitude log-linearly for a particular seismic source. It is defined as

$$\log N(M) = a - bM \tag{6.22}$$

Where, N(M) is the cumulative frequency of occurrence of earthquakes of magnitude greater than M, and a and b are the seismicity parameters for a given source zone.

The recurrence relationship commonly used in PSHA application is defined with a lower threshold magnitude M_{min} and upper bound magnitude M_{max} to replicate the realistic scenario (Cornell and Vanmarcke, 1969). In the study, the constant seismicity model is used for this purpose and it is represented as

$$N(M) = N(M_{min}) \times \frac{e^{-\beta M} - e^{-\beta M_{max}}}{e^{-\beta M_{min}} - e^{-\beta M_{max}}} \tag{6.23}$$

Where, $N(M_{min})$ is the total number of earthquakes with magnitude greater than or equal to M_{min} and β is related to the parameter b as

$$\beta = b \ln 10 \tag{6.24}$$

The parameter β can be evaluated by using the maximum likelihood method (Utsu, 1965) and it is defined as

$$\beta = \frac{1}{\overline{M} - Mmin}; \tag{6.25}$$

$$\overline{M} = \frac{\sum M_i \times n_i}{N} \tag{6.26}$$

Where, N is total number of earthquakes and n_i is the number of earthquakes for different lower threshold magnitude M_{min} for different period of completeness.

As discussed in sec. 6.4.1, Entire Magnitude Range (EMR) method has been used to estimate M_{min} for each seismogenic source zone. The periods of completeness for different magnitude range have been estimated by Stepp (1972) method. In this present study, observed value of M_{max} from earthquake catalogue is used. The magnitude-completeness by EMR method for each sesimogenic source zone is shown in Fig. 6.2. The seismicity parameters for each zone used in this study are presented in Table 6.2.
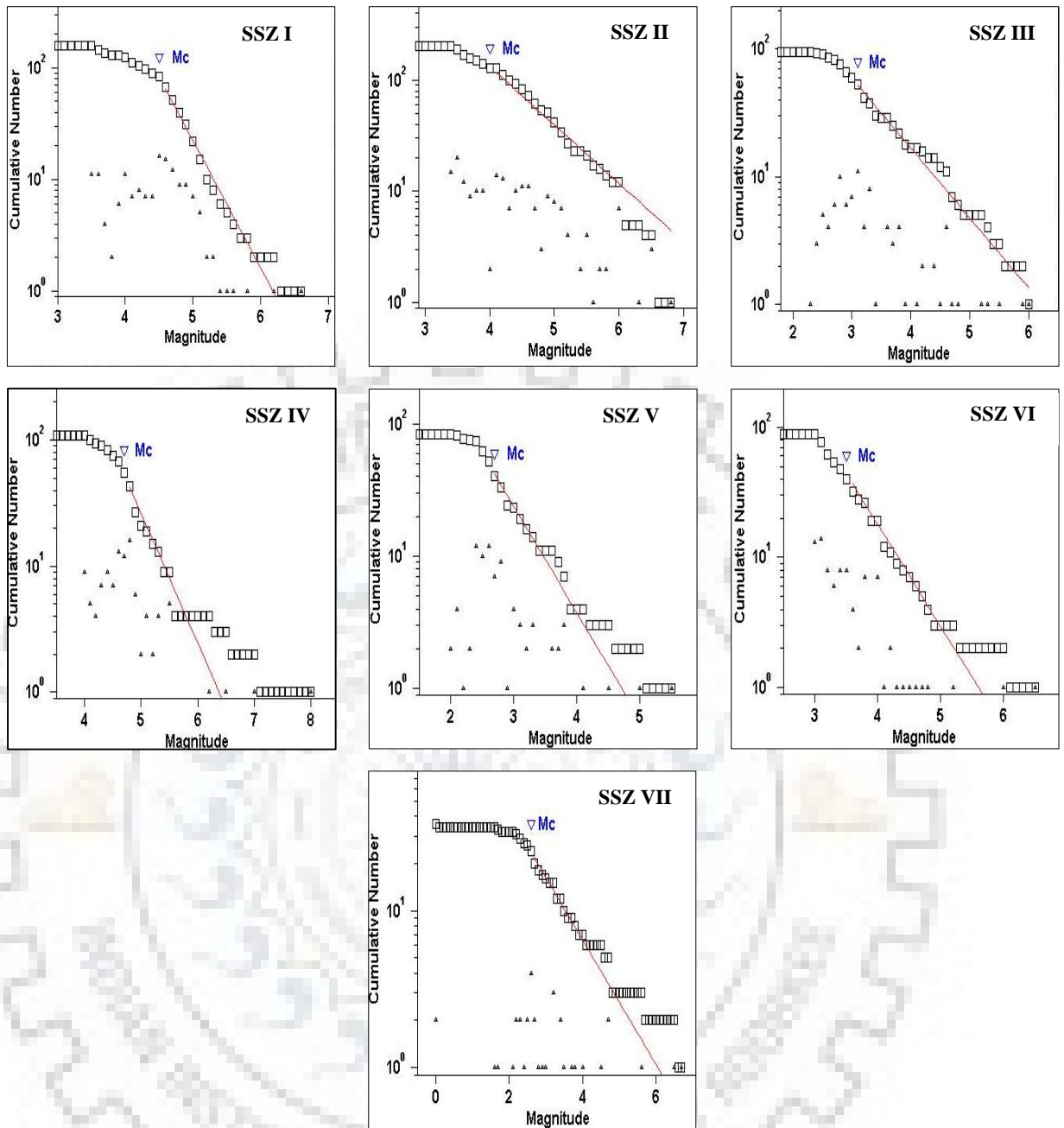
Fig. 6.2: Magnitude Completeness EMR Graphs for Seismogenic Sources

Table 6.2: Computed Seismicity Parameters for Seismogenic Sources

Seismogenic Source Zone	M_{max}	M_{min}	β	a	$N(M_{min})$
SSZ I	6.5	4.5	2.23	4.26	2.40
SSZ II	5.5	4.0	1.93	3.87	3.24
SSZ III	8.0	3.1	1.70	2.66	0.50
SSZ IV	6.6	4.7	2.20	4.08	2.51
SSZ V	6.0	2.7	2.00	2.67	0.15
SSZ VI	6.8	3.5	2.14	3.40	0.47
SSZ VII	6.7	2.6	1.49	1.83	0.17

6.6 Attenuation Relationship

Both deterministic and probabilistic seismic hazard assessments apply ground motion attenuation models. The main purpose of using attenuation relationships is to specify the expected level of ground shaking as a function of predictor variables describing earthquake source, path, and site effects. They were historically developed as equations that express ground motion as a function of magnitude and distance with occasional inclusion of other variables like type of faulting etc. However, with time, they have become more and more comprehensive and now-a-days most of the models include a set of primary variables and a set of secondary variables. Ground motion attenuation relationships are determined either empirically (where previously recorded ground motions are used) or theoretically (using seismological models to generate synthetic ground motions which incorporate source, site and path effect). Yet, there exists an overlap in both these methods since empirical approaches often fit data to a functional form (equation) suggested by theory and theoretical approaches often use empirical data to determine some parameters.

In this present study, attenuation relationship developed by Boore and Atkinson in 2008 (BA08) has been used. The attenuation relationships was developed as a function of earthquake magnitude, distance from source to site, local average shear-wave velocity, and fault type, for PGA (Peak Ground Acceleration), PGV (Peak Ground Velocity) and PSA (Pseudo Acceleration Spectra) at time periods between 0.01 and 10 sec. BA08 attenuation relationship is relatively simple and more user friendly compared to other complicated relationships. The basic empirical relationship is given as:

$$Y = F_M(M) + F_D(R_{JB}, M) + F_S(V_{S30}, R_{JB}, M) + \varepsilon\sigma\tau \tag{6.27}$$

Where, Y represents a ground motion intensity measure (PGA/PGV/PSA), F_M represents the magnitude scaling, F_D represents the distance function, F_S represents the site amplification, M denotes the moment magnitude, R_{JB} is Joyner- Boore distance defined as the closest distance to the surface projection of the fault (considered to be approximately equal to epicentral distance for events of M < 6), V_{S30} represents the inverse of the average shear wave slowness from the surface to a depth of 30 m and ε is the standard deviation of a predicted mean value of the Y. σ_τ is a period dependent variable and is computed as given as

$$\sigma_\tau = \sqrt{\sigma^2 + \tau^2} \tag{6.28}$$

Where, σ is the intra-event aleatory uncertainty and τ is the inter- event aleatory uncertainty.

The magnitude scaling relations (F_M) in Eq. 6.27 are given by

$$F_M(M) = \begin{cases} e_1U + e_2SS + e_3NS + e_4RS + e_5(M - M_h) + e_6(M - M_h)^2, & M \leq M_h \\ e_1U + e_2SS + e_3NS + e_4RS + e_7(M - M_h), & M > M_h \end{cases} \quad (6.29)$$

Where, U, SS, NS and RS are the dummy variables used to represent unspecified , strike-slip, normal –slip, and reverse-slip fault types, respectively, and M_h, the "hinge magnitude" for the shape of the magnitude scaling (the value of which is to be set during the analysis).

The distance function (F_D) in Eq. 6.27 is given by

$$F_D(R_{JB}, M) = [C_1 + C_2(M - M_{ref})] \ln(R/R_{ref}) + C_3(R - R_{ref}) \quad (6.30)$$

Where, $R = \sqrt{R_{JB}^2 + h^2}$ and C$_1$, C$_2$, C$_3$, M_{ref}, R_{ref} and h are the coefficients to be estimated in the analysis.

The site amplification factor (F$_S$) in Eq. 6.27 is given by

$$F_S = F_{LIN} + F_{NL} \quad (6.31)$$

Where, F_{LIN} and F_{NL} represent the linear and nonlinear terms, respectively.

The linear term (F_{LIN}) is given by:

$$F_{LIN} = b_{lin} \ln(V_{S30}/V_{ref}) \quad (6.32)$$

Where, b_{lin} represents a period-dependent coefficient, and V$_{ref}$ is the specified reference velocity (760 m/s) corresponding to National Earthquake Hazards Reduction Program (NEHRP) boundary site conditions.

The linear term is given by:

$$F_{NL} = \begin{cases} b_{nl} \ln(pga_{low}/0.1), & pga4nl \leq a_1 \\ \text{bnl} \ln\left(\frac{\text{pga}_{\text{low}}}{0.1}\right) + c \ln\left[\frac{\text{pga4nl}}{\text{a1}}\right]2 + d \ln\left[\frac{\text{pga4nl}}{\text{a1}}\right], & a1 \leq pga4nl \leq a2 \\ \text{bnl} \ln\left(\frac{\text{pga4nl}}{0.1}\right), & a2 < pga4nl \end{cases} \quad (6.32)$$

Where, a$_1$ (0.03g) and a$_2$ (0.09g) are used as threshold levels for linear and nonlinear amplification, respectively. pga_{low} (0.06g) is a variable used for transition between linear and nonlinear behaviours, and pga4nl is the predicted PGA in g for V$_{ref}$ = 760 m/s, with F$_S$ = 0 and $\varepsilon = 0$.

The attenuation relationship (BA08) was developed based on simplest formulation and regression analyses. The equation indicates a reliable description of recorded ground motion amplitudes for shallow crustal earthquakes in active tectonic regions over a wide range of magnitude and distances**.** The equation should be used for predictor variables in the magnitude range of 5-8 (for all fault types), R$_{JB}$<200 km and V$_{S30}$ range of 180-1300 m/s. These limiting

ranges are subjective estimates, based on the distributions of the recordings used to develop the equations. After careful examination of various attenuation relationships available for the study area, BA08 has been selected mainly due to the availability of required data for such analysis. The simpler form of the attenuation relationship also encourages the inclination towards its use.

6.7 Generation of Peak Ground Acceleration (PGA) Maps

The probabilistic frame work of seismic hazard assessment provides with the scope of examining the effects of an entire range of earthquake sizes (in terms of return periods) for any IM parameter. For this research work, PGA is selected as the output IM parameter as discussed in section 6.1. The final results of this PSHA study is presented as PGA maps (Fig. 6.3) for five earthquake scenarios with return periods of 10 years, 50 years, 100 years, 225 years and 475 years. The selection criteria for the specified earthquake scenarios are discussed in the next chapter. Each PGA map is further classified into five classes so as to facilitate their application in seismically induced LHZ mapping. Table 6.3 shows the minimum and maximum PGA obtained for the study area corresponding to each earthquake scenario.

Table 6.3: Minimum and Maximum PGA values for Different Earthquake Sizes

Earthquake Return Period	PGAmin (g)	PGAmax (g)
10	0.031	0.056
50	0.039	0.071
100	0.049	0.093
225	0.069	0.140
475	0.097	0.190
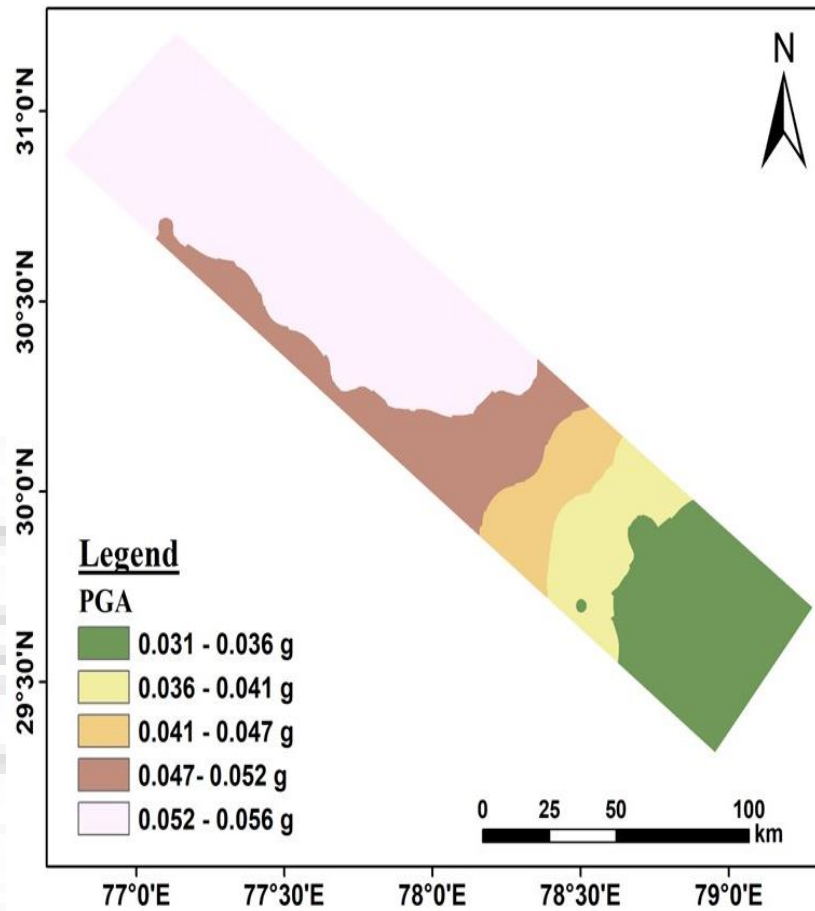
Fig. 6.3(a): PGA Map of the Study Area for Earthquake with Return Period of 10 Years
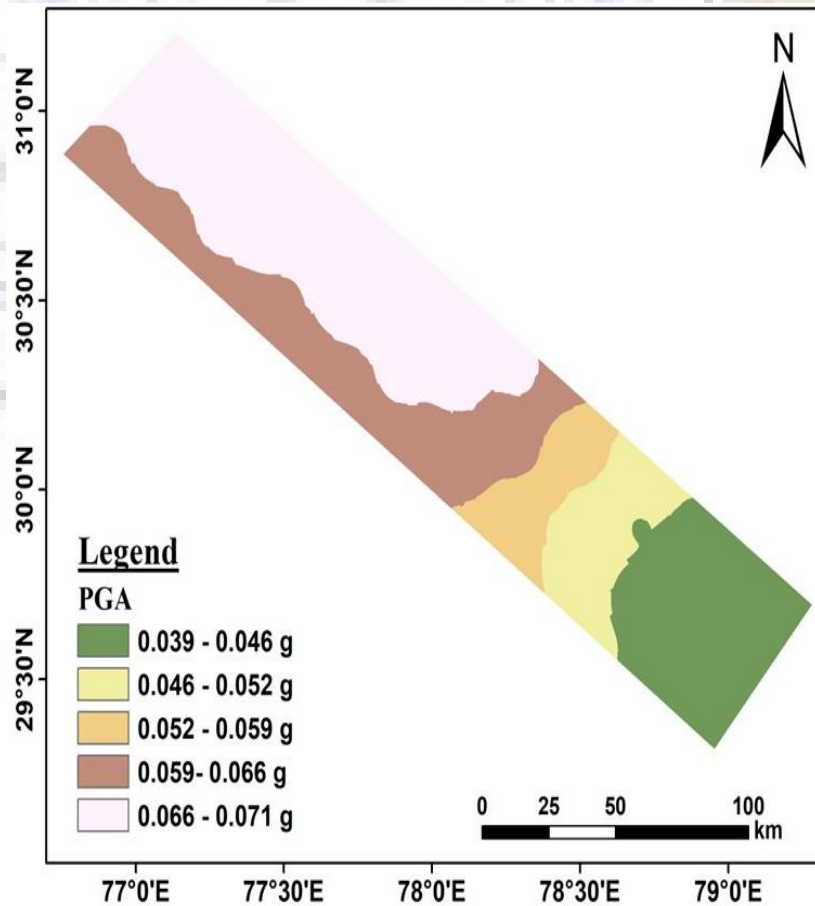
Fig. 6.3(b): PGA Map of the Study Area for Earthquake with Return Period of 50 Years
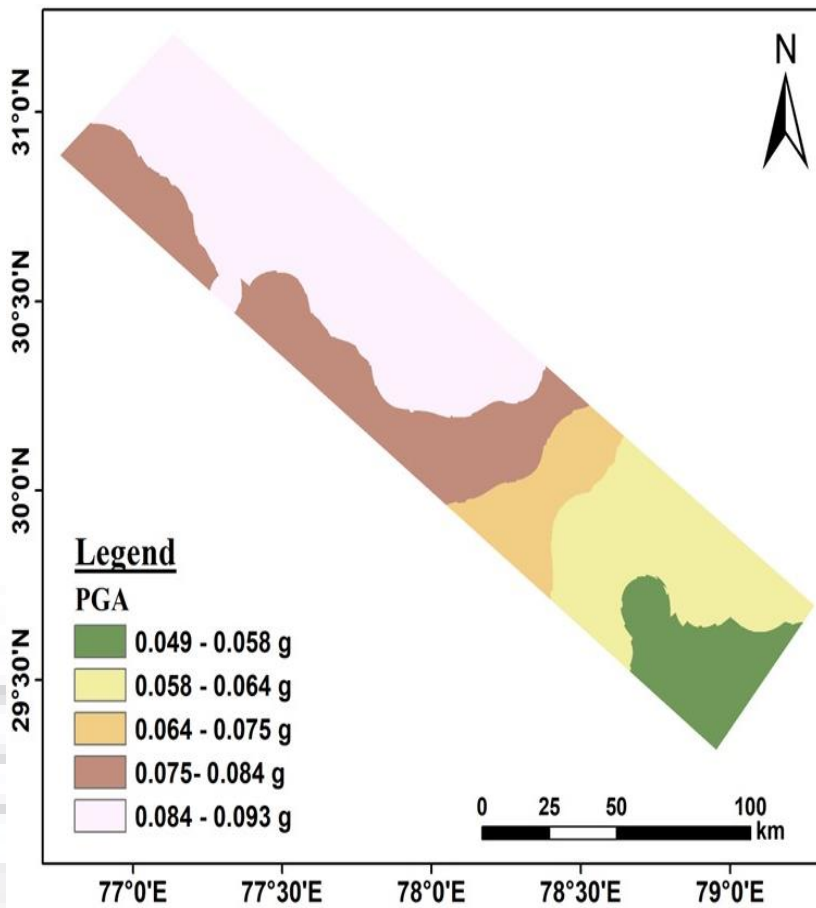
Fig. 6.3(c): PGA Map of the Study Area for Earthquake with Return Period of 100 Years
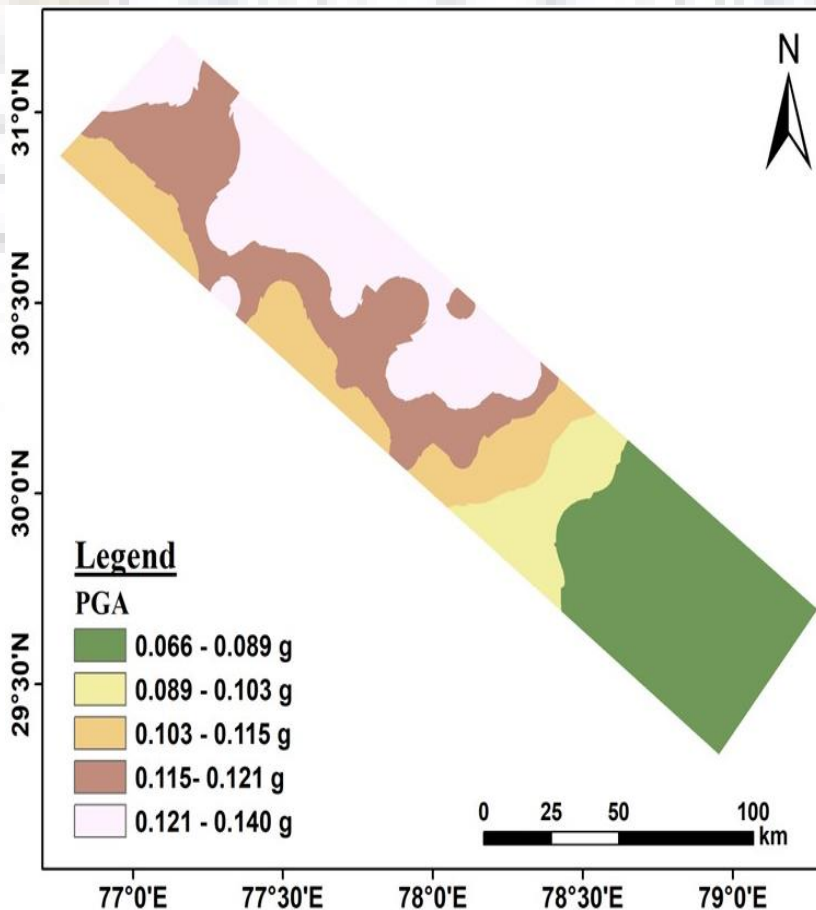
Fig. 6.3(d): PGA Map of the Study Area for Earthquake with Return Period of 225 Years
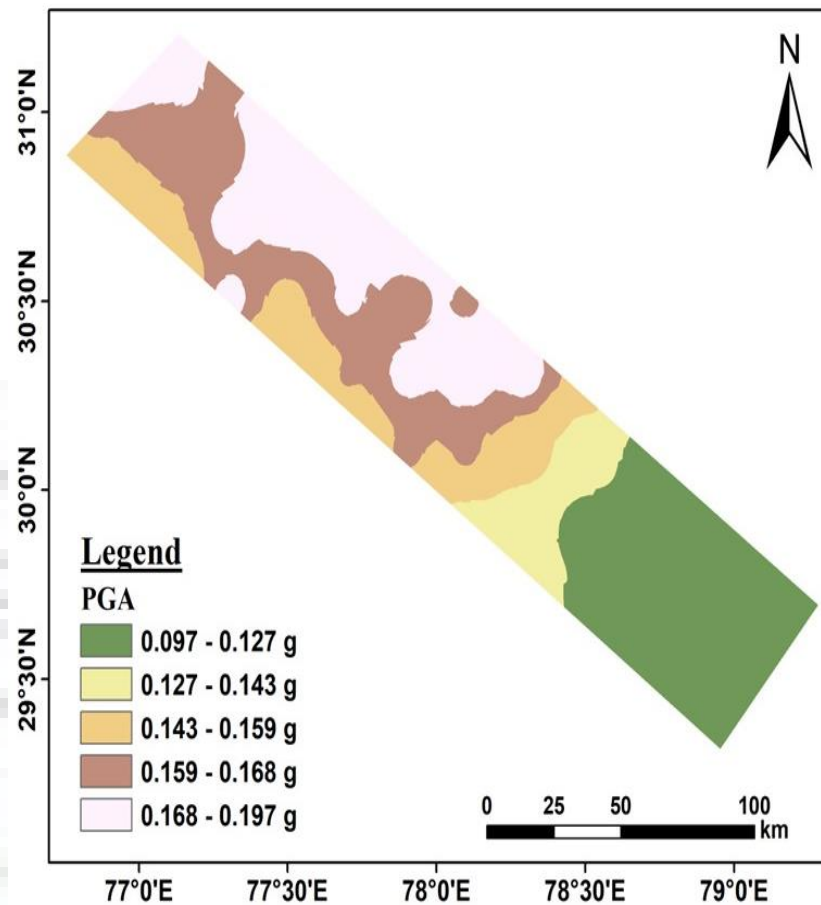
Fig. 6.3(e): PGA Map of the Study Area for Earthquake with Return Period of 475 Years

As per the current Indian code of practice, IS 1893 (Part-I): 2016 (BIS, 2016) the study area lies in zone IV of seismic hazard level. This corresponds to a PGA value of 0.24g for earthquake scenario with return period of 475 years. However, the present study estimates a PGA of 0.197g for the same earthquake scenario, which is slightly smaller (17%) than the code specified value. Bhatiya et al. (1999) reported a PGA value of 0.10g to 0.30g for 475 years return period in the Garhwal Himalaya region. Sharma and Dimri (2003) estimated a PGA of 0.35g for earthquake scenario with 225 years return period for the Dehradun area. Mahajan et al. (2010) estimated PGA for the study area as 0.25g for 475 years return period scenario. Nath et al. (2012) predicted a PGA value of 0.47g for 2475 years return period in and around Dehradun city. This roughly translate into a PGA of 0.23g for 475 years return period earthquake. Sitharam et al. (2013) predicted a PGA value of 0.21g for earthquake scenario of 475 years return period for Delhi region which is in close proximity of the study area. It is worth mentioning that these studies are carried out for a much bigger area considering the whole Himalaya as seismogenic source. Invariably, the seismicity parameters estimated by these studies are greater than that estimated in the research work. Taking that into account, the

PSHA results of the present research work seem to satisfy the lower bound values of PGA parameter suggested by the past studies.

6.8   Summary

A comprehensive seismic hazard analysis for the study area has been performed. The results of the PSHA study are presented in terms of PGA maps for five earthquake scenarios with return periods of 10 years, 50 years, 100 years, 225 years and 475 years. The maximum PGA estimated for the study area is 0.197g for an earthquake scenario with return period of 475 years. Detailed discussions on past PSHA studies in India, PSHA methodology, compilation and treatment of earthquake catalogue and selection of attenuation relationship are included in this chapter.

One of the key challenges in carrying out seismically induced landslide hazard zonation (LHZ) mapping is the selection of an appropriate earthquake motion and choice of a suitable parameter, through which an earthquake is described. The conventional studies mainly focus on correlating earthquake magnitude and spatial distribution of landslides in an area. However, applicability of such methods has been severely challenged due to the regional and characteristic biasness of the dataset used and the earthquake scenario (generally a single event) selected. Alternatively, earthquake generated strong ground motion scenarios, formed through the frame work of PSHA could be effectively used. This will increase the overall applicability of the input earthquake motion for carrying out seismically induced LHZ mapping.

LANDSLIDE HAZARD ZONATION (LHZ)
UNDER SEISMIC CONDITIONS

7.1 Preamble

In the Himalayan mountain chains, two of the most persistent natural hazards are its inherent seismicity and perennial slope failures. Landslides seem ubiquitous throughout the Himalayan arc, mainly due to its fragile geo-morphology and active tectonism. In this research work, the effect of seismicity on landslide occurrence and distribution has been examined for a part of lower Indian Himalaya. As discussed in the previous chapters, the main challenges in carrying out seismically induced landslide hazard zonation (LHZ) mapping are the lack of a globally recognized statistical technique and lack of consensus in selection of input earthquake parameter. In this chapter, inclusion and implications of probabilistic peak ground acceleration (PGA) parameter in LHZ mapping have been described. The chapter includes detail discussions on the impact of various scenario earthquakes in spatial distribution of hazard zones and quantify the role and effect of seismicity in LHZ mapping.

7.2 Multi-Hazard Integration

The most critical aspect of carrying out seismically induce LHZ mapping is coalescing the two hazards at a same scale i.e. integrating seismic and landslide hazard. The choice of an adopted method is governed by the aim and scope of the study. If the study is carried out post a major seismic event, distance magnitude frequency correlation becomes an automatic choice. The results of such studies will greatly improve the knowledge of the investigated terrain and its response during an earthquake shaking. The studies by Keefer (1984), Yin et al. (2008), Pareek et al. (2010) are some successful examples of such research. On the hindsight, such studies are limited to the particular region and ground motion only. For micro-scale, site specific LHZ studies, physical based models might represent a better estimate of co-seismic displacements, but the main disadvantage of such model is the complex and robust analytical processes associated with it. The selection of an appropriate statistical LHZ technique is a complicated decision as discussed in section 5.2, and as an alternative approach, map combination method has been considered for the research work to carry out seismically induced LHZ mapping of the study area. For that purpose, a landslide susceptibility scale has been developed (section 5.4), which is used to incorporate both static and seismic parameters in this study. Considering that the study is carried out at a regional level, the objective is here to

quantify the impact of earthquakes on spatial distribution of landslide hazard zones for different scenarios of strong ground motion.

The landslide susceptibility scale, developed for the study area, is based on the linguistic variables of perceived susceptibility level for a particular data layer. The linguistic variables are determined judging the concurrency of statistical correlations. Weights are then assigned to various thematic classes on a scale from 1 to 9; 9 being the highest represents very high level of susceptibility, whereas 1 represents very low susceptibility level. Five crisp values *viz.* 1, 3, 5, 7 and 9 are used to denote five distinct susceptibility levels, with the sporadic use intermediate values like 8 or 2 to denote H-VH or VL-L susceptibility levels. The same scale is applied to assess the perceived hazard level of earthquake thematic classes, albeit with little modifications.

7.2.1   Assignment of Weights ($W_{E,K}$) to PGA Thematic Classes

Assignment of weights to various thematic classes require classification of PGA maps, which is done following their probability distribution pattern. This is derived from the same procedure used to segment the LPI values (section 5.7 in chapter 5). However, for segmenting the LPI values, an optimization scheme has been suggested by Saha et al. (2005), where a positive, non-zero entity (m) is introduced to maximize the success rate of the LSZ map. As the PGA map is represented more discretely, and it is not possible to optimize the classification based on success rate, segmentation of PGA values is done on the basis of predicted mean and standard error. The probability distribution of PGA classes for earthquake scenario with 475 years return period is shown in Fig. 7.1 for illustrative purpose. The PGA classes for all earthquake scenarios follow an binomial distribution pattern as shown in Fig. 7.1. For the distribution pattern, values of predicted mean (μ_p) and predicted standard error (σ_p) have been calculated.   Each PGA map is then categorized into five classes at (μ_p-1.5σ_p), (μ_p-0.5σ_p), (μ_p+0.5σ_p) and (μ_p+1.5σ_p). The classified maps are shown in Fig. 6.3 (a-e) in chapter 6. The assignment of weights ($W_{E,K}$) to PGA thematic classes are shown in Table 7.1.
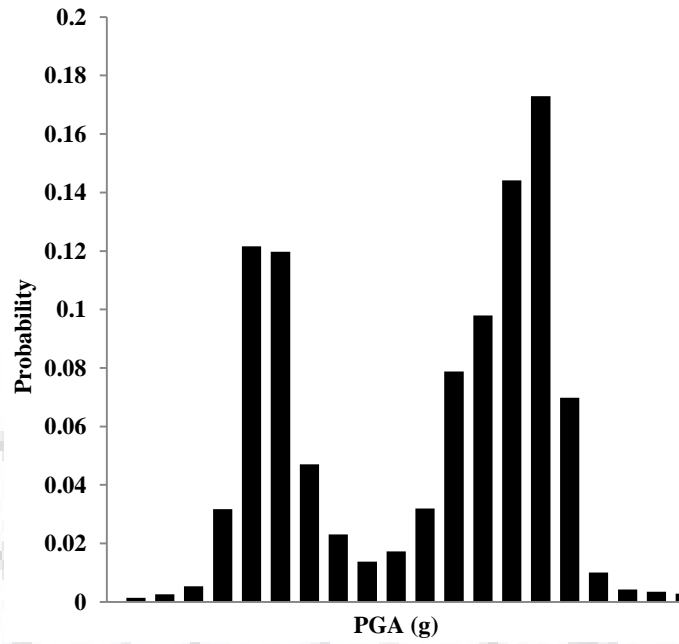
Fig. 7.1: Probability Distribution of PGA Classes for Earthquake Return Period 475 yrs

Table 7.1: Assignment of Weights ($W_{E,K}$) to PGA Thematic Classes

PGA Thematic Class	Perceived Hazard Level (Linguistic Variable)	$W_{E,K}$
Earthquake Return Period 10 Years		
0.031-0.036g	VL	1
0.036-0.041g	L	3
0.041-0.047g	M	5
0.047-0.052g	H	7
0.052-0.056g	VH	9
Earthquake Return Period 50 Years		
0.039-0.046g	VL	1
0.046-0.052g	L	3
0.052-0.059g	M	5
0.059-0.066g	H	7
0.066-0.071g	VH	9
Earthquake Return Period 100 Years		
0.049-0.058g	VL	1
0.058-0.064g	L	3
0.064-0.075g	M	5

0.075-0.084g	H	7
0.084-0.093g	VH	9
Earthquake Return Period 225 Years		
0.069-0.089g	VL	1
0.089-0.103g	L	3
0.103-0.115g	M	5
0.115-0.121g	H	7
0.121-0.140g	VH	9
Earthquake Return Period 475 Years		
0.097-0.127g	VL	1
0.127-0.143g	L	3
0.143-0.159g	M	5
0.159-0.168g	H	7
0.168-0.197g	VH	9

Once, the weights are assigned, it is important to check the consistency of the decision made. For that purpose, AHP is used. The methodology followed for checking the consistency through AHP has already been discussed in section 5.3 in chapter 5. Table 7.2 shows the decision matrix for weight assignment procedure.

Table 7.2: Decision Matrix for Weight Assignment Procedure to PGA Thematic Class

Perceived Hazard Level	VH	H	M	L	VL	Normalized Principle Eigen Vector
[1] Very High	1					0.5132
[2] High	1/3	1				0.2621
[3] Moderate	1/5	1/3	1			0.1295
[4] Low	1/7	1/5	1/3	1		0.0631
[5] Very Low	1/9	1/7	1/5	1/3	1	0.0334

For the above decision matrix 10 pair-wise comparisons are made. Solution of the decision matrix yields the following results:

$$N = 5, \qquad \lambda_{max} = 5.237, \qquad CI = 0.05925 \qquad RI = 1.12$$
$$CR = CI/RI = 0.0529$$

Since CR (5.29%) < 10%, the decision made i.e. weights assigned are consistent.

7.2.2 Assignment of Ranks ($R_{E,K}$) to Scenario Earthquakes

In this research work, probabilistic scenario earthquakes are considered as input seismicity parameter to carry out seismically induced LHZ mapping for a part of lower Himalayan belt. Use of probabilistic scenario earthquakes in LHZ mapping becomes popular since the early part of last decade (Nadim et al., 2006; Saygili and Rathje, 2009; Yin et al., 2009; Abou-Jaoude and Wartman, 2017). However, n such studies, only one scenario earthquake (generally earthquake with return period 475 years as a conservative approach) has been considered. It is understood that different earthquake sizes will have different effects on landslide occurrence and their spatial distribution in an area. Earthquakes with higher return periods (e.g. 225 years or 475 years) have lower probability of occurrence, but would generate bigger ground accelerations. On the other hand, smaller earthquakes with lower return periods (e.g. 10 years or 50 years) will impart much smaller ground accelerations, but have a higher frequency of occurrence. Thus, it is imperative to assign different ranks to different earthquake sizes corresponding o different return periods.

Assignment of ranks to various earthquake size is subjective as there is no literature available for the same. In this research work, a novel methodology has been suggested to assign ranks to various earthquake sizes to reduce the subjectivity in weight assignment process. It is based on the normalized PGA values for the entire range of earthquakes considered. The size dependent dynamic ranking of earthquake sizes will facilitate to comprehend the effect and implications of scenario earthquakes in LHZ mapping objectively.

Mathematically, Dynamic Ranking ($R_{E,K}$) of different earthquake sizes may be computed as follows:

$$R_{E,K} = \frac{a_k}{a_{max}} \times R_{max} \tag{7.1}$$

Where, $R_{E,K}$ and a_k denote the rank and maximum PGA value of earthquake size with k^{th} return period respectively, a_{max} represents the maximum PGA value corresponding to the largest earthquake size (475 years return period in this study) and R_{max} is the rank assigned to the largest earthquake size (the same 475 years return period earthquake).

Dynamic ranking system is developed to assign ranks to different scenario earthquakes (in terms of PGA values) objectively. Physically, it denotes the relative importance of a specified earthquake size (measured in terms of return period) in the entire range of earthquakes considered for the LHZ mapping.

There are three steps in calculation of dynamic ranks: (i) selection of the *"worst case"* scenario earthquake corresponding to which maximum PGA (a_{max}) is recorded, (ii) assignment

of the highest earthquake rank to the "worst case" scenario earthquake and (iii) calculation of normalized PGA factors (a_k/a_{max}). In this present study, maximum PGA is recorded corresponding to the earthquake with return period of 475 years, which is, therefore; considered as the *"worst case"* scenario. The perceived hazard level for this scenario earthquake is very high and therefore, it is assigned the highest rank of 9 using the same LSZ scale (section 5.3) developed for the study area. Now the dynamic rankings ($R_{E,K}$), which will signify the relative importance of other earthquake scenarios, have been estimated w.r.to the assigned rank of the *"worst case"* scenario earthquake (i.e. Rank of 9 for earthquake with return period 475 years). In the present study, it is proposed that the maximum value of normalized PGA factor ($a_k/a_{max}=$ 1) would be assigned to the biggest earthquake size (highest return period) considered in a particular study and 475 years is a reasonable approximation. But if one is to consider an earthquake with greater return period, say 1000 years, the value of a_k/a_{max} becomes 1 for 1000 years return period. In that case the dynamic ranking 475 years will be changed and should be calculated accordingly. For PSHA method, earthquake with highest return period will be the *"worst case"* scenario automatically and that should be given the highest rank. It is also to be noted that for different seismotectonic environment, the dynamic ranks will be different. Since the present study is carried out for seismically hyper-active Himalayan belt, the earthquake with return period 475 years is assigned a rank of 9. Assignment of rank to the *"worst case"* earthquake scenario would be based on the professional experience and judgment of the investigators. Thus, the proposed method could quantify the relative importance of various earthquake sizes effectively. Table 7.3 illustrates the results.

Table 7.3: Calculation of Dynamic Rankings ($R_{E, K}$)

Earthquake Return Period	Normalized PGA Factor	Highest Rank	Dynamic Rank	Perceived Hazard Level
10 yrs	0.284	-----	2.5	VL
50 yrs	0.359	-----	3.5	L
100 yrs	0.475	-----	4.5	M
225 yrs	0.711	-----	6.5	H
475 yrs	1.000	9	9	VH

From table 7.3, it is observed that, earthquakes with lower return periods (10 years and 50 years) have dynamic rankings of 2.5 and 3.5 respectively. This implies that their effects on LHZ mapping is compatible to static causative parameters like slope aspect and LULC patterns. Their perceived level of hazard is thus considered to be very low and low. In other words, there is little possibility of these earthquakes rendering widespread landslides in the study area. On

the other hand, earthquakes with higher return periods (225 years and 475 years) have relative importance as high as geological units and slope angle and are likely to produce landslides of multitude proportion. The computed dynamic ranks ($R_{E,K}$) and weights ($W_{E,K}$) are used to calculate the dynamic landslide potential (LPI_D) of the study area.

7.3 Landslide Hazard Zonation under Seismic Condition: Results and Discussion

7.3.1 Computation of Dynamic Landslide Potential Index (LPI_D)

Assuming that $R_{E,K}$ and $W_{E,K}$ denote the dynamic rank and weight of an earthquake size with k^{th} return period respectively, the dynamic Landslide Potential Index (LPI_D) is computed as

$$LPI_D = \sum_{i=1}^{n} \sum_{j=1}^{m} R_i \times W_{i,j} + \sum_{k=1}^{l} R_{E,k} \times W_{E,K} \qquad (7.2)$$

The dynamic LPI_D in Eq (7.2) is an extension of Eq. (5.1) in chapter 5. It has two parts: the static part as given by Eq. (1) and the size-dependent dynamic part. Introducing a dummy variable, a combined equation may be derived as

$$LPI_E = \sum_{i=1}^{n} \sum_{j=1}^{m} R_i \times W_{i,j} + \left(\sum_{k=1}^{l} R_{E,k} \times W_{E,K} \right) \delta(e) \qquad (7.3)$$

Where, $\delta(e) = \begin{cases} 1, & \text{if seismcity is considered} \\ 0, & \text{otherwise} \end{cases}$

If seismicity is not considered, LPI_D will become static and will be computed as given by Eq. (5.1). The computed LPI_D values are used to generate seismically induced LHZ maps for the study area.

7.3.2 Generation of Seismically Induced LHZ Maps for the Study Area

The computed dynamic ranks and weights of scenario earthquakes are appended to each PGA map in Arc-GIS 10.6. The reclassified maps are then numerically integrated with LSZ_Static (Fig. 5.2, chapter 5) to generate five dynamic LHZ map of the study area, which are shown in Fig. 7.2 (a-e). The dynamic LHZ maps are denoted as LHZ_D10, LHZ_D50, LHZ_D100, LHZ_D225 and LHZ_D475 respectively, corresponding to the scenario earthquake used. Each map is categorized into five distinct zones of landslide hazard. As the research work envisages to quantify the impact of scenario earthquakes on the spatial distribution of landslides in the study area, the dynamic LHZ maps are further analyzed w.r.t. the LSZ_Static map prepared for the study area. Therefore, the class boundaries of LSZ_Static map has been retained for segmenting the LPI_D values of each map.
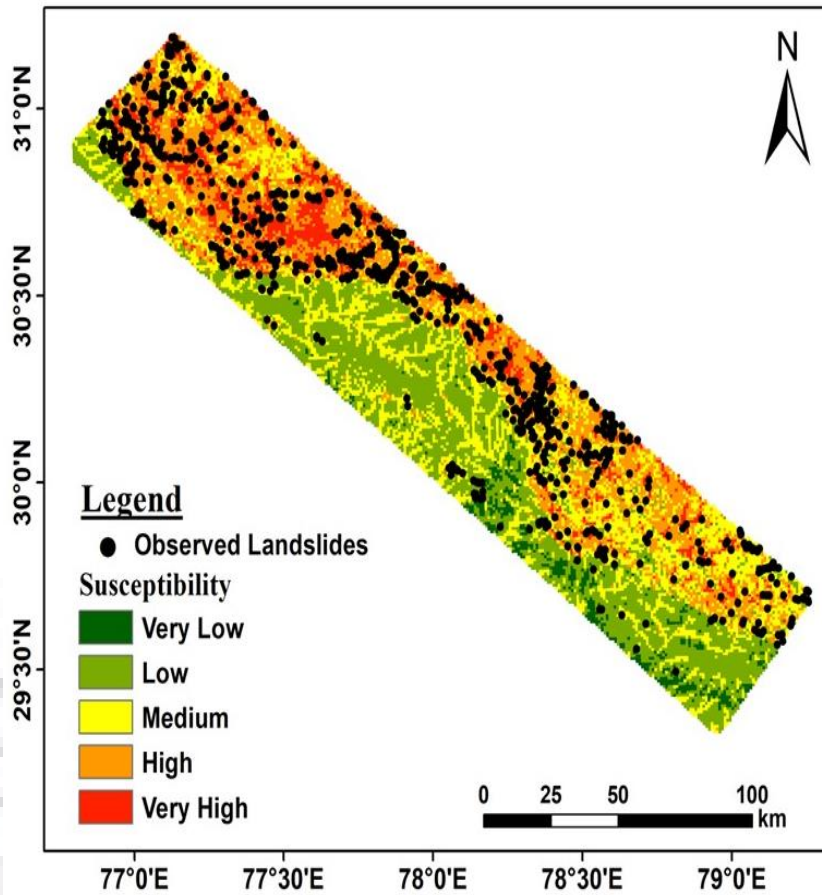
Fig. 7.2(a): Seismically Induced LHZ Map for Earthquake Return Period 10 Years
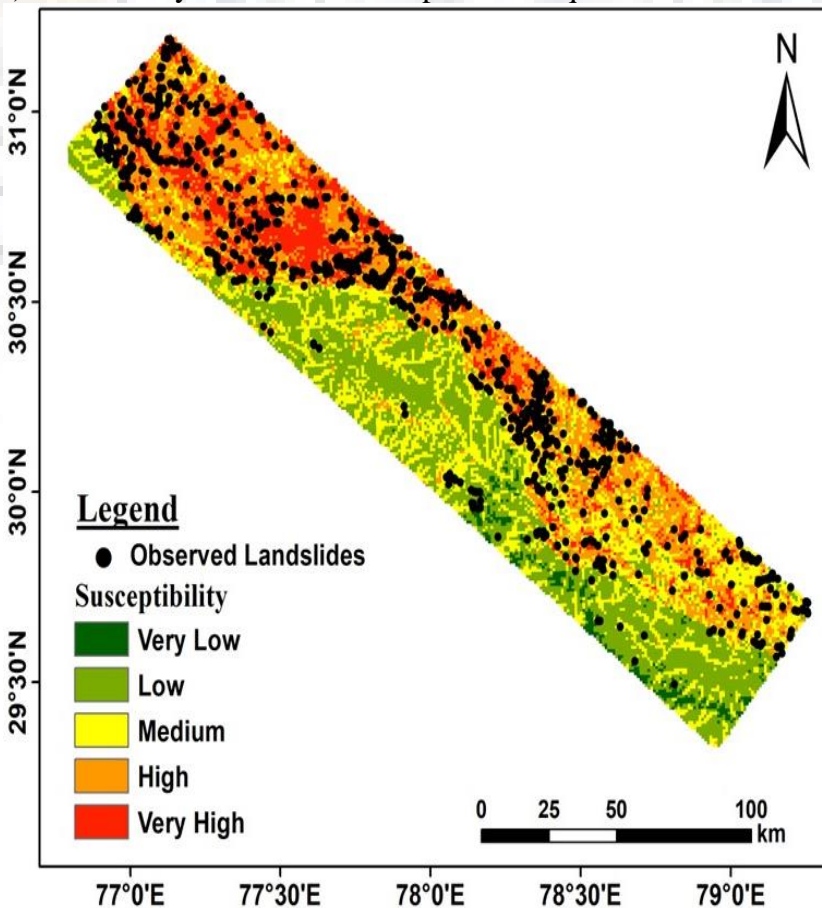
Fig. 7.2(b): Seismically Induced LHZ Map for Earthquake Return Period 50 Years
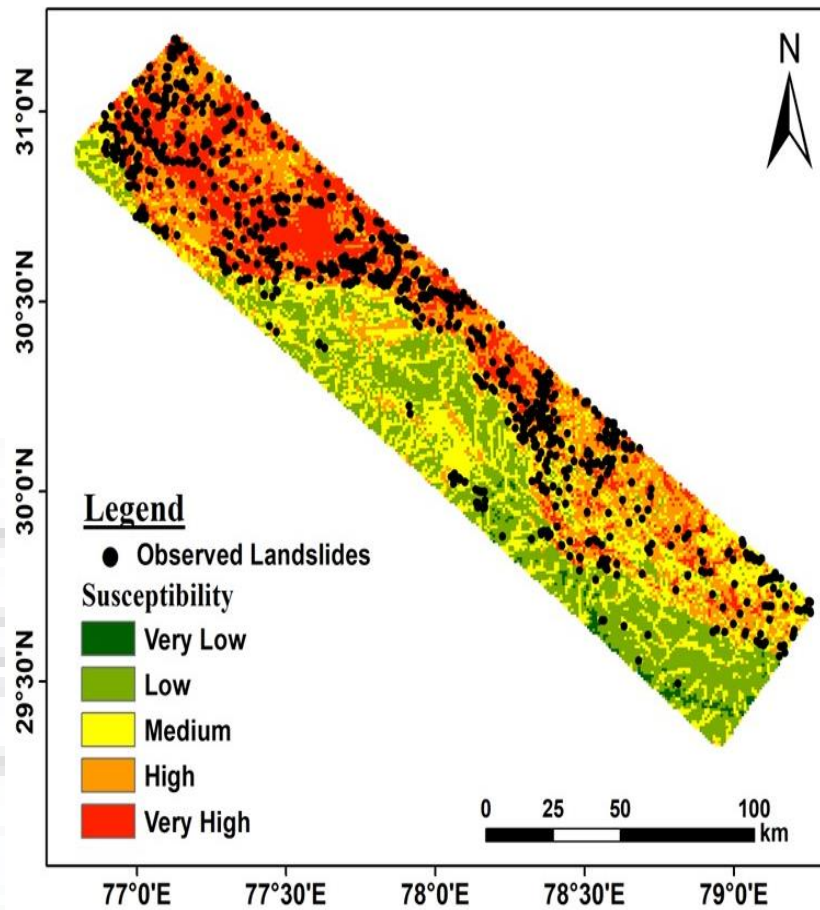
Fig. 7.2(c): Seismically Induced LHZ Map for Earthquake Return Period 100 Years
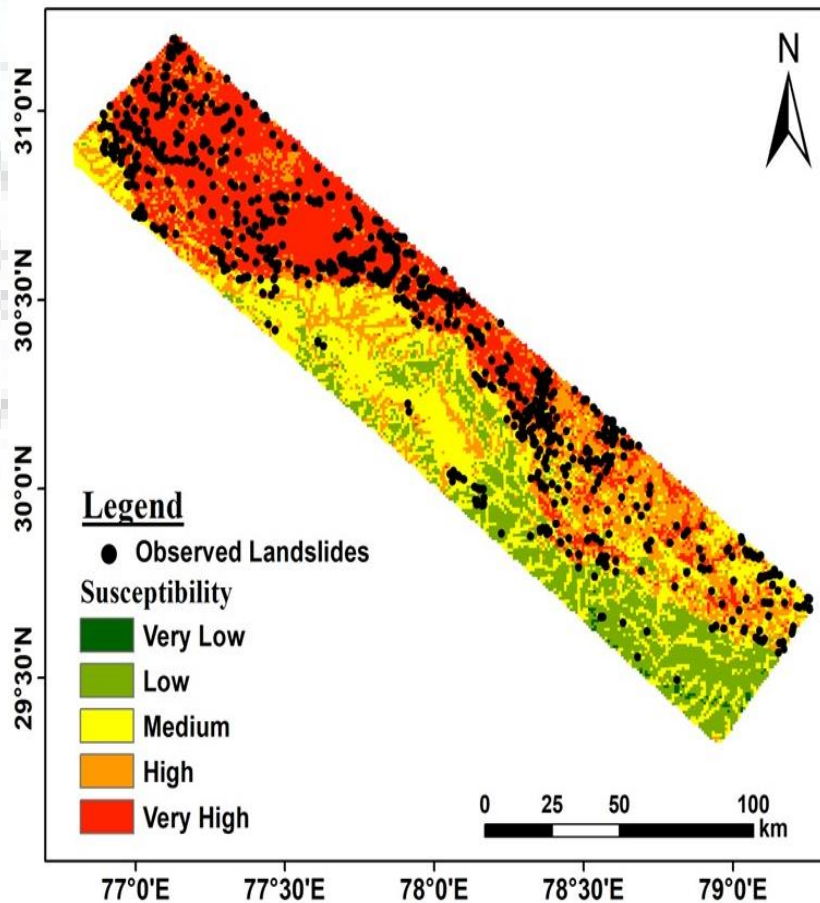
Fig. 7.2(d): Seismically Induced LHZ Map for Earthquake Return Period 225 Years
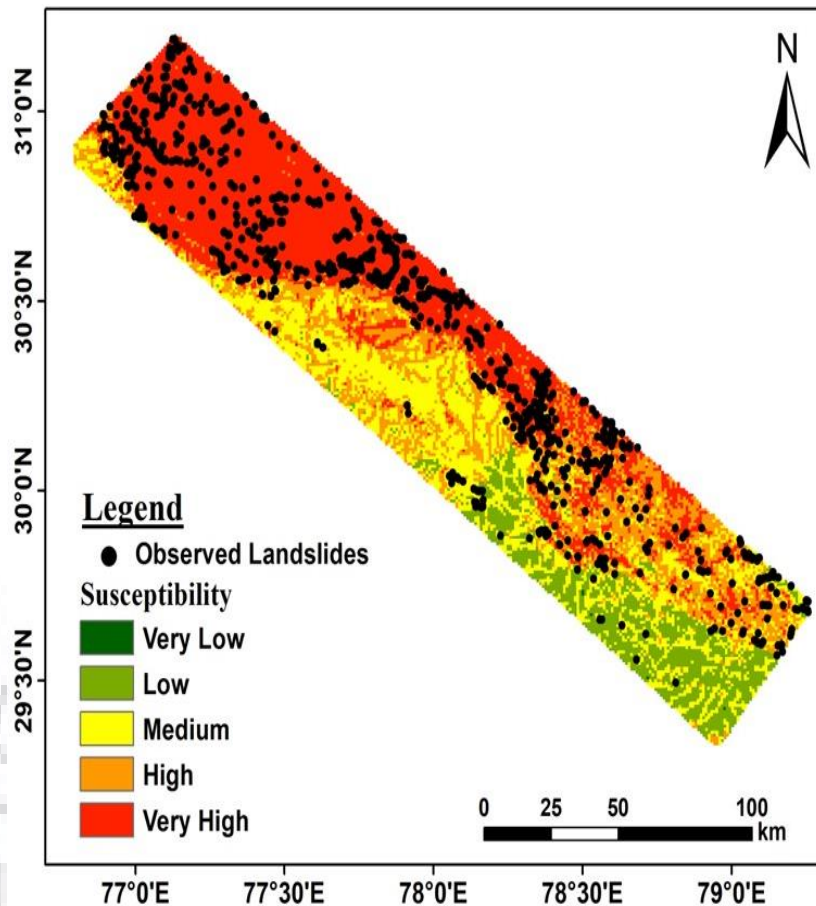
Fig. 7.2(e): Seismically Induced LHZ Map for Earthquake Return Period 475 Years

From Fig. 7.2 (a-e), it is clearly evident that with the change in input scenario earthquakes, there has been a distinct change in the area of the landslide hazard zones. More precisely, the changes indicate a paradigm shift of zones from very low (VL) towards very (VH) as the size of the input earthquake increases (i.e. higher earthquake return periods). To quantify these observations, the dynamic LHZ maps are compared with the LSZ_ Static map. For that purpose, ratios of zone area to the total area for all the maps are calculated. Table 7.4 shows the results of this comparisons.

Table 7.4: Change in Area Ratio of LHZ maps

Maps	Ratio of the Area of the Zone to the Total Study Area				
	VL	L	M	H	VH
LSZ_Static	0.17	0.24	0.27	0.23	0.09
LHZ_D10	0.08	0.21	0.25	0.27	0.20
LHZ_D50	0.06	0.19	0.24	0.27	0.25
LHZ_D100	0.04	0.18	0.23	0.26	0.28
LHZ_D225	0.02	0.13	0.20	0.25	0.40
LHZ_D475	0.01	0.08	0.17	0.23	0.51

Table 7.4 quantifies the impact of earthquake scenarios in LHZ mapping in terms of zone areas. Under the static landslide causative parameters, the Very Low (VL) and Low (L) susceptibility zones constitute almost 41% of the total area, whereas the corresponding figure for High (H) and Very High (VH) zones is 32%. With the input of earthquake scenario of 10 years return period, there is a perceivable increment (~14%) in the area of H and VH hazard zones, which is compensated in terms of shrinkage of areas of VL and L hazard zones (~12%) and Moderate (M) hazard zone (~2%). The same trend is observed for all earthquake scenarios, where areas of H and VH hazard zones increase significantly as the size of input earthquake scenario increases. For earthquake scenarios with return periods 225 years and 475 years, the figures are even more astounding, when approximately 40% and 51% of the study area fall under the zone of VH landslide hazard respectively. The same has been shown in Fig. 7.3, where the percentage change of different LHZ area for different earthquake return periods are plotted.
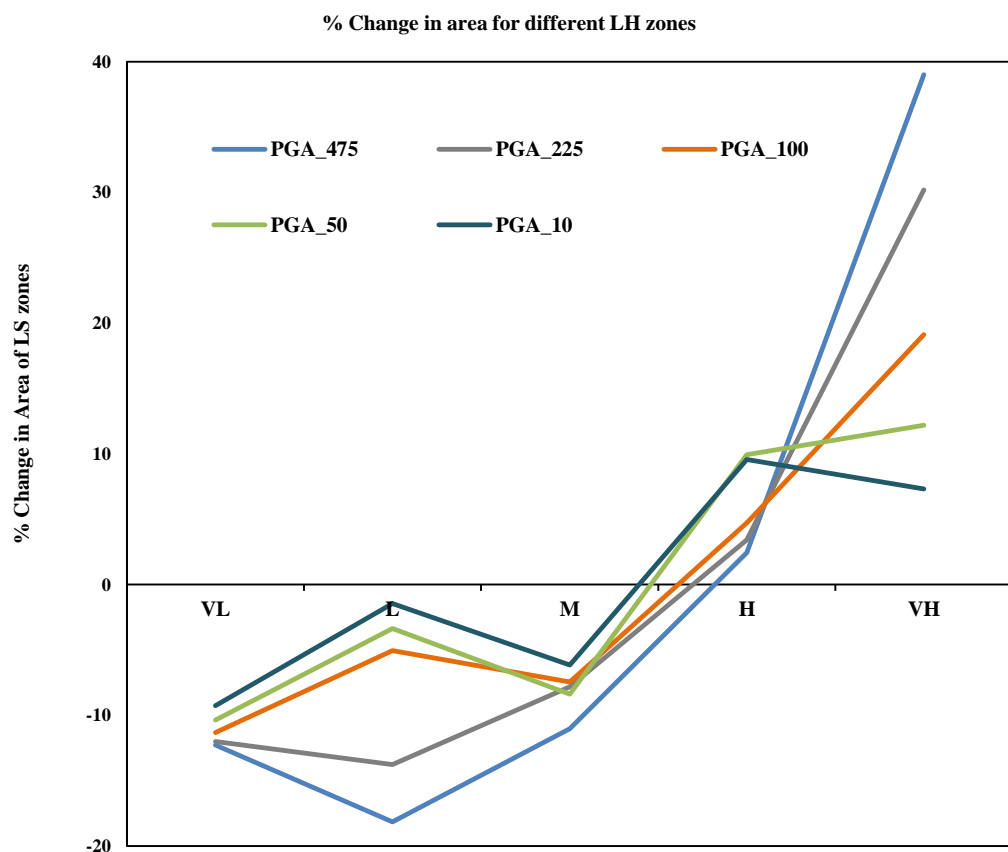
Fig. 7.3: Percentage change of different LHZ area for different earthquake return periods

From Fig. 7.3, there is a clear indication that the trend of percentage change of LHZ area, for all earthquake scenarios, remains the same but with varying degree. The change is most prominent when earthquake scenario with return period 475 years has been considered. Table 7.5 shows the percentage change of zone areas when scenario earthquake with return

period 475 years is integrated with LSZ_Static map. Even for dynamic LHZ maps under different seismic scenarios, the effect of earthquake size is palpable, which is shown in table 7.6. Compared to LHZ_D10, there is a significant area gain of VH zone in LHZ_D475 (~31%). The negative values in tables 7.5 and 7.6 indicate the shrinkage of zone areas.

Table 7.5: Percentage Change of LHZ Area from LHZ_Static to LHZ_D475

Landslide Hazard Zone	% change in LHZ area
VL	-15.50
L	-14.11
M	-9.64
H	-0.39
VH	39.64

Table 7.6: Percentage Change of LHZ Area from LHZ_D10 to LHZ_D475

Landslide Hazard Zone	% change in LHZ area
VL	-7.04
L	-12.75
M	-7.57
H	-4.50
VH	31.86

It will be also interesting to examine the change in LPI_D values under seismic conditions. For that purpose, maximum and minimum LPI values of LSZ_ Static map and dynamic LHZ maps are compared and percentage change in LPI (ΔLPI) values are calculated. It is given in table 7.7 below:

Table 7.7: Percentage Change of LPI values under different conditions

LHZ Map	LPI_{min}	LPI_{max}	%Δ LPI_{min}	%ΔLPI_{max}
LSZ_Static	80.0	338.0	-----	-----
LHZ_D10	97.5	355.5	0.125	0.096
LHZ_D50	106.0	362.5	0.185	0.135
LHZ_D100	108.0	369.5	0.199	0.173
LHZ_D225	112.0	383.5	0.228	0.250
LHZ_D475	117.0	401.0	0.263	0.346

Table 7.7 indicates that under seismic conditions, both LPI_{min} and LPI_{max} increase rapidly as the size of the input earthquake increases. For smaller earthquakes with return periods less than

100 years, the increment of LPI_{min} is more than that of LPI_{max}. This in turn would cause lesser area falling in H and VH hazard zones (for earthquake scenario with 100 years return period, ΔA is 22% for H and VH zones, and for 50 years return period the corresponding figure is 15%). This shows that in such scenarios, static landslide causative factors still play the dominant role. However, for earthquake scenarios of 225 years and 475 years, the increase in both LPI_{min} and LPI_{max} is significant (LPI_{max} increases by 25% and 34.6% respectively). Such increment transpires to a paradigm shift in LHZ mapping, especially for the zones of H and VH landslide hazard (ΔA is 31% and 42% for VH zone for the two earthquake scenarios respectively). The present study, thus suggests that seismicity has major impact on landslide hazard zonation mapping for moderate to great earthquakes.

For a more generalized comprehension of variation of ΔLPI_{min} and ΔLPI_{max} with different earthquake return periods for the lower Himalayan belt, a chart has been prepared, which is presented in Fig. 7.4.
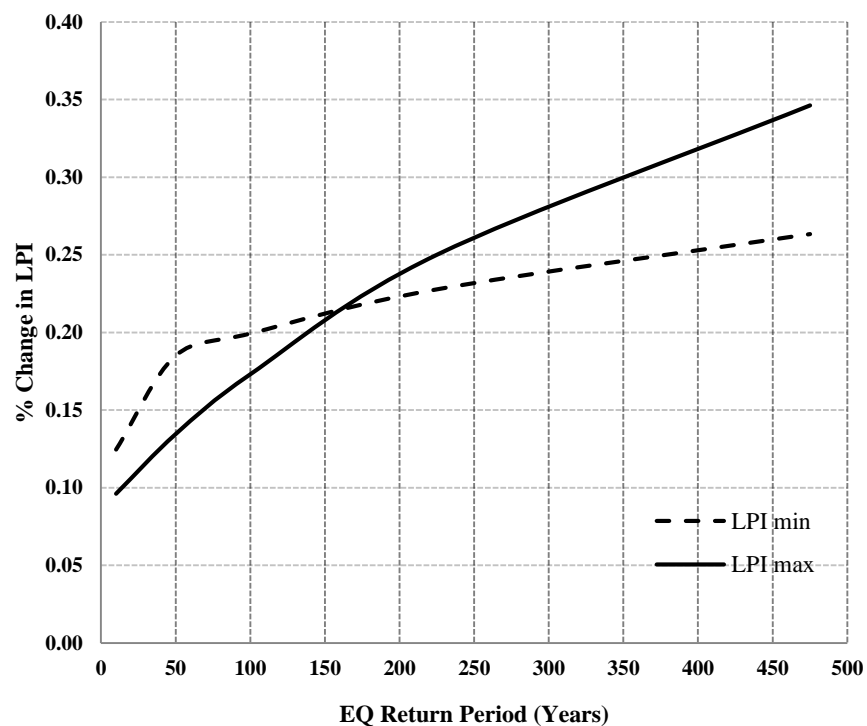
Fig. 7.4: Percentage Change of LPI_{min} and LPI_{max} for Different Earthquake Return Periods

Consideration of a single scenario earthquake may not be adequate enough to understand the impact and implications of strong ground motion on landslide occurrence and their spatial distribution. While the landslides produced by moderate to great earthquakes are of catastrophic nature, one should not neglect the effect of smaller earthquake sizes in LHZ mapping. Smaller microseisms having very low stress drops (Sharma and Wason, 1994) prevent the slope from natural arresting of failures and this in turn increases the overall

landslide susceptibility manifold. In that context, five scenario earthquakes with varying sizes have been considered in the present research work, so as to quantify the role and effect of seismicity in LHZ mapping.

7.4   Summary

This chapter includes preparation of landslide hazard zonation maps under seismic condition for the study area. Map combination method of LHZ mapping has been used. Five scenario earthquakes generated through PSHA, have been used as landslide triggering parameters, along with the identified preparatory causative parameters. The ranks of different scenario earthquakes are calculated based on normalize PGA values to reduce the subjectivity of weight assignment procedure. The PGA thematic maps are classified statistically, and weights of different thematic classes are assigned using the prepared landslide susceptibility scale developed for the study area. The ranks and weights of scenario earthquakes are numerically integrated with static causative parameters to generate the dynamic LPI (LPI_D), which is used to produce the final seismically induced LHZ maps for the study area. The dynamic maps are further analyzed w.r.t. LSZ_Static to quantify the role and effect of scenario earthquakes in LHZ mapping. The study shows that as input earthquake size increases, the existing landslide potential increases exponentially. This transpires to a paradigm shift in hazard zones from low towards very high. For earthquake scenario with return period 475 years, the increment in LPI_{max} is 34%, due to which   almost 51% of the study area falls in the zone of very high landslide hazard. The study, thus, concluded that in case of moderate to great earthquakes, seismicity assumes a bigger role in landslide occurrence and their spatial distribution in lower Himalayan belt.

8.1   Preamble

The research work presents seismically induced landslide hazard zonation for the lower Himalayan belt, which is a major scientific challenge and a pressing societal imperative owing to its socio-economic aspects. Seismically induced landslides have drawn worldwide attention mainly due to increasing awareness and pressure of urbanization in mountain regions. Earthquakes are globally recognized as one of the most important landslide triggering factors, especially in seismically active mountain chains like the Himalaya. The frequent recurrence of landslide events in the Himalayan arc has been a major burden to the long term economic growth of the country, and necessitates accurate and updated landslide hazard zoning for this region. An accurate LHZ map incorporating both static and seismic factors, will be of immense practical use for decision based future land-use planning.

In this research work, eight static landslide preparatory causative parameters have been identified for the study area. Seismicity in terms of probabilistic scenario earthquakes, is considered as landslide triggering parameter. Different techniques of landslide hazard zonation have been explored. An integrated landslide susceptibility scale has been developed statistically, which is used for multi hazard integration. The research work discusses at length the challenges in carrying out seismically induced LHZ for the Himalayan belt and suggested a novel approach that considers probabilistically generated scenario earthquakes as the seismicity factor. A detailed seismic hazard assessment within the probabilistic frame-work has been put forth for the study area. The results of PSHA have been discussed in terms of peak ground acceleration parameter, which is further incorporated in LHZ mapping. The research wok presents five dynamic LHZ maps for the study area, which are analyzed to quantify the role and effect of seismicity in landslide occurrence and their spatial distribution in lower Indian Himalaya. This chapter includes the final conclusions of the present research and scope for future work.

8.2   Conclusions

The main conclusions of the research work can be briefly summarized as follows:

i.   In seismically active mountainous regions, the transitory earth stresses, generated due to spatial and temporal variation of plate tectonics, are one of the strongest geodetic forces forming and controlling the landscapes in an area. Thus consideration of the seismicity as a landslide triggering factor becomes a priority in LHZ mapping for seismically active areas

like the Himalaya. The perceived levels of landslide hazard follow the trends of isoseismal maps in lower Indian Himalaya. In case of moderate to large earthquakes, seismicity becomes the major landslide causative parameter in the study area.

ii. The pattern of landslide distribution depicts a strong inverse correlation with the tectonic features present in the study area.

iii. Consideration of seismicity in LHZ mapping is a difficult task mainly due to lack of a globally recognized methodology for earthquake induced LHZ mapping, paucity of earthquake induced landslide inventory, rarity of an extreme earthquake event along with its regional and characteristic biasness, and complexity in collating various static landslide causative parameters with earthquake characteristics. As an alternative, strong ground motion parameter (PGA values) derived from PSHA studies may be used as a landslide triggering factor for LHZ mapping.

iv. Use of probabilistic PGA values in LHZ mapping has two distinct advantages: it allows incorporation of (a) seismotectonic environment (in terms of faults and lineaments) of a bigger area (R~300 km) which would likely to produce earthquakes in the study area and (b) recorded past seismicity. The PGA values are representative of an entire range of earthquake sizes, rather than a single event. Thus, characteristic biasness of a single event could be avoided which in turn increases the applicability of the whole method. Consideration of an entire range of earthquake sizes quantifies the impact and implications of seismicity in landslide hazard comprehensively.

Based on the results, the present study concludes that inclusion of earthquake scenarios will enhance the understanding of landslide hazard with a more pragmatic vision, especially for seismically active mountainous belts like the Himalaya.

The primary outputs of the research work can be enumerated in the following points:

i. A comprehensive landslide inventory of 1062 existing landslides has been prepared for the study area. The prepared inventory provides information on the location of existing landslides, their slope morphometry, geological units, elevation profiles and distance from major geological discontinuities. The inventory identifies the areas with higher landslide potential and forms the backbone for statistical analyses of LSZ mapping.

ii. The results of the study quantify a strong inverse relationship between landslide distribution and fault distance for the lower Himalaya, which is presented in the form of an equation. The equation will be useful for other micro/meso-scale city specific landslide studies in the Himalayan region, where it is difficult to create a relevant dataset correlating fault distance and landslide distribution.

iii. An accurate and updated LSZ map has been prepared for the study area considering 8 static landslide causative parameters. An integrated LSZ scale correlating three statistical methods has been developed for the lower Himalayan region. The LSZ scale is used to incorporate seismic parameters in LHZ mapping. The study concludes that developed scale produces the best LSZ map for the study area in terms of both spatial and statistical success of the predictive maps. The final LSZ map shows the current level of landslide susceptibility for different prominent cities of Uttarakhand and Himachal Pradesh states of India.

iv. Detailed probabilistic seismic hazard assessment of the study area has been carried out. The results of the PSHA study is discussed in terms of peak ground acceleration maps for five different scenario earthquakes. The scenario earthquakes are considered as landslide triggering factor for analyzing seismically induced landslide hazard in the study area.

v. The research work presents a quantitative approach to assign ranks of different scenario earthquakes objectively. Five dynamic LHZ maps under seismic conditions have been prepared for the study area. Analyses of the dynamic LHZ maps quantify the role and impact of earthquakes on LHZ mapping in terms of percentage change in LPI (landslide potential index) and zone areas. The results of the research work shows that in case of moderate to great earthquakes, there is paradigm shift of hazard zones from very low towards very high.

8.3   Scope for Future Work

The success of any landslide hazard zonation endeavour is dependent on the quality of the dataset used and selection of mapping technique. In the present study, data has been collected from various sources, which are then collated in GIS environment. There is always scope to improve the quality of remote sensing data in terms of their spatial resolution and source to ground aspects. The selection of a particular mapping technique is dictated by the aim and scope of the study and the size and quality of dataset. The present research work incorporates both qualitative and statistical techniques of landslide hazard zonation. In future, machine learning techniques may be applied to such huge data set to establish correlation between various landslide causative parameters and landslide occurrence. The research work identifies zones of high landslide potential in the study area. Quantification of co-seismic displacements for some selected active landslides may be undertaken as a next phase of the study. Also, finite element based models may be applied to estimate the expected displacements of some selected active landslides in the study area.

BIBLIOGRAPHY

1. Abou-Jaoude, G., Wartman, J. 2017.Landslide hazard mapping for Lebanon. In *Proceedings of the 19th International Conference on Soil Mechanics and Geotechnical Engineering*, Seoul.

2. Akgun, A., Sezer, E.A., Nefeslioglu, H.A., Gokceoglu, C. and Pradhan, B., 2012. An easy-to-use MATLAB program (MamLand) for the assessment of landslide susceptibility using a Mamdani fuzzy algorithm. *Computers & Geosciences*, *38*(1), pp.23-34.

3. Aleotti, P., Chowdhury, R. 1999. Landslide hazard assessment: summary review and new perspectives. *Bulletin of Engineering Geology and the environment*, 58(1), 21-44.

4. Alexander, E.D., 1989. Urban landslides. *Progress in Physical Geography,*13, 157–191.

5. Alexander, D. E. 1995. A survey of the field of natural hazards and disaster studies. In *Proceedings of Geographical information systems in assessing natural hazards*, Dordrecht.

6. Anbalagan, R., Singh, B. 1996. Landslide hazard and risk assessment mapping of mountainous terrains—a case study from Kumaun Himalaya, India. *Engineering Geology*, 43(4), 237-246.

7. Anbalagan, R. 1992. Landslide hazard evaluation and zonation mapping in mountainous terrain. *Engineering Geology*, 32(4), 269-277.

8. Anbalagan, R., Kumar, R., Lakshmanan, K., Parida, S., Neethu, S. 2015. Landslide hazard zonation mapping using frequency ratio and fuzzy logic approach, a case study of Lachung Valley, Sikkim. *Geo-environmental Disasters*, 2(1), 6.

9. Arnone, E., Francipane, A., Scarbaci, A., Puglisi, C. and Noto, L.V., 2016. Effect of raster resolution and polygon-conversion algorithm on landslide susceptibility mapping. *Environmental modelling & software*, *84*, pp.467-481.

10. Arora, M. K., Das Gupta, A. S., Gupta, R. P. 2004. An artificial neural network approach for landslide hazard zonation in the Bhagirathi (Ganga) Valley, Himalayas. *International Journal of Remote Sensing*, 25(3), 559-572.

11. Atkinson, P. M., Massari, R. 1998. Generalised linear modelling of susceptibility to landsliding in the central Apennines, Italy. *Computers & Geosciences*, 24(4), 373-385.

12. Ayalew, L., Yamagishi, H. 2005. The application of GIS-based logistic regression for landslide susceptibility mapping in the Kakuda-Yahiko Mountains, Central Japan. *Geomorphology*, 65, 15-31.

13. Bandooni, S. K., Laishram, M. 2018. Eco-environmental vulnerability evaluation in Mountain regions using Remote Sensing and Geographical Information System: A case study of Pasol Gad Watershed of Garhwal Himalaya, India. *International Journal of*

Geological and Environmental Engineering,12(1), 1-8.

14. Basu, S., Nigam, N., C., 1977. Seismic risk analysis of Indian peninsula. *In Proceedings of sixth world conference on earthquake engineering, New Delhi* (Vol. 1, pp. 782-788).

15. Behera, K.K., Rocky, W. S. 2010. Landslide hazard zonation of a two km wide strip along NH-44 between Shillong and Khliehriat, East Khasi hills district, Meghalaya. *Rec. Geological Survey of India*, 143(4), 54-56.

16. Bhatia, S. C., Ravi Kumar, M., Gupta, H. K. 1999. A probabilistic seismic hazard map of India and adjoining region. *Annali di Geofisica,* 42(6):1153–1166.

17. Bhattacharya, A., Arora, M. K., Sharma, M. L., Vöge, M., Bhasin, R. 2014. Surface displacement estimation using space-borne SAR interferometry in a small portion along Himalayan Frontal Fault. *Optics and Lasers in Engineering*, 53, 164-178.

18. Bhattacharya, A., Mukherjee, K., Kuri, M., Vöge, M., Sharma, M. L., Arora, M. K., Bhasin, R. K. 2015. Potential of SAR intensity tracking technique to estimate displacement rate in a landslide-prone area in Haridwar region, India. *Natural Hazards*, 79(3), 2101-2121.

19. Bhattacharya, A., Sharma, M. L., Arora, M. K. 2012. Surface displacement estimation along Himalayan frontal fault using differential SAR interferometry. *Natural Hazards*, 64(2), 1105-1123.

20. Bhattacharya, A., Arora, M.K. and Sharma, M.L., 2012. Usefulness of synthetic aperture radar (SAR) interferometry for digital elevation model (DEM) generation and estimation of land surface displacement in Jharia coal field area. *Geocarto International*, *27*(1), pp.57-77.

21. Bhattacharya, A., Vöge, M., Arora, M.K., Sharma, M.L. and Bhasin, R.K., 2013. Surface displacement estimation using multi-temporal SAR interferometry in a seismically active region of the Himalaya. *Georisk: Assessment and Management of Risk for Engineered Systems and Geohazards*, *7*(3), pp.184-197.

22. Bhasin, R., Kaynia, A. M. 2004. Static and dynamic simulation of a 700-m high rock slope in western Norway. Engineering Geology, 71(3-4), 213-226.

23. Bhasin, R., Grimstad, E., Larsen, J.O., Dhawan, A.K., Singh, R., Verma, S.K. and Venkatachalam, K., 2002. Landslide hazards and mitigation measures at Gangtok, Sikkim Himalaya. *Engineering Geology*, *64*(4), pp.351-368.

24. Bird, J.F. and Bommer, J.J., 2004. Earthquake losses due to ground failure. *Engineering geology*, *75*(2), pp.147-179.

25. Blong, R. J. 1973. A numerical classification of selected landslides of the debris slide-avalanche-flow type. *Engineering Geology*, 7(2), 99-114.

26. Bosi, C. 1984. Considerazioni e propostemetodologichesullaelaborazione di carte di

stabilita. *Geol. Appl*. Ed Idrogeol, 13, 246-281.

27. Brabb, E. E. 1985. Innovative approaches to landslide hazard and risk mapping. In *Proceedings of International Landslide Symposium*, Toronto, 17-22.

28. Brabb, E. E. 1995. The San Mateo County California GIS project for predicting the consequences of hazardous geologic processes. In *Proceedings of Geographical Information Systems in Assessing Natural Hazards*, Dordrecht.

29. Brabb, E.E., Pampeyan, E.H., Bonilla, M.G., 1978. Landslide susceptibility in San Mateo County, California. *US Geological Survey Misc. Field Studies Map, MF-360, map at 1:62,500 scale*.

30. BUREAU OF INDIAN STANDARDS, 1998. Preparation of landslide hazards zonation maps in mountainous terrains, guidelines, part-2 Macrozonation: ICS 07.040. IS 4496 (part-2).

31. Bui, D.T., Pradhan, B., Lofman, O., Revhaug, I. and Dick, O.B., 2012. Spatial prediction of landslide hazards in Hoa Binh province (Vietnam): a comparative assessment of the efficacy of evidential belief functions and fuzzy logic models. *Catena*, *96*, pp.28-40.

32. Bui, D.T., Pradhan, B., Lofman, O., Revhaug, I. and Dick, O.B., 2012. Landslide susceptibility mapping at Hoa Binh province (Vietnam) using an adaptive neuro-fuzzy inference system and GIS. *Computers & Geosciences*, *45*, pp.199-211.

33. Bui, D.T., Tuan, T.A., Klempe, H., Pradhan, B. and Revhaug, I., 2016. Spatial prediction models for shallow landslide hazards: a comparative assessment of the efficacy of support vector machines, artificial neural networks, kernel logistic regression, and logistic model tree. *Landslides*, *13*(2), pp.361-378.

34. Canuti, P., Rodolfi, G. 1979. Dinamicamorfologica di unambientesoggetto a fenomenifranosi e ad intensaattivitàagricola. Tip. R. Coppini & C.

35. Carrara, A. 1989, June. Landslide hazard mapping by statistical methods: a" black-box" model approach. In *Proceedings ofInternational Workshop on Natural Disasters in European–Mediterranean Countries*, Perugia, 27, 427-445.

36. Carrara, A. 1983. Multivariate models for landslide hazard evaluation. *Journal of the International Association for Mathematical Geology*, 15(3), 403-426.

37. Carrara, A. 1988. Drainage and divide networks derived from high-fidelity digital terrain models. In *Quantitative analysis of mineral and energy resources*, Dordrecht.

38. Carrara, A. 1993. Potentials and pitfalls of GIS technology in assessing natural hazards. In *Proceedings of Geographical Information Systems in Assessing Natural Hazards*, Perugia.

39. Carrara, A., Cardinali, M., Detti, R., Guzzetti, F., Pasqui, V., Reichenbach, P. 1991. GIS

techniques and statistical models in evaluating landslide hazard. *Earth Surface Processes and Landforms*, 16(5), 427-445.

40. Chakraborty, I., Ghosh, S., Bhattacharya, D., Bora, A. 2011. Earthquake induced landslides in the Sikkim-Darjeeling Himalayas— An aftermath of the 18th September 2011 Sikkim earthquake. *Geological Survey of India*, Kolkata.

41. Champati Ray, P. K. 2005. Geoinformatics and its application in Geosciences. *Journal of Earth System Science and Environment*, 2(1), 4-12.

42. Champati Ray, P. K., Lakhera, R. C. 2004, September. Landslide Hazards in India. In *Proceedings ofAsian Workshop on Regional Capacity Enhancement for Landslide Mitigation (RECLAIM)*, Bangkok.

43. Champati-ray, P., K., Dimri, S., Lakhera, R., C., Sati, S., 2007. Fuzzy-based method for landslide hazard assessment in active seismic zone of Himalaya. Landslides 4(2): 101-109.

44. Chauhan, G.S., Nainwal H.C., Vikram Gupta 2017. Stability analysis of rock cut slopes along the Minas road between Ichhari Dam and Minas Bridge, Tons valley, Garhwal Himalaya. *Himalayan Geology*, 39(1), 68-84

45. Chauhan, S., Sharma, M., Arora, M. K. 2010. Landslide susceptibility zonation of the Chamoli region, Garhwal Himalayas, using logistic regression model. *Landslides*, 7(4), 411-423.

46. Chen, W., Panahi, M. and Pourghasemi, H.R., 2017. Performance evaluation of GIS-based new ensemble data mining techniques of adaptive neuro-fuzzy inference system (ANFIS) with genetic algorithm (GA), differential evolution (DE), and particle swarm optimization (PSO) for landslide spatial modelling. *Catena*, *157*, pp.310-324.

47. Chigira, M., Wang, W. N., Furuya, T., Kamai, T. 2003. Geological causes and geomorphological precursors of the Tsaoling landslide triggered by the 1999 Chi-Chi Earthquake, Taiwan. *Engineering Geology*, 68, 259 – 273.

48. Chigira, M., Yagi, H. 2006. Geological and geomorphological characteristics of landslides triggered by the 2004 Mid Niigta prefecture earthquake in Japan. *Engineering Geology*, 82(4), 202-221.

49. Chorley RJ, Schumm SA, Sugden DE 1984. *Geomorphology*. Methuen, London, 607 pp

50. Chaudhary, C. and Sharma, M.L., 2017. Probabilistic models for earthquakes with large return periods in Himalaya region. *Pure and Applied Geophysics*, *174*(12), pp.4313-4327.

51. Choudhary, C. and Sharma, M.L., 2018. Global strain rates in western to central Himalayas and their implications in seismic hazard assessment. *Natural Hazards*, *94*(3), pp.1211-1224.

52. Choudhary, C., and Sharma, M.L. (2018). Implications of Constant Seismicity and Constant Moment Release models on seismic hazard, *16th Symposium on Earthquake Engineering*

53. Chung, C. F. 1998. Three Bayesian prediction models for landslide hazard. In *Proceedings of International Association for Mathematical Geology 1998 Annual Meeting*.

54. Chung, C. J. F., Fabbri, A. G. 1999. Probabilistic prediction models for landslide hazard mapping. *Photogrammetric Engineering and Remote Sensing*, 65(12), 1389-1399.

55. Clerici, A., Perego, S., Tellini, C., Vescovi, P. 2002. A procedure for landslide susceptibility zonation by the conditional analysis method. *Geomorphology*, 48(4), 349-364.

56. Collins, B.D. and Jibson, R.W., 2015. Assessment of existing and potential landslide hazards resulting from the April 25, 2015 Gorkha, Nepal earthquake sequence (No. 2015-1142). *US Geological Survey*.

57. Cornell, C.A. and Vanmarcke, E.H., 1969, January. The major influences on seismic risk. In *Proceedings of the fourth world conference on earthquake engineering* (Vol. 1, pp. 69-83).

58. Crozier, M. J. 1984. Field assessment of slope instability. *Slope Instability*, 103-142.

59. Crozier, M. J. 1986. *Landslides: causes, consequences and environment*. Croom Helm, London.

60. Cruden, D. M. 1991. A simple definition of a landslide. *Bulletin of Engineering Geology and the Environment*, 43(1), 27-29.

61. Cruden, D.M., Fell, R., 1997. Landslide Risk Assessment. In *Proceedings International Workshop on Landslide Risk Assessment*, Honolulu.

62. Das, I., Sahoo, S., van Westen, C., Stein, A., Hack, R., 2010. Landslide susceptibility assessment using logistic regression and its comparison with a rock mass classification system, along a road section in the northern Himalayas (India). *Geomorphology*, 114(4), 627-637.

63. Das, R., Wason, H.R., Gonzalez, G., Sharma, M.L., Choudhury, D., Lindholm, C., Roy, N., Salazar, P 2018. Earthquake magnitude conversion problem, *Bulletin of the Seismological Society of America*, 108 (4), 1995-2007.

64. Das, S., Gupta, I.D. and Gupta, V.K., 2006. A probabilistic seismic hazard analysis of northeast India. *Earthquake Spectra*, *22*(1), pp.1-27.

65. Desai, S., S., Choudhury, D., 2014. Spatial variation of probabilistic seismic hazard for Mumbai and surrounding region. *Natural hazards*, 71(3), 1873-1898.

66. Dickson, M.E. and Perry, G.L., 2016. Identifying the controls on coastal cliff landslides using machine-learning approaches. *Environmental Modelling & Software*, *76*, pp.117-127.

67. Dietrich, W. E., Reiss, R., Hsu, M. L., Montgomery, D. R. 1995. A process-based model for colluvial soil depth and shallow landsliding using digital elevation data. *Hydrological Processes*, 9(3-4), 383-400.

68. Dikau, R., Brunsden, D., Schrott, L., Ibsen, M.L., 1996. *Landslide recognition. Identification, movements and causes*, Wiley, England, p 251.

69. Dimri, S., Lakhera, R. C., Sati, S. 2007. Fuzzy-based method for landslide hazard assessment in active seismic zone of Himalaya. *Landslides*, 4(2), 101-109.

70. Dunning, S. A., Mitchell, W. A., Rosser, N. J., Petley, D. N. 2007. The Hattian Bala rock avalanche and associated landslides triggered by the Kashmir Earthquake of 8 October 2005. *Engineering Geology*, 93(3-4), 130-144.

71. Ercanoglu, M., Gokceoglu, C. 2004. Use of fuzzy relations to produce landslide susceptibility map of a landslide prone area (West Black Sea Region, Turkey). *Engineering Geology*, 75(3-4), 229-250.

72. Espizua, L. E., Bengochea, J. D. 2002. Landslide hazard and risk zonation mapping in the Rio Grande Basin, Central Andes of Mendoza, Argentina. *Mountain Research and Development*, 22(2), 177-185.

73. Fell, R. 1994. Landslide risk assessment and acceptable risk. *Canadian Geotechnical Journal*, 31(2), 261-272.

74. Felicísimo, Á.M., Cuartero, A., Remondo, J. and Quirós, E., 2013. Mapping landslide susceptibility with logistic regression, multiple adaptive regression splines, classification and regression trees, and maximum entropy methods: a comparative study. *Landslides*, *10*(2), pp.175-189.

75. France. Bureau de rechercheygéologiquesetminières, Meneroud, J. P., & Calvino, A. 1976. Carte ZERMOS, zones exposées à des risquesliés aux mouvements du sol et du sous-sol 1: 25,000: région de la MoyenneVésubie (Alpes-Maritimes). Bureau de recherches géologiquesetminières.

76. Gorsevski, P. V., Gessler, P. E., Jankowski, P. 2003. Integrating a fuzzy k-means classification and a Bayesian approach for spatial prediction of landslide hazard. *Journal of Geographical Systems*, 5(3), 223-251.

77. Gorum, T., Korup, O., van Westen, C.J., van der Meijde, M., Xu, C. and van der Meer, F.D., 2014. Why so few? Landslides triggered by the 2002 Denali earthquake, Alaska. *Quaternary Science Reviews*, *95*, pp.80-94.

78. GSI, 2005. Modified BIS guidelines for macro level landslide hazard zonation mapping.

Geological Survey of India.

79. Gubin, I.E., 1993, November. Seismic zoning of Indian peninsula. In *DOKLADY AKADEMII NAUK* (Vol. 333, No. 2, pp. 218-219). 39 DIMITROVA UL., 113095 MOSCOW, RUSSIA: MEZHDUNARODNAYA KNIGA.

80. Guha, S., K., 1962. Seismic regionalization of India. *In Proceedings of Second Symposium on Earthquake Engineering* (pp. 191-207).

81. Gupta, R. P., Saha, A. K., Arora, M. K., Kumar, A. 1999. Landslide hazard zonation in a part of the Bhagirathi Valley. Garhwal Himalyas, using integrated remote sensing–GIS, *Himalayan Geology*, 20, 71-85.

82. Gupta, R. P., Joshi, B. C. 1990. Landslide hazard zoning using the GIS approach—a case study from the Ramganga catchment, Himalayas. *Engineering Geology*, 28(1-2), 119-131.

83. Gupta, V., Bhasin, R. K., Kaynia, A. M., Kumar, V., Saini, A. S., Tandon, R. S., Pabst, T. 2016. Finite element analysis of failed slope by shear strength reduction technique: a case study for Surabhi Resort Landslide, Mussoorie township, Garhwal Himalaya. *Geomatics, Natural Hazards and Risk*, 7(5), 1677-1690.

84. Gupta, V., Mahajan, A.K., Thakur V.C. 2015. A study on landslides triggered during Sikkim Earthquake of September 18, 2011. *Himalayan Geology*, 36 (1), 81-90

85. Gupta, V., Nautiyal, H., Kumar, V., Jamir, I., Tandon, R. S. 2016. Landslide hazards around Uttarkashi township, Garhwal Himalaya, after the tragic flash flood in June 2013. *Natural Hazards*, 80(3), 1689-1707.

86. Guzzetti, F., Carrara, A., Cardinali, M., Reichenbach, P. 1999. Landslide hazard evaluation: a review of current techniques and their application in a multi-scale study, Central Italy. *Geomorphology*, 31(1), 181-216.

87. Hancox, G.T., Perrin, N.D. and Dellow, G.D., 2002. Recent studies of historical earthquake-induced landsliding, ground damage, and MM intensity in New Zealand. *Bulletin-New Zealand Society forEarthquake Engineering*, *35*(2), pp.59-95.

88. Hansen, A. 1984. Landslide hazard analysis. *Slope Instability*, 523-602.

89. Hansen, A., Franks, C. A. M., Kirk, P. A., Brimicombe, A. J., Tung, F. 1995. Application of GIS to hazard assessment, with particular reference to landslides in Hong Kong. In *Proceedings of Geographical Information Systems in Assessing Natural Hazards*, Dordrecht.

90. Harp, E.L., Jibson, R.W. 1996. Landslides triggered by the 1994 Northridge, California earthquake. *Bulletin of the Seismological Society of America*, 86, 319 – 332.

91. Hearn, G. J. 1995. Landslide and erosion hazard mapping at Ok Tedi copper mine, Papua New Guinea. *Quarterly Journal of Engineering Geology and Hydrogeology*, 28(1), 47-60.

92. Hong, H., Pradhan, B., Xu, C. and Bui, D.T., 2015. Spatial prediction of landslide hazard at the Yihuang area (China) using two-class kernel logistic regression, alternating decision tree and support vector machines. *Catena*, *133*, pp.266-281.

93. Hong, H., Naghibi, S.A., Pourghasemi, H.R. and Pradhan, B., 2016. GIS-based landslide spatial modeling in Ganzhou City, China. *Arabian Journal of Geosciences*, *9*(2), p.112.

94. Hong, H., Pourghasemi, H.R. and Pourtaghi, Z.S., 2016. Landslide susceptibility assessment in Lianhua County (China): a comparison between a random forest data mining technique and bivariate and multivariate statistical models. *Geomorphology*, *259*, pp.105-118.

95. Humbert, M. 1977. Risk mapping of areas exposed to movements of soil and sub-soil: French "ZERMOS" maps. *Bulletin of International Association of Engineering Geologists*, 16, 80-82.

96. Hutchinson, J. N. 1989, March. General report: morphological and geotechnical parameters of landslides in relation to geology and hydrogeology. In *Proceedings of 5th International Symposium on Landslides*, Lausanne.

97. Hutchinson, J. N. 1995. Landslide hazard assessment. *Landslides*, 1805-1841.

98. Hutchinson, J. N., Chandler, M. P. 1991. A preliminary landslide hazard zonation of the Undercliff of the Isleof Wight. In Slope stability engineering developments and applications: In *Proceedings of International conference on slope stability organized by the Institution of Civil Engineers*, the Isle of Wight.

99. Japan Geographical Institute, 2004. Earthquake hazards map by the 2004 Mid-Niigata prefecture earthquake.

100. Jade, S., & Sarkar, S. 1993. Statistical models for slope instability classification. *Engineering Geology*, 36(3), 91-98.

101. Jaiswal, K. and Sinha, R., 2006. Probabilistic modeling of earthquake hazard in stable continental shield of the Indian Peninsula. *ISET J Earthq Technol*, *43*(3), pp.49-64.

102. Jibson, R. W. 1993. Predicting earthquake-induced landslide displacements using Newmark's sliding block analysis. *Transportation Research Record*, 1411.

103. Jibson, R.W. and Harp, E.L., 2012. Extraordinary Distance Limits of Landslides Triggered by the 2011 Mineral, Virginia, EarthquakeExtraordinary Distance Limits of Landslides Triggered by the 2011 Mineral, Virginia, Earthquake. *Bulletin of the Seismological Society of America*, *102*(6), pp.2368-2377.

104. Kaila, K.L. and Rao, M., 1979. Seismic zoning maps of Indian subcontinent. *Geophys. Res. Bull*, *17*(4), pp.293-301.

105. Kanungo, D.P., Arora, M.K., Gupta, R.P. and Sarkar, S., 2008. Landslide risk assessment

using concepts of danger pixels and fuzzy set theory in Darjeeling Himalayas. *Landslides*, *5*(4), pp.407-416.

106. Kanungo, D. P., Arora, M. K., Sarkar, S.,Gupta, R. P. 2006. A comparative study of conventional, ANN black box, fuzzy and combined neural and fuzzy weighting procedures for landslide susceptibility zonation in Darjeeling Himalayas. *Engineering Geology*, 85(3-4), 347-366.

107. Kanungo, D. P., Arora, M. K., Sarkar, S., Gupta, R. P. 2009. Landslide Susceptibility Zonation (LSZ) Mapping–A Review. *Journal of South Asia Disaster Studies*, 2(1), 81-105.

108. Kayastha, P., 2012. Application of fuzzy logic approach for landslide susceptibility mapping in Garuwa sub-basin, East Nepal. *Frontiers of Earth Science*, *6*(4), pp.420-432.

109. Kayastha, P., Dhital, M., R., De, Smedt, F., 2013. Application of the analytical hierarchy process (AHP) for landslide susceptibility mapping: a case study from the Tinau watershed, West Nepal. *Computers & Geosciences* 52:398-408.

110. Kavzoglu, T., Sahin, E.K. and Colkesen, I., 2015. An assessment of multivariate and bivariate approaches in landslide susceptibility mapping: a case study of Duzkoy district. *Natural Hazards*, *76*(1), pp.471-496.

111. Keefer, D., K., 1984. Landslides caused by earthquakes. *Geological Society of America Bulletin*, 95(4), 406-421.

112. Keefer, D. K. 2000. Statistical analysis of an earthquake-induced landslide distribution—the 1989 Loma Prieta, California event. *Engineering Geology*, 58(3-4), 231-249.

113. Keefer, D. K. 2002. Investigating landslides caused by earthquakes–a historical review. *Surveys in Geophysics*, 23(6), 473-510.

114. Khan, P., K., Ansari, A., Singh, D., 2017. Insights into the great Mw 7.9 April 25, 2015 Nepal earthquake, *Current Science*, 113, 2014-2020.

115. Khan, P. K., 2003. Stress state, seismicity and subduction geometry of the descending lithosphere below the Hindukush and Pamir, *Gondwana Research*, 6, 867-877.

116. Khan, P. K., Mohanty, S. and Mohanty, M., 2010. Geodynamic implications for the 8 October 2005 North Pakistan earthquake, Surveys in Geophysics, 31, 85–106.

117. Khattri, K.N., Rogers, A.M., Perkins, D.M. and Algermissen, S.T., 1984. A seismic hazard map of India and adjacent areas. *Tectonophysics*, *108*(1-2), pp.93-134.

118. Korup, O., 2006. Effects of deep-seated bedrock landslides on hillslope morphology, Southern Alps, New Zealand. *Journal of Geophysical Research*, *111*, p.F01018.

119. Kornejady, A., Ownegh, M. and Bahremand, A., 2017. Landslide susceptibility assessment using maximum entropy model with two different data sampling methods. *Catena*, *152*, pp.144-162.

120. Krishna, J., 1959, February. Seismic zoning of India. In *Earthquake Engineering Seminar, Roorkee University, India*(pp. 32-38).

121. Kumar, D., Thakur, M., Dubey, C., S., Shukla, D., P., 2017. Landslide susceptibility mapping & prediction using support vector machine for Mandakini River Basin, Garhwal Himalaya, India. *Geomorphology* 295:115-125.

122. Kumar, S., Wesnousky, S., G., Rockwell, T., K., Ragona, D., Thakur V., C., Seitz, G., G., 2001. Earthquake recurrence and rupture dynamics of Himalayan Frontal Thrust, *India. Science* 294(5550):2328-2331.

123. Kumar, P., Singh, C.D. 2008. Landslide hazard zonation and evaluation of Lunglei Town, Mizoram – its utility in planning and development. *Journal of Engineering Geology*, 35 (1-4), 313-319.

124. Kumar, R., Anbalagan, R., 2015. Landslide susceptibility zonation in part of Tehri reservoir region using frequency ratio, fuzzy logic and GIS. *Journal of Earth System Science* 124(2): 431-448.

125. Kumar, V., Gupta V. Jamir, I. & Chattoraj S.L. (2018) Evaluation of Potential Landslide Damming; Case study of Urni landslide, Kinnaur, Satluj valley, India. *Geoscience Frontiers*, 2(10), 753-767

126. Kumar V., Gupta, V. and Jamir I. (2018) Hazard Evaluation of Progressive Pawari Landslide Zone, Satluj Valley, Higher Himalaya, India. *Natural Hazards* 93 (2), 1029-1047

127. Kveldsvik, V., Kaynia, A. M., Nadim, F., Bhasin, R., Nilsen, B., & Einstein, H. H. (2009). Dynamic distinct-element analysis of the 800 m high Åknes rock slope. *International journal of rock mechanics and mining sciences*, 46(4), 686-698.

128. Ladd, G.E., 1935. Landslides, subsidences and rock-falls. *AmericanRailway Engineering Association*.

129. Landry, J., 1979 carte ZERMOS. Zones exposes a des risques lies aux mouvements du sol et du sous-sol, region de Lons-le-Saunier a Poligny (Jura), Orleans, *Bur. de Rech. Geol. Et Miniere*, 1 Map, 14.

130. Lee, S., Min, K. 2001. Statistical analysis of landslide susceptibility at Yongin, Korea. *Environmental Geology*, 40(9), 1095-1113.

131. Lee, S., Choi, J., Min, K. 2002. Landslide susceptibility analysis and verification using the Bayesian probability model. *Environmental Geology*, 43(1-2), 120-131.

132. Lee, S., Ryu, J. H., Won, J. S., Park, H. J. 2004. Determination and application of the weights for landslide susceptibility mapping using an artificial neural network. *Engineering Geology*, 71(3-4), 289-302.

133. Lee, S., Sambath, T., 2006. Landslide susceptibility mapping in the Damrei Romel area, Cambodia using frequency ratio and logistic regression models. *Environmental Geology* 50(6): 847-855.

134. Lee, S., Pradhan, B., 2007. Landslide hazard mapping at Selangor, Malaysia using frequency ratio and logistic regression models. *Landslides*, *4*(1), pp.33-41.

135. Liao, H., W., Lee, C., T., 2000. Landslides triggered by the Chi-Chi earthquake. In Proceedings of the 21stAsian conference on remote sensing, Taipei.

136. Long, N., T., De, Smedt, F., 2012. Application of an analytical hierarchical process approach for landslide susceptibility mapping in A Luoi district, ThuaThien Hue Province, Vietnam. *Environmental Earth Sciences* 66 (7):1739–1752.

137. Luo, J., Pei, X., Evans, S.G., Huang, R. 2018. Mechanics of the earthquake-induced Hongshiyan landslide in the 2014 Mw 6.2 Ludian earthquake, Yunnan, China. *Engineering Geology*. (doi.org/10.1016/j.enggeo.2018.11.011)

138. Maheshwari, B.K., 2019. Earthquake-Induced Landslide Hazard Assessment of Chamoli District, Uttarakhand Using Relative Frequency Ratio Method. *Indian Geotechnical Journal*, *49*(1), pp.108-123.

139. Marano, K.D., Wald, D.J. and Allen, T.I., 2010. Global earthquake casualties due to secondary effects: a quantitative analysis for improving rapid loss analyses. *Natural hazards*, *52*(2), pp.319-328.

140. Mark, R. K. 1992. Map of debris-flow probability, San Mateo County, California (No. 1257-M).

141. Marjanović, M., Kovačević, M., Bajat, B. and Voženílek, V., 2011. Landslide susceptibility assessment using SVM machine learning algorithm. *Engineering Geology*, *123*(3), pp.225-234.

142. Marui, H. and Nadim, F., 2009. Landslides and multi-hazards. In *Landslides–Disaster Risk Reduction* (pp. 435-450). *Springer, Berlin, Heidelberg*.

143. McKean, J., Buechel, S. Gaydos, L. 1991. Remote sensing and landslide hazard assessment. *Photogrammetric Engineering and Remote Sensing*, 57(9), 1185-1193.

144. Mehrotra, G. S., Sarkar, S., Kanungo, D. P., Mahadevaiah, K. 1996. Terrain analysis and spatial assessment of landslide hazards in parts of Sikkim Himalaya. *Journal of Geological Society of India*, 47, 491-498.

145. Micheletti, N., Foresti, L., Kanevski, M., Pedrazzini, A. and Jaboyedoff, M., 2011. Landslide susceptibility mapping using adaptive support vector machines and feature selection. *Geophysical Research Abstracts, EGU*, *13*.

146. Mishra, A. K., Maruthi, K.V., Pradhan, U. K. 2012. Landslide hazard zonation on

macroscale of Charmudighat section from Charmudi to Kalasa, Sakleshpur to Uppinangadi, DakshinKanada and Chikmagulardistrcts, Karnataka. *Rec.Geol. Surv. India*, 144 (5), 165-167.

147. Molnar P, Tapponnier P. 1977. The collision between India and Eurasia. Scientific American 236(4):30-41

148. Mondal S, Maiti R (2012) Landslide susceptibility analysis of Shiv-Khola watershed, Darjiling: a remote sensing & GIS based Analytical Hierarchy Process (AHP). *Journal of the Indian Society of Remote Sensing* 40 (3):483–496

149. Mridula, S., Sinvhal, A., Wason, H.R. and Rajput, S.S., 2016. Segmentation of Main Boundary Thrust and Main Central Thrust in Western Himalaya for assessment of seismic hazard. *Natural Hazards*, *84*(1), pp.383-403.

150. Mukhopadhyay, B., Acharyya, A., Bhattacharyya, D., Dasgupta, S. and Pande, P., 2011. Seismotectonics at the terminal ends of the Himalayan Arc. *Geomatics, Natural Hazards and Risk*, *2*(2), pp.159-181.

151. Nadim, F., Kjekstad, O., Peduzzi, P., Herold, C., Jaedicke, C. 2006. Global landslide and avalanche hotspots. *Landslides*, 3(2), 159-173.

152. Naik, N. and Choudhury, D., 2015. Deterministic seismic hazard analysis considering different seismicity levels for the state of Goa, India. *Natural Hazards*, *75*(1), pp.557-580.

153. Naithani, A. K., 1999. The Himalayan Landslides, *Employment News*, 23(47), 20-26 February, 1-2

154. Nath, R. R., Kumar, G., Sharma, M. L., Gupta, S. C. 2018. Estimation of bedrock depth for a part of Garhwal Himalayas using two different geophysical techniques. *Geoscience Letters*, 5(1), 1-9.

155. Nath, S., K., Thingbaijam, K., K., S., 2012. Probabilistic Seismic Hazard Assessment of India. *Seismological Research Letters* 83(1):135–149

156. Nath, S., K., Thingbaijam, K., K., S., S., K., Ghosh, 2010. Earthquake Catalogue of South Asia –A Generic MW Scale Framework (www.earthqhaz.net/sacat/)

157. Neely, M. K., RICE, R. M. 1990. Estimating risk of debris slides after timber harvest in northwestern California. *Bulletin of the Association of Engineering Geologists*, 27(3), 281-289.

158. Nefeslioglu, H.A., Sezer, E., Gokceoglu, C., Bozkir, A.S. and Duman, T.Y., 2010. Assessment of landslide susceptibility by decision trees in the metropolitan area of Istanbul, Turkey. *Mathematical Problems in Engineering*, *2010*.

159. Oh, H.J. and Pradhan, B., 2011. Application of a neuro-fuzzy model to landslide-susceptibility mapping for shallow landslides in a tropical hilly area. *Computers & Geosciences*, *37*(9), pp.1264-1276.

160. Pachauri, A. K., Pant, M. 1992. Landslide hazard mapping based on geological attributes. *Engineering Geology*, 32(1-2), 81-100.

161. Pachauri, A. K., Gupta, P. V., Chander, R. 1998. Landslide zoning in a part of the Garhwal Himalayas. *Environmental Geology*, 36(3-4), 325-334.

162. Pain, A., Kanungo, D. P., Sarkar, S. 2014. Rock slope stability assessment using finite element based modelling–examples from the Indian Himalayas. *Geomechanics and Geoengineering*, 9(3), 215-230.

163. Pal, S., Kaynia, A.M., Bhasin, R.K. and Paul, D.K., 2012. Earthquake stability analysis of rock slopes: a case study. *Rock Mechanics and Rock Engineering*, *45*(2), pp.205-215.

164. Pande, P. (2000). Recent damaging earthquakes of India and related societal issues. In Proceedings of 12th World Conference on Earthquake Engineering, Auckland, New Zealand, January-2000, Paper No. 2728.

165. Pande, P., Parvez, I. A. (2008). Seismic microzonation: the Indian scene. Glimpses of Geoscience Research in India; IUGS Book 2004–2008, 113-118.

166. Pande, P., Kumar, R., Suresh, N., Sangode, S. J., Pandey, A. K. (2009). Soft-sediment deformation in contemporary reservoir sediment: a repository of recent major earthquake events in Garhwal Himalaya. The Journal of Geology, 117(2), 200-209.

167. Pandey VK, Pourghasemi HR, Sharma MC (2018) Landslide susceptibility mapping using maximum entropy and support vector machine models along the Highway Corridor, Garhwal Himalaya. Geocarto International 1-38.

168. Papadakis, M., Karimalis, A., 2017. Producing a landslide susceptibility map through the use of Analytic Hierarchical Process in Finikas Watershed, North Peloponnese, Greece. American *Journal of Geographic Information System* 6(1A):14-22.

169. Papadopoulos, G.A. and Plessa, A., 2000. Magnitude–distance relations for earthquake-induced landslides in Greece. *Engineering Geology*, *58*(3-4), pp.377-386.

170. Patil, N.S., Das, J., Kumar, A., Rout, M.M. and Das, R., 2014. Probabilistic seismic hazard assessment of Himachal Pradesh and adjoining regions. *Journal of earth system science*, *123*(1), pp.49-62.

171. Pareek, N., Sharma, M. L., Arora, M. K. 2010. Impact of seismic factors on landslide susceptibility zonation: a case study in part of Indian Himalayas. *Landslides*, 7(2), 191-201.

172. Pareek, N., Pal, S., Sharma, M. L., Arora, M. K. 2013. Study of effect of seismic displacements on landslide susceptibility zonation (LSZ) in Garhwal Himalayan region of

India using GIS and remote sensing techniques. *Computers & Geosciences*, 61, 50-63.

173. Pareek, N., Sharma, M. L., Arora, M. K., Pal, S. 2013. Inclusion of earthquake strong ground motion in a geographic information system-based landslide susceptibility zonation in Garhwal Himalayas. *Natural Hazards*, 65(1), 739-765.

174. Parkash, S., 2013. Earthquake related landslides in the Indian Himalaya: experiences from the past and implications for the future. In *Landslide Science and Practice* (pp. 327-334). Springer, Berlin, Heidelberg.

175. Parker, R.N., Hancox, G.T., Petley, D.N., Massey, C.I., Densmore, A.L. and Rosser, N.J., 2015. Spatial distributions of earthquake-induced landslides and hillslope preconditioning in northwest South Island, New Zealand. *Earth surface dynamics.*, *3*(4), pp.501-525.

176. Park, N.W., 2015. Using maximum entropy modeling for landslide susceptibility mapping with multiple geoenvironmental data sets. *Environmental earth sciences*, *73*(3), pp.937-949.

177. Peethambaran, B., Anbalagan, R. and Shihabudheen, K.V., 2019. Landslide susceptibility mapping in and around Mussoorie Township using fuzzy set procedure, MamLand and improved fuzzy expert system-A comparative study. *Natural Hazards*, *96*(1), pp.121-147.

178. Peethambaran, B., Anbalagan, R., Shihabudheen, K.V. and Goswami, A., 2019. Robustness evaluation of fuzzy expert system and extreme learning machine for geographic information system-based landslide susceptibility zonation: A case study from Indian Himalaya. *Environmental Earth Sciences*, *78*(6), p.231.

179. Petley, D., 2012. Global patterns of loss of life from landslides. *Geology*, *40*(10), pp.927-930.

180. Pourghasemi, H. R., Pradhan, B., & Gokceoglu, C. 2012. Application of fuzzy logic and analytical hierarchy process (AHP) to landslide susceptibility mapping at Haraz watershed, Iran. *Natural hazards*, 63(2), 965-996.

181. Pourghasemi, H.R., Jirandeh, A.G., Pradhan, B., Xu, C. and Gokceoglu, C., 2013. Landslide susceptibility mapping using support vector machine and GIS at the Golestan Province, Iran. *Journal of Earth System Science*, *122*(2), pp.349-369.

182. Pourghasemi, H.R. and Kerle, N., 2016. Random forests and evidential belief function-based landslide susceptibility assessment in Western Mazandaran Province, Iran. *Environmental earth sciences*, *75*(3), p.185.

183. Pradhan, B., Lee, S. and Buchroithner, M.F., 2009. Use of geospatial data and fuzzy algebraic operators to landslide-hazard mapping. *Applied Geomatics*, *1*(1-2), pp.3-15.

184. Pradhan, B., Sezer, E.A., Gokceoglu, C. and Buchroithner, M.F., 2010. Landslide susceptibility mapping by neuro-fuzzy approach in a landslide-prone area (Cameron

Highlands, Malaysia). *IEEE Transactions on Geoscience and Remote Sensing*, *48*(12), pp.4164-4177.

185. Pradhan, B., & Lee, S. 2010. Regional landslide susceptibility analysis using back-propagation neural network model at Cameron Highland, Malaysia. Landslides, 7(1), 13-30.

186. Pradhan, B., & Lee, S. 2010. Landslide susceptibility assessment and factor effect analysis: backpropagation artificial neural networks and their comparison with frequency ratio and bivariate logistic regression modelling. Environmental Modelling & Software, 25(6), 747-759.

187. Pradhan, B., 2010a. Application of an advanced fuzzy logic model for landslide susceptibility analysis. *International Journal of Computational Intelligence Systems*, *3*(3), pp.370-381.

188. Pradhan, B., 2010b. Landslide susceptibility mapping of a catchment area using frequency ratio, fuzzy logic and multivariate logistic regression approaches. *Journal of the Indian Society of Remote Sensing*, *38*(2), pp.301-320.

189. Pradhan, B., 2011a. Manifestation of an advanced fuzzy logic model coupled with Geo-information techniques to landslide susceptibility mapping and their comparison with logistic regression modelling. *Environmental and Ecological Statistics*, *18*(3), pp.471-493.

190. Pradhan, B., 2011b. Use of GIS-based fuzzy logic relations and its cross application to produce landslide susceptibility maps in three test areas in Malaysia. *Environmental Earth Sciences*, *63*(2), pp.329-349.

191. Pradhan, B., Mansor, S., Pirasteh, S., & Buchroithner, M. F. 2011. Landslide hazard and risk analyses at a landslide prone catchment area using statistical based geospatial model. International Journal of Remote Sensing, 32(14), 4075-4087.

192. Pradhan, B., 2013. A comparative study on the predictive ability of the decision tree, support vector machine and neuro-fuzzy models in landslide susceptibility mapping using GIS. *Computers & Geosciences*, *51*, pp.350-365.

193. Raghukanth S. T. G. 2010. Catalogue of Earthquakes of Moment Magnitude 4.0 in and Around India, Appendix I, in Development of Probabilistic Seismic Hazard Map of India, Report, *National Disaster Management Authority*, New Delhi, India

194. Rib, H. T., Liang, T. 1978. Recognition and identification. *Transportation Research Board Special Report*, 176.

195. Roback, K., Clark, M. K., West, A. J., Zekkos, D., Li, G., Gallen, S. F., Godt, J. W. 2018. The size, distribution, and mobility of landslides caused by the 2015 Mw7. 8 Gorkha earthquake, Nepal. *Geomorphology*, 301, 121-138.

196. Rodrıguez, C. E., Bommer, J. J., Chandler, R. J. 1999. Earthquake-induced landslides:

1980–1997. *Soil Dynamics and Earthquake Engineering*, 18(5), 325-346.

197. Rosenfeld, C. L. 1994. The geomorphological dimensions of natural disasters. *Geomorphology and Natural Hazards*, 27-36.

198. Roth, R. A. 1983. Factors affecting landslide-susceptibility in San Mateo county, California. *Bulletin of the Association of Engineering Geologists*, 20(4), 353-372.

199. Saaty, T., L., 1980. The analytic hierarchy process: planning, priority setting, resource allocation. *McGraw-Hill Book Co*, USA.

200. Saaty, T., L., 2000. The Fundamentals of Decision Making and Priority Theory with the Analytic Hierarchy Process, Vol VI. *RWS Publications*, Pitsburg.

201. Saha, A. K., Gupta, R. P., Arora, M. K. 2002. GIS-based landslide hazard zonation in the Bhagirathi (Ganga) valley, Himalayas. *International Journal of Remote Sensing*, 23(2), 357-369.

202. Saha, A. K., Gupta, R. P., Sarkar, I., Arora, M. K., Csaplovics, E. 2005. An approach for GIS-based statistical landslide susceptibility zonation—with a case study in the Himalayas. *Landslides*, 2(1), 61-69.

203. Saito, H., Nakayama, D. and Matsuyama, H., 2009. Comparison of landslide susceptibility based on a decision-tree model and actual landslide occurrence: the Akaishi Mountains, Japan. *Geomorphology*, *109*(3-4), pp.108-121.

204. Sarkar, S., Kanungo, D. P., Mehrotra, G. S. 1995. Landslide hazard zonation: a case study in Garhwal Himalaya, India. *Mountain Research and Development*, 301-309.

205. Sarkar, I., Pachauri, A. K., Israil, M. 2001. On the damage caused by the Chamoli earthquake of 29 March, 1999. *Journal of Asian Earth Sciences*, 19(1-2), 129-134.

206. Sarkar, S., Kanungo, D. P. 2004. An integrated approach for landslide susceptibility mapping using remote sensing and GIS. *Photogrammetric Engineering & Remote Sensing*, 70(5), 617-625.

207. Sassa, K. 1989, March. Special lecture: geotechnical model for the motion of landslides: In *Proceedings of 5th International Symposium on Landslides*, Lausanne.

208. Saygili, G., Rathje, E. M. 2009. Probabilistically based seismic landslide hazard maps: an application in Southern California. *Engineering Geology*, 109(3-4), 183-194.

209. Schuster, R. L., Fleming, R. W. 1986. Economic losses and fatalities due to landslides. *Bulletin of the Association of Engineering Geologists*, 23(1), 11-28.

210. Scordilis, E., M., 2006. Empirical global relations converting MS and Mb to moment magnitude. *Journal of Seismology* 10:225-236

211. Sharma, M., L., Wason, H., R., 1994. Occurrence of low stress drop earthquakes in the Garhwal Himalaya region. Physics of the Earth and Planetary Interiors 85(3-4):265-272

212. Sharma, M., L., Dimri, R., 2003. Seismic hazard estimation and zonation of northern Indian region for bed rock ground motion. Journal of Seismology and Earthquake Engineering 5(2):23-34

213. Sharma, M.L., Wason, H.R. and Dimri, R., 2003. Seismic zonation of the Delhi region for bedrock ground motion. *Pure and applied geophysics*, *160*(12), pp.2381-2398.

214. Sharma, M., L., Lindholm, C., 2012. Earthquake hazard assessment for Dehradun, Uttarakhand, India, including a characteristic earthquake recurrence model for the Himalaya Frontal Fault (HFF). Pure and Applied Geophysics 169:1601-1617

215. Sharma, M.L. and Malik, S.H.I.P.R.A., 2006, October. Probabilistic seismic hazard analysis and estimation of spectral strong ground motion on bed rock in north east India. In *4th international conference on earthquake engineering* (pp. 12-13).

216. Shroder Jr, J. F. 1998. Slope failure and denudation in the western Himalaya. *Geomorphology*, 26(1-3), 81-105.

217. Shukla, J. and Choudhury, D., 2012. Estimation of seismic ground motions using deterministic approach for major cities of Gujarat. *Natural Hazards and Earth System Sciences*, *12*(6), p.2019.

218. Siddle, H. J., Jones, D. B., Payne, H. R. 1991. Development of a methodology for landslip potential mapping in the Rhondda Valley. In *Proceedings of International Conference on Slope Stability organized by the Institution of Civil Engineers*, Isle of Wight.

219. Singh, C.D., Behera, K., K., Singh, J. 2011. Comparison of different methodologies of landslide hazard zonation in and around Guwahati, Assam. *Indian Landslides*, 4 (2), 11-16.

220. Singh, C. D., Kohli, A., Kumar, P. 2014. Comparison of results of BIS and GSI guidelines on macrolevel landslide hazard zonation—A case study along highway from Bhalukpong to Bomdila, West Kameng district, Arunachal Pradesh. *Journal of the Geological Society of India*, 83(6), 688-696.

221. Sitharam, T.G. and Anbazhagan, P., 2007. Seismic hazard analysis for the Bangalore region. *Natural Hazards*, *40*(2), pp.261-278.

222. Sitharam, T.G., Kolathayar, S. and James, N., 2015. Probabilistic assessment of surface level seismic hazard in India using topographic gradient as a proxy for site condition. *Geoscience Frontiers*, *6*(6), pp.847-859.

223. Skempton, A. W. 1953. Soil mechanics in relation to geology. In *Proceedings of Yorkshire Geological Society*, 28, 33-62.

224. Skempton, A. W., Hutchinson, J. 1969. Stability of natural slopes and embankment foundations. In *Proceedings of International Conference on Soil Mechanics & Foundation Engineering*, Mexico.

225. Soeters, R., van Westen, C. J. 1996. Landslides: Investigation and mitigation. Chapter 8-Slope instability recognition, analysis, and zonation. *Transportation Research Board Special Report*, 247.

226. Stepp, J.C., 1972, October. Analysis of completeness of the earthquake sample in the Puget Sound area and its effect on statistical estimates of earthquake hazard. In *Proc. of the 1st Int. Conf. on Microzonazion, Seattle* (Vol. 2, pp. 897-910).

227. Tandon, A., N., 1956. Zones of India liable to earthquake damage Indian Journal of Meteorological Geophysics 10:13-146

228. Tang, C., Ma, G., Chang, M., Li, W., Zhang, D., Jia, T., Zhou, Z. 2015. Landslides triggered by the 20 April 2013 Lushan earthquake, Sichuan Province, China. *Engineering Geology*, 187, 45-55.

229. Tang, C, van Westen C., J., Tanyas, H., Jetten, V., G., 2016. Analysing post-earthquake landslide activity using multi-temporal landslide inventories near the epicentral area of the 2008 Wenchuan earthquake. Natural Hazards and Earth System Sciences 16(12): 2641–2655.

230. Tanyaş, H., Van Westen, C. J., Allstadt, K. E., Jessee, M. A. N., Görüm, T., Jibson, R. W. et al. 2017. Presentation and analysis of a worldwide database of earthquake-induced landslide inventories. *Journal of Geophysical Research: Earth Surface*, 122(10), 1991-2015.

231. Terzaghi, K. 1950. Mechanism of landslides. *Geological Society of America, Geology (Berkeley),* 83-123.

232. Thanh, L., N., De, Smedt, F, 2012. Application of an analytical hierarchical process approach for landslide susceptibility mapping in A Luoi district, ThuaThien Hue Province, Vietnam. *Environmental Earth Sciences* 66(7): 1739-1752

233. Thai Pham, B., Tien Bui, D., Pourghasemi, H.R., Indra, P., Dholakia, M.B., 2015. Landslidesusceptibility assesssment in the Uttarakhand area (India) using GIS: a comparisonstudy of prediction capability of naïve bayes, multilayer perceptron neural networks, and functional trees methods. Theor. Appl. Climatol.http://dx.doi.org/10.1007/s00704-015-1702-9

234. Tianchi, L., Kathmandu, N. E. P. A. L. 1987. Landslide management in the mountain areas of China. *ICIMOD occasional paper*, 15.

235. Trigila, A., Iadanza, C., Esposito, C. and Scarascia-Mugnozza, G., 2015. Comparison of Logistic Regression and Random Forests techniques for shallow landslide susceptibility assessment in Giampilieri (NE Sicily, Italy). *Geomorphology*, *249*, pp.119-136.

236. Tsangaratos, P. and Ilia, I., 2016. Comparison of a logistic regression and Naïve Bayes classifier in landslide susceptibility assessments: The influence of models complexity and training dataset size. *Catena*, *145*, pp.164-179.

237. Turner, A.K., Schuster, R.L. Eds. 1995. Landslides, investigation and mitigation. *Transportation Research Board Special Report,* 247.

238. Uhrhammer, R., 1986. Characterization of northern and central California Seismicity. Earthquake Notes 57(1):21

239. Utsu, T., 1965. A method for determining the value of" b" in a formula log n= a-bM showing the magnitude-frequency relation for earthquakes. *Geophys. Bull. Hokkaido Univ.*, *13*, pp.99-103.

240. Van Westen, C.J. 1993. Application of Geographical Information System to landslide hazard zonation. *ITC Publication,*15.

241. Van Westen, C. J. 1994. GIS in landslide hazard zonation: a review, with examples from the Andes of Colombia. In *Mountain Environments & Geographic Information Systems*, Taylor & Francis.

242. Van Westen, C. J. 1997. Statistical landslide hazard analysis. *ILWIS*, 2, 73-84.

243. Van Westen, C. J., Rengers, N., Soeters, R. 2003. Use of geomorphological information in indirect landslide susceptibility assessment. *Natural Hazards*, 30(3), 399-419.

244. Vahidnia, M.H., Alesheikh, A.A., Alimohammadi, A. and Hosseinali, F., 2010. A GIS-based neuro-fuzzy procedure for integrating knowledge and data in landslide susceptibility mapping. *Computers & Geosciences*, *36*(9), pp.1101-1114.

245. Varnes, D. J. 1958. Landslide types and processes.*Landslides and Engineering Practice*, 29(3), 20-45.

246. Varnes, D. J. 1978. Slope movement types and processes. *Special Report*, 176, 11-33.

247. Varnes, D. J. 1984. Landslide hazard zonation: a review of principles and practice (No. 3).

248. Wang, W.N., Nakamura, H., Tsuchiya, S., Chen, C.C. 2002. Distributions of landslides triggered by the Chi-Chi earthquake in Central Taiwan on September 21, 1999. *Journal of the Japan Landslide Society*, 38 (4), 318 – 326.

249. Wason, H.R., Sharma, M.L., Khan, P.K., Kapoor, K., Nandini, D. and Kara, V., 2002. Analysis of aftershocks of the Chamoli Earthquake of March 29, 1999 using broadband seismic data. *J. Himalayan Geol*, *23*, pp.7-18.

250. Wieczorek, G. F. 1984. Preparing a detailed landslide-inventory map for hazard evaluation and reduction. *Bulletin of the Association of Engineering Geologists*, 21(3), 337-342.

251. Wieczorek, G. F., Gori, P. L., Jager, S., Kappel, W. M., Negussey, D. 1996. Assessment and management of landslide hazards near Tully Valley landslide, Syracuse, New York, USA.

In *Proceedings of 7th International Symposium on Landslides*, Rotterdam.

252. Woessner, J. and Wiemer, S., 2005. Assessing the quality of earthquake catalogues: Estimating the magnitude of completeness and its uncertainty. *Bulletin of the Seismological Society of America*, *95*(2), pp.684-698.

253. Wright, R. H., Nilsen, T. H. 1974. Isopleth map of landslide deposits, southern San Francisco Bay Region, California (No. 550). *US Geological Survey*.

254. Wu, X., Ren, F. and Niu, R., 2014. Landslide susceptibility assessment using object mapping units, decision tree, and support vector machine models in the Three Gorges of China. *Environmental earth sciences*, *71*(11), pp.4725-4738.

255. Xu, C., Xu, X., Lee, Y. H., Tan, X., Yu, G., Dai, F., 2012. The 2010 Yushu earthquake triggered landslide hazard mapping using GIS and weight of evidence modeling. *Environmental Earth Sciences*, 66(6), 1603-1616.

256. Yagi, H., Sato, G., Higaki, D., Yamamoto, M., Yamasaki, T. 2009. Distribution and characteristics of landslides induced by the Iwate–Miyagi Nairiku Earthquake in 2008 in Tohoku District, Northeast Japan. *Landslides*, 6(4), 335.

257. Yao, X., Tham, L.G. and Dai, F.C., 2008. Landslide susceptibility mapping based on support vector machine: a case study on natural slopes of Hong Kong, China. *Geomorphology*, *101*(4), pp.572-582.

258. Yesilnacar, E. and Topal, T., 2005. Landslide susceptibility mapping: a comparison of logistic regression and neural networks methods in a medium scale study, Hendek region (Turkey). *Engineering Geology*, *79*(3-4), pp.251-266.

259. Yin, K. L., 1988. Statistical prediction model for slope instability of metamorphosed rocks. In *Proceedings of 5th International Symposium on Landslides*, 2, 1269-1272.

260. Yin, Y., Wang, F., Sun, P., 2009. Landslide hazards triggered by the 2008 Wenchuan earthquake, Sichuan, China. *Landslides*, 6(2), 139-152. Yilmaz, I., 2010. The effect of the sampling strategies on the landslide susceptibility mapping by conditional probability and artificial neural networks. *Environmental Earth Sciences*, *60*(3), pp.505-519.

261. Youssef, A.M., Pourghasemi, H.R., Pourtaghi, Z.S. and Al-Katheeri, M.M., 2016. Landslide susceptibility mapping using random forest, boosted regression tree, classification and regression tree, and general linear models and comparison of their performance at Wadi Tayyah Basin, Asir Region, Saudi Arabia. *Landslides*, *13*(5), pp.839-856.

262. Zare, M., Pourghasemi, H.R., Vafakhah, M. and Pradhan, B., 2013. Landslide susceptibility mapping at Vaz Watershed (Iran) using an artificial neural network model: a comparison between multilayer perceptron (MLP) and radial basic function (RBF) algorithms. *Arabian Journal of Geosciences*, *6*(8), pp.2873-2888.

Table A1: Landslide Inventory

Object Id	POINT_X	POINT_Y	Aspect	Slope (Degree)	Elevation (m)	Lithology	Drainage ED (m)	Fault ED (m)	Road ED (m)	LULC
1	131585.25	3456820.53	N-E	31.76	1225	Simla Gp	0	2422	1664	Sparsely Vegetated
2	130723.26	3457059.01	E	26.54	1415	Simla Gp	848	3087	1663	Sparsely Vegetated
3	133965.22	3454607.29	S-W	33.08	1366	Simla Gp	0	856	4322	Sparsely Vegetated
4	132370.95	3455087.05	N-E	38.00	1364	Simla Gp	0	856	3407	Sparsely Vegetated
5	131515.03	3454304.52	S-E	30.29	1596	Simla Gp	848	856	4192	Sparsely Vegetated
6	131212.46	3454279.31	S-E	32.82	1690	Simla Gp	848	856	4239	Sparsely Vegetated
7	129665.07	3454318.76	N-W	23.54	1900	Simla Gp	848	1712	3918	Sparsely Vegetated
8	130344.08	3453645.70	S-W	35.72	1828	Simla Gp	1199	856	4148	Sparsely Vegetated
9	130497.73	3451995.05	S-E	39.15	1691	Simla Gp	848	0	3098	Sparsely Vegetated
10	129406.17	3451942.63	S-E	8.46	1797	Simla Gp	1199	0	2198	Sparsely Vegetated
11	129589.25	3452462.61	E	21.17	1915	Simla Gp	1199	0	2739	Sparsely Vegetated
12	129393.07	3452876.20	S-E	13.94	1985	Simla Gp	1199	856	2981	Sparsely Vegetated
13	132378.55	3453578.26	W	29.64	1540	Simla Gp	0	0	4906	Sparsely Vegetated
14	135834.71	3450876.41	N	44.67	1808	Simla Gp	1199	3425	2605	Evergreen Forest
15	130175.36	3451633.92	S-W	32.95	1724	Simla Gp	848	856	2611	Sparsely Vegetated
16	130227.31	3451654.62	S-W	22.19	1755	Simla Gp	848	856	2664	Sparsely Vegetated
17	130212.94	3451714.37	S-E	14.43	1757	Simla Gp	848	856	2700	Sparsely Vegetated
18	136246.54	3448763.83	E	17.96	1914	Simla Gp	1896	3530	820	Sparsely Vegetated
19	134556.31	3447879.28	N-E	40.44	2100	Simla Gp	3058	1712	0	Sparsely Vegetated
20	122539.71	3449161.30	N-W	11.95	1265	Jaunsar Gp of W. Himalaya	848	0	3049	Sparsely Vegetated
21	128049.29	3448940.79	W	32.01	1769	Jutogh Gp of W.Himalaya	3058	1914	32	Sparsely Vegetated
22	128660.06	3448749.27	S-E	37.38	1794	Jutogh Gp of W.Himalaya	3058	1211	160	Shrub Land
23	128258.81	3446271.39	N	25.15	1543	Jutogh Gp of W.Himalaya	2399	3087	64	Sparsely Vegetated
24	137055.41	3447467.61	N-E	26.00	2205	Simla Gp	2544	2422	0	Evergreen Forest
25	133050.66	3444304.79	S	12.22	1557	Jutogh Gp of W.Himalaya	0	856	1426	Sparsely Vegetated

26	133105.87	3443760.14	S-W	8.27	1507	Jutogh Gp of W.Himalaya	0	856	1640	Sparsely Vegetated
27	132911.12	3443880.44	E	29.90	1606	Jutogh Gp of W.Himalaya	0	856	1417	Sparsely Vegetated
28	117901.40	3444610.44	S	19.20	1148	Krol, Infrakrol & Blaini Formation	1896	856	32	Sparsely Vegetated
29	128080.08	3446104.88	S	20.58	1607	Jutogh Gp of W.Himalaya	1896	3087	0	Sparsely Vegetated
30	131134.30	3444024.64	W	41.55	1841	Jutogh Gp of W.Himalaya	1696	1914	45	Evergreen Forest
31	119970.92	3445438.83	S-E	25.44	1065	Simla Gp	0	1712	1793	Sparsely Vegetated
32	123053.04	3445666.71	W	10.27	1440	Jaunsar Gp of W. Himalaya	848	856	362	Sparsely Vegetated
33	127338.77	3446062.79	N-W	20.15	1471	Jutogh Gp of W.Himalaya	1696	2422	45	Sparsely Vegetated
34	141600.85	3445817.35	W	41.23	1965	Simla Gp	1896	1914	1855	Evergreen Forest
35	141645.95	3444978.20	W	32.41	1964	Simla Gp	1199	2422	1856	Evergreen Forest
36	147567.23	3444798.61	E	24.27	2433	Simla Gp	3058	6687	453	Sparsely Vegetated
37	133290.11	3443482.23	S-W	35.02	1539	Jutogh Gp of W.Himalaya	0	856	1925	Sparsely Vegetated
38	133491.81	3442787.80	S-W	23.62	1411	Jutogh Gp of W.Himalaya	0	0	1941	Sparsely Vegetated
39	134001.15	3442738.70	S	40.03	1543	Jutogh Gp of W.Himalaya	0	856	1444	Deciduous Forest
40	132403.95	3443195.48	E	11.20	1668	Jutogh Gp of W.Himalaya	848	856	1335	Sparsely Vegetated
41	121593.57	3442471.53	S-E	18.34	1467	Simla Gp	2399	856	0	Sparsely Vegetated
42	121970.04	3443580.11	E	28.33	1492	Simla Gp	2399	0	32	Shrub Land
43	133009.83	3443288.61	E	49.00	1509	Jutogh Gp of W.Himalaya	0	0	1751	Shrub Land
44	128761.25	3442791.94	S	7.79	1383	Jutogh Gp of W.Himalaya	848	1914	1539	Sparsely Vegetated
45	127653.04	3442837.36	S	44.88	1279	Jutogh Gp of W.Himalaya	0	1211	880	Sparsely Vegetated
46	130511.73	3439944.72	S	19.65	1691	Jutogh Gp of W.Himalaya	2682	0	666	Deciduous Forest
47	130534.00	3440179.68	E	16.44	1743	Jutogh Gp of W.Himalaya	2682	856	525	Sparsely Vegetated
48	116074.90	3439819.94	E	15.71	960	Simla Gp	0	1211	1590	Sparsely Vegetated
49	124286.23	3439945.23	S	33.50	1217	Simla Gp	0	856	3350	Sparsely Vegetated

50	124345.75	3440469.86	W	25.83	1246	Jaunsar Gp of W. Himalaya	0	0	3270	Shrub Land
51	123462.32	3440374.10	S-E	27.71	1168	Simla Gp	0	856	2745	Sparsely Vegetated
52	123431.44	3440275.22	S-E	31.60	1141	Simla Gp	0	856	2799	Sparsely Vegetated
53	123064.15	3440168.86	S	33.87	1116	Simla Gp	0	1211	2656	Sparsely Vegetated
54	127131.35	3439676.84	S	36.61	1633	Jaunsar Gp of W. Himalaya	2544	856	490	Sparsely Vegetated
55	124943.17	3439655.03	S	39.45	1364	Jaunsar Gp of W. Himalaya	848	856	2648	Sparsely Vegetated
56	127263.53	3441024.34	S-W	39.93	1416	Jaunsar Gp of W. Himalaya	1696	856	1482	Sparsely Vegetated
57	127443.42	3440836.26	S-W	27.29	1396	Jaunsar Gp of W. Himalaya	1696	856	1258	Sparsely Vegetated
58	135624.71	3439787.36	S	24.80	1436	Simla Gp	0	1712	0	Evergreen Forest
59	153507.50	3439571.73	N-W	18.92	1171	Simla Gp	848	6520	8363	Sparsely Vegetated
60	115363.22	3438539.08	S-W	25.45	878	Subathu Fm of W. Himalaya	0	2422	427	Sparsely Vegetated
61	109993.85	3438146.11	S-W	12.22	1057	Subathu Fm of W. Himalaya	3497	856	660	Sparsely Vegetated
62	115124.44	3438851.12	S-W	40.35	852	Subathu Fm of W. Himalaya	0	2422	258	Sparsely Vegetated
63	129957.37	3438259.91	S-E	22.95	1689	Jutogh Gp of W.Himalaya	1896	856	1517	Sparsely Vegetated
64	127723.54	3437874.05	S-E	11.01	1723	Jaunsar Gp of W. Himalaya	1896	0	0	Sparsely Vegetated
65	127855.10	3438025.88	S-E	28.75	1711	Jaunsar Gp of W. Himalaya	2399	0	202	Sparsely Vegetated
66	127359.03	3439426.61	S-W	20.88	1688	Jaunsar Gp of W. Himalaya	2544	856	302	Sparsely Vegetated
67	126778.23	3438840.10	S-W	20.39	1505	Jaunsar Gp of W. Himalaya	2544	0	810	Sparsely Vegetated
68	134981.69	3439199.21	S-E	37.73	1344	Jutogh Gp of W.Himalaya	0	1211	750	Sparsely Vegetated
69	135278.26	3439162.15	S-W	16.45	1330	Jaunsar Gp of W. Himalaya	0	1211	638	Sparsely Vegetated
70	140722.77	3439636.06	S-E	25.54	2206	Simla Gp	2399	856	0	Sparsely Vegetated
71	133263.07	3436415.94	E	38.60	1532	Jaunsar Gp of W. Himalaya	848	856	659	Sparsely Vegetated
72	121488.87	3435834.73	S	20.48	959	Simla Gp	0	0	4870	Sparsely Vegetated
73	121356.91	3435906.10	S	27.19	982	Simla Gp	0	0	4781	Sparsely Vegetated

74	117683.00	3436880.04	S-E	24.13	984	Simla Gp	848	2707	2054	Sparsely Vegetated
75	117686.46	3436600.01	W	19.88	954	Simla Gp	848	2707	2049	Sparsely Vegetated
76	155752.74	3437202.33	S-W	16.82	1408	Simla Gp	848	3530	11614	Sparsely Vegetated
77	111995.06	3435598.12	N-W	19.41	1216	Subathu Fm of W. Himalaya	2399	1914	916	Sparsely Vegetated
78	142424.38	3437622.84	S	25.83	1751	Simla Gp	848	2569	2118	Evergreen Forest
79	137074.85	3437579.10	S	34.84	1490	Jaunsar Gp of W. Himalaya	0	2569	32	Evergreen Forest
80	139230.45	3437721.49	W	26.92	1941	Simla Gp	1696	856	784	Sparsely Vegetated
81	133973.51	3435670.03	S-W	46.08	1254	Jaunsar Gp of W. Himalaya	0	856	0	Sparsely Vegetated
82	133837.31	3436421.09	S	25.88	1333	Jaunsar Gp of W. Himalaya	0	1211	226	Sparsely Vegetated
83	133637.50	3436553.26	S-W	32.37	1281	Jaunsar Gp of W. Himalaya	0	1914	462	Sparsely Vegetated
84	147191.66	3436543.19	W	32.62	1212	Simla Gp	0	6849	5867	Sparsely Vegetated
85	146316.73	3436114.84	S	31.52	1436	Simla Gp	0	5993	5798	Sparsely Vegetated
86	107623.08	3435887.60	S-W	24.85	1151	Lower Siwalik Group	1896	856	3501	Sparsely Vegetated
87	120942.20	3435883.57	N	23.74	1001	Simla Gp	0	0	4409	Sparsely Vegetated
88	121495.68	3435667.85	N-E	5.06	966	Simla Gp	0	0	4807	Sparsely Vegetated
89	127507.02	3437180.29	N-W	32.71	1646	Jaunsar Gp of W. Himalaya	1896	1211	32	Sparsely Vegetated
90	127288.93	3437062.37	N-E	9.06	1659	Jaunsar Gp of W. Himalaya	2682	1211	32	Evergreen Forest
91	126955.21	3437072.87	N-E	20.64	1681	Simla Gp	2682	1211	0	Shrub Land
92	150952.07	3435741.03	S	40.95	1303	Simla Gp	0	5743	8990	Sparsely Vegetated
93	156047.16	3436844.22	S-W	22.76	1429	Simla Gp	0	3425	12065	Sparsely Vegetated
94	107976.53	3435494.57	E	37.73	1064	Lower Siwalik Group	1199	856	2991	Sparsely Vegetated
95	120925.13	3435308.97	E	21.58	1054	Simla Gp	848	0	4142	Sparsely Vegetated
96	120996.11	3435465.35	S-E	23.46	1054	Simla Gp	0	0	4291	Sparsely Vegetated
97	120340.43	3435009.24	S-W	13.08	1154	Simla Gp	1199	856	3492	Sparsely Vegetated
98	143664.22	3435379.30	S	50.54	1881	Simla Gp	1696	3425	3798	Sparsely Vegetated
99	144385.03	3435350.18	Flat	28.15	1932	Simla Gp	1199	4281	4495	Sparsely Vegetated

100	144812.99	3435305.61	N-E	28.55	1888	Simla Gp	1696	4992	4898	Sparsely Vegetated
101	115576.05	3433680.61	E	19.26	962	Dagshai and Kausauli Fm of W. Himalayas	0	5137	115	Sparsely Vegetated
102	115911.32	3433804.26	S-W	24.24	1007	Dagshai and Kausauli Fm of W. Himalayas	0	4611	72	Sparsely Vegetated
103	115048.76	3435528.55	W	37.12	878	Dagshai and Kausauli Fm of W. Himalayas	0	5208	513	Sparsely Vegetated
104	115123.16	3435314.76	S-W	30.01	898	Dagshai and Kausauli Fm of W. Himalayas	0	5208	516	Sparsely Vegetated
105	126432.59	3435175.67	S-W	21.91	1548	Simla Gp	1199	3087	224	Sparsely Vegetated
106	124924.07	3434546.32	S-W	23.34	1228	Krol, Infrakrol & Blaini Formation	848	2422	1862	Sparsely Vegetated
107	138995.62	3435373.31	S	30.03	2109	Jaunsar Gp of W. Himalaya	2399	856	32	Sparsely Vegetated
108	151169.36	3434850.10	W	37.81	1200	Simla Gp	0	5137	9209	Sparsely Vegetated
109	110153.48	3431856.31	N-E	30.44	780	Lower Siwalik Group	848	0	32	Sparsely Vegetated
110	110379.80	3431837.15	W	22.51	801	Lower Siwalik Group	848	0	101	Sparsely Vegetated
111	110436.99	3431735.98	S-W	42.86	808	Lower Siwalik Group	848	0	45	Sparsely Vegetated
112	109939.62	3431991.51	N	23.26	751	Lower Siwalik Group	848	0	45	Sparsely Vegetated
113	107687.02	3432084.98	S-W	21.38	730	Lower Siwalik Group	0	2569	365	Sparsely Vegetated
114	107844.12	3432989.65	S-E	16.68	894	Lower Siwalik Group	848	2569	1255	Sparsely Vegetated
115	109855.65	3431987.64	N-E	28.98	770	Lower Siwalik Group	848	0	0	Sparsely Vegetated
116	106762.33	3431670.96	N	24.22	711	Lower Siwalik Group	0	3425	320	Sparsely Vegetated
117	148465.73	3432106.19	N	37.08	1089	Simla Gp	0	2422	6049	Sparsely Vegetated
118	120926.46	3432740.22	N	13.20	1162	Krol, Infrakrol & Blaini Formation	1896	856	3285	Sparsely Vegetated
119	115842.71	3432752.85	W	24.00	976	Dagshai and Kausauli Fm of W. Himalayas	0	4366	45	Sparsely Vegetated

120	117380.11	3432022.97	W	22.68	1263	Subathu Fm of W. Himalaya	1199	2569	0	Sparsely Vegetated
121	109522.91	3432100.32	N	15.34	724	Lower Siwalik Group	0	856	32	Sparsely Vegetated
122	115566.76	3433137.48	N-E	19.26	985	Dagshai and Kausauli Fm of W. Himalayas	0	5137	0	Sparsely Vegetated
123	114815.91	3433001.74	S-E	40.13	1023	Dagshai and Kausauli Fm of W. Himalayas	848	5137	233	Deciduous Forest
124	113904.52	3432423.16	E	32.25	1168	Dagshai and Kausauli Fm of W. Himalayas	1696	4281	192	Sparsely Vegetated
125	115394.59	3431937.05	E	13.12	1054	Dagshai and Kausauli Fm of W. Himalayas	848	5137	484	Shrub Land
126	132708.71	3431753.59	S	28.37	1597	Simla Gp	1199	3087	32	Sparsely Vegetated
127	159695.39	3433436.61	S-W	41.02	1384	Simla Gp	0	1211	13509	Sparsely Vegetated
128	159754.98	3432526.33	E	40.69	1486	Jaunsar Gp of W. Himalaya	0	856	13098	Sparsely Vegetated
129	158643.20	3432771.76	S-E	41.30	1683	Simla Gp	848	0	12257	Sparsely Vegetated
130	121676.74	3430212.08	S-E	20.59	1389	Krol, Infrakrol & Blaini Formation	1696	856	2811	Sparsely Vegetated
131	111490.58	3429938.79	W	45.66	1079	Subathu Fm of W. Himalaya	1199	1712	0	Sparsely Vegetated
132	117874.37	3429452.53	E	27.87	1132	Dagshai and Kausauli Fm of W. Himalayas	0	3087	187	Evergreen Forest
133	117073.05	3431317.85	W	23.98	1113	Dagshai and Kausauli Fm of W. Himalayas	0	3425	0	Sparsely Vegetated
134	118208.31	3430810.71	S-W	20.07	1282	Subathu Fm of W. Himalaya	848	1712	0	Shrub Land
135	119206.14	3430763.50	S-E	19.56	1343	Subathu Fm of W. Himalaya	1199	856	859	Sparsely Vegetated
136	146123.59	3429887.24	N	50.14	1194	Simla Gp	0	3087	4418	Shrub Land
137	146934.68	3430227.99	N	37.32	1296	Simla Gp	848	2422	4402	Sparsely Vegetated
138	147112.27	3430099.62	N-E	40.67	1293	Simla Gp	848	2422	4221	Sparsely Vegetated
139	147279.69	3430433.71	S-W	27.98	1226	Simla Gp	848	2422	4486	Sparsely Vegetated
140	147363.26	3430292.12	S-W	35.02	1201	Simla Gp	848	1914	4339	Sparsely Vegetated

141	148870.68	3431425.86	S-E	39.35	1185	Simla Gp	0	2422	5368	Sparsely Vegetated
142	113333.90	3428101.60	S	35.61	1192	Subathu Fm of W. Himalaya	0	3425	273	Sparsely Vegetated
143	132321.12	3427872.87	S	25.84	1051	Krol, Infrakrol & Blaini Formation	0	6054	0	Sparsely Vegetated
144	130856.47	3429118.91	S-E	24.92	1331	Krol, Infrakrol & Blaini Formation	848	5415	417	Sparsely Vegetated
145	121575.55	3427951.30	W	36.17	1776	Krol, Infrakrol & Blaini Formation	1896	1914	1404	Deciduous Forest
146	121625.69	3427677.96	S-W	17.20	1733	Krol, Infrakrol & Blaini Formation	1199	1211	1229	Sparsely Vegetated
147	121790.86	3427714.36	S-W	33.10	1786	Krol, Infrakrol & Blaini Formation	1896	1211	1376	Sparsely Vegetated
148	108063.48	3427626.03	E	22.08	745	Lower Siwalik Group	1696	1712	2204	Sparsely Vegetated
149	111630.25	3428059.42	S	31.57	1007	Lower Siwalik Group	0	1712	588	Sparsely Vegetated
150	118207.53	3428640.68	E	22.68	1171	Dagshai and Kausauli Fm of W. Himalayas	0	3087	458	Sparsely Vegetated
151	118628.82	3428126.26	N-E	5.51	1178	Dagshai and Kausauli Fm of W. Himalayas	0	3087	673	Sparsely Vegetated
152	117956.73	3428953.66	N-E	28.44	1167	Dagshai and Kausauli Fm of W. Himalayas	848	3087	244	Evergreen Forest
153	139500.47	3427565.78	S-E	28.44	1693	Jaunsar Gp of W. Himalaya	1199	3425	4750	Sparsely Vegetated
154	151656.56	3428993.16	S-E	29.51	1556	Jaunsar Gp of W. Himalaya	0	856	4398	Sparsely Vegetated
155	161722.45	3427902.01	S	26.64	2204	Jaunsar Gp of W. Himalaya	1199	4366	13468	Evergreen Forest
156	135670.49	3425616.15	S	39.45	984	Krol, Infrakrol & Blaini Formation	0	6174	3284	Sparsely Vegetated
157	130917.74	3426499.38	E	17.44	1417	Krol, Infrakrol & Blaini Formation	848	4281	295	Sparsely Vegetated
158	123502.89	3425513.99	W	38.68	1808	Krol, Infrakrol & Blaini Formation	2399	1211	724	Sparsely Vegetated
159	123396.83	3425727.57	W	38.78	1789	Krol, Infrakrol & Blaini Formation	2399	1211	930	Deciduous Forest
160	122455.82	3426773.65	S-W	26.23	1705	Krol, Infrakrol & Blaini Formation	1696	1914	1576	Sparsely Vegetated

161	122380.29	3426856.87	S-W	30.75	1712	Krol, Infrakrol & Blaini Formation	1896	1914	1539	Sparsely Vegetated
162	126465.79	3425851.81	N-E	16.62	1529	Krol, Infrakrol & Blaini Formation	1896	0	0	Sparsely Vegetated
163	126303.81	3425777.57	S-W	21.96	1521	Krol, Infrakrol & Blaini Formation	1896	0	45	Sparsely Vegetated
164	111409.84	3426139.81	S-W	35.70	1037	Lower Siwalik Group	1199	1712	1482	Sparsely Vegetated
165	110160.56	3425816.98	S-W	29.08	1056	Lower Siwalik Group	1696	0	1975	Sparsely Vegetated
166	111320.71	3426431.93	W	27.02	1044	Lower Siwalik Group	1199	856	1180	Shrub Land
167	110016.07	3426180.90	N-W	28.43	1041	Lower Siwalik Group	1896	0	1749	Sparsely Vegetated
168	107619.30	3426303.22	E	17.92	680	Dagshai and Kausauli Fm of W. Himalayas	848	2569	2281	Sparsely Vegetated
169	107323.74	3425635.12	S	15.47	667	Dagshai and Kausauli Fm of W. Himalayas	0	2569	1682	Sparsely Vegetated
170	115992.13	3425576.37	S-E	25.59	1627	Dagshai and Kausauli Fm of W. Himalayas	3058	5415	0	Sparsely Vegetated
171	110339.27	3425442.56	S-W	32.37	1048	Lower Siwalik Group	1696	0	2257	Sparsely Vegetated
172	120381.07	3427153.57	S-W	23.32	1327	Subathu Fm of W. Himalaya	0	2422	0	Sparsely Vegetated
173	123645.15	3427324.92	E	22.41	1476	Krol, Infrakrol & Blaini Formation	1199	0	2336	Evergreen Forest
174	135521.13	3425504.02	S-E	21.96	1002	Krol, Infrakrol & Blaini Formation	0	6174	3326	Sparsely Vegetated
175	139140.25	3425570.17	S	37.87	1258	Simla Gp	848	5137	4349	Sparsely Vegetated
176	140405.68	3426168.75	E	22.53	1062	Simla Gp	0	5208	4877	Sparsely Vegetated
177	140633.40	3426343.08	S	12.14	1080	Simla Gp	0	4611	5057	Sparsely Vegetated
178	124315.15	3424040.57	S-W	39.32	1830	Krol, Infrakrol & Blaini Formation	2682	1914	64	Sparsely Vegetated
179	124317.67	3423946.06	S-W	19.63	1763	Krol, Infrakrol & Blaini Formation	2682	1914	32	Sparsely Vegetated
180	125751.19	3424293.34	S	28.86	1640	Krol, Infrakrol & Blaini Formation	1199	1211	32	Sparsely Vegetated
181	113188.85	3423839.73	N-W	45.70	1225	Lower Siwalik Group	1896	2569	2514	Evergreen Forest

182	113352.53	3424176.66	S	34.83	1268	Subathu Fm of W. Himalaya	1896	2569	2164	Sparsely Vegetated
183	114065.86	3424353.86	S-W	49.01	1457	Subathu Fm of W. Himalaya	3058	3425	1539	Evergreen Forest
184	113587.16	3424430.16	S-E	32.89	1417	Subathu Fm of W. Himalaya	2399	2569	1830	Sparsely Vegetated
185	115754.30	3424789.06	E	31.19	1499	Dagshai and Kausauli Fm of W. Himalayas	3058	5208	528	Sparsely Vegetated
186	109863.50	3424158.80	W	30.51	765	Lower Siwalik Group	848	856	1360	Sparsely Vegetated
187	107841.84	3424461.72	S	27.34	630	Dagshai and Kausauli Fm of W. Himalayas	848	2707	1088	Deciduous Forest
188	111649.60	3424942.56	W	33.33	1071	Lower Siwalik Group	1696	1211	2694	Deciduous Forest
189	118251.48	3423484.95	S-E	20.33	1175	Dagshai and Kausauli Fm of W. Himalayas	1696	6687	375	Deciduous Forest
190	136299.24	3424700.85	S-W	22.78	928	Krol, Infrakrol & Blaini Formation	0	6520	4411	Sparsely Vegetated
191	135889.48	3423780.94	E	22.62	1302	Krol, Infrakrol & Blaini Formation	848	6054	4835	Sparsely Vegetated
192	141713.24	3423866.40	S	33.25	1188	Simla Gp	0	5415	2989	Sparsely Vegetated
193	146633.02	3424730.57	S-E	32.65	1553	Jaunsar Gp of W. Himalaya	848	1211	1728	Sparsely Vegetated
194	145048.01	3423561.34	S-E	27.94	1412	Jaunsar Gp of W. Himalaya	0	1914	3296	Sparsely Vegetated
195	145191.19	3423618.58	S	34.11	1418	Jaunsar Gp of W. Himalaya	0	1914	3136	Sparsely Vegetated
196	163840.40	3424873.66	S-W	42.78	2462	Jutogh Gp of W.Himalaya	848	7658	15456	Evergreen Forest
197	168562.63	3423913.27	N-E	32.44	2252	Jutogh Gp of W.Himalaya	0	6054	14584	Evergreen Forest
198	117501.57	3422657.65	Flat	0.89	722	Dagshai and Kausauli Fm of W. Himalayas	848	6520	32	Sparsely Vegetated
199	127205.65	3421598.92	E	16.40	1640	Dagshai and Kausauli Fm of W. Himalayas	848	1712	45	Sparsely Vegetated
200	126899.89	3421661.46	S	26.61	1681	Dagshai and Kausauli Fm of W. Himalayas	848	1712	32	Sparsely Vegetated

201	127046.58	3421624.54	S	28.69	1658	Dagshai and Kausauli Fm of W. Himalayas	848	1712	32	Sparsely Vegetated
202	126786.35	3421672.22	S-W	23.84	1659	Dagshai and Kausauli Fm of W. Himalayas	848	1712	32	Sparsely Vegetated
203	126651.25	3421749.72	S-W	32.98	1650	Dagshai and Kausauli Fm of W. Himalayas	848	2422	0	Sparsely Vegetated
204	125907.28	3422319.22	S	31.23	1652	Dagshai and Kausauli Fm of W. Himalayas	1199	1914	0	Sparsely Vegetated
205	125757.73	3422365.51	S	29.87	1670	Dagshai and Kausauli Fm of W. Himalayas	1199	2422	32	Sparsely Vegetated
206	125669.70	3422253.51	S-W	20.98	1586	Dagshai and Kausauli Fm of W. Himalayas	1896	2422	96	Sparsely Vegetated
207	125408.96	3422763.78	S-W	18.52	1652	Dagshai and Kausauli Fm of W. Himalayas	1696	2422	0	Sparsely Vegetated
208	125282.35	3422909.55	S	35.82	1711	Dagshai and Kausauli Fm of W. Himalayas	1696	1914	0	Sparsely Vegetated
209	125137.53	3422878.23	W	26.23	1646	Dagshai and Kausauli Fm of W. Himalayas	1696	1914	0	Sparsely Vegetated
210	125055.78	3423013.18	S-W	40.13	1679	Dagshai and Kausauli Fm of W. Himalayas	1696	1914	32	Sparsely Vegetated
211	112865.02	3422604.07	S-W	35.56	1163	Lower Siwalik Group	1199	1712	1953	Sparsely Vegetated
212	113060.74	3422854.97	N	36.33	1128	Lower Siwalik Group	1696	2569	2178	Shrub Land
213	112858.52	3421185.92	S-W	32.71	952	Lower Siwalik Group	1896	1712	521	Sparsely Vegetated
214	130696.69	3421725.82	S-W	24.12	1412	Krol, Infrakrol & Blaini Formation	848	856	3520	Sparsely Vegetated
215	131863.61	3421298.55	S	18.51	1399	Krol, Infrakrol & Blaini Formation	2544	1211	4683	Sparsely Vegetated
216	136408.23	3421172.86	S-E	26.23	1101	Krol, Infrakrol & Blaini Formation	848	4843	3649	Sparsely Vegetated
217	136826.15	3421386.62	S-E	33.46	1066	Krol, Infrakrol & Blaini Formation	0	4843	3233	Sparsely Vegetated

218	110733.90	3422752.97	S-E	33.23	864	Lower Siwalik Group	0	0	373	Sparsely Vegetated
219	118112.34	3423226.71	S	18.98	1158	Dagshai and Kausauli Fm of W. Himalayas	848	6849	405	Sparsely Vegetated
220	124913.81	3423145.92	W	28.03	1633	Dagshai and Kausauli Fm of W. Himalayas	1696	2422	0	Sparsely Vegetated
221	129131.10	3421301.91	S-W	28.95	1183	Krol, Infrakrol & Blaini Formation	0	0	1978	Sparsely Vegetated
222	127055.44	3421984.32	N-E	35.91	1640	Krol, Infrakrol & Blaini Formation	848	1211	0	Sparsely Vegetated
223	146313.62	3421205.91	E	31.58	1335	Jaunsar Gp of W. Himalaya	0	856	1763	Sparsely Vegetated
224	150452.62	3423161.48	S-E	24.11	1855	Jutogh Gp of W.Himalaya	848	2422	2112	Sparsely Vegetated
225	117468.43	3420648.43	E	26.57	1112	Dagshai and Kausauli Fm of W. Himalayas	0	6054	45	Sparsely Vegetated
226	117726.05	3420692.49	E	31.44	1014	Dagshai and Kausauli Fm of W. Himalayas	0	6054	202	Sparsely Vegetated
227	117546.81	3420378.59	E	28.23	1144	Dagshai and Kausauli Fm of W. Himalayas	0	6054	32	Sparsely Vegetated
228	117438.21	3420179.66	S	30.03	1100	Dagshai and Kausauli Fm of W. Himalayas	0	5743	32	Sparsely Vegetated
229	117313.41	3419230.35	N	39.17	914	Dagshai and Kausauli Fm of W. Himalayas	0	4611	429	Shrub Land
230	118373.56	3420143.16	S-W	32.62	1021	Dagshai and Kausauli Fm of W. Himalayas	0	6520	737	Shrub Land
231	134024.07	3420728.69	S-W	20.66	1222	Krol, Infrakrol & Blaini Formation	1199	2422	6041	Sparsely Vegetated
232	115881.23	3419639.16	S-E	28.02	1407	Subathu Fm of W. Himalaya	1199	4281	800	Sparsely Vegetated
233	117287.77	3419747.86	S-E	33.61	935	Dagshai and Kausauli Fm of W. Himalayas	0	4992	226	Sparsely Vegetated
234	116904.62	3419332.35	S-E	31.89	1031	Dagshai and Kausauli Fm of W. Himalayas	848	4611	32	Sparsely Vegetated

235	117605.76	3419832.12	S-E	19.73	936	Dagshai and Kausauli Fm of W. Himalayas	0	5743	290	Sparsely Vegetated
236	135889.66	3420662.36	S	34.05	1045	Krol, Infrakrol & Blaini Formation	848	3632	4204	Sparsely Vegetated
237	138728.48	3419337.64	E	27.18	1185	Krol, Infrakrol & Blaini Formation	848	4611	2080	Sparsely Vegetated
238	144865.83	3420336.27	E	36.64	1585	Jaunsar Gp of W. Himalaya	1199	856	891	Sparsely Vegetated
239	116343.82	3417589.78	N-W	45.02	1029	Subathu Fm of W. Himalaya	0	3087	747	Sparsely Vegetated
240	116280.85	3417415.83	W	38.66	1090	Subathu Fm of W. Himalaya	848	3087	859	Sparsely Vegetated
241	123060.08	3418322.91	S	22.78	1409	Dagshai and Kausauli Fm of W. Himalayas	2544	6903	1219	Sparsely Vegetated
242	123009.42	3418328.40	S	23.68	1406	Dagshai and Kausauli Fm of W. Himalayas	2544	6903	1250	Sparsely Vegetated
243	122976.33	3418258.29	S	29.28	1366	Dagshai and Kausauli Fm of W. Himalayas	2544	6903	1328	Sparsely Vegetated
244	122949.06	3418398.42	S-W	27.09	1430	Dagshai and Kausauli Fm of W. Himalayas	1696	6903	1299	Sparsely Vegetated
245	175778.48	3417645.33	N	38.09	1914	Jaunsar Gp of W. Himalaya	848	4281	5282	Sparsely Vegetated
246	115097.87	3418142.77	S-E	22.11	783	Subathu Fm of W. Himalaya	0	2707	224	Sparsely Vegetated
247	114999.68	3418422.32	S-W	21.90	861	Subathu Fm of W. Himalaya	848	2707	32	Deciduous Forest
248	115219.01	3418368.12	S	16.39	885	Subathu Fm of W. Himalaya	848	2707	32	Sparsely Vegetated
249	114875.34	3417773.18	N-E	32.33	721	Subathu Fm of W. Himalaya	0	2707	618	Evergreen Forest
250	114566.76	3418225.31	S-E	27.29	773	Subathu Fm of W. Himalaya	0	1914	202	Sparsely Vegetated
251	116510.50	3418893.79	S	22.88	1035	Subathu Fm of W. Himalaya	0	4611	64	Sparsely Vegetated
252	116497.74	3419109.03	E	30.18	1034	Subathu Fm of W. Himalaya	0	4611	45	Sparsely Vegetated
253	121133.37	3419132.63	S	40.17	1491	Dagshai and Kausauli Fm of W. Himalayas	1896	7894	3136	Sparsely Vegetated

254	140965.27	3417602.08	S-W	37.78	964	Krol, Infrakrol & Blaini Formation	0	5208	994	Sparsely Vegetated
255	127472.73	3415476.50	S-W	34.62	1329	Dagshai and Kausauli Fm of W. Himalayas	2544	6054	45	Sparsely Vegetated
256	114951.84	3414345.86	S-E	32.74	866	Lower Siwalik Group	3058	856	3921	Sparsely Vegetated
257	169660.34	3413739.58	S-W	31.48	2052	Jutogh Gp of W.Himalaya	0	0	11180	Sparsely Vegetated
258	128313.36	3414699.61	W	32.01	1470	Dagshai and Kausauli Fm of W. Himalayas	2544	6054	0	Sparsely Vegetated
259	114577.30	3414678.76	S-W	32.85	881	Lower Siwalik Group	2399	0	3471	Sparsely Vegetated
260	116223.49	3415055.27	S	23.78	1118	Subathu Fm of W. Himalaya	2544	1712	3152	Sparsely Vegetated
261	117433.72	3414195.04	S-W	35.08	1142	Subathu Fm of W. Himalaya	3793	2422	4285	Sparsely Vegetated
262	121522.08	3414405.02	E	27.79	916	Dagshai and Kausauli Fm of W. Himalayas	0	4992	4033	Sparsely Vegetated
263	135106.39	3414375.77	S-W	23.31	1408	Krol, Infrakrol & Blaini Formation	1896	0	4924	Sparsely Vegetated
264	147884.64	3414201.11	S-W	30.60	1744	Jutogh Gp of W.Himalaya	1896	1211	1231	Sparsely Vegetated
265	142097.79	3413567.15	N-E	21.63	1040	Krol, Infrakrol & Blaini Formation	0	4843	1083	Sparsely Vegetated
266	148733.50	3413286.02	S-E	32.44	1584	Jutogh Gp of W.Himalaya	848	1211	544	Sparsely Vegetated
267	149044.02	3413108.63	S-E	43.02	1487	Jutogh Gp of W.Himalaya	0	856	224	Sparsely Vegetated
268	151659.20	3412954.64	E	33.01	1229	Jutogh Gp of W.Himalaya	0	856	2401	Sparsely Vegetated
269	156169.88	3415067.73	S-W	22.01	2122	Jutogh Gp of W.Himalaya	848	4611	6942	Sparsely Vegetated
270	178325.44	3413364.54	S	34.98	1173	Deoban Gp of W. India	0	8432	2528	Sparsely Vegetated
271	185543.39	3409138.22	S	38.02	959	Deoban Gp of W. India	848	4281	32	Evergreen Forest
272	180007.17	3409291.46	N-W	41.76	910	Jaunsar Gp of W. Himalaya	0	6687	1385	Sparsely Vegetated
273	179229.39	3409290.68	S	35.39	1107	Jaunsar Gp of W. Himalaya	0	7365	2173	Sparsely Vegetated

274	163782.83	3409929.02	W	24.70	2011	Jutogh Gp of W.Himalaya	1696	1712	14680	Sparsely Vegetated
275	163541.39	3410110.25	S	37.24	1973	Jutogh Gp of W.Himalaya	1696	2422	14408	Sparsely Vegetated
276	163462.51	3410167.93	S	26.99	1999	Jutogh Gp of W.Himalaya	1696	2422	14338	Sparsely Vegetated
277	163289.08	3410072.53	S-E	39.92	2027	Jutogh Gp of W.Himalaya	1696	2422	14157	Sparsely Vegetated
278	162984.18	3409887.21	S-E	38.92	2041	Jutogh Gp of W.Himalaya	1696	1712	13892	Sparsely Vegetated
279	161616.12	3409288.53	S-E	37.95	1599	Jutogh Gp of W.Himalaya	848	856	12616	Sparsely Vegetated
280	161064.59	3409407.75	S	33.92	1630	Jutogh Gp of W.Himalaya	0	856	12064	Sparsely Vegetated
281	161388.15	3409322.57	S-W	36.14	1620	Jutogh Gp of W.Himalaya	848	856	12390	Sparsely Vegetated
282	138544.15	3409529.22	S-W	33.33	1636	Dagshai and Kausauli Fm of W. Himalayas	1896	0	5340	Sparsely Vegetated
283	145801.54	3409355.18	N-E	42.84	833	Krol, Infrakrol & Blaini Formation	0	5482	559	Sparsely Vegetated
284	154288.67	3408519.83	S-E	43.56	1997	Jutogh Gp of W.Himalaya	1896	1211	5911	Sparsely Vegetated
285	156456.77	3409194.96	S-W	40.89	1427	Jutogh Gp of W.Himalaya	848	0	7630	Evergreen Forest
286	162819.26	3409707.35	S-E	33.94	1988	Jutogh Gp of W.Himalaya	848	1712	13754	Sparsely Vegetated
287	165347.68	3409283.21	N	31.31	1810	Jutogh Gp of W.Himalaya	1199	1211	15820	Sparsely Vegetated
288	168087.17	3409307.11	W	8.89	2406	Jaunsar Gp of W. Himalaya	3393	0	13136	Sparsely Vegetated
289	168952.64	3409539.06	S-E	40.92	2490	Jaunsar Gp of W. Himalaya	3058	0	12247	Sparsely Vegetated
290	172776.37	3408626.49	S	40.61	1900	Jaunsar Gp of W. Himalaya	1896	3530	8623	Sparsely Vegetated
291	174387.88	3407517.77	S	40.93	1743	Jaunsar Gp of W. Himalaya	1199	5415	7244	Sparsely Vegetated
292	174566.06	3407772.32	E	37.32	1671	Jaunsar Gp of W. Himalaya	1199	5415	7010	Sparsely Vegetated
293	174681.31	3407805.21	S-E	42.11	1635	Jaunsar Gp of W. Himalaya	1199	5415	6910	Sparsely Vegetated
294	175488.33	3407728.62	S	43.28	1474	Jaunsar Gp of W. Himalaya	1696	6174	6134	Sparsely Vegetated

295	176023.49	3408208.29	S	39.10	1465	Jaunsar Gp of W. Himalaya	1896	6903	5513	Sparsely Vegetated
296	149411.51	3407628.03	S	34.35	1150	Jaunsar Gp of W. Himalaya	848	4281	2422	Sparsely Vegetated
297	117956.97	3406893.98	N	22.46	717	Lower Siwalik Group	0	856	32	Sparsely Vegetated
298	118859.99	3407685.75	S-W	22.86	727	Subathu Fm of W. Himalaya	0	1914	1135	Sparsely Vegetated
299	118924.65	3408237.35	N-E	21.98	663	Subathu Fm of W. Himalaya	0	1914	1391	Shrub Land
300	128812.32	3407259.58	S	17.82	996	Dagshai and Kausauli Fm of W. Himalayas	848	4992	480	Sparsely Vegetated
301	173030.00	3408394.55	S-W	46.51	1863	Jaunsar Gp of W. Himalaya	1896	4281	8410	Sparsely Vegetated
302	176187.45	3407350.98	S-W	38.31	1310	Jaunsar Gp of W. Himalaya	848	7315	5508	Sparsely Vegetated
303	165169.42	3405649.21	S	45.40	1856	Jutogh Gp of W.Himalaya	848	2569	12756	Evergreen Forest
304	164981.82	3405622.07	S	26.76	1837	Jutogh Gp of W.Himalaya	848	2569	12675	Evergreen Forest
305	164823.87	3405836.11	S-E	44.27	1886	Jutogh Gp of W.Himalaya	1199	1712	12849	Sparsely Vegetated
306	164658.28	3405660.86	S-E	36.58	1873	Jutogh Gp of W.Himalaya	0	2569	12621	Sparsely Vegetated
307	163909.75	3405349.06	S	37.38	1812	Jutogh Gp of W.Himalaya	0	2569	12116	Sparsely Vegetated
308	163371.12	3405724.64	S-E	32.01	1762	Jutogh Gp of W.Himalaya	848	1712	12343	Sparsely Vegetated
309	163215.96	3405628.05	S-E	27.03	1693	Jutogh Gp of W.Himalaya	0	2569	12209	Sparsely Vegetated
310	162857.73	3405817.57	S	42.53	1632	Jutogh Gp of W.Himalaya	848	1712	12302	Sparsely Vegetated
311	162746.78	3405830.62	S	54.62	1653	Jutogh Gp of W.Himalaya	848	1712	12268	Sparsely Vegetated
312	162656.94	3405837.15	S	39.82	1645	Jutogh Gp of W.Himalaya	848	1712	12282	Sparsely Vegetated
313	162277.64	3406684.91	S	33.97	1636	Jutogh Gp of W.Himalaya	1199	856	12981	Built-up
314	134694.10	3405159.78	S-W	29.40	1608	Dagshai and Kausauli Fm of W. Himalayas	1696	5415	45	Sparsely Vegetated

315	134614.78	3405209.99	S-W	20.88	1589	Dagshai and Kausauli Fm of W. Himalayas	1696	5415	0	Sparsely Vegetated
316	187219.28	3405002.10	S	43.05	799	Manjir Fm of W. Himalaya	0	1211	32	Sparsely Vegetated
317	116729.73	3405694.48	W	0.90	722	Lower Siwalik Group	1199	1211	32	Deciduous Forest
318	117809.61	3406312.30	E	19.81	752	Lower Siwalik Group	848	0	0	Sparsely Vegetated
319	119669.97	3405024.80	N	30.22	850	Lower Siwalik Group	848	856	96	Sparsely Vegetated
320	119231.37	3405113.80	N	23.34	856	Lower Siwalik Group	848	856	32	Sparsely Vegetated
321	119598.12	3405682.46	S-W	28.46	729	Lower Siwalik Group	0	856	703	Sparsely Vegetated
322	118376.65	3405616.31	N-E	16.36	711	Lower Siwalik Group	848	0	358	Sparsely Vegetated
323	119672.60	3406015.86	N	29.72	666	Subathu Fm of W. Himalaya	0	1211	1017	Sparsely Vegetated
324	117858.53	3405336.05	S-W	26.47	803	Lower Siwalik Group	1199	856	45	Sparsely Vegetated
325	118148.93	3405068.35	S-W	18.00	763	Lower Siwalik Group	848	856	192	Sparsely Vegetated
326	141450.64	3405785.69	S-W	13.96	1454	Krol, Infrakrol & Blaini Formation	1696	856	4937	Sparsely Vegetated
327	141635.71	3405015.67	S	21.99	1414	Dagshai and Kausauli Fm of W. Himalayas	1199	0	5123	Sparsely Vegetated
328	149379.36	3405015.75	S	27.46	1157	Jaunsar Gp of W. Himalaya	848	4843	1863	Sparsely Vegetated
329	149629.73	3404612.42	S-W	27.04	1120	Jaunsar Gp of W. Himalaya	848	4281	2080	Sparsely Vegetated
330	156607.22	3405095.27	S	33.83	1053	Jaunsar Gp of W. Himalaya	848	4281	9059	Sparsely Vegetated
331	188548.73	3403098.91	S-W	57.38	742	Manjir Fm of W. Himalaya	0	1211	32	Sparsely Vegetated
332	151933.84	3402979.39	S-W	27.26	1016	Jaunsar Gp of W. Himalaya	0	4281	4384	Sparsely Vegetated
333	158107.34	3403373.15	S	40.93	1247	Jaunsar Gp of W. Himalaya	1199	5415	9088	Sparsely Vegetated
334	187653.19	3403576.65	S-W	42.75	739	Manjir Fm of W. Himalaya	0	856	0	Sparsely Vegetated
335	188610.75	3402708.79	S-W	28.11	732	Manjir Fm of W. Himalaya	0	1211	0	Sparsely Vegetated

336	158456.97	3401346.10	N	13.30	1745	Krol, Infrakrol & Blaini Formation	3058	6520	7041	Sparsely Vegetated
337	145215.50	3400114.29	S	26.84	1121	Dagshai and Kausauli Fm of W. Himalayas	848	1914	2304	Sparsely Vegetated
338	145280.76	3400136.81	S	33.04	1127	Dagshai and Kausauli Fm of W. Himalayas	848	1914	2208	Sparsely Vegetated
339	159949.71	3402427.57	S	37.04	1833	Jaunsar Gp of W. Himalaya	2399	5743	8284	Sparsely Vegetated
340	160101.72	3402514.97	S	30.83	1845	Jaunsar Gp of W. Himalaya	2399	5743	8410	Sparsely Vegetated
341	160407.04	3402469.84	S-E	24.43	1832	Jaunsar Gp of W. Himalaya	2399	5415	8413	Sparsely Vegetated
342	160376.48	3402439.04	S-E	20.88	1832	Jaunsar Gp of W. Himalaya	2399	5415	8374	Sparsely Vegetated
343	160513.98	3402522.59	S-E	30.81	1815	Jaunsar Gp of W. Himalaya	1896	5415	8506	Sparsely Vegetated
344	163497.22	3402499.89	S	45.46	1657	Krol, Infrakrol & Blaini Formation	848	5137	9262	Sparsely Vegetated
345	163673.68	3402509.78	S-E	29.91	1654	Krol, Infrakrol & Blaini Formation	848	5137	9336	Sparsely Vegetated
346	163985.26	3402315.59	S-E	30.12	1678	Krol, Infrakrol & Blaini Formation	848	5137	9235	Sparsely Vegetated
347	164100.52	3402370.89	S	47.60	1704	Krol, Infrakrol & Blaini Formation	848	5137	9299	Sparsely Vegetated
348	125794.94	3400726.92	S-W	29.46	1032	Subathu Fm of W. Himalaya	848	1712	1645	Sparsely Vegetated
349	125284.48	3401238.70	S-W	18.99	1056	Subathu Fm of W. Himalaya	1199	1712	1409	Sparsely Vegetated
350	193756.76	3401823.65	S	34.96	1786	Manjir Fm of W. Himalaya	1199	4611	3310	Sparsely Vegetated
351	194012.24	3401721.09	S	33.73	1784	Manjir Fm of W. Himalaya	1199	4611	3364	Sparsely Vegetated
352	194833.58	3401619.09	S	36.50	1836	Manjir Fm of W. Himalaya	1896	4992	3824	Sparsely Vegetated
353	195296.91	3401170.60	S-E	30.98	1879	Manjir Fm of W. Himalaya	3058	4843	3906	Sparsely Vegetated
354	157772.12	3401936.35	E	17.25	1541	Krol, Infrakrol & Blaini Formation	1896	6903	7656	Shrub Land
355	157837.14	3401567.86	N	36.58	1582	Krol, Infrakrol & Blaini Formation	1896	6903	7270	Shrub Land
356	122454.07	3402281.42	S-E	32.03	889	Lower Siwalik Group	1696	1211	1122	Sparsely Vegetated

357	123479.71	3401462.27	W	28.17	997	Subathu Fm of W. Himalaya	1896	1914	1954	Sparsely Vegetated
358	126001.70	3401763.24	N-W	29.30	853	Dagshai and Kausauli Fm of W. Himalayas	0	856	607	Sparsely Vegetated
359	149443.04	3402356.24	E	55.31	1272	Krol, Infrakrol & Blaini Formation	848	3087	1920	Sparsely Vegetated
360	158280.64	3402388.04	S-W	32.65	1418	Jaunsar Gp of W. Himalaya	1896	6233	8096	Sparsely Vegetated
361	157826.99	3401090.41	S	30.03	1687	Krol, Infrakrol & Blaini Formation	2399	6174	6790	Sparsely Vegetated
362	155297.63	3401329.84	S	40.32	1036	Jaunsar Gp of W. Himalaya	848	4843	7238	Sparsely Vegetated
363	153133.31	3400095.10	N	39.53	786	Krol, Infrakrol & Blaini Formation	0	2707	5632	Sparsely Vegetated
364	188873.39	3402122.87	S-W	55.47	737	Manjir Fm of W. Himalaya	0	856	32	Sparsely Vegetated
365	146603.83	3399070.00	S-E	27.35	1144	Dagshai and Kausauli Fm of W. Himalayas	1199	1211	800	Sparsely Vegetated
366	146880.23	3399294.12	S-W	23.43	1292	Dagshai and Kausauli Fm of W. Himalayas	1199	1211	567	Sparsely Vegetated
367	146993.20	3399177.82	S-W	27.82	1280	Dagshai and Kausauli Fm of W. Himalayas	1896	1211	421	Sparsely Vegetated
368	184640.63	3398730.66	S-E	44.57	1805	Jaunsar Gp of W. Himalaya	3393	3829	0	Sparsely Vegetated
369	125994.45	3399747.11	N-E	16.32	834	Subathu Fm of W. Himalaya	1696	1211	2599	Sparsely Vegetated
370	129626.79	3399813.53	S-E	21.16	1137	Dagshai and Kausauli Fm of W. Himalayas	1896	1211	4066	Shrub Land
371	154523.67	3399028.73	S-E	34.08	918	Jaunsar Gp of W. Himalaya	0	3087	5092	Sparsely Vegetated
372	188541.56	3399986.51	W	52.42	776	Jaunsar Gp of W. Himalaya	0	856	32	Sparsely Vegetated
373	183949.01	3398992.42	S-W	31.52	1798	Jaunsar Gp of W. Himalaya	2682	4366	91	Sparsely Vegetated
374	192297.44	3396735.26	S	33.38	809	Jaunsar Gp of W. Himalaya	0	0	345	Sparsely Vegetated
375	201859.84	3396251.04	S-E	31.08	1863	Jaunsar Gp of W. Himalaya	2682	2569	224	Sparsely Vegetated

376	201699.79	3396351.66	S	23.18	1969	Jaunsar Gp of W. Himalaya	3497	3425	132	Sparsely Vegetated
377	201240.76	3396808.34	S-W	35.51	2046	Jaunsar Gp of W. Himalaya	3497	3425	0	Built-up
378	150976.94	3397939.11	S-W	9.15	1546	Krol, Infrakrol & Blaini Formation	2399	0	3662	Sparsely Vegetated
379	195568.50	3398175.69	S	38.25	1745	Manjir Fm of W. Himalaya	1696	3530	1811	Sparsely Vegetated
380	195614.13	3397838.96	S-W	43.54	1714	Manjir Fm of W. Himalaya	1696	3087	1694	Sparsely Vegetated
381	195863.00	3397696.57	S	45.78	1723	Manjir Fm of W. Himalaya	1696	3087	1886	Sparsely Vegetated
382	196403.93	3397081.31	N-E	29.54	1615	Jaunsar Gp of W. Himalaya	848	2569	1979	Sparsely Vegetated
383	196047.61	3397665.76	S	33.44	1688	Manjir Fm of W. Himalaya	1696	3087	2065	Sparsely Vegetated
384	196386.94	3396979.75	E	26.19	1621	Jaunsar Gp of W. Himalaya	848	2569	1944	Sparsely Vegetated
385	195260.51	3397218.79	S	35.54	1499	Jaunsar Gp of W. Himalaya	1696	3087	1216	Sparsely Vegetated
386	196691.09	3395923.55	E	29.19	1610	Jaunsar Gp of W. Himalaya	848	1712	1576	Sparsely Vegetated
387	181187.70	3397347.21	S	25.84	1578	Jaunsar Gp of W. Himalaya	848	7315	226	Sparsely Vegetated
388	181499.45	3396848.30	S	41.19	1496	Jaunsar Gp of W. Himalaya	848	7658	0	Sparsely Vegetated
389	181809.67	3397008.40	E	28.99	1506	Jaunsar Gp of W. Himalaya	1696	6903	32	Sparsely Vegetated
390	183072.52	3397945.49	E	28.34	1659	Jaunsar Gp of W. Himalaya	1896	5743	32	Sparsely Vegetated
391	198153.09	3396790.36	S	44.58	1473	Jaunsar Gp of W. Himalaya	848	2569	435	Sparsely Vegetated
392	200469.18	3396968.53	S-W	35.38	1740	Jaunsar Gp of W. Himalaya	3058	3425	72	Evergreen Forest
393	202079.84	3396477.08	S	32.45	2015	Jaunsar Gp of W. Himalaya	3598	3425	0	Sparsely Vegetated
394	202855.38	3396390.88	S	22.38	1976	Manjir Fm of W. Himalaya	3598	3530	365	Sparsely Vegetated
395	202886.00	3396447.99	S-E	12.33	1981	Manjir Fm of W. Himalaya	3058	3530	416	Sparsely Vegetated
396	156526.98	3398011.76	S-W	51.14	1000	Jaunsar Gp of W. Himalaya	0	3087	3824	Sparsely Vegetated
397	185507.61	3397666.15	S	36.52	1738	Jaunsar Gp of W. Himalaya	2544	3530	1223	Sparsely Vegetated

398	185276.17	3397544.66	S	26.93	1730	Jaunsar Gp of W. Himalaya	2544	3530	1120	Sparsely Vegetated
399	141426.98	3394651.13	S	27.25	1337	Dagshai and Kausauli Fm of W. Himalayas	1896	2569	0	Sparsely Vegetated
400	163800.38	3395355.27	S-W	37.01	1378	Krol, Infrakrol & Blaini Formation	0	3087	2734	Sparsely Vegetated
401	141302.18	3395068.67	S-W	27.42	1320	Dagshai and Kausauli Fm of W. Himalayas	1896	2569	0	Sparsely Vegetated
402	197126.41	3395604.21	E	27.09	1554	Jaunsar Gp of W. Himalaya	0	1712	1206	Sparsely Vegetated
403	197541.65	3395110.35	E	25.91	1409	Jaunsar Gp of W. Himalaya	0	856	707	Sparsely Vegetated
404	197682.01	3394802.73	N-E	27.59	1364	Jaunsar Gp of W. Himalaya	0	856	653	Sparsely Vegetated
405	198886.07	3394622.22	S-W	26.68	1579	Jaunsar Gp of W. Himalaya	848	1211	172	Sparsely Vegetated
406	146427.87	3395867.05	N	28.64	1032	Dagshai and Kausauli Fm of W. Himalayas	0	4281	329	Shrub Land
407	141662.25	3394826.85	S	24.58	1330	Dagshai and Kausauli Fm of W. Himalayas	1896	2569	32	Deciduous Forest
408	192582.14	3392661.61	S	37.74	862	Jaunsar Gp of W. Himalaya	0	2422	72	Sparsely Vegetated
409	192211.61	3392596.41	S	35.90	802	Jaunsar Gp of W. Himalaya	0	2422	0	Sparsely Vegetated
410	192733.49	3392748.92	S	41.71	943	Jaunsar Gp of W. Himalaya	0	1914	160	Sparsely Vegetated
411	143883.28	3392188.13	S	27.45	1211	Dagshai and Kausauli Fm of W. Himalayas	3793	856	32	Evergreen Forest
412	144325.18	3392884.26	N-W	28.59	1205	Subathu Fm of W. Himalaya	3793	1211	0	Evergreen Forest
413	143850.51	3393561.33	W	35.55	1246	Subathu Fm of W. Himalaya	3497	856	32	Sparsely Vegetated
414	142716.93	3394269.22	S-W	36.11	1276	Dagshai and Kausauli Fm of W. Himalayas	2544	1712	32	Shrub Land
415	160181.88	3393208.81	S	33.19	927	Krol, Infrakrol & Blaini Formation	848	856	547	Sparsely Vegetated
416	160613.23	3392998.75	S	19.87	888	Krol, Infrakrol & Blaini Formation	0	856	647	Sparsely Vegetated

417	196858.10	3393251.10	N-E	20.03	1590	Jaunsar Gp of W. Himalaya	1696	856	1985	Sparsely Vegetated
418	197782.54	3393408.24	S-E	27.67	1414	Jaunsar Gp of W. Himalaya	848	856	1076	Sparsely Vegetated
419	197872.87	3393539.51	S-E	45.10	1413	Jaunsar Gp of W. Himalaya	0	856	930	Sparsely Vegetated
420	197969.69	3393493.94	S-E	29.16	1349	Jaunsar Gp of W. Himalaya	0	856	862	Sparsely Vegetated
421	197967.89	3393572.30	S-E	36.31	1399	Jaunsar Gp of W. Himalaya	0	856	830	Sparsely Vegetated
422	198034.04	3393573.52	E	40.75	1351	Jaunsar Gp of W. Himalaya	0	856	774	Sparsely Vegetated
423	198027.83	3393656.32	E	47.47	1360	Jaunsar Gp of W. Himalaya	0	856	731	Sparsely Vegetated
424	198020.75	3393698.45	E	47.53	1356	Jaunsar Gp of W. Himalaya	0	856	719	Sparsely Vegetated
425	198663.27	3393185.94	N-E	38.91	1266	Jaunsar Gp of W. Himalaya	0	0	595	Sparsely Vegetated
426	199025.38	3392807.09	S-E	37.14	1253	Jaunsar Gp of W. Himalaya	0	856	446	Sparsely Vegetated
427	199088.09	3392895.05	N-E	23.05	1238	Jaunsar Gp of W. Himalaya	0	0	358	Sparsely Vegetated
428	190603.85	3391818.34	S	28.62	847	Jaunsar Gp of W. Himalaya	0	4281	707	Sparsely Vegetated
429	192573.65	3392230.58	S-W	35.42	699	Jaunsar Gp of W. Himalaya	0	2422	64	Sparsely Vegetated
430	200248.75	3392182.28	S-E	24.71	1203	Jaunsar Gp of W. Himalaya	0	856	0	Sparsely Vegetated
431	200163.00	3392109.14	S-E	23.98	1205	Jaunsar Gp of W. Himalaya	0	856	0	Sparsely Vegetated
432	200548.52	3392789.91	N-W	48.87	1295	Jaunsar Gp of W. Himalaya	0	856	72	Sparsely Vegetated
433	200417.50	3392929.20	S-E	35.36	1246	Jaunsar Gp of W. Himalaya	0	0	32	Sparsely Vegetated
434	200474.46	3393472.06	N-E	23.02	1407	Jaunsar Gp of W. Himalaya	0	0	384	Sparsely Vegetated
435	199951.05	3392961.30	S	36.22	1352	Jaunsar Gp of W. Himalaya	848	0	64	Sparsely Vegetated
436	199785.93	3392881.12	S-E	30.81	1324	Jaunsar Gp of W. Himalaya	0	0	32	Sparsely Vegetated
437	199309.48	3393557.86	S	25.99	1324	Jaunsar Gp of W. Himalaya	0	0	64	Sparsely Vegetated
438	199084.53	3394007.79	S-W	33.12	1403	Jaunsar Gp of W. Himalaya	848	856	32	Sparsely Vegetated

439	157415.91	3394134.15	N-E	40.45	769	Krol, Infrakrol & Blaini Formation	0	0	96	Sparsely Vegetated
440	158564.85	3391724.92	E	32.84	751	Krol, Infrakrol & Blaini Formation	0	1712	1056	Sparsely Vegetated
441	144195.72	3392066.75	S-W	39.79	1233	Dagshai and Kausauli Fm of W. Himalayas	3058	856	45	Evergreen Forest
442	150118.71	3393497.44	N-E	18.05	1030	Subathu Fm of W. Himalaya	0	2569	416	Sparsely Vegetated
443	151838.34	3392031.16	N	36.76	970	Subathu Fm of W. Himalaya	848	1712	1159	Sparsely Vegetated
444	149463.41	3393960.77	E	13.62	1002	Subathu Fm of W. Himalaya	0	3425	937	Shrub Land
445	159172.02	3394144.11	S-W	27.05	990	Krol, Infrakrol & Blaini Formation	848	856	64	Sparsely Vegetated
446	158940.78	3394565.03	S-W	33.37	982	Krol, Infrakrol & Blaini Formation	848	856	396	Sparsely Vegetated
447	156346.48	3394547.61	E	29.02	891	Krol, Infrakrol & Blaini Formation	848	856	405	Sparsely Vegetated
448	161273.72	3394238.15	N-E	31.98	858	Jaunsar Gp of W. Himalaya	0	1712	708	Sparsely Vegetated
449	161276.62	3393711.59	S-E	30.72	832	Krol, Infrakrol & Blaini Formation	0	856	224	Sparsely Vegetated
450	183501.11	3391908.43	S-E	34.63	1740	Krol, Infrakrol & Blaini Formation	2399	4281	32	Sparsely Vegetated
451	192970.79	3393132.48	N-W	49.57	1045	Jaunsar Gp of W. Himalaya	848	1211	181	Sparsely Vegetated
452	204717.50	3391963.90	S	19.51	1931	Jaunsar Gp of W. Himalaya	1696	0	0	Sparsely Vegetated
453	203296.02	3391850.36	W	42.25	1463	Jaunsar Gp of W. Himalaya	1199	0	1268	Sparsely Vegetated
454	160081.49	3390541.98	S	37.13	785	Krol, Infrakrol & Blaini Formation	848	856	1136	Sparsely Vegetated
455	143935.02	3390749.83	S-E	29.37	1117	Subathu Fm of W. Himalaya	2399	856	32	Sparsely Vegetated
456	182256.06	3391205.97	S-E	46.02	1703	Krol, Infrakrol & Blaini Formation	1896	3530	32	Sparsely Vegetated
457	182600.15	3391433.87	S-E	34.75	1736	Krol, Infrakrol & Blaini Formation	3058	3829	32	Sparsely Vegetated
458	183614.26	3390857.66	S-W	22.03	1434	Krol, Infrakrol & Blaini Formation	1896	3632	859	Sparsely Vegetated
459	192555.50	3390837.52	N-E	36.71	809	Jaunsar Gp of W. Himalaya	0	3829	45	Sparsely Vegetated

460	200187.52	3391112.37	N-E	26.26	1058	Jaunsar Gp of W. Himalaya	0	2569	132	Sparsely Vegetated
461	189079.81	3390771.05	S	44.52	952	Jaunsar Gp of W. Himalaya	848	6174	864	Sparsely Vegetated
462	190755.08	3391113.49	N	30.80	800	Jaunsar Gp of W. Himalaya	0	4843	45	Sparsely Vegetated
463	191406.40	3390874.99	N-E	23.64	834	Jaunsar Gp of W. Himalaya	0	4281	0	Sparsely Vegetated
464	191462.11	3391386.13	S-E	44.52	770	Jaunsar Gp of W. Himalaya	0	3632	396	Sparsely Vegetated
465	155146.06	3390574.75	N-E	25.49	829	Subathu Fm of W. Himalaya	0	0	3157	Shrub Land
466	205687.29	3391442.58	S-E	16.68	2057	Jaunsar Gp of W. Himalaya	1696	856	0	Sparsely Vegetated
467	145954.39	3389111.05	S-E	32.45	769	Subathu Fm of W. Himalaya	1896	2422	1056	Shrub Land
468	144817.29	3388555.24	S-W	19.90	753	Lower Siwalik Group	1896	1914	0	Shrub Land
469	144845.48	3389897.71	W	29.61	838	Subathu Fm of W. Himalaya	2682	1712	32	Sparsely Vegetated
470	162251.71	3390017.62	S-W	14.61	853	Krol, Infrakrol & Blaini Formation	0	0	1376	Sparsely Vegetated
471	161702.15	3389994.14	S	48.82	904	Krol, Infrakrol & Blaini Formation	848	0	1480	Sparsely Vegetated
472	161325.98	3389782.65	S-E	26.04	869	Krol, Infrakrol & Blaini Formation	848	0	1479	Sparsely Vegetated
473	187025.46	3387516.59	N-E	42.45	1403	Krol, Infrakrol & Blaini Formation	1696	4281	1824	Evergreen Forest
474	186296.25	3387980.83	N-E	40.40	1302	Krol, Infrakrol & Blaini Formation	1199	5137	2080	Sparsely Vegetated
475	186468.34	3388458.99	E	12.11	1190	Krol, Infrakrol & Blaini Formation	1199	5137	1660	Deciduous Forest
476	185675.62	3388581.03	N-E	28.31	1447	Krol, Infrakrol & Blaini Formation	1696	4281	2369	Deciduous Forest
477	184759.23	3389061.04	N-E	29.26	1423	Krol, Infrakrol & Blaini Formation	1199	3530	2722	Shrub Land
478	184011.86	3389345.00	E	45.40	1466	Krol, Infrakrol & Blaini Formation	1896	2707	1934	Sparsely Vegetated
479	182577.93	3389511.07	N-E	39.24	1773	Tal Fm of W. Himalaya	2544	2422	566	Shrub Land
480	176065.26	3388475.31	S-W	35.30	1016	Krol, Infrakrol & Blaini Formation	848	856	2736	Evergreen Forest
481	175729.18	3388424.35	S	36.86	875	Krol, Infrakrol & Blaini Formation	0	856	3088	Evergreen Forest

482	176689.69	3388328.61	S-W	38.15	1294	Krol, Infrakrol & Blaini Formation	1696	0	2163	Sparsely Vegetated
483	179427.95	3387698.94	S-E	26.47	960	Tal Fm of W. Himalaya	0	0	32	Evergreen Forest
484	178932.98	3388978.84	S-W	18.93	1175	Tal Fm of W. Himalaya	848	856	64	Sparsely Vegetated
485	178815.79	3389844.81	S	34.59	1556	Krol, Infrakrol & Blaini Formation	1199	1712	659	Sparsely Vegetated
486	179587.25	3389010.88	S-E	32.12	1218	Tal Fm of W. Himalaya	0	1211	32	Sparsely Vegetated
487	179931.42	3388958.41	S	32.38	1140	Tal Fm of W. Himalaya	0	1211	334	Sparsely Vegetated
488	200329.35	3390392.58	E	58.08	1124	Jaunsar Gp of W. Himalaya	848	2569	0	Sparsely Vegetated
489	200302.72	3389827.92	E	30.34	1102	Jaunsar Gp of W. Himalaya	848	3425	32	Sparsely Vegetated
490	200495.70	3388634.10	S-E	50.40	1106	Jaunsar Gp of W. Himalaya	0	3632	0	Sparsely Vegetated
491	200474.31	3388488.26	E	54.08	1069	Jaunsar Gp of W. Himalaya	0	4281	0	Sparsely Vegetated
492	200359.30	3388178.85	E	41.45	1106	Jaunsar Gp of W. Himalaya	0	4843	0	Sparsely Vegetated
493	200183.65	3387914.18	S-E	43.03	1111	Jaunsar Gp of W. Himalaya	848	4843	32	Sparsely Vegetated
494	200064.30	3387707.97	S	42.32	1066	Jaunsar Gp of W. Himalaya	0	5482	32	Sparsely Vegetated
495	199921.72	3387712.55	S-E	44.57	1066	Jaunsar Gp of W. Himalaya	0	5482	0	Sparsely Vegetated
496	200117.82	3387752.72	E	23.00	1071	Jaunsar Gp of W. Himalaya	0	4843	0	Sparsely Vegetated
497	199833.72	3387645.94	S-E	43.34	1077	Jaunsar Gp of W. Himalaya	0	5482	0	Sparsely Vegetated
498	199737.85	3387545.95	S-E	44.31	1073	Jaunsar Gp of W. Himalaya	0	5482	0	Sparsely Vegetated
499	189297.42	3387549.28	W	50.04	668	Krol, Infrakrol & Blaini Formation	0	4281	32	Sparsely Vegetated
500	187792.48	3387970.11	N-E	28.72	1049	Krol, Infrakrol & Blaini Formation	848	5137	950	Shrub Land
501	188942.39	3388901.02	S-W	20.33	977	Krol, Infrakrol & Blaini Formation	848	5993	506	Sparsely Vegetated
502	187042.34	3389808.22	S-W	16.92	737	Krol, Infrakrol & Blaini Formation	0	6233	847	Sparsely Vegetated
503	186801.14	3390052.95	S	33.50	841	Krol, Infrakrol & Blaini Formation	0	6233	1090	Sparsely Vegetated

504	186024.59	3390267.94	S-E	39.35	977	Krol, Infrakrol &Blaini Formation	0	5415	1878	Sparsely Vegetated
505	185477.41	3390097.96	S	39.76	966	Krol, Infrakrol & Blaini Formation	0	4611	2403	Sparsely Vegetated
506	188300.85	3389462.51	W	38.07	703	Krol, Infrakrol & Blaini Formation	0	6849	128	Sparsely Vegetated
507	188276.13	3389991.39	N	42.45	622	Jaunsar Gp of W. Himalaya	0	6849	0	Shrub Land
508	188433.58	3389929.80	N-E	54.43	628	Jaunsar Gp of W. Himalaya	0	6687	32	Shrub Land
509	148105.78	3390142.47	S-W	39.62	1323	Subathu Fm of W. Himalaya	2544	856	2886	Sparsely Vegetated
510	160328.54	3390101.48	S-W	37.78	672	Krol, Infrakrol & Blaini Formation	0	0	1417	Sparsely Vegetated
511	165682.01	3389831.45	W	37.76	840	Krol, Infrakrol & Blaini Formation	0	0	1002	Sparsely Vegetated
512	161762.80	3388159.02	N-E	45.04	1071	Subathu Fm of W. Himalaya	848	1712	0	Sparsely Vegetated
513	161647.93	3388571.89	N-E	11.86	954	Subathu Fm of W. Himalaya	848	1712	320	Sparsely Vegetated
514	171286.24	3387595.45	S	42.66	807	Krol, Infrakrol & Blaini Formation	848	2569	5252	Sparsely Vegetated
515	169657.59	3388217.24	S-W	48.77	1060	Krol, Infrakrol & Blaini Formation	848	1914	3633	Sparsely Vegetated
516	168239.45	3388391.52	W	44.74	883	Krol, Infrakrol & Blaini Formation	848	2569	2267	Sparsely Vegetated
517	175231.11	3389727.70	S-W	46.34	1032	Krol, Infrakrol & Blaini Formation	0	856	3615	Evergreen Forest
518	175652.70	3388666.87	W	51.72	860	Krol, Infrakrol & Blaini Formation	0	0	3120	Sparsely Vegetated
519	178304.44	3388163.46	S-E	53.63	1388	Tal Fm of W. Himalaya	848	0	679	Sparsely Vegetated
520	152096.83	3386404.43	S-E	31.32	761	Lower Siwalik Group	1199	2569	5068	Sparsely Vegetated
521	205361.21	3386415.54	S	29.45	1912	Jaunsar Gp of W. Himalaya	1896	5137	1222	Sparsely Vegetated
522	206308.02	3387038.95	S	28.75	2040	Jaunsar Gp of W. Himalaya	2544	4366	160	Sparsely Vegetated
523	206451.51	3387107.49	S	46.77	2074	Jaunsar Gp of W. Himalaya	2544	4281	143	Sparsely Vegetated
524	199707.93	3387381.54	E	36.15	1031	Jaunsar Gp of W. Himalaya	0	5482	0	Sparsely Vegetated
525	199498.45	3387186.67	S-W	32.02	1031	Jaunsar Gp of W. Himalaya	0	5743	0	Sparsely Vegetated

526	199100.35	3386952.67	S-E	45.47	1109	Jaunsar Gp of W. Himalaya	0	5743	64	Sparsely Vegetated
527	199119.12	3386755.15	E	30.07	1049	Jaunsar Gp of W. Himalaya	0	4992	32	Sparsely Vegetated
528	199066.17	3386463.44	S-E	46.89	1031	Jaunsar Gp of W. Himalaya	0	4992	0	Sparsely Vegetated
529	178933.54	3387016.45	S	13.89	869	Tal Fm of W. Himalaya	848	856	32	Sparsely Vegetated
530	179015.63	3387282.28	E	21.71	929	Tal Fm of W. Himalaya	848	0	0	Sparsely Vegetated
531	180482.10	3387511.34	E	26.76	1048	Tal Fm of W. Himalaya	0	856	1064	Evergreen Forest
532	193762.99	3386883.30	S	22.43	1541	Jaunsar Gp of W. Himalaya	1696	5137	1677	Sparsely Vegetated
533	194473.13	3386440.49	S-W	43.54	1265	Jaunsar Gp of W. Himalaya	1696	4281	1096	Sparsely Vegetated
534	152400.19	3386375.22	S-W	24.11	780	Lower Siwalik Group	1199	2569	5224	Sparsely Vegetated
535	151218.80	3386327.27	S	29.29	675	Lower Siwalik Group	848	2422	4313	Sparsely Vegetated
536	150379.72	3385755.39	N-E	6.37	768	Lower Siwalik Group	848	1211	3302	Sparsely Vegetated
537	149504.91	3385805.03	E	14.41	737	Lower Siwalik Group	1199	856	2670	Sparsely Vegetated
538	203601.17	3383720.69	S-E	24.91	907	Jaunsar Gp of W. Himalaya	848	5482	1131	Evergreen Forest
539	205676.31	3385782.70	S	30.14	1552	Jaunsar Gp of W. Himalaya	1896	6054	1222	Sparsely Vegetated
540	160716.77	3385536.40	S-W	31.98	889	Lower Siwalik Group	3393	4281	0	Shrub Land
541	160967.68	3385842.79	S-W	28.79	1020	Subathu Fm of W. Himalaya	3393	4281	0	Deciduous Forest
542	185463.71	3383980.09	S-E	36.27	1025	Jaunsar Gp of W. Himalaya	3058	856	4766	Sparsely Vegetated
543	184633.37	3384378.62	S-E	14.26	910	Jaunsar Gp of W. Himalaya	2682	1712	4367	Sparsely Vegetated
544	184779.51	3383625.10	W	42.55	848	Jaunsar Gp of W. Himalaya	2682	856	4014	Sparsely Vegetated
545	187116.20	3384636.63	S	40.08	1351	Jaunsar Gp of W. Himalaya	2682	1712	3120	Sparsely Vegetated
546	186596.18	3385107.73	S-W	29.89	1527	Krol, Infrakrol & Blaini Formation	3497	1712	3438	Deciduous Forest
547	198941.02	3386232.32	S	24.83	990	Jaunsar Gp of W. Himalaya	0	4992	0	Sparsely Vegetated

548	198688.50	3385729.76	E	19.98	998	Jaunsar Gp of W. Himalaya	0	4281	0	Sparsely Vegetated
549	198542.17	3385581.55	S-E	37.92	1015	Jaunsar Gp of W. Himalaya	848	3829	32	Sparsely Vegetated
550	198383.01	3385518.48	S	41.57	965	Jaunsar Gp of W. Himalaya	848	3829	32	Evergreen Forest
551	197924.10	3385717.52	S-E	39.74	1056	Jaunsar Gp of W. Himalaya	848	3829	115	Sparsely Vegetated
552	197861.29	3385465.55	S	35.02	959	Jaunsar Gp of W. Himalaya	848	3829	32	Evergreen Forest
553	197948.38	3385193.05	E	26.11	937	Jaunsar Gp of W. Himalaya	0	3829	32	Shrub Land
554	197570.01	3384848.18	S-E	27.45	964	Jaunsar Gp of W. Himalaya	848	2707	0	Sparsely Vegetated
555	197415.17	3384063.89	N-E	28.22	799	Jaunsar Gp of W. Himalaya	0	1914	0	Sparsely Vegetated
556	197304.81	3383896.19	S	37.20	847	Jaunsar Gp of W. Himalaya	0	1914	0	Sparsely Vegetated
557	197214.58	3383856.48	S	35.72	839	Jaunsar Gp of W. Himalaya	0	1914	32	Deciduous Forest
558	197092.43	3383820.75	S-E	31.53	853	Jaunsar Gp of W. Himalaya	0	1914	32	Deciduous Forest
559	197088.52	3383566.83	E	43.81	843	Jaunsar Gp of W. Himalaya	0	1914	45	Sparsely Vegetated
560	196980.79	3383407.68	S-E	31.75	917	Jaunsar Gp of W. Himalaya	0	1211	101	Sparsely Vegetated
561	196714.18	3383568.08	S	40.86	972	Jaunsar Gp of W. Himalaya	848	1712	322	Sparsely Vegetated
562	194606.81	3383677.08	E	37.03	699	Jaunsar Gp of W. Himalaya	0	1712	275	Sparsely Vegetated
563	194831.41	3385308.13	S-W	52.35	577	Jaunsar Gp of W. Himalaya	0	3425	45	Sparsely Vegetated
564	194581.66	3385382.71	S-E	46.16	600	Jaunsar Gp of W. Himalaya	848	3425	32	Evergreen Forest
565	193764.96	3384845.96	S-E	54.57	597	Jaunsar Gp of W. Himalaya	0	2569	32	Evergreen Forest
566	193216.87	3385482.75	S	38.24	1016	Jaunsar Gp of W. Himalaya	848	3425	481	Sparsely Vegetated
567	193119.78	3385183.37	S	44.47	791	Jaunsar Gp of W. Himalaya	0	3425	160	Sparsely Vegetated
568	192688.57	3384703.57	S-E	46.24	610	Jaunsar Gp of W. Himalaya	0	2569	32	Evergreen Forest
569	191571.51	3385652.34	S	50.45	806	Jaunsar Gp of W. Himalaya	0	3087	320	Sparsely Vegetated

570	208680.66	3383981.11	S-E	24.11	1183	Jaunsar Gp of W. Himalaya	2399	6233	256	Sparsely Vegetated
571	209628.21	3384057.94	S	45.09	1007	Jaunsar Gp of W. Himalaya	1696	6054	304	Sparsely Vegetated
572	156491.71	3385657.94	S-W	25.36	830	Lower Siwalik Group	1696	3087	3650	Sparsely Vegetated
573	168091.81	3386254.28	N-E	40.56	737	Krol, Infrakrol & Blaini Formation	848	4281	2560	Evergreen Forest
574	175352.05	3385367.75	S	33.37	780	Krol, Infrakrol & Blaini Formation	0	3087	1482	Sparsely Vegetated
575	171830.16	3383727.25	S	42.64	1280	Lower Siwalik Group	2544	5743	5099	Deciduous Forest
576	182937.08	3383810.97	S-W	34.48	844	Jaunsar Gp of W. Himalaya	1896	856	2854	Deciduous Forest
577	193659.40	3385714.68	E	40.84	1040	Jaunsar Gp of W. Himalaya	848	3425	795	Sparsely Vegetated
578	194942.49	3384196.64	E	45.92	650	Jaunsar Gp of W. Himalaya	0	1712	202	Evergreen Forest
579	196581.34	3385108.67	S-E	32.00	1368	Jaunsar Gp of W. Himalaya	1199	2569	883	Sparsely Vegetated
580	202679.90	3384352.08	S	26.23	1094	Jaunsar Gp of W. Himalaya	1199	5482	1568	Sparsely Vegetated
581	207959.37	3384084.12	S-E	33.77	1261	Jaunsar Gp of W. Himalaya	2544	6520	136	Sparsely Vegetated
582	207614.56	3384010.84	E	35.27	1417	Jaunsar Gp of W. Himalaya	2544	6520	101	Sparsely Vegetated
583	215494.90	3386388.10	S-E	50.85	1170	Jaunsar Gp of W. Himalaya	848	4281	609	Sparsely Vegetated
584	202023.71	3382431.69	W	31.21	711	Jaunsar Gp of W. Himalaya	0	3087	72	Evergreen Forest
585	202633.60	3383048.10	S-E	40.46	862	Jaunsar Gp of W. Himalaya	848	4281	295	Sparsely Vegetated
586	203166.47	3383165.08	S	31.02	732	Jaunsar Gp of W. Himalaya	0	4843	416	Evergreen Forest
587	161371.19	3382331.50	S-W	44.39	559	Lower Siwalik Group	848	1211	862	Sparsely Vegetated
588	196955.76	3383133.69	S	35.08	799	Jaunsar Gp of W. Himalaya	0	1211	0	Sparsely Vegetated
589	196668.03	3383254.91	S	25.16	749	Jaunsar Gp of W. Himalaya	848	856	0	Sparsely Vegetated
590	161092.83	3382795.13	S-E	21.24	561	Lower Siwalik Group	848	1914	1028	Deciduous Forest
591	207713.29	3382808.09	S	33.76	1210	Jaunsar Gp of W. Himalaya	2544	7315	32	Sparsely Vegetated

592	208284.00	3382530.65	E	23.87	1109	Jaunsar Gp of W. Himalaya	1696	7658	32	Sparsely Vegetated
593	195586.06	3382983.82	W	54.79	703	Jaunsar Gp of W. Himalaya	848	856	365	Sparsely Vegetated
594	157203.14	3381282.81	S-W	31.76	584	Lower Siwalik Group	848	856	1431	Deciduous Forest
595	157014.94	3381570.99	S-W	39.68	646	Lower Siwalik Group	848	856	1603	Shrub Land
596	201002.45	3381350.39	E	27.79	730	Jaunsar Gp of W. Himalaya	0	1914	0	Sparsely Vegetated
597	201508.46	3382259.40	S-E	45.65	771	Jaunsar Gp of W. Himalaya	0	3087	91	Sparsely Vegetated
598	159737.01	3380884.21	S	34.17	608	Lower Siwalik Group	0	0	1462	Deciduous Forest
599	203126.76	3382098.00	E	52.61	705	Jaunsar Gp of W. Himalaya	0	4281	32	Shrub Land
600	207593.34	3379723.78	E	46.72	738	Jaunsar Gp of W. Himalaya	0	4992	566	Sparsely Vegetated
601	208619.97	3379848.05	S-W	25.13	777	Jaunsar Gp of W. Himalaya	0	5482	101	Sparsely Vegetated
602	209419.76	3379865.38	S	40.20	867	Jaunsar Gp of W. Himalaya	0	6054	0	Sparsely Vegetated
603	209453.95	3379558.37	S-E	31.04	737	Jaunsar Gp of W. Himalaya	0	6054	226	Sparsely Vegetated
604	209727.27	3379768.04	S	41.49	815	Jaunsar Gp of W. Himalaya	0	6054	91	Sparsely Vegetated
605	210518.35	3379499.63	E	43.87	875	Jaunsar Gp of W. Himalaya	0	6520	32	Evergreen Forest
606	210773.18	3381433.57	S-W	56.66	766	Jaunsar Gp of W. Himalaya	0	8432	0	Sparsely Vegetated
607	211219.78	3380990.39	S	32.42	905	Jaunsar Gp of W. Himalaya	0	8432	143	Shrub Land
608	212314.82	3380885.68	S	39.95	1395	Jaunsar Gp of W. Himalaya	848	8562	101	Sparsely Vegetated
609	213742.83	3380384.80	S-E	29.31	1010	Krol, Infrakrol & Blaini Formation	848	9101	0	Sparsely Vegetated
610	214157.01	3380082.25	S-W	30.14	1032	Krol, Infrakrol & Blaini Formation	0	9101	45	Sparsely Vegetated
611	214367.00	3379888.99	S-E	21.98	1027	Krol, Infrakrol & Blaini Formation	0	8562	0	Sparsely Vegetated
612	215226.37	3379576.89	S-E	39.10	898	Krol, Infrakrol & Blaini Formation	0	7894	724	Shrub Land
613	215402.65	3380302.47	S	32.64	1153	Krol, Infrakrol & Blaini Formation	848	8476	545	Sparsely Vegetated

614	215704.51	3380090.79	S-W	34.75	1096	Krol, Infrakrol & Blaini Formation	848	8476	847	Sparsely Vegetated
615	215934.36	3380185.54	S	30.77	1209	Krol, Infrakrol & Blaini Formation	848	7894	1058	Sparsely Vegetated
616	216109.02	3379366.91	S	30.09	1022	Krol, Infrakrol & Blaini Formation	848	7265	1536	Sparsely Vegetated
617	217000.69	3379612.94	S-E	40.34	1265	Krol, Infrakrol & Blaini Formation	848	6687	2237	Sparsely Vegetated
618	215219.24	3379164.04	N-W	48.42	924	Krol, Infrakrol & Blaini Formation	0	7894	1060	Evergreen Forest
619	221248.56	3379165.47	S	25.39	1623	Krol, Infrakrol & Blaini Formation	848	5137	3423	Sparsely Vegetated
620	221202.76	3380091.31	E	27.06	1850	Krol, Infrakrol & Blaini Formation	1696	5993	3807	Sparsely Vegetated
621	202067.74	3378682.12	W	19.21	871	Jaunsar Gp of W. Himalaya	1696	856	1306	Sparsely Vegetated
622	201982.01	3378641.93	S-W	29.66	833	Jaunsar Gp of W. Himalaya	848	856	1288	Sparsely Vegetated
623	200077.27	3378475.05	S-W	25.45	715	Jaunsar Gp of W. Himalaya	0	856	244	Sparsely Vegetated
624	209166.49	3378813.02	N-W	56.16	863	Jaunsar Gp of W. Himalaya	0	5415	803	Evergreen Forest
625	207574.77	3378888.28	N-E	35.68	940	Jaunsar Gp of W. Himalaya	848	4281	1296	Evergreen Forest
626	216785.20	3378853.54	S-E	34.22	940	Krol, Infrakrol & Blaini Formation	0	6054	1802	Sparsely Vegetated
627	217415.49	3378512.50	W	37.10	1017	Krol, Infrakrol & Blaini Formation	0	6054	2016	Sparsely Vegetated
628	218061.73	3378597.98	S-E	30.94	1215	Krol, Infrakrol & Blaini Formation	848	5482	2592	Sparsely Vegetated
629	218748.46	3378547.44	S-E	31.34	1194	Krol, Infrakrol & Blaini Formation	1199	4992	3128	Sparsely Vegetated
630	219096.84	3379126.49	S-E	33.40	1327	Krol, Infrakrol & Blaini Formation	1896	4992	3752	Sparsely Vegetated
631	215939.87	3378545.27	N-E	33.22	998	Krol, Infrakrol & Blaini Formation	0	6687	1226	Shrub Land
632	221888.18	3378208.01	S	43.26	1166	Krol, Infrakrol & Blaini Formation	0	3425	2722	Sparsely Vegetated
633	203738.30	3376538.16	S	40.73	1109	Jaunsar Gp of W. Himalaya	2682	0	2139	Sparsely Vegetated
634	203728.05	3376836.85	W	38.21	1100	Jaunsar Gp of W. Himalaya	1696	856	2315	Sparsely Vegetated
635	203580.14	3376973.14	S-W	32.94	1095	Jaunsar Gp of W. Himalaya	1696	856	2308	Sparsely Vegetated

636	203457.91	3377228.35	S-W	31.74	1132	Jaunsar Gp of W. Himalaya	1696	856	2439	Sparsely Vegetated
637	203131.55	3377477.13	S	27.49	1049	Jaunsar Gp of W. Himalaya	1696	1211	2235	Sparsely Vegetated
638	202926.43	3377610.07	S	19.23	1057	Jaunsar Gp of W. Himalaya	1696	856	2135	Sparsely Vegetated
639	202564.64	3377267.95	S	17.71	958	Jaunsar Gp of W. Himalaya	848	0	1661	Sparsely Vegetated
640	216816.94	3375984.91	N	30.39	1618	Krol, Infrakrol & Blaini Formation	848	4611	64	Shrub Land
641	216546.73	3375626.10	N-E	29.75	1753	Krol, Infrakrol & Blaini Formation	1199	5208	32	Shrub Land
642	216997.77	3375437.08	N	22.94	1755	Krol, Infrakrol & Blaini Formation	1199	4366	101	Evergreen Forest
643	206140.51	3375805.64	S	41.17	1784	Jaunsar Gp of W. Himalaya	4241	1211	2085	Sparsely Vegetated
644	205627.27	3376628.46	S	36.05	1744	Jaunsar Gp of W. Himalaya	3393	1914	2774	Evergreen Forest
645	217353.47	3378161.19	S-W	36.01	889	Krol, Infrakrol & Blaini Formation	0	5482	1775	Sparsely Vegetated
646	218408.09	3378020.89	N-W	50.52	1074	Krol, Infrakrol & Blaini Formation	848	4281	2534	Sparsely Vegetated
647	222783.45	3377754.47	S-W	42.18	1088	Krol, Infrakrol & Blaini Formation	0	3425	1903	Sparsely Vegetated
648	224303.25	3376458.77	N-E	44.22	1401	Krol, Infrakrol & Blaini Formation	848	1914	1087	Evergreen Forest
649	220408.77	3376925.08	S-E	30.12	1092	Tal Fm of W. Himalaya	0	2707	2895	Evergreen Forest
650	219779.25	3376167.71	N-W	31.71	1175	Krol, Infrakrol & Blaini Formation	0	2422	2442	Evergreen Forest
651	158533.69	3372441.23	W	17.56	460	Middle Siwalik Gp of w. & e. Himalayas	1896	8122	2407	Sparsely Vegetated
652	207741.55	3373374.56	S-W	31.67	1756	Jaunsar Gp of W. Himalaya	1896	0	1184	Sparsely Vegetated
653	205524.23	3372097.60	E	9.74	1031	Lower Siwalik Group	2682	1914	329	Shrub Land
654	206818.54	3370851.70	S-W	22.92	883	Lower Siwalik Group	848	2422	997	Deciduous Forest
655	210851.88	3371933.34	S-E	39.54	1566	Jaunsar Gp of W. Himalaya	1696	856	4544	Shrub Land
656	216812.59	3373713.96	N-E	26.00	1972	Krol, Infrakrol & Blaini Formation	2682	4281	202	Evergreen Forest

657	219324.27	3371316.32	S	37.01	1559	Krol, Infrakrol & Blaini Formation	1896	2422	202	Shrub Land
658	216128.45	3370834.16	S	51.21	1357	Jaunsar Gp of W. Himalaya	0	2422	2139	Shrub Land
659	216181.72	3371267.68	S-E	38.17	1548	Jaunsar Gp of W. Himalaya	848	2422	1770	Shrub Land
660	160629.14	3370500.36	N-E	18.90	529	Middle Siwalik Gp of w. & e. Himalayas	0	9687	3559	Deciduous Forest
661	218643.41	3370436.40	S-E	37.65	1406	Jaunsar Gp of W. Himalaya	848	3087	668	Evergreen Forest
662	233299.38	3370496.95	E	37.58	2369	Krol, Infrakrol & Blaini Formation	3058	3087	32	Evergreen Forest
663	174352.26	3366907.08	S-E	40.52	568	Middle Siwalik Gp of w. & e. Himalayas	1696	0	3134	Sparsely Vegetated
664	213247.03	3369821.82	S-W	26.00	1007	Jaunsar Gp of W. Himalaya	848	856	4820	Shrub Land
665	225829.64	3368043.92	W	40.78	1279	Tal Fm of W. Himalaya	848	0	1316	Evergreen Forest
666	223483.79	3369348.24	E	32.27	1228	Tal Fm of W. Himalaya	0	856	160	Shrub Land
667	225040.18	3368324.93	S-E	31.14	1474	Tal Fm of W. Himalaya	0	0	704	Sparsely Vegetated
668	229124.60	3369779.92	W	38.72	1720	Krol, Infrakrol & Blaini Formation	1199	856	1411	Shrub Land
669	227063.50	3366608.70	W	32.76	1658	Tal Fm of W. Himalaya	1696	1712	0	Evergreen Forest
670	225538.79	3366776.84	N	53.04	1095	Tal Fm of W. Himalaya	0	0	187	Evergreen Forest
671	174320.30	3366527.52	S	47.36	503	Middle Siwalik Gp of w. & e. Himalayas	848	0	2920	Sparsely Vegetated
672	176096.60	3365338.79	W	39.70	509	Middle Siwalik Gp of w. & e. Himalayas	0	1914	4417	Sparsely Vegetated
673	222670.31	3365877.56	S	25.13	1095	Krol, Infrakrol & Blaini Formation	1199	1211	160	Sparsely Vegetated
674	223451.29	3364017.36	W	39.66	1071	Krol, Infrakrol & Blaini Formation	848	2569	774	Evergreen Forest
675	227062.52	3365026.74	E	45.72	1159	Tal Fm of W. Himalaya	848	1712	684	Evergreen Forest
676	230097.62	3359780.50	N-E	23.82	1321	Tal Fm of W. Himalaya	0	3425	5181	Shrub Land

677	235037.85	3360840.48	N	31.93	1634	Tal Fm of W. Himalaya	1696	2422	8144	Shrub Land
678	236039.40	3359354.51	S-E	30.10	1799	Tal Fm of W. Himalaya	1199	3087	8959	Sparsely Vegetated
679	227971.70	3356139.38	S	48.79	900	Krol, Infrakrol & Blaini Formation	0	0	4659	Sparsely Vegetated
680	224583.13	3355529.40	S	35.83	873	Jaunsar Gp of W. Himalaya	1696	3087	1279	Sparsely Vegetated
681	225302.20	3354868.38	N-W	27.67	868	Jaunsar Gp of W. Himalaya	2399	3087	1792	Deciduous Forest
682	225975.78	3354203.00	S	43.54	864	Jaunsar Gp of W. Himalaya	2399	3632	2554	Sparsely Vegetated
683	233249.05	3355621.08	N-E	48.60	1110	Krol, Infrakrol &Blaini Formation	0	1712	7215	Sparsely Vegetated
684	232157.47	3356807.50	S-E	29.19	1179	Krol, Infrakrol & Blaini Formation	0	1914	8081	Sparsely Vegetated
685	233207.26	3357137.72	W	31.50	1295	Krol, Infrakrol & Blaini Formation	848	3087	8659	Evergreen Forest
686	234563.60	3357235.90	S-E	26.81	1493	Krol, Infrakrol & Blaini Formation	848	3530	9188	Sparsely Vegetated
687	244431.87	3355929.37	E	38.92	1068	Tal Fm of W. Himalaya	0	0	160	Deciduous Forest
688	244438.09	3355578.55	E	45.04	1132	Tal Fm of W. Himalaya	848	0	195	Deciduous Forest
689	243813.65	3356382.06	N-E	55.29	1064	Tal Fm of W. Himalaya	0	0	647	Evergreen Forest
690	248427.80	3355683.67	S-W	32.43	1443	Krol, Infrakrol & Blaini Formation	2399	3087	702	Sparsely Vegetated
691	245774.75	3354284.25	S	44.04	957	Krol, Infrakrol & Blaini Formation	0	0	64	Shrub Land
692	247986.04	3356120.02	S-E	46.10	1838	Krol, Infrakrol & Blaini Formation	2399	3087	1335	Evergreen Forest
693	246631.87	3354841.16	S-E	27.21	1316	Krol, Infrakrol & Blaini Formation	848	1211	830	Deciduous Forest
694	245695.42	3354287.95	S	32.94	951	Krol, Infrakrol & Blaini Formation	0	0	64	Shrub Land
695	245312.74	3354607.79	S-W	38.83	911	Tal Fm of W. Himalaya	0	0	32	Sparsely Vegetated
696	245416.30	3354473.48	S-W	31.41	914	Tal Fm of W. Himalaya	0	0	45	Sparsely Vegetated
697	245970.86	3354242.71	S-W	43.29	975	Krol, Infrakrol & Blaini Formation	0	0	91	Deciduous Forest
698	230481.81	3351348.32	S	41.29	1023	Jaunsar Gp of W. Himalaya	1896	3087	2523	Shrub Land

699	229548.66	3352308.87	S-E	36.47	925	Jaunsar Gp of W. Himalaya	2544	2707	3402	Shrub Land
700	227303.80	3352952.39	S	35.61	1132	Jaunsar Gp of W. Himalaya	1896	3087	3753	Shrub Land
701	226472.13	3352844.36	S	35.27	863	Jaunsar Gp of W. Himalaya	1696	3530	3263	Deciduous Forest
702	237228.02	3351833.33	S-E	43.71	1282	Krol, Infrakrol & Blaini Formation	848	856	4766	Shrub Land
703	236985.52	3351782.47	S	45.24	1420	Krol, Infrakrol & Blaini Formation	848	0	4572	Sparsely Vegetated
704	236710.70	3351755.49	S	29.21	1501	Krol, Infrakrol & Blaini Formation	1199	856	4430	Sparsely Vegetated
705	236030.01	3351836.32	E	26.39	1396	Jaunsar Gp of W. Himalaya	1199	0	4156	Evergreen Forest
706	233888.78	3353046.99	S-W	30.25	1313	Jaunsar Gp of W. Himalaya	1696	0	5002	Sparsely Vegetated
707	232878.37	3353345.63	N	2.92	1516	Jaunsar Gp of W. Himalaya	1896	856	4938	Sparsely Vegetated
708	237971.32	3351731.05	S-W	27.71	1024	Krol, Infrakrol & Blaini Formation	0	0	5145	Evergreen Forest
709	247313.78	3350994.89	S-W	50.37	836	Krol, Infrakrol & Blaini Formation	0	1712	115	Deciduous Forest
710	245696.35	3351663.17	S-W	31.98	1125	Tal Fm of W. Himalaya	0	0	750	Evergreen Forest
711	245928.25	3351260.89	S	31.49	954	Krol, Infrakrol & Blaini Formation	0	856	326	Deciduous Forest
712	245321.41	3352399.73	S-W	37.86	1354	Tal Fm of W. Himalaya	848	0	1282	Sparsely Vegetated
713	247028.18	3352719.06	W	35.51	849	Krol, Infrakrol & Blaini Formation	848	856	32	Deciduous Forest
714	247113.18	3352451.47	N-W	27.11	952	Krol, Infrakrol & Blaini Formation	848	1211	72	Deciduous Forest
715	247360.73	3352782.54	W	42.37	1078	Krol, Infrakrol & Blaini Formation	848	856	195	Sparsely Vegetated
716	248463.31	3353279.69	N-W	20.88	1088	Krol, Infrakrol & Blaini Formation	848	2569	32	Shrub Land
717	246674.98	3352953.73	E	23.58	939	Krol, Infrakrol & Blaini Formation	0	856	172	Sparsely Vegetated
718	246398.64	3352374.06	S-E	33.04	945	Krol, Infrakrol & Blaini Formation	0	856	226	Sparsely Vegetated
719	246630.93	3352115.07	N-E	44.69	848	Krol, Infrakrol & Blaini Formation	0	1211	32	Sparsely Vegetated
720	244788.54	3350310.32	S-E	38.15	1300	Tal Fm of W. Himalaya	1199	856	1589	Evergreen Forest

721	246888.11	3349892.97	E	46.54	971	Krol, Infrakrol &Blaini Formation	0	1712	0	Shrub Land
722	256593.62	3350398.22	S	38.36	857	Jaunsar Gp of W. Himalaya	0	1211	481	Evergreen Forest
723	249928.99	3349946.87	N	36.15	1549	Krol, Infrakrol & Blaini Formation	1199	4281	0	Evergreen Forest
724	246425.53	3349694.16	S	39.29	1091	Krol, Infrakrol & Blaini Formation	0	856	72	Deciduous Forest
725	238434.00	3349369.01	S-E	47.85	1397	Jaunsar Gp of W. Himalaya	1199	1211	4172	Evergreen Forest
726	236475.01	3346112.51	N-W	32.37	1187	Jaunsar Gp of W. Himalaya	2399	4992	2626	Shrub Land
727	235763.61	3346798.68	W	35.74	978	Krol, Infrakrol & Blaini Formation	1199	4611	1632	Sparsely Vegetated
728	246135.33	3348324.74	S-W	43.04	1062	Krol, Infrakrol & Blaini Formation	848	1211	96	Shrub Land
729	202731.86	3347705.11	S-E	24.12	732	Lower Siwalik Group	848	6174	1632	Shrub Land
730	238616.95	3348773.27	W	30.67	1335	Jaunsar Gp of W. Himalaya	2399	1914	4155	Shrub Land
731	240643.88	3347698.26	W	38.19	1343	Jaunsar Gp of W. Himalaya	1696	1712	2740	Sparsely Vegetated
732	242564.27	3345775.06	S-W	43.61	1448	Jaunsar Gp of W. Himalaya	1696	2569	346	Evergreen Forest
733	245252.65	3346748.78	S	32.68	1085	Krol, Infrakrol & Blaini Formation	1696	1712	387	Sparsely Vegetated
734	243864.37	3347639.66	S-E	45.11	1578	Krol, Infrakrol & Blaini Formation	2544	856	329	Shrub Land
735	244168.82	3347294.51	S	34.53	1284	Krol, Infrakrol & Blaini Formation	2544	1712	32	Sparsely Vegetated
736	246939.96	3345969.19	S-W	42.50	866	Krol, Infrakrol & Blaini Formation	0	3087	1180	Evergreen Forest
737	248898.51	3348778.63	S-W	44.23	1183	Krol, Infrakrol & Blaini Formation	1199	3425	476	Deciduous Forest
738	259364.44	3347232.08	S	26.76	1151	Jaunsar Gp of W. Himalaya	848	1914	2104	Sparsely Vegetated
739	260326.03	3347527.71	S	46.74	1007	Jaunsar Gp of W. Himalaya	0	1211	2489	Sparsely Vegetated
740	260027.20	3347418.11	S	39.65	973	Jaunsar Gp of W. Himalaya	0	1211	2353	Evergreen Forest
741	203101.32	3345445.41	E	23.71	603	Middle Siwalik Gp of w. & e. Himalayas	0	4611	181	Sparsely Vegetated

742	242235.39	3345514.71	S-W	18.14	1302	Jaunsar Gp of W. Himalaya	1696	3530	497	Evergreen Forest
743	237148.07	3343401.16	E	35.77	778	Jaunsar Gp of W. Himalaya	0	4366	1983	Sparsely Vegetated
744	237837.78	3343664.14	S-E	35.91	717	Jaunsar Gp of W. Himalaya	0	5208	2144	Evergreen Forest
745	234578.89	3342413.15	W	17.21	621	Jaunsar Gp of W. Himalaya	2544	1712	1222	Shrub Land
746	243104.53	3345007.73	N-E	13.96	1474	Jaunsar Gp of W. Himalaya	2682	3425	458	Evergreen Forest
747	240944.13	3341949.99	N-W	36.34	1350	Krol, Infrakrol & Blaini Formation	2544	6174	0	Evergreen Forest
748	241368.78	3342394.79	S	30.28	1405	Krol, Infrakrol & Blaini Formation	2399	6233	0	Sparsely Vegetated
749	241966.31	3343270.95	N-W	7.96	1427	Jaunsar Gp of W. Himalaya	2682	5208	32	Sparsely Vegetated
750	238940.71	3342790.38	S	12.28	927	Jaunsar Gp of W. Himalaya	1199	6054	1539	Shrub Land
751	237372.69	3343524.89	S-E	22.81	696	Jaunsar Gp of W. Himalaya	0	5208	2021	Sparsely Vegetated
752	240678.62	3344396.82	N-W	28.15	1164	Jaunsar Gp of W. Himalaya	848	4611	1135	Shrub Land
753	249436.37	3344786.79	S-E	32.15	1299	Jaunsar Gp of W. Himalaya	1696	1211	3610	Evergreen Forest
754	247355.54	3342707.54	N-W	34.13	834	Jaunsar Gp of W. Himalaya	848	2569	4467	Evergreen Forest
755	247988.28	3342285.93	W	29.17	892	Jaunsar Gp of W. Himalaya	1696	1712	5007	Evergreen Forest
756	247903.86	3342875.17	S	27.32	904	Jaunsar Gp of W. Himalaya	1696	1712	4426	Evergreen Forest
757	245030.60	3345164.86	S-E	16.03	1052	Jaunsar Gp of W. Himalaya	1199	3425	1875	Evergreen Forest
758	245670.40	3344480.71	N-E	30.51	633	Jaunsar Gp of W. Himalaya	0	4281	2686	Deciduous Forest
759	245392.08	3342223.28	E	46.32	643	Krol, Infrakrol & Blaini Formation	848	3087	3399	Shrub Land
760	245254.67	3342864.93	S-W	37.53	806	Jaunsar Gp of W. Himalaya	848	3632	3078	Deciduous Forest
761	245966.59	3343137.14	S	35.06	861	Jaunsar Gp of W. Himalaya	848	3087	3601	Shrub Land
762	244381.46	3343564.40	S	55.92	1164	Jaunsar Gp of W. Himalaya	1896	4843	1961	Shrub Land
763	244935.93	3341751.95	N	45.63	812	Krol, Infrakrol & Blaini Formation	0	3087	2942	Evergreen Forest

764	245839.47	3341648.70	N-E	35.80	596	Krol, Infrakrol & Blaini Formation	0	2422	3417	Sparsely Vegetated
765	250651.93	3342364.00	S-W	38.98	1487	Jaunsar Gp of W. Himalaya	1696	856	2946	Sparsely Vegetated
766	262514.86	3345095.32	S-E	35.91	1287	Jaunsar Gp of W. Himalaya	1896	1914	5770	Sparsely Vegetated
767	266645.15	3341688.14	S-E	25.51	761	Jaunsar Gp of W. Himalaya	0	7265	4198	Evergreen Forest
768	263736.60	3343468.04	S	53.23	866	Jaunsar Gp of W. Himalaya	0	4281	7388	Evergreen Forest
769	268680.50	3339295.29	E	20.36	580	Jaunsar Gp of W. Himalaya	0	10310	1125	Sparsely Vegetated
770	268311.86	3340980.87	S	18.32	836	Jaunsar Gp of W. Himalaya	0	9101	2701	Sparsely Vegetated
771	268771.34	3340582.07	W	43.50	769	Jaunsar Gp of W. Himalaya	0	9687	2068	Sparsely Vegetated
772	268341.41	3341100.09	S-W	28.22	843	Jaunsar Gp of W. Himalaya	0	9101	2754	Sparsely Vegetated
773	268722.71	3341081.57	W	26.86	956	Jaunsar Gp of W. Himalaya	0	9101	2444	Sparsely Vegetated
774	236864.97	3340337.44	W	33.03	535	Krol, Infrakrol & Blaini Formation	848	2422	1421	Evergreen Forest
775	239534.57	3340438.60	W	43.02	1084	Krol, Infrakrol & Blaini Formation	1896	3829	32	Evergreen Forest
776	239661.58	3340431.28	N	27.35	1140	Krol, Infrakrol & Blaini Formation	1896	3829	0	Evergreen Forest
777	239585.28	3341164.64	S-W	40.63	1007	Krol, Infrakrol & Blaini Formation	1896	4611	417	Evergreen Forest
778	249105.53	3340198.93	W	38.15	952	Jaunsar Gp of W. Himalaya	1896	856	3144	Evergreen Forest
779	246955.82	3340082.22	W	38.81	567	Krol, Infrakrol &Blaini Formation	0	856	3502	Evergreen Forest
780	246698.43	3340739.24	S	34.98	635	Krol, Infrakrol & Blaini Formation	0	1211	3545	Shrub Land
781	246499.92	3340664.64	S	38.17	531	Krol, Infrakrol & Blaini Formation	0	1914	3348	Shrub Land
782	247924.87	3338931.54	S-W	27.19	738	Krol, Infrakrol & Blaini Formation	848	856	2088	Sparsely Vegetated
783	245000.69	3340461.19	N	5.37	913	Krol, Infrakrol & Blaini Formation	848	1914	2004	Shrub Land
784	243025.22	3339715.97	E	26.49	1287	Krol, Infrakrol & Blaini Formation	2399	3530	635	Sparsely Vegetated
785	242072.90	3338934.98	S-W	31.29	1133	Krol, Infrakrol & Blaini Formation	2682	4281	1363	Shrub Land

786	241999.38	3338530.26	S-W	29.40	964	Krol, Infrakrol & Blaini Formation	1896	3530	1526	Deciduous Forest
787	239947.26	3338124.46	W	25.27	740	Krol, Infrakrol & Blaini Formation	2399	2707	588	Sparsely Vegetated
788	239552.53	3337583.77	S-E	23.54	682	Krol, Infrakrol & Blaini Formation	1896	1712	385	Shrub Land
789	239402.99	3339971.49	W	36.64	1146	Krol, Infrakrol & Blaini Formation	2399	3829	32	Evergreen Forest
790	238290.06	3337643.05	S	29.83	628	Krol, Infrakrol & Blaini Formation	1696	1211	72	Shrub Land
791	248374.22	3337355.01	S-W	35.49	497	Krol, Infrakrol & Blaini Formation	0	2422	458	Shrub Land
792	253661.13	3338464.54	S-E	31.54	944	Jaunsar Gp of W. Himalaya	848	0	3012	Shrub Land
793	266867.23	3340765.63	S-E	42.35	910	Jaunsar Gp of W. Himalaya	848	7894	3311	Deciduous Forest
794	267451.87	3341108.44	E	17.35	616	Jaunsar Gp of W. Himalaya	0	8476	3292	Sparsely Vegetated
795	265988.59	3338701.06	S	29.69	1602	Jaunsar Gp of W. Himalaya	1896	8815	2664	Sparsely Vegetated
796	266449.75	3338040.56	S-W	43.48	1104	Jaunsar Gp of W. Himalaya	2544	9261	2027	Sparsely Vegetated
797	268303.17	3337589.09	S	34.76	619	Jaunsar Gp of W. Himalaya	0	10310	128	Sparsely Vegetated
798	269841.49	3338334.94	S	54.29	806	Jaunsar Gp of W. Himalaya	848	12108	320	Sparsely Vegetated
799	269422.28	3338057.22	S	35.96	734	Jaunsar Gp of W. Himalaya	848	10897	205	Sparsely Vegetated
800	271936.87	3337879.01	S	38.97	839	Jaunsar Gp of W. Himalaya	2682	12728	1492	Sparsely Vegetated
801	268367.51	3337224.50	S-E	33.90	583	Jaunsar Gp of W. Himalaya	0	10310	32	Sparsely Vegetated
802	242861.38	3336744.07	S-E	19.90	461	Krol, Infrakrol & Blaini Formation	0	1914	32	Sparsely Vegetated
803	240010.86	3336930.72	S-W	32.57	582	Krol, Infrakrol & Blaini Formation	1199	1211	903	Deciduous Forest
804	239231.62	3336566.16	W	20.62	517	Krol, Infrakrol & Blaini Formation	1199	856	32	Shrub Land
805	242913.09	3334935.61	W	31.42	545	Krol, Infrakrol & Blaini Formation	848	856	358	Evergreen Forest
806	243304.66	3334840.49	S-W	33.82	719	Krol, Infrakrol & Blaini Formation	848	0	484	Evergreen Forest
807	243676.65	3335330.38	N-W	28.68	806	Krol, Infrakrol & Blaini Formation	848	0	226	Evergreen Forest

808	249065.89	3336015.17	S-W	36.52	518	Tal Fm of W. Himalaya	0	856	466	Evergreen Forest
809	248585.29	3335730.04	E	47.40	496	Tal Fm of W. Himalaya	848	856	0	Evergreen Forest
810	248036.40	3335458.21	S	48.76	598	Tal Fm of W. Himalaya	848	0	115	Sparsely Vegetated
811	247708.44	3335372.06	S	41.10	507	Tal Fm of W. Himalaya	848	0	45	Deciduous Forest
812	248341.58	3335930.36	N	37.40	526	Tal Fm of W. Himalaya	848	856	45	Evergreen Forest
813	251723.31	3335266.47	S-W	36.84	514	Krol, Infrakrol & Blaini Formation	0	0	0	Evergreen Forest
814	251651.11	3335354.68	W	38.09	476	Krol, Infrakrol & Blaini Formation	0	0	0	Evergreen Forest
815	249901.36	3337019.09	S	43.73	433	Krol, Infrakrol & Blaini Formation	848	1712	32	Shrub Land
816	251269.13	3336229.14	S-W	49.26	472	Krol, Infrakrol & Blaini Formation	848	0	0	Evergreen Forest
817	254971.64	3333795.37	N	46.01	947	Krol, Infrakrol & Blaini Formation	1696	856	1568	Evergreen Forest
818	263914.21	3337107.05	S	33.07	1556	Jaunsar Gp of W. Himalaya	848	7315	4070	Sparsely Vegetated
819	265649.59	3336690.94	S-W	55.15	1369	Jaunsar Gp of W. Himalaya	1696	8077	2406	Sparsely Vegetated
820	269313.31	3336068.10	S	49.02	870	Jaunsar Gp of W. Himalaya	848	9687	1041	Sparsely Vegetated
821	266456.41	3335494.42	S-W	45.92	836	Jaunsar Gp of W. Himalaya	1696	7265	1086	Shrub Land
822	268420.11	3335108.43	S	45.66	641	Jaunsar Gp of W. Himalaya	0	8476	0	Sparsely Vegetated
823	268612.26	3335190.96	S-E	26.19	585	Jaunsar Gp of W. Himalaya	0	8476	32	Evergreen Forest
824	268251.45	3335467.20	E	36.37	590	Jaunsar Gp of W. Himalaya	0	8476	32	Sparsely Vegetated
825	268282.88	3336310.06	E	23.98	567	Jaunsar Gp of W. Himalaya	0	9101	64	Sparsely Vegetated
826	268229.60	3336437.19	E	35.76	605	Jaunsar Gp of W. Himalaya	0	9687	0	Sparsely Vegetated
827	268249.02	3336507.33	E	37.47	612	Jaunsar Gp of W. Himalaya	0	9687	0	Sparsely Vegetated
828	268213.63	3336670.13	E	28.10	657	Jaunsar Gp of W. Himalaya	0	9687	32	Sparsely Vegetated
829	268375.20	3336789.64	E	25.99	541	Jaunsar Gp of W. Himalaya	0	9687	72	Sparsely Vegetated

830	268326.38	3337051.92	E	40.43	586	Jaunsar Gp of W. Himalaya	0	9687	0	Sparsely Vegetated
831	268356.48	3337158.81	E	28.77	573	Jaunsar Gp of W. Himalaya	0	9687	0	Sparsely Vegetated
832	271939.22	3334134.67	W	47.65	1025	Jaunsar Gp of W. Himalaya	848	9985	3501	Deciduous Forest
833	272008.46	3334864.90	S-W	33.70	1357	Jaunsar Gp of W. Himalaya	1696	10728	3410	Sparsely Vegetated
834	272537.45	3333612.43	S	35.26	904	Jaunsar Gp of W. Himalaya	848	9762	4219	Sparsely Vegetated
835	268543.88	3334271.24	S-E	36.72	674	Jaunsar Gp of W. Himalaya	0	7894	838	Sparsely Vegetated
836	268574.90	3334841.15	N	44.70	552	Jaunsar Gp of W. Himalaya	0	8476	286	Evergreen Forest
837	268872.75	3336523.77	W	43.35	662	Jaunsar Gp of W. Himalaya	0	10310	608	Evergreen Forest
838	269190.62	3336639.70	N	44.71	779	Jaunsar Gp of W. Himalaya	0	10310	704	Evergreen Forest
839	274324.93	3334354.70	S-W	39.08	1217	Jaunsar Gp of W. Himalaya	848	11519	5483	Sparsely Vegetated
840	274354.20	3333431.75	S-E	26.74	1056	Jaunsar Gp of W. Himalaya	0	10897	6002	Sparsely Vegetated
841	276899.43	3333511.99	S-E	44.40	1154	Jaunsar Gp of W. Himalaya	0	12728	4442	Sparsely Vegetated
842	244994.37	3333103.96	N-E	20.87	1162	Krol, Infrakrol & Blaini Formation	1896	0	1135	Shrub Land
843	260139.54	3333089.90	W	31.76	929	Krol, Infrakrol & Blaini Formation	0	2422	2906	Shrub Land
844	247966.48	3332465.43	S-E	17.90	461	Subathu Fm. of W. Himalaya	0	0	45	Evergreen Forest
845	246872.09	3330594.02	S-E	40.11	620	Amri Tectonic unit	848	0	64	Evergreen Forest
846	244187.01	3331393.44	E	22.91	972	Tal Fm of W. Himalaya	2544	1211	45	Sparsely Vegetated
847	246453.83	3329315.66	S	28.85	682	Amri Tectonic unit	0	856	1165	Deciduous Forest
848	249809.81	3331923.28	N	45.81	1134	Subathu Fm. of W. Himalaya	1696	856	1884	Evergreen Forest
849	255674.59	3330298.12	S	38.71	882	Subathu Fm. of W. Himalaya	1696	856	1131	Shrub Land
850	260975.32	3332177.61	S-E	34.93	1059	Krol, Infrakrol & Blaini Formation	848	1914	1772	Sparsely Vegetated
851	260967.57	3329809.16	S	43.86	757	Subathu Fm. of W. Himalaya	0	0	32	Evergreen Forest

852	260781.81	3329584.27	E	38.05	797	Subathu Fm. of W. Himalaya	0	0	0	Sparsely Vegetated
853	259827.74	3332244.19	E	38.32	887	Krol, Infrakrol & Blaini Formation	0	1712	2318	Sparsely Vegetated
854	258198.98	3329772.23	S-E	47.52	644	Subathu Fm. of W. Himalaya	0	1211	160	Shrub Land
855	262527.92	3329363.79	N-E	28.99	567	Subathu Fm. of W. Himalaya	0	0	1042	Evergreen Forest
856	261606.43	3329489.99	N	56.79	508	Subathu Fm. of W. Himalaya	0	856	644	Evergreen Forest
857	263228.24	3329881.40	S	38.87	784	Krol, Infrakrol & Blaini Formation	0	1211	1021	Sparsely Vegetated
858	267194.06	3330133.27	S-E	33.12	598	Jaunsar Gp of W. Himalaya	0	4281	716	Evergreen Forest
859	266945.28	3329772.23	S-E	38.33	554	Jaunsar Gp of W. Himalaya	0	3632	792	Sparsely Vegetated
860	265858.79	3330226.90	S-W	33.59	945	Krol, Infrakrol & Blaini Formation	1199	3087	32	Sparsely Vegetated
861	266564.68	3330865.96	S-W	31.62	894	Jaunsar Gp of W. Himalaya	848	4281	32	Sparsely Vegetated
862	268138.39	3330534.18	W	49.60	548	Jaunsar Gp of W. Himalaya	0	5415	1094	Shrub Land
863	272031.89	3330528.04	S-W	38.50	1546	Jaunsar Gp of W. Himalaya	2399	7265	4911	Sparsely Vegetated
864	216985.88	3327563.39	S	20.27	635	Middle Siwalik Gp of w. & e. Himalayas	2399	12169	7365	Sparsely Vegetated
865	218753.82	3325906.86	S-W	5.39	662	Middle Siwalik Gp of w. & e. Himalayas	3793	12728	6203	Sparsely Vegetated
866	218389.09	3326273.99	S	21.54	657	Middle Siwalik Gp of w. & e. Himalayas	4241	13319	6387	Sparsely Vegetated
867	217424.01	3326391.14	E	8.66	636	Middle Siwalik Gp of w. & e. Himalayas	3598	12728	6257	Deciduous Forest
868	215852.23	3326711.99	W	31.30	464	Middle Siwalik Gp of w. & e. Himalayas	2399	12108	6475	Sparsely Vegetated
869	220232.23	3325060.25	N-W	48.81	656	Middle Siwalik Gp of w. & e. Himalayas	3497	10897	6114	Shrub Land

870	218481.65	3325981.61	S-E	7.27	702	Middle Siwalik Gp of w. & e. Himalayas	4241	12728	6150	Deciduous Forest
871	244320.49	3326417.05	N-W	28.31	766	Subathu Fm. of W. Himalaya	1896	0	1020	Sparsely Vegetated
872	243870.32	3325156.44	W	40.19	667	Subathu Fm. of W. Himalaya	1199	856	2116	Deciduous Forest
873	247070.10	3327628.05	N-E	37.30	842	Amri Tectonic unit	848	1914	1255	Evergreen Forest
874	259961.49	3328768.72	E	54.43	716	Subathu Fm. of W. Himalaya	0	856	0	Evergreen Forest
875	253951.68	3328070.02	E	21.21	1151	Jaunsar Gp of W. Himalaya	848	1712	1334	Shrub Land
876	252418.07	3327557.16	S-W	35.17	799	Jaunsar Gp of W. Himalaya	848	3087	2626	Shrub Land
877	253156.86	3325729.21	S-W	42.29	742	Jaunsar Gp of W. Himalaya	0	4281	3769	Sparsely Vegetated
878	260530.90	3327199.84	N-E	39.22	527	Subathu Fm. of W. Himalaya	0	856	885	Sparsely Vegetated
879	267696.59	3328666.69	S-E	36.05	567	Krol, Infrakrol & Blaini Formation	0	3530	2110	Sparsely Vegetated
880	264617.19	3328735.74	N	43.23	666	Krol, Infrakrol & Blaini Formation	0	1914	1403	Deciduous Forest
881	266635.38	3327373.61	N-E	35.09	633	Krol, Infrakrol & Blaini Formation	0	1712	2694	Sparsely Vegetated
882	266142.27	3326363.40	E	49.18	1046	Subathu Fm. of W. Himalaya	1199	856	3535	Deciduous Forest
883	241967.08	3324726.56	N	43.45	851	Krol, Infrakrol & Blaini Formation	848	0	3708	Shrub Land
884	264122.71	3324786.20	N-W	35.92	1252	Subathu Fm. of W. Himalaya	3058	856	5153	Evergreen Forest
885	216539.08	3324575.69	W	10.52	477	Middle Siwalik Gp of w. & e. Himalayas	2544	13374	4330	Sparsely Vegetated
886	224840.38	3322229.57	W	18.59	659	Lower Siwalik Group	3058	6054	3593	Deciduous Forest
887	223661.29	3322834.70	S	15.87	699	Lower Siwalik Group	2544	7265	4594	Deciduous Forest
888	225426.17	3322097.89	S	13.49	700	Lower Siwalik Group	2682	5482	3007	Shrub Land
889	226438.41	3322104.51	E	6.74	639	Lower Siwalik Group	2399	4843	2080	Deciduous Forest
890	245008.87	3323305.32	N	38.09	790	Subathu Fm. of W. Himalaya	0	856	2390	Shrub Land

891	248718.15	3323042.48	N-W	27.71	1001	Amri Tectonic unit	2682	4281	833	Sparsely Vegetated
892	246595.16	3322026.12	E	24.92	876	Subathu Fm. of W. Himalaya	0	1712	2336	Sparsely Vegetated
893	246298.20	3321590.78	E	26.53	1033	Subathu Fm. of W. Himalaya	848	1712	2661	Sparsely Vegetated
894	246171.16	3322143.08	N-E	28.47	789	Subathu Fm. of W. Himalaya	0	1712	2557	Sparsely Vegetated
895	245841.33	3322086.27	N	46.66	813	Subathu Fm. of W. Himalaya	0	1712	2836	Evergreen Forest
896	245281.30	3322316.40	N	35.97	741	Subathu Fm. of W. Himalaya	0	856	3128	Evergreen Forest
897	250584.74	3321521.82	S	40.73	1199	Amri Tectonic unit	2544	5993	0	Sparsely Vegetated
898	253880.85	3322431.37	N	13.79	654	Jaunsar Gp of W. Himalaya	0	6903	2805	Shrub Land
899	262114.12	3321044.78	S-E	31.74	1069	Amri Tectonic unit	0	3632	7155	Sparsely Vegetated
900	263474.67	3323154.90	S-W	24.92	1517	Jaunsar Gp of W. Himalaya	1896	1914	5875	Sparsely Vegetated
901	274137.70	3323702.67	N	39.00	809	Jaunsar Gp of W. Himalaya	0	4281	3057	Evergreen Forest
902	280345.81	3321641.93	W	44.47	1535	Jaunsar Gp of W. Himalaya	1696	6687	3299	Sparsely Vegetated
903	224185.44	3317599.42	S	20.52	416	Middle Siwalik Gp of w. & e. Himalayas	2399	4281	618	Built-up
904	223774.26	3318950.89	E	30.63	470	Middle Siwalik Gp of w. & e. Himalayas	1896	4611	1109	Built-up
905	224322.94	3318734.11	N-W	21.42	482	Middle Siwalik Gp of w. & e. Himalayas	1896	4611	618	Built-up
906	226683.30	3319424.39	E	13.62	349	Lower Siwalik Group	0	3087	375	Built-up
907	225902.83	3317346.87	S	21.26	462	Middle Siwalik Gp of w. & e. Himalayas	848	2422	375	Built-up
908	226438.43	3317443.01	S-E	6.50	447	Middle Siwalik Gp of w. & e. Himalayas	848	1712	32	Built-up
909	226457.78	3317802.18	S-E	20.75	358	Middle Siwalik Gp of w. & e. Himalayas	848	1914	72	Built-up
910	252647.99	3318026.76	N-W	34.26	1082	Amri Tectonic unit	1199	6054	0	Sparsely Vegetated

911	249356.46	3317251.38	E	40.56	1221	Amri Tectonic unit	1696	3087	1832	Sparsely Vegetated
912	271101.39	3318625.77	S	40.38	766	Jaunsar Gp of W. Himalaya	0	1211	1970	Sparsely Vegetated
913	280074.54	3319583.42	E	25.13	1397	Jaunsar Gp of W. Himalaya	848	5482	2986	Sparsely Vegetated
914	259616.63	3315342.15	N-W	50.23	837	Jaunsar Gp of W. Himalaya	0	8077	1775	Sparsely Vegetated
915	259541.32	3315222.40	N-W	49.35	855	Jaunsar Gp of W. Himalaya	0	8077	1617	Sparsely Vegetated
916	266350.65	3314981.11	N-E	23.88	1587	Amri Tectonic unit	1896	6174	6116	Evergreen Forest
917	279187.56	3315637.49	S	46.08	975	Jaunsar Gp of W. Himalaya	848	1914	1600	Shrub Land
918	275863.22	3315925.18	S-E	38.17	704	Tal Fm of W. Himalaya	0	0	967	Sparsely Vegetated
919	277288.36	3313106.11	E	40.02	1201	Tal Fm of W. Himalaya	1199	0	1050	Sparsely Vegetated
920	232034.52	3308895.78	S	6.12	548	Middle Siwalik Gp of w. & e. Himalayas	2399	1914	3825	Sparsely Vegetated
921	247511.37	3309076.11	N-W	50.88	917	Lower Siwalik Group	848	856	2291	Shrub Land
922	244574.16	3309281.99	S-E	7.27	815	Lower Siwalik Group	848	1914	4717	Deciduous Forest
923	244497.65	3309702.18	W	5.93	880	Lower Siwalik Group	848	1914	4918	Deciduous Forest
924	245276.02	3310123.98	W	31.08	897	Lower Siwalik Group	1696	856	4509	Shrub Land
925	246615.72	3310066.18	S-W	32.80	931	Lower Siwalik Group	848	856	3168	Deciduous Forest
926	249687.59	3311352.13	E	46.96	1064	Subathu Fm. of W. Himalaya	0	856	1699	Deciduous Forest
927	273026.97	3311999.79	S-E	28.07	1669	Jaunsar Gp of W. Himalaya	3058	3632	1933	Sparsely Vegetated
928	288668.67	3309830.70	W	40.58	752	Jaunsar Gp of W. Himalaya	0	4281	7068	Sparsely Vegetated
929	297146.11	3309647.48	N-E	24.75	1223	Jaunsar Gp of W. Himalaya	0	2422	288	Sparsely Vegetated
930	246661.00	3308380.04	W	39.83	871	Subathu Fm. of W. Himalaya	0	856	3292	Shrub Land
931	266747.97	3307976.44	S-E	40.56	1164	Amri Tectonic unit	1896	3087	295	Sparsely Vegetated
932	292090.82	3308193.62	S-W	30.04	1330	Jaunsar Gp of W. Himalaya	848	4843	5408	Sparsely Vegetated

933	309676.94	3304934.48	N	27.53	1246	Jaunsar Gp of W. Himalaya	848	2569	0	Sparsely Vegetated
934	309784.69	3305191.02	N-W	50.96	1241	Jaunsar Gp of W. Himalaya	1199	2569	0	Evergreen Forest
935	309504.45	3306193.36	S-W	50.89	1218	Jaunsar Gp of W. Himalaya	1696	2707	0	Sparsely Vegetated
936	241400.90	3307837.32	S	27.28	527	Lower Siwalik Group	1696	0	1385	Sparsely Vegetated
937	253808.84	3306962.46	E	21.96	1267	Krol, Infrakrol &Blaini Formation	1199	0	3188	Shrub Land
938	250978.65	3305819.02	W	23.06	863	Lower Siwalik Group	1199	856	3947	Sparsely Vegetated
939	251152.49	3305774.76	W	17.43	929	Lower Siwalik Group	1199	856	4030	Sparsely Vegetated
940	260142.17	3306801.38	S	28.92	1014	Subathu Fm. of W. Himalaya	0	856	215	Sparsely Vegetated
941	259687.89	3306356.77	N	42.87	969	Subathu Fm. of W. Himalaya	0	0	362	Shrub Land
942	261797.47	3307335.39	S-W	28.88	1383	Jaunsar Gp of W. Himalaya	1199	1712	385	Sparsely Vegetated
943	262645.89	3306655.78	S-W	19.90	1232	Jaunsar Gp of W. Himalaya	848	856	707	Sparsely Vegetated
944	264028.29	3305636.78	W	47.89	1174	Jaunsar Gp of W. Himalaya	1696	856	1726	Sparsely Vegetated
945	280289.08	3305699.15	W	12.41	1409	Jaunsar Gp of W. Himalaya	1696	1712	3019	Sparsely Vegetated
946	290970.81	3307098.10	E	27.91	829	Jaunsar Gp of W. Himalaya	0	2422	6564	Sparsely Vegetated
947	286423.05	3304981.97	S	31.37	1152	Tal Fm of W. Himalaya	848	1211	4893	Sparsely Vegetated
948	278845.97	3304217.47	E	33.74	989	Jaunsar Gp of W. Himalaya	0	3829	1096	Sparsely Vegetated
949	313382.69	3300975.67	E	31.17	1363	Jaunsar Gp of W. Himalaya	0	856	0	Sparsely Vegetated
950	312387.17	3301309.46	S-W	34.38	1329	Jaunsar Gp of W. Himalaya	0	0	64	Sparsely Vegetated
951	312356.73	3301892.65	S-W	26.88	1432	Jaunsar Gp of W. Himalaya	848	0	32	Sparsely Vegetated
952	311455.15	3301771.16	S	21.45	1537	Jaunsar Gp of W. Himalaya	0	856	32	Sparsely Vegetated
953	311527.48	3301491.52	S-W	37.77	1386	Jaunsar Gp of W. Himalaya	0	856	91	Evergreen Forest
954	310831.87	3302368.12	S-E	38.21	1572	Jaunsar Gp of W. Himalaya	848	0	0	Sparsely Vegetated

955	310736.77	3302270.57	S-E	27.67	1591	Jaunsar Gp of W. Himalaya	848	856	32	Sparsely Vegetated
956	315722.41	3300720.94	W	30.26	1597	Almora Crystallines Fm of W.Himalaya.	848	3425	769	Sparsely Vegetated
957	313990.96	3300548.03	E	52.05	1424	Jaunsar Gp of W. Himalaya	0	1712	358	Sparsely Vegetated
958	311745.70	3301010.17	N-W	32.43	1306	Jaunsar Gp of W. Himalaya	0	0	101	Shrub Land
959	253612.77	3302647.56	S-E	19.73	1023	Subathu Fm. of W. Himalaya	1696	856	4056	Shrub Land
960	256754.67	3302316.84	W	27.18	832	Lower Siwalik Group	1199	856	4429	Sparsely Vegetated
961	257073.96	3302040.90	S-W	35.66	923	Lower Siwalik Group	1696	0	4378	Sparsely Vegetated
962	264232.45	3301397.06	N-E	18.40	1357	Krol, Infrakrol & Blaini Formation	3393	856	3841	Sparsely Vegetated
963	265766.52	3301239.58	S-W	30.29	1292	Krol, Infrakrol & Blaini Formation	1896	856	2415	Sparsely Vegetated
964	279519.25	3303246.40	E	36.16	911	Amri Tectonic unit	0	4281	731	Sparsely Vegetated
965	295916.88	3302846.19	S-E	44.85	1177	Jaunsar Gp of W. Himalaya	0	1914	3882	Sparsely Vegetated
966	305376.11	3302924.85	S-E	12.79	1139	Jaunsar Gp of W. Himalaya	0	3632	2084	Sparsely Vegetated
967	305298.21	3302922.51	N	21.33	1160	Jaunsar Gp of W. Himalaya	0	3632	2073	Sparsely Vegetated
968	305068.62	3302722.65	S-E	41.68	1154	Jaunsar Gp of W. Himalaya	0	3632	1815	Sparsely Vegetated
969	304869.10	3302307.91	E	22.67	1097	Jaunsar Gp of W. Himalaya	0	3632	1375	Sparsely Vegetated
970	306457.48	3300508.34	E	26.71	1402	Jaunsar Gp of W. Himalaya	0	1914	373	Sparsely Vegetated
971	311375.71	3301028.75	E	40.75	1275	Jaunsar Gp of W. Himalaya	0	856	192	Evergreen Forest
972	313400.02	3300283.21	N-E	27.98	1450	Jaunsar Gp of W. Himalaya	848	1712	32	Sparsely Vegetated
973	315061.57	3299833.57	N-E	30.83	1551	Almora Crystallines Fm of W.Himalaya.	0	2569	0	Sparsely Vegetated
974	263240.31	3299966.79	S-W	37.25	1075	Lower Siwalik Group	3058	856	3163	Shrub Land
975	265167.35	3299616.98	S-E	8.18	1267	Lower Siwalik Group	1696	856	2113	Deciduous Forest

976	264980.67	3299593.50	S-E	5.09	1303	Lower Siwalik Group	1696	856	2127	Deciduous Forest
977	268828.49	3300119.52	S-E	42.00	858	Krol, Infrakrol & Blaini Formation	0	856	317	Sparsely Vegetated
978	296784.79	3300305.00	N-E	37.63	993	Jaunsar Gp of W. Himalaya	0	2422	1219	Sparsely Vegetated
979	320022.27	3296394.64	S-E	33.52	1830	Almora Crystallines Fm of W.Himalaya.	3497	0	0	Sparsely Vegetated
980	320085.32	3296473.07	S-E	43.73	1798	Almora Crystallines Fm of W.Himalaya.	3497	0	0	Evergreen Forest
981	256717.87	3298382.72	W	46.75	695	Lower Siwalik Group	2544	1914	2344	Deciduous Forest
982	265383.79	3299407.24	S-W	34.62	1071	Lower Siwalik Group	1696	856	1922	Shrub Land
983	265087.60	3299440.60	S-E	40.85	1177	Lower Siwalik Group	1696	856	1959	Shrub Land
984	264884.70	3299476.61	S	34.24	1233	Lower Siwalik Group	1696	856	2015	Sparsely Vegetated
985	265284.75	3298978.96	N-E	19.75	907	Lower Siwalik Group	1696	856	1472	Shrub Land
986	265437.91	3299145.17	S	28.92	953	Lower Siwalik Group	1696	856	1669	Shrub Land
987	265344.96	3298699.50	N-E	43.17	923	Lower Siwalik Group	848	856	1218	Shrub Land
988	265645.59	3298403.90	E	35.65	755	Lower Siwalik Group	848	856	885	Shrub Land
989	268674.25	3296831.41	S-E	17.28	1128	Lower Siwalik Group	1199	1914	1565	Shrub Land
990	276990.31	3296878.77	E	32.74	655	Subathu Fm. of W. Himalaya	0	1712	32	Deciduous Forest
991	296138.61	3297431.15	S-W	13.06	1152	Tal Fm of W. Himalaya	0	0	91	Sparsely Vegetated
992	297347.08	3296976.68	S-W	28.31	1452	Tal Fm of W. Himalaya	1696	1211	1323	Sparsely Vegetated
993	291781.90	3296316.03	E	30.71	1364	Lower Siwalik Group	2399	1914	275	Sparsely Vegetated
994	298986.77	3296979.94	N	43.08	1601	Krol, Infrakrol & Blaini Formation	848	2422	2530	Sparsely Vegetated
995	320092.09	3296209.66	E	25.48	1791	Almora Crystallines Fm of W.Himalaya.	2682	0	32	Sparsely Vegetated

996	320111.05	3296236.45	N-E	29.92	1770	Almora Crystallines Fm of W.Himalaya.	2682	0	32	Sparsely Vegetated
997	320118.24	3295333.42	S	34.24	1768	Almora Crystallines Fm of W.Himalaya.	1896	0	0	Sparsely Vegetated
998	319121.28	3295301.51	E	18.74	1797	Almora Crystallines Fm of W.Himalaya.	1696	856	0	Evergreen Forest
999	261829.96	3295512.82	S	23.22	663	Lower Siwalik Group	848	2422	831	Shrub Land
1000	291681.69	3296187.61	S-E	31.44	1343	Jaunsar Gp of W. Himalaya	3058	1914	295	Sparsely Vegetated
1001	325910.53	3292265.84	S-E	26.83	1782	Almora Crystallines Fm of W.Himalaya.	3058	856	195	Deciduous Forest
1002	321752.85	3294786.43	E	19.03	1844	Almora Crystallines Fm of W.Himalaya.	3058	856	136	Sparsely Vegetated
1003	320260.19	3295089.70	S	24.60	1770	Almora Crystallines Fm of W.Himalaya.	1896	856	32	Deciduous Forest
1004	318916.00	3294883.26	S	30.73	1849	Almora Crystallines Fm of W.Himalaya.	1896	856	0	Sparsely Vegetated
1005	318742.64	3294974.00	S-W	34.50	1859	Almora Crystallines Fm of W.Himalaya.	1896	856	0	Sparsely Vegetated
1006	318253.72	3294769.61	S	20.09	1878	Jaunsar Gp of W. Himalaya	1896	1211	0	Sparsely Vegetated
1007	318059.62	3294891.95	S	33.53	1926	Jaunsar Gp of W. Himalaya	2399	1211	0	Shrub Land
1008	317006.24	3294685.92	S-E	22.95	1762	Jaunsar Gp of W. Himalaya	2544	1914	0	Sparsely Vegetated
1009	316967.06	3294541.51	E	33.19	1760	Jaunsar Gp of W. Himalaya	1696	1914	0	Sparsely Vegetated
1010	316073.50	3294024.37	S	11.49	1616	Jaunsar Gp of W. Himalaya	1896	2569	275	Sparsely Vegetated
1011	315877.94	3294580.69	S	30.82	1783	Jaunsar Gp of W. Himalaya	2682	3425	0	Sparsely Vegetated
1012	315637.60	3294588.66	S	25.10	1775	Jaunsar Gp of W. Himalaya	2399	3425	32	Sparsely Vegetated
1013	315353.67	3293651.00	S	13.22	1803	Jaunsar Gp of W. Himalaya	1696	3425	0	Sparsely Vegetated

1014	306810.62	3293364.19	N	37.79	1545	Jaunsar Gp of W. Himalaya	848	4281	905	Sparsely Vegetated
1015	287813.01	3292035.22	N-E	20.09	1029	Jaunsar Gp of W. Himalaya	848	2422	736	Evergreen Forest
1016	319347.51	3292049.86	W	30.84	1350	Jaunsar Gp of W. Himalaya	0	856	865	Sparsely Vegetated
1017	299685.61	3290517.41	W	24.24	1536	Lower Siwalik Group	1896	0	6858	Sparsely Vegetated
1018	321191.18	3290315.06	S	27.87	1729	Jaunsar Gp of W. Himalaya	1896	3632	385	Sparsely Vegetated
1019	331346.65	3287750.33	S	33.37	877	Almora Crystallines Fm of W.Himalaya.	848	856	466	Sparsely Vegetated
1020	331153.16	3287843.16	S	20.31	959	Almora Crystallines Fm of W.Himalaya.	0	856	641	Sparsely Vegetated
1021	330989.90	3287961.41	S	27.49	1013	Almora Crystallines Fm of W.Himalaya.	0	856	801	Sparsely Vegetated
1022	330711.53	3287951.46	S	38.82	997	Almora Crystallines Fm of W.Himalaya.	848	856	1088	Sparsely Vegetated
1023	310800.70	3288083.77	S-E	45.44	1267	Krol, Infrakrol & Blaini Formation	0	4611	1559	Sparsely Vegetated
1024	331263.83	3284682.76	W	36.30	982	Almora Crystallines Fm of W.Himalaya.	1199	1211	1518	Sparsely Vegetated
1025	331153.78	3284767.25	S-W	17.60	932	Almora Crystallines Fm of W.Himalaya.	1199	1211	1591	Sparsely Vegetated
1026	331253.53	3285212.24	W	36.05	885	Almora Crystallines Fm of W.Himalaya.	1199	856	1344	Sparsely Vegetated
1027	329604.68	3285894.97	S	23.44	1190	Almora Crystallines Fm of W.Himalaya.	848	1914	1619	Sparsely Vegetated
1028	329787.61	3285566.08	S	36.45	1057	Almora Crystallines Fm of W.Himalaya.	848	1712	1972	Sparsely Vegetated
1029	327962.83	3285341.79	S-W	32.46	1391	Almora Crystallines Fm of W.Himalaya.	2544	1712	1531	Sparsely Vegetated
1030	327181.57	3285592.17	S-W	28.19	1431	Jaunsar Gp of W. Himalaya	1696	856	1316	Sparsely Vegetated

1031	302946.77	3286626.87	S-W	33.33	1494	Tal Fm of W. Himalaya	1696	3829	4184	Sparsely Vegetated
1032	308405.27	3284756.29	S-E	17.25	1582	Krol, Infrakrol & Blaini Formation	2399	4366	0	Deciduous Forest
1033	316551.03	3286892.53	E	46.56	964	Jaunsar Gp of W. Himalaya	0	6520	480	Sparsely Vegetated
1034	317683.83	3286749.29	S	37.62	1251	Jaunsar Gp of W. Himalaya	0	6054	1364	Sparsely Vegetated
1035	318655.25	3286716.87	S	27.58	1221	Jaunsar Gp of W. Himalaya	848	5993	2166	Sparsely Vegetated
1036	323226.12	3286699.12	E	24.21	1108	Jaunsar Gp of W. Himalaya	848	3425	1361	Sparsely Vegetated
1037	263571.99	3283732.50	S-W	15.84	814	Lower Siwalik Group	3058	856	2920	Sparsely Vegetated
1038	264255.84	3283702.37	E	32.95	624	Lower Siwalik Group	2399	1211	3419	Sparsely Vegetated
1039	317989.63	3282885.67	E	39.12	769	Jaunsar Gp of W. Himalaya	0	7315	750	Sparsely Vegetated
1040	270770.20	3281838.37	S-E	7.77	506	Middle Siwalik Gp of w. & e. Himalayas	848	2707	7826	Sparsely Vegetated
1041	300821.29	3280376.10	N-E	40.66	650	Krol, Infrakrol & Blaini Formation	0	1914	45	Deciduous Forest
1042	306246.34	3281853.23	E	18.58	1072	Krol, Infrakrol & Blaini Formation	1896	1211	295	Sparsely Vegetated
1043	278505.16	3279170.23	S-W	35.11	726	Lower Siwalik Group	2399	2422	9131	Sparsely Vegetated
1044	299609.80	3279596.62	S	16.40	917	Lower Siwalik Group	848	3530	704	Shrub Land
1045	303411.83	3279600.16	W	41.86	587	Krol, Infrakrol & Blaini Formation	0	1914	885	Shrub Land
1046	309926.87	3278634.48	N-W	31.77	949	Krol, Infrakrol & Blaini Formation	848	0	2906	Sparsely Vegetated
1047	310136.56	3279386.36	W	31.03	944	Krol, Infrakrol & Blaini Formation	848	856	2661	Sparsely Vegetated
1048	315013.06	3278648.31	E	26.67	886	Krol, Infrakrol & Blaini Formation	0	1914	163	Sparsely Vegetated
1049	325735.87	3278540.05	N-W	44.07	734	Jaunsar Gp of W. Himalaya	0	6174	2585	Sparsely Vegetated
1050	325977.98	3279751.71	W	39.20	766	Jaunsar Gp of W. Himalaya	0	6054	1356	Sparsely Vegetated
1051	314836.95	3275964.62	E	35.52	665	Jaunsar Gp of W. Himalaya	848	0	329	Sparsely Vegetated
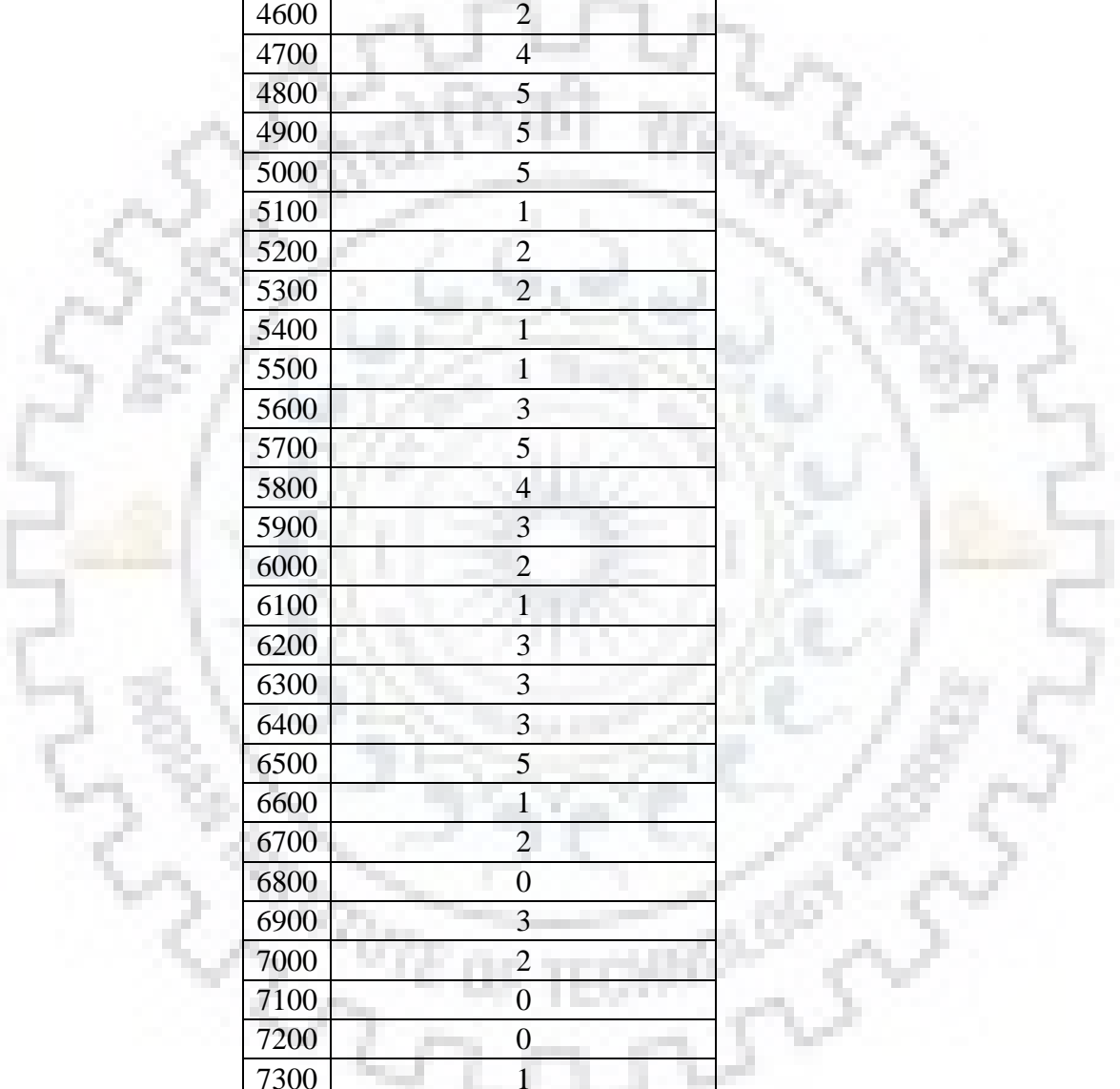
1052	314831.11	3275839.07	E	23.60	655	Jaunsar Gp of W. Himalaya	0	0	407	Sparsely Vegetated
1053	313702.48	3276689.22	S	25.28	628	Jaunsar Gp of W. Himalaya	0	0	1406	Shrub Land
1054	316517.67	3276245.60	E	57.24	536	Jaunsar Gp of W. Himalaya	0	856	761	Shrub Land
1055	325411.53	3277753.08	N-E	39.53	716	Jaunsar Gp of W. Himalaya	0	5482	3442	Sparsely Vegetated
1056	315905.71	3275475.57	S-W	39.86	715	Jaunsar Gp of W. Himalaya	848	856	132	Shrub Land
1057	321375.91	3275039.27	N	27.35	951	Jaunsar Gp of W. Himalaya	0	1712	2310	Sparsely Vegetated
1058	322552.94	3275283.90	S-W	39.52	1077	Jaunsar Gp of W. Himalaya	848	1712	2290	Sparsely Vegetated
1059	320978.96	3272117.99	W	28.50	894	Jaunsar Gp of W. Himalaya	2399	1712	1656	Evergreen Forest
1060	322765.79	3273217.04	S-E	29.17	1399	Jaunsar Gp of W. Himalaya	2682	0	3704	Sparsely Vegetated
1061	275334.29	3271650.41	S-E	35.13	559	Lower Siwalik Group	3058	0	5024	Shrub Land
1062	287866.47	3264745.58	S-E	18.02	533	Lower Siwalik Group	1199	856	2813	Sparsely Vegetated
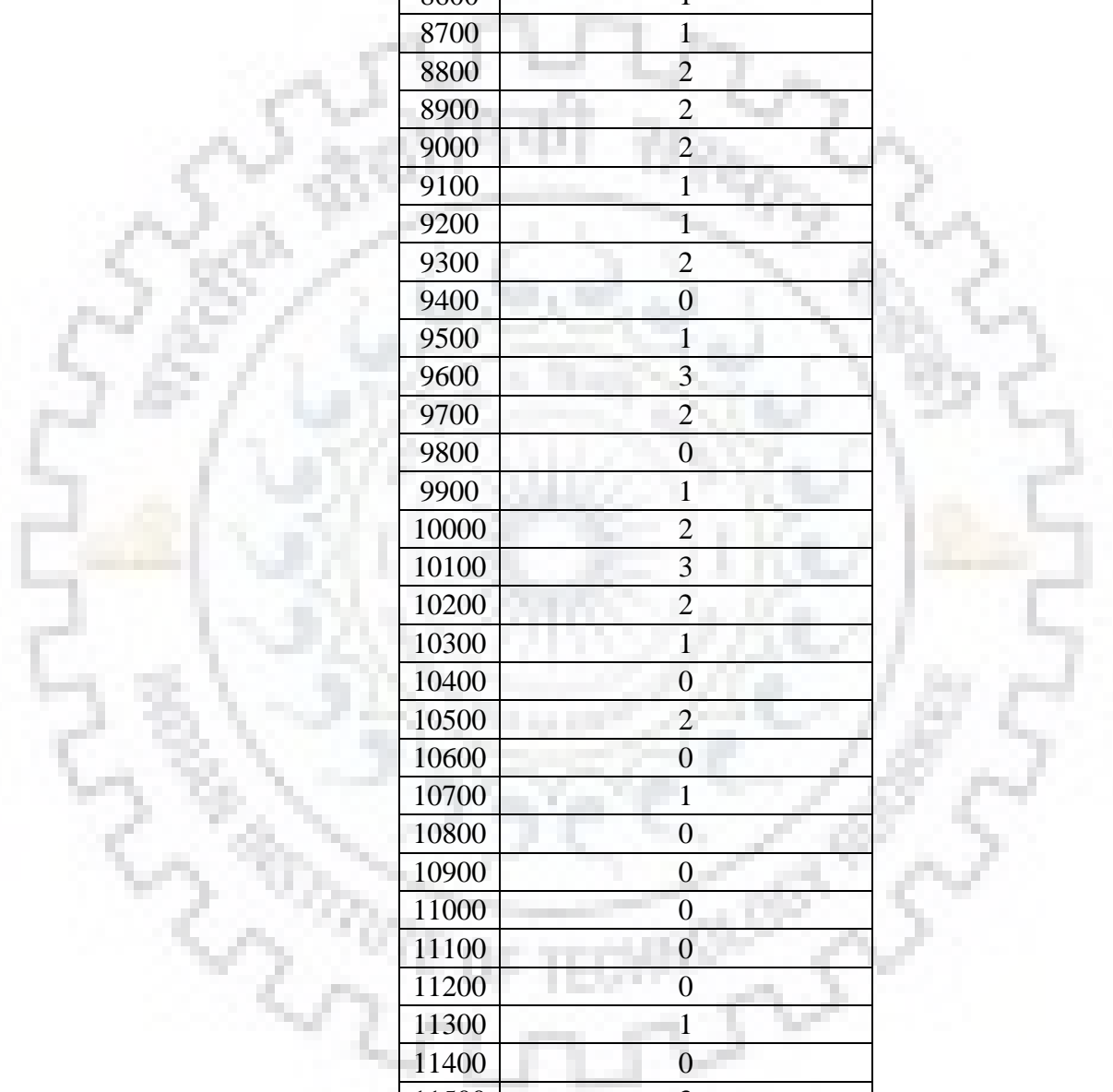
Table A2: No. of observed landslides for fault Euclidean distance

Fault Euclidian Distance (m)	No. of Observed Landslides
0	3
100	16
200	14
300	14
400	13
500	23
600	17
700	19
800	8
900	14
1000	8
1100	13
1200	6
1300	13
1400	10
1500	5
1600	10
1700	9
1800	6
1900	8
2000	3
2100	11
2200	9
2300	7
2400	6
2500	7
2600	3
2700	6
2800	4
2900	3
3000	5
3100	6
3200	6
3300	5
3400	3
3500	8
3600	8
3700	5
3800	5

3900	4
4000	6
4100	2
4200	2
4300	3
4400	7
4500	3
4600	2
4700	4
4800	5
4900	5
5000	5
5100	1
5200	2
5300	2
5400	1
5500	1
5600	3
5700	5
5800	4
5900	3
6000	2
6100	1
6200	3
6300	3
6400	3
6500	5
6600	1
6700	2
6800	0
6900	3
7000	2
7100	0
7200	0
7300	1
7400	2
7500	2
7600	1
7700	3
7800	2
7900	0

8000	0
8100	7
8200	1
8300	2
8400	0
8500	3
8600	1
8700	1
8800	2
8900	2
9000	2
9100	1
9200	1
9300	2
9400	0
9500	1
9600	3
9700	2
9800	0
9900	1
10000	2
10100	3
10200	2
10300	1
10400	0
10500	2
10600	0
10700	1
10800	0
10900	0
11000	0
11100	0
11200	0
11300	1
11400	0
11500	3
11600	0
11700	1
11800	1
11900	1
12000	1

12100	0
12200	0
12300	0
12400	0
12500	0
12600	0
12700	0
12800	1
12900	0
13000	1
13100	1
13200	1
13300	0
13400	0
13500	2
13600	1
13700	2
13800	2
13900	0
14000	0
14100	0
14200	0
14300	0
14400	0
14500	0
14600	0
14700	0
14800	1

Table A3: Earthquake Catalogue

Longitude	Latitude	Year	Month	Date	Magnitude	Depth	Time	
							Hour	Minute
80	30	1720	7	25	7.5	1	0	0
80	31.3	1751	1	1	7	1	0	0
80	30	1803	5	22	6.4	5	17	0
79	31.5	1803	9	1	7.5	5	1	30
78.5	30.7	1809	1	1	5.5	5	0	0
79	30	1809	1	1	6.3	5	0	0
79	30.9	1816	5	26	6.4	5	22	30
81	30	1816	8	28	7.5	5	0	0
77.2	28.53	1825	3	22	4.3	5	12	35
77.2	28.53	1830	7	17	4.3	5	1	15
77.2	28.53	1831	10	24	5.4	5	12	30
79.6	29.4	1831	12	25	5.1	5	21	0
79.6	29.4	1832	7	2	4.5	5	23	0
79.6	29.4	1832	9	23	4	5	22	0
79.6	29.4	1833	5	30	6	5	0	0
79.6	29.4	1835	1	4	4	5	7	0
79.6	29.4	1835	1	14	5.1	5	1	30
77.2	28.7	1842	1	2	4.3	5	0	0
78	27	1842	1	16	5.5	5	19	30
78.1	30.45	1842	3	5	5.4	5	21	10
77.2	28.7	1842	7	4	4.8	5	14	50
78.07	30.43	1842	9	7	4.3	5	13	58
77.2	28.53	1842	9	26	4.8	5	9	0
77.2	28.53	1842	11	6	4.3	5	13	30
80	30	1843	4	11	4.8	5	8	50
77.75	29	1852	3	31	4.8	5	0	0
77.17	31.1	1856	4	7	5.1	5	0	0
77.17	31.12	1858	8	11	6	5	0	0
77.17	31.12	1865	4	11	5.4	5	0	0
78.1	30.3	1869	3	25	4	5	0	0
79.42	29.33	1869	7	25	4.8	5	0	0
77.17	31.12	1878	3	2	5.1	5	0	0
77	32	1901	11	18	6.2	5	0	4
79	30	1902	6	16	5.9	5	1	36
76.2	32.3	1905	4	4	7.8	35	0	50
79	31	1906	6	13	6	5	0	0
80.28	30.76	1911	10	14	6.5	20	23	24
77	31	1913	6	26	5.1	5	23	30
76.18	32.6	1914	10	9	6.3	20	2	39
80.75	29.73	1916	8	28	7.2	20	6	39

80.05	30.5	1926	7	27	6	5	7	23
80.5	30.5	1927	10	8	6	5	10	34
77	31.7	1930	5	11	5.5	5	11	30
80	29.5	1933	5	18	3.3	5	0	0
75.5	29	1934	4	14	5.1	5	0	0
80.4	29.6	1935	3	5	5.8	5	22	15
78	31	1937	10	20	5.4	5	1	23
77	31.5	1940	4	17	4	5	0	0
80	30.3	1945	6	4	6.4	60	12	9
76.13	32.78	1945	6	22	6.3	60	18	1
76.14	32.83	1947	7	10	5.6	60	10	19
79.09	31.2	1947	8	19	5.9	5	20	7
78.75	30.44	1948	5	5	4	5	8	31
79.05	31.2	1949	2	5	5.5	5	0	0
75.9	32.6	1950	8	12	5.5	5	3	59
77.02	32.17	1950	10	6	4.5	5	21	20
74.8	31.2	1952	12	27	5.5	5	18	45
76.49	32.25	1955	4	14	5.1	5	1	1
78.55	32.38	1955	6	27	6	5	10	14
77.7	28.2	1956	10	10	6.2	33	15	31
79.95	29.99	1958	12	28	6.5	5	5	34
78.59	32.29	1959	5	12	5.1	5	0	35
76.72	28.59	1960	8	27	5.5	5	15	58
80.83	29.43	1961	12	24	5.4	59	0	0
79.6	30.5	1962	7	13	5.5	25	0	0
76.2	31.9	1962	9	15	5.5	5	12	35
80.9	29.5	1963	1	30	5.5	5	0	0
78.82	31.94	1963	4	12	5.8	23	0	41
78.5	30.3	1963	7	14	5.5	33	14	48
78.35	32.06	1963	11	12	4.7	5	15	29
79.1	30.8	1963	11	27	5.3	33	21	10
77.78	29.33	1964	2	16	4.4	5	0	0
76.9	28.93	1964	5	4	4	5	0	0
77.07	28.83	1964	8	12	3.5	5	0	0
80.46	29.96	1964	9	26	6	50	0	46
80.98	29.4	1964	10	6	5.4	11	20	19
78.7	31.84	1964	10	19	4.9	72	2	16
81.1	29.35	1964	12	20	5.4	9	3	31
76.9	32.79	1965	2	21	5	33	3	25
80.26	29.55	1965	3	18	5.3	67	2	41
78.1	31.76	1965	3	30	4.8	5	22	31
77.1	31.3	1965	4	13	4.3	5	0	0
80.19	29.62	1965	5	13	5.1	75	10	51
77.99	32.65	1965	5	31	5.5	28	2	4

77.2	31.5	1965	5	31	5.6	5	0	0
80.3	29.9	1965	11	18	5.5	5	0	0
76.95	31.42	1966	1	25	4.1	5	0	0
77	28.5	1966	2	13	5.1	5	0	0
80.5	31.49	1966	3	6	6.6	50	2	15
76.98	28.5	1966	6	20	5	53	13	42
79.61	32.76	1966	8	5	5.5	31	1	3
78.93	28.67	1966	8	15	5.8	5	2	15
81.23	29.3	1966	10	5	4.9	33	7	57
80.19	31.41	1966	10	13	4.9	29	12	42
80.79	29.62	1966	12	16	5.9	19	20	52
79.13	30.6	1967	1	2	4.9	25	22	17
76.1	32.6	1967	9	20	4.3	59	0	0
79.25	30.41	1968	1	5	5.3	7	6	42
80.51	29.76	1968	5	27	5.2	27	18	35
79.92	29.91	1968	5	31	5.3	33	3	1
76.1	31.6	1968	10	12	4.9	160	19	6
76.48	32.28	1968	11	5	5.2	33	2	2
76	32.19	1969	1	23	4.3	64	20	1
79.84	30.04	1969	3	3	5.4	18	6	20
81.02	29.46	1969	3	5	5.3	22	11	14
79.4	30.5	1969	6	22	5.5	15	1	33
80.95	29.13	1969	12	5	5.2	33	18	45
76	32.5	1970	1	2	4.5	96	20	1
76.64	32.7	1970	1	17	5	22	18	33
76.61	32.32	1970	3	5	5	33	18	34
76.6	28.95	1970	3	18	5	18	7	40
74.9	32.8	1970	4	28	4.9	116	14	12
78.97	30.54	1971	1	30	5	56	20	15
77.1	29.1	1971	10	14	3.8	5	0	0
76.61	31.79	1972	6	20	4.6	57.9	15	34
78.42	30.75	1972	8	17	5.5	33	18	14
78.51	32.49	1972	9	6	5.3	14	2	51
76.35	32.05	1972	10	26	4.8	82.3	14	5
77.13	32.06	1972	10	26	5	68	0	0
80.34	30.51	1973	2	10	4.9	5	6	51
77.83	32.12	1973	4	1	5.8	90.1	9	45
75.2	27	1973	6	26	4.4	5	0	0
77.85	29.38	1973	9	28	4	5	0	0
76.19	32.36	1973	12	16	5.1	18	9	16
78.47	30.97	1974	2	24	5.2	0.6	21	32

78.48	30.55	1974	7	7	5	96	20	56
78.5	32.39	1975	1	19	7	1.4	8	1
78.94	28.22	1975	4	30	4.9	33	3	8
79.4	30.69	1975	8	23	4.5	33	3	8
76.25	32.34	1975	9	16	4.9	58.8	4	20
77.5	31.4	1975	11	20	3.8	5	0	0
77.03	31.24	1976	2	5	5.3	5.5	12	4
78.63	32.35	1976	2	24	5.2	148.4	22	26
75.3	32.59	1976	3	4	4.2	121	18	45
76.39	32.65	1976	4	10	4.7	62	7	9
76.22	32.68	1976	4	16	4.3	92	20	15
77	32	1976	5	6	4.3	5	0	0
78.59	31.53	1976	5	6	4.9	87	8	21
78.35	32.44	1976	7	6	5.4	24.6	2	55
79.1	31.2	1976	9	8	5.1	5	0	0
78.76	32.03	1976	9	8	5.5	9	20	13
79.4	30.1	1976	9	22	4.6	5	0	0
78.4	31.83	1976	9	29	5.2	20.4	7	47
75.98	32.76	1977	1	21	4.9	51	14	57
78.04	31.42	1977	1	28	5	50.1	3	48
78.43	31.8	1977	2	19	5.1	40	6	15
78.66	32.67	1977	3	27	5.4	26	5	36
79.45	30.49	1977	4	20	5.2	35.8	4	21
81.06	29.57	1977	9	20	4.7	23	5	51
78.8	31.4	1977	10	18	5.1	5	0	0
78.47	32.78	1977	10	19	4.8	33	7	14
79.4	29.8	1977	10	21	4.4	5	0	0
81.14	30.02	1978	1	1	4.7	83.3	11	25
79.4	30.51	1978	1	7	4.9	33	7	23
78.28	31.07	1978	1	15	4.6	33	0	17
78.37	31.85	1978	1	15	4.9	60	2	30
75.27	31.79	1978	2	19	4.4	45	18	56
80.69	29.34	1978	2	28	5	53.6	17	26
78.46	32.69	1978	3	30	4.6	50	23	44
78.72	32.73	1978	4	11	4.9	33	7	55
77.87	31.51	1978	5	21	4.6	70.1	23	7
76.61	32.24	1978	6	14	5.3	6.7	16	12
78.78	32.04	1978	8	24	4.9	33	7	22
77.05	28.5	1978	10	16	3.7	5	0	0
80.94	29.2	1978	12	12	4.8	56	10	0
80.4	29.64	1978	12	14	4.5	33	20	16

79.6	30.33	1979	3	5	4.6	8.4	23	54
78.65	32.2	1979	3	27	4.6	33	5	27
80.31	29.9	1979	3	29	4.6	33	1	58
78.88	32.09	1979	5	11	4.8	33	21	56
80.27	29.93	1979	5	20	5.8	15.8	22	59
81.18	31.43	1979	11	30	4.4	33	20	13
78	32.08	1979	12	22	5.5	5	0	0
78.58	30.82	1979	12	28	5.3	23	1	59
80	30	1980	1	16	4.2	5	0	0
81.01	29.37	1980	2	15	4.4	33	1	15
77.89	28.65	1980	4	27	5	33	17	0
76.45	31.46	1980	5	29	4.6	16	22	40
81.09	29.63	1980	7	29	6.5	23.3	14	58
80.31	29.63	1980	7	30	4.8	33	5	30
78	29.2	1980	8	16	4.2	5	0	0
77	32	1980	9	4	4	5	0	0
75.68	31.29	1980	9	4	4.9	121.8	1	48
80.36	29.92	1980	9	8	4.8	33	7	42
78.55	32.57	1980	9	22	4.9	65	20	37
80.66	29.8	1981	3	6	5.4	23.6	5	58
77.47	29.06	1981	5	15	3.3	5	0	0
78.44	31.83	1981	5	28	5.5	5	23	14
78.89	30.44	1981	6	19	4.9	64	10	41
80.31	30.77	1981	7	1	4.5	33	20	38
76.09	32.73	1981	7	12	5	35.9	8	45
75.08	30.98	1981	7	31	4.5	5	5	49
77.82	31.1	1981	8	10	4.9	33	10	58
81.14	29.43	1981	9	10	5.1	33	3	47
79.63	30.67	1981	12	2	4.3	5	12	46
76.01	32.62	1982	5	7	5.1	39.7	7	44
78.58	30.37	1982	6	22	4.5	33	2	38
78.38	30.91	1982	7	7	4.8	5	22	36
77.68	30.89	1982	7	16	4.5	67.4	4	15
76.14	32.59	1982	9	4	4.7	33	12	33
79.9	30.1	1982	9	15	4.3	5	0	0
79.25	30.42	1982	10	16	4.9	25.5	2	22
81.05	28.8	1982	11	21	4.8	5	8	10
80.65	29.84	1982	12	6	4.6	5	11	52
78.96	31.39	1982	12	14	4.9	10.9	23	57
79.89	30.05	1982	12	29	5	21.7	0	9
78.57	32.6	1983	2	27	5.2	40	20	33

79.77	30.36	1983	5	20	4.6	33	12	52
75.49	32.71	1983	5	30	4.9	41.4	8	39
80.87	29.3	1983	7	5	4.9	33	17	26
79.66	32.19	1984	1	8	4.8	36.3	1	53
80.54	29.84	1984	2	19	5.4	21	15	46
81.12	29.18	1984	3	14	5.3	14.8	1	32
78.56	30.54	1984	5	3	4.9	59.8	13	18
77.35	31.32	1984	6	1	4.1	61.9	3	51
80.13	29.56	1984	10	24	4.6	56	8	19
76.85	32.39	1984	11	12	4.8	33	22	30
81.23	29.22	1984	11	23	4.8	72	6	14
79.13	30.21	1984	11	26	4.8	63.1	3	35
77.61	31.27	1984	12	15	4.9	63.5	10	54
80.9	29.35	1984	12	18	4.9	33	22	46
77.26	31.39	1985	3	11	5	40.9	14	36
79.4	29.72	1985	6	14	4.3	33	17	19
76.1	32.68	1985	12	29	5.2	5	21	31
78.21	30.65	1986	3	28	4.9	33	18	5
76.95	31.85	1986	4	22	4.9	32.2	9	29
76.41	32.15	1986	4	26	5.5	33	7	35
78.59	31.53	1986	6	14	4.2	33	13	36
78.71	31.77	1986	6	30	4.9	33	13	1
78	31.05	1986	7	16	5.4	4.4	22	3
78.49	32.56	1986	9	11	5.1	18.4	4	22
76.62	32.3	1986	11	21	4.3	40	17	31
79.12	30.36	1987	6	6	5.2	36	11	2
77.95	31	1987	7	18	5	49.5	16	29
80.67	29.94	1987	7	23	4.6	33	21	1
80.05	31.68	1987	8	21	4.9	33.6	0	26
76.4	32.07	1987	10	6	5	51.1	16	33
76.94	32.15	1987	12	26	4.8	33	1	3
81.12	29.09	1988	3	13	4.6	55.6	11	13
79.56	32.74	1988	4	30	4.1	33	22	17
80.44	29.76	1988	5	15	5.2	6	20	23
79.19	30.52	1988	6	9	5	40.7	12	11
78.28	30.85	1988	7	14	4.7	33	3	53
78.7	31.59	1988	7	27	4.7	46.5	7	7
79.88	32.62	1988	9	23	4.9	33	4	23
79.38	32.05	1988	9	26	4.6	154.6	18	4
78.57	32.34	1988	10	3	4.4	33	7	24
77.92	30.58	1988	12	26	4.7	45.4	11	11

78.68	30.64	1989	1	27	4.3	33	11	3
79.98	29.32	1989	8	28	4.7	10	19	8
76.04	32.63	1989	11	4	4.7	71.7	13	22
80.64	29.89	1990	2	9	4.9	33	15	51
78.54	31.67	1990	4	3	4.7	28.9	1	8
76.71	29.19	1990	5	15	4.5	25.4	17	19
76.58	28.96	1990	8	27	4.4	33	16	38
76.16	32.66	1990	9	5	4.4	33	21	15
79.91	29.99	1990	9	21	5.4	18.7	16	8
78.5	31.09	1990	10	3	4.7	33	18	20
77.29	31.48	1990	12	13	5	33	8	28
79.16	30.35	1990	12	18	5.1	34.5	2	40
77.4	31.59	1991	1	20	5.2	33	12	43
79.28	30.62	1991	2	12	4.8	51.2	14	2
77.46	32.42	1991	3	23	4.4	33	1	48
79.72	30.06	1991	4	22	5	35.8	8	48
80.12	31.68	1991	5	18	4.9	31.8	4	52
80.28	29.5	1991	5	27	5.2	28	21	6
76.76	32.38	1991	6	23	4.9	22.9	2	45
78.55	30.82	1991	8	16	4.5	33	1	23
79.7	30.4	1991	8	20	4.6	10	5	6
80.92	30.7	1991	9	14	5	64.4	5	29
79.29	30.61	1991	10	15	4.9	23.1	19	10
78.79	30.77	1991	10	19	6.8	13.2	21	23
81.02	28.38	1992	1	11	4.2	33	13	3
76.44	32.31	1992	1	26	4.8	41.4	23	48
81.18	29.42	1992	1	30	4.8	10.7	5	55
76.61	32.76	1992	2	13	4.9	17.6	22	43
80.73	32.2	1992	3	31	4	33	0	28
80.62	31.99	1992	5	22	4.1	33	22	22
78.01	31.45	1992	7	21	4.3	34.6	5	6
80.71	32.95	1992	8	3	4.4	33	2	5
78.49	30.87	1992	8	9	4.4	39.5	15	16
76.53	32.7	1992	9	6	4.8	38.3	14	10
80.4	28.98	1992	10	22	4.5	33	7	7
80.75	31.8	1992	10	25	4	33	0	16
80.63	29.01	1992	11	11	3.8	33	8	32
80.2	27.7	1993	1	2	3.3	5	13	31
81.13	29.15	1993	1	2	5.1	17.7	14	53
80.33	31.25	1993	1	12	5	25.7	8	52
80.56	29.68	1993	3	25	4.7	30.1	20	16

80.22	31.61	1993	7	28	4.8	36.4	14	16
78.44	30.94	1993	7	31	4.3	15.8	19	44
78.95	30.94	1993	8	16	4.7	33	2	9
79.98	30.09	1993	8	19	4.8	37.3	3	49
80.61	32.17	1993	9	25	4.5	33	23	24
80.03	30.23	1993	11	14	4.8	36.4	13	20
76.72	28.9	1993	12	3	4.3	40.4	9	48
79.39	30.58	1994	3	29	4.4	43.2	0	26
75.95	32.55	1994	5	13	4.7	33	9	19
76.77	27.97	1994	6	1	3.8	10	18	22
76.35	32.79	1994	7	2	4.3	33	20	34
78.43	31.62	1994	7	10	4.7	33	8	16
80.07	31.62	1994	7	31	5	35.9	23	53
79.62	30.67	1994	12	8	5.1	20.1	13	1
80.59	29.53	1994	12	12	4.7	38	10	41
81.07	29.46	1995	2	8	4.2	44	0	0
76.17	32.67	1995	3	24	5	29.2	11	52
79.98	31.43	1995	6	12	4.4	52	11	30
79.38	29.88	1995	7	15	4.6	33	6	39
79.61	30.09	1995	7	24	4.3	5	22	11
77.78	31.12	1995	9	5	4.5	49.9	7	44
74.89	32.27	1995	9	26	4.6	5	20	31
78.96	31.39	1995	10	21	5.2	33	19	39
76.65	28.97	1995	11	15	4.4	24.9	21	44
78.47	31.97	1995	11	26	4.6	28.6	20	21
79.23	30.71	1995	11	27	4.9	38.2	21	44
79.81	31.47	1995	12	10	4.5	15.4	1	56
79.42	30.46	1996	1	23	4.7	27	17	34
80.39	29.59	1996	2	7	4.5	47.6	10	56
79.1	30.69	1996	3	26	4.9	41.8	8	30
80.92	29.41	1996	4	4	4	92	23	3
76.34	32.82	1996	5	9	4.4	56	8	25
76.15	32.87	1996	5	16	4.3	65.3	17	18
76.5	32.78	1996	5	23	4.6	48.4	23	51
79.26	30.57	1996	6	18	4.6	42	2	46
81.04	29.55	1996	7	14	4.3	55	0	0
76.49	32.55	1996	7	14	4.5	39.2	0	40
78.55	31.41	1996	7	17	4.7	40.5	6	56
75.09	27.22	1996	7	28	4	33	20	54
78.91	30.83	1996	8	3	4.3	33	13	33
78.3	30.8	1996	9	14	4.6	46.5	2	12

76.4	32.82	1996	9	14	4.8	45	0	22
78.57	30.5	1996	9	25	4.7	30.8	7	12
78.2	30.95	1996	10	1	4.3	73.5	11	24
78.3	31.21	1996	10	3	4.2	39.7	21	9
78.07	30.81	1996	10	9	4.4	33	21	45
77.21	29.93	1996	11	12	4.5	55.5	4	20
76.89	32.39	1996	12	23	3.9	33	21	52
77.62	31.04	1997	1	2	4.2	72.3	3	52
80.5	29.8	1997	1	5	5.7	16	0	0
76.23	32.73	1997	1	19	4.3	58.7	14	38
75.79	31.77	1997	2	24	4.3	5	19	37
76.48	31.61	1997	2	25	4.3	5	10	10
80.4	29.42	1997	5	2	4.3	30.2	20	9
76.59	28.98	1997	5	4	4.3	28.8	7	19
78.31	30.1	1997	6	29	4.5	33	20	11
76.86	31.56	1997	7	29	4.7	49.2	18	0
76.69	31.41	1997	8	13	4.3	62.9	23	10
79.06	32.62	1997	9	11	4	33	3	1
78.64	31.86	1997	9	21	4	33	15	21
75.77	31.62	1997	10	17	4.6	38	17	36
76.34	32.73	1997	11	9	4.1	33	1	56
80.87	32.4	1997	12	4	4	33	7	46
81.12	29.77	1998	1	19	4.2	7	0	0
78.11	29.1	1998	2	7	4	35.3	8	45
81.26	28.97	1998	2	15	4.3	2	0	0
77.75	31.11	1998	3	19	4.1	58.3	17	1
76.26	32.51	1998	3	19	4.2	63.8	23	34
76.38	32.7	1998	3	20	4.3	19.3	1	3
76.32	28.22	1998	3	30	4.4	10.5	23	55
78.42	31.21	1998	4	5	4.3	33	6	52
79.46	30.08	1998	5	1	4.5	42.6	11	57
76.87	28.85	1998	5	28	4.2	24.8	0	16
79.62	30.45	1998	5	31	4.1	33	10	52
77.46	31.65	1998	6	6	4.1	10	17	8
76.53	32.42	1998	10	17	4.7	11.1	9	24
78.23	31.44	1998	10	26	3.8	62.4	14	34
76.01	32.3	1998	11	6	4.3	34.1	14	29
80.19	31.57	1998	11	10	4.2	33	2	51
79.26	30.56	1998	11	19	4.7	45.2	16	34
77.26	31.62	1999	2	3	4	5	10	17
78.85	30.62	1999	2	25	4.3	50.5	11	13

79.31	30.34	1999	2	28	4.9	10	19	47
78.42	28.84	1999	3	15	4.3	54.8	23	17
76.71	28.88	1999	3	22	4.4	36.9	9	55
78.61	28.79	1999	3	23	4.3	25.4	7	29
76.81	32.33	1999	3	28	4.2	190.3	19	20
75.13	30.72	1999	3	28	6	33	19	4
79.42	30.51	1999	3	28	6.5	22.9	19	5
80.39	32.44	1999	4	16	3.6	5	17	22
78.46	32.61	1999	5	16	4.6	44	5	41
77.5	32.1	1999	5	21	3.6	33	19	18
80.93	29.49	1999	5	28	4.4	25.2	19	0
81.21	27.96	1999	6	12	2.9	17	17	8
78.66	30.68	1999	6	13	4.2	54.6	13	40
80	28.77	1999	6	17	4.6	33	4	33
81.11	29.15	1999	6	17	4.7	2	0	0
75.58	32.78	1999	7	13	4.2	33	3	17
76.47	32.58	1999	7	27	4.3	10	20	19
77.89	30.59	1999	8	29	4.1	19.5	0	27
80.83	30.89	1999	9	5	4.3	33	13	48
77.77	31.13	1999	9	12	4.7	44.3	9	0
79.22	27.06	1999	10	24	3	10	15	10
77.24	31.31	1999	11	8	4.7	16.2	21	45
81.19	27.69	1999	11	28	4.2	55	0	0
77.14	31.35	2000	2	22	4.1	17.2	20	53
77.97	27.97	2000	3	26	2.8	10	2	33
77.36	27.1	2000	3	30	3.6	15	7	14
78.84	32.06	2000	4	11	4.3	56.7	18	12
78.73	32.51	2000	4	14	3.8	33	15	28
78.29	31.51	2000	4	28	4.6	46.6	0	17
79.95	29.92	2000	5	4	4.3	33	2	0
77.07	27.48	2000	6	17	3.6	19	16	51
79.49	32.81	2000	6	17	4.3	39.6	2	47
78.41	32	2000	6	17	5.1	38.8	16	34
79.17	30.51	2000	6	21	4	39.7	16	11
81.05	29.58	2000	7	10	4.2	19	0	0
76.32	32.16	2000	7	26	4.2	10	23	30
74.9	29.62	2000	8	5	4.4	5	0	0
78.65	31.81	2000	8	31	4.4	15	2	17
78.46	32.09	2000	8	31	4.9	37.9	2	8
77.65	31.66	2000	9	13	4.3	5	14	43
78.23	30.86	2000	9	26	4.6	53.1	7	22

78.34	32.68	2000	10	12	4.4	33	0	8
76.52	32.81	2000	10	13	4.6	38.2	2	38
81.18	29.93	2000	10	27	4.4	58.7	19	7
78.06	31.17	2000	11	22	4.4	33	8	40
79.6	30.36	2000	11	27	4.2	42.9	3	20
76.67	32.37	2000	12	26	4.5	5.6	5	37
78.26	30.98	2001	2	20	4.5	10	8	42
76.04	28.47	2001	2	28	4.3	33	2	41
79.23	30.52	2001	3	12	4.5	33	11	34
77.8	31.27	2001	4	8	4.5	5	5	28
78.56	30.92	2001	4	14	4.4	10	10	55
76.66	32.8	2001	4	25	4.4	15	18	28
77.04	28.59	2001	4	28	4.7	15.4	3	6
77.62	31.75	2001	6	1	4.2	10	19	11
80.65	30.94	2001	6	17	4.2	33	5	57
78.45	32.56	2001	6	17	4.7	54	1	49
77.54	30.28	2001	6	23	3.9	0.5	2	33
80.21	30.21	2001	7	25	4.2	21	19	1
79.31	30.61	2001	8	9	4.4	33	5	56
77.31	28.94	2001	8	10	4.3	14	12	19
76.49	28.69	2001	9	12	4.2	6.4	14	22
77.49	29.2	2001	9	13	4.4	15	10	19
80.57	29.87	2001	9	13	4.8	15	6	20
79.64	30.46	2001	9	17	4.3	41.4	23	25
76.16	32.52	2001	10	14	4.9	21.4	21	14
78.9	32.56	2001	11	26	4	33	15	57
80.9	29.51	2001	12	7	4.4	42.6	4	50
75.62	29.56	2001	12	29	4.2	5	19	6
80.35	30.6	2002	2	20	4	33	21	16
75.89	27.78	2002	2	24	4.3	5	16	37
78.49	30.8	2002	2	27	4.9	10	22	59
80.11	30.11	2002	3	9	3.7	5	18	42
78.11	30.81	2002	3	12	4.2	7.3	10	32
76.26	32.81	2002	3	18	4.4	10.5	4	29
76.96	32.76	2002	4	21	4.2	10	15	32
75.73	27.45	2002	5	2	4.5	15	14	29
81.02	30.05	2002	6	4	4	67.9	14	45
81.13	28.77	2002	6	7	4.3	10	0	0
75.34	29.08	2002	6	8	4.2	5	5	9
76.34	29.19	2002	6	19	4.3	33	10	10
77.95	29.97	2002	7	15	4.1	5	23	36

77.91	31.41	2002	9	4	4.3	33	16	11
77.73	31.52	2002	9	13	4.7	33	22	39
80.09	29.98	2002	9	29	4.4	10	14	3
77.3	31.65	2002	10	8	4.1	10	4	48
76.88	32.4	2002	11	30	3.8	15	22	54
76.76	28.93	2002	12	15	4	10	1	30
78.2	30.86	2003	1	31	3.8	9.7	16	34
77	31.95	2003	2	3	4.1	12.8	23	2
76.93	30.62	2003	2	11	4.1	4.7	15	0
78.48	30.87	2003	2	16	4.2	19.7	23	41
78.1	30.97	2003	3	5	3.9	15	8	1
78.38	31.42	2003	3	5	4.4	4	8	24
78.61	31.45	2003	3	5	4.6	19.1	8	22
81.17	28.82	2003	3	21	4.4	10	0	0
80.04	30.09	2003	4	4	4.9	27.7	7	2
77.42	28.38	2003	4	9	3.9	17	13	29
77.72	31.44	2003	4	21	4.2	4.1	23	50
76.69	32.85	2003	4	27	4.2	12.7	19	17
77.68	30.55	2003	4	29	4.2	33	0	31
79.34	30.56	2003	5	27	5.3	28.9	4	23
77.34	28.38	2003	6	16	4	28.4	19	46
77.87	31.46	2003	7	3	4.1	16.6	1	8
80.84	30.27	2003	7	4	4.2	22.9	23	51
75.98	27.38	2003	8	10	4.4	10	11	17
76.66	29.16	2003	8	28	4.3	15.2	13	1
80.51	30.27	2003	8	28	4.3	15	22	45
78.44	32.58	2003	9	3	4.3	33	8	27
80.31	30.64	2003	9	3	4.8	33	23	21
76.67	28.92	2003	9	13	3.8	9.5	18	32
76.57	28.98	2003	9	13	3.9	5	19	36
76.03	32.79	2003	9	15	4.1	32.1	12	28
76.12	31.54	2003	9	27	4.7	15	15	40
77.39	32.89	2003	9	30	4.3	3.2	9	8
76.49	32.38	2003	11	24	4.3	23.9	22	47
79.22	30.62	2003	11	30	4.1	31.1	12	58
78.24	31.66	2003	12	2	4.2	25.9	11	38
80.51	30.44	2003	12	11	4.3	3.9	14	44
79.35	30.78	2003	12	12	4.5	14.5	1	2
80.71	30.78	2003	12	14	4.3	33	17	12
78.43	31.49	2003	12	15	4.1	10	23	51
78.29	31.65	2003	12	15	4.3	10	23	51

78.12	31.56	2003	12	15	4.7	24.3	23	56
76.61	32.4	2003	12	21	4.3	33	2	14
76.38	29.32	2003	12	22	4.3	16.1	20	19
80.86	29.57	2004	2	14	4.1	31.3	7	30
80.89	30.48	2004	2	18	4.3	10	8	37
76.22	32.56	2004	2	22	4.3	15	8	23
80.36	30.3	2004	3	1	4.9	23.3	17	41
78.88	30.02	2004	4	1	3.9	33	1	43
78.24	29.19	2004	4	7	4.2	22.4	9	2
80.99	29.45	2004	4	17	4.3	33.9	7	15
79.67	30.4	2004	5	28	4.2	10	21	43
76.8	32.56	2004	7	22	4.1	18.9	3	31
76.69	28.96	2004	7	27	4.3	12.6	0	10
80.26	29.38	2004	9	9	4.4	25.6	5	55
80.04	30.42	2004	9	28	4.1	12.5	0	39
81.08	31.04	2004	10	26	5.6	4	2	11
77.07	31.65	2004	11	1	4	17	4	3
78.4	31.42	2004	11	11	4.1	63.9	6	1
76.61	32.37	2004	11	11	5.1	15	2	13
77.11	30.65	2004	11	26	4.2	43.3	23	53
80.95	29.45	2005	1	15	4.7	10	22	32
80.69	29.65	2005	1	16	5	10	8	43
78.86	28.89	2005	1	30	4.1	33	10	6
78.46	30.82	2005	2	20	4.3	12.1	11	1
76.27	32.49	2005	2	28	4.1	37.6	16	4
76.53	32.45	2005	2	28	4.9	4.8	18	1
80.9	29.99	2005	3	1	3.9	10	10	16
76.4	32.62	2005	4	14	4.9	25.7	7	11
78.64	31.1	2005	5	23	3.8	10	0	25
76.26	32.84	2005	6	18	4.2	33	4	1
76.32	32.78	2005	7	4	5	10	19	44
80.82	29.56	2005	8	1	4.3	8.6	20	0
78.53	30.93	2005	8	16	4.6	17	3	45
80.83	30.07	2005	8	21	4	33	19	53
79.25	30.45	2005	9	5	4.6	48.3	1	45
80.57	32.97	2005	9	7	4.3	10	2	57
81.19	30.99	2005	10	3	4.1	7.1	18	18
81.21	29.95	2005	10	25	4.3	61.5	2	51
81.11	30.13	2005	10	25	4.9	41.5	1	51
80.09	30.03	2005	11	20	4.1	15	4	46
79.25	30.52	2005	12	14	5.1	36.9	7	9

77.96	31.55	2005	12	20	4	10	8	26
80.54	31.46	2006	1	8	3.8	35	19	16
80.28	30.23	2006	1	30	4.2	10	1	57
80.41	30.29	2006	2	14	4.8	22	19	17
76.6	29.2	2006	2	15	4.3	0.1	1	37
81	30.47	2006	2	25	3.8	10	18	51
75.53	32.71	2006	3	29	4	17.8	10	56
80.29	30.09	2006	3	31	3.9	33	6	25
76.5	28.83	2006	3	31	4.1	2.4	11	25
76.93	28.93	2006	4	7	3.6	5	18	56
81.2	29.49	2006	4	15	4	35	13	39
76.71	32.36	2006	4	21	4.2	9.4	23	20
80.91	29.48	2006	5	5	5.1	22.7	8	0
76.64	28.71	2006	5	7	4.4	12.8	16	1
76.63	32.72	2006	5	9	4.7	35.9	13	30
80.33	30.1	2006	6	13	4.2	33.6	5	30
75.46	31.78	2006	6	22	3.2	15	23	21
77.41	32.81	2006	7	18	4.3	50.1	10	42
78.23	31.75	2006	7	20	4.3	7.5	0	10
78.35	31.8	2006	7	21	4.1	1	22	32
80.19	29.87	2006	8	5	4.7	14.5	7	33
76.74	32.77	2006	9	13	3.9	10	4	23
80.51	29.77	2006	9	26	4.9	47.9	4	4
80.55	29.88	2006	10	27	4.3	18.7	1	7
80.15	29.89	2006	10	27	4.7	10	7	55
75.49	27.83	2006	11	6	3.2	1.3	0	20
80.78	29.74	2006	11	12	4	28.2	13	46
76.73	27.53	2006	11	29	4.2	5.5	5	41
77.05	31.53	2006	12	10	4.4	17.5	8	19
80.17	31.32	2007	1	29	3.9	51.8	5	28
78.61	32.1	2007	2	3	4.4	36.2	0	51
80.48	29.84	2007	2	5	4.3	5	7	57
77.73	31.36	2007	2	21	4.3	25.2	0	33
79.61	30.43	2007	3	17	3.6	17.7	10	4
78.15	30.95	2007	3	27	4.3	37.6	11	19
76.66	28.93	2007	4	3	4.1	25.1	15	35
76.63	28.93	2007	5	14	3.9	8.7	7	22
77.76	31.41	2007	6	3	4.3	13.1	8	9
76.69	32.41	2007	6	14	4.2	4.2	19	52
76.57	32.71	2007	6	17	4.3	4.6	23	55
80.49	30.25	2007	6	20	3.9	65.2	19	38

79.02	32.2	2007	6	30	3.9	3.2	19	55
78.29	30.87	2007	7	22	5.3	32.8	23	2
80.28	31.39	2007	8	9	4.4	9.1	20	33
80.59	29.56	2007	8	11	3.8	10	9	52
80.34	30.31	2007	8	16	3.9	10	13	11
76.16	32.53	2007	10	4	4.4	12.6	5	14
77.75	28.24	2007	10	18	4.2	14.7	5	54
78.65	29.41	2007	11	8	4.2	6.5	4	42
77.13	28.55	2007	11	25	4.8	33.7	23	12
81.02	29.48	2007	12	18	3.8	10	0	19
77.35	31.42	2008	1	7	3.8	6.8	4	8
79.44	30.68	2008	1	25	3.9	27.4	15	24
76.23	28.59	2008	2	17	3	15	1	51
76.35	29.11	2008	3	2	4.2	0.6	7	41
80.71	29.9	2008	3	29	4.3	10	16	11
77.34	28.84	2008	4	3	3.8	18.9	17	26
76.38	32.6	2008	4	13	3.8	10	10	45
77.29	31.89	2008	4	25	3.8	33	6	40
76.2	32.84	2008	5	2	3.9	32.9	20	20
77.1	31.61	2008	5	6	4	10	17	28
75.9	32.76	2008	5	20	4.1	22.1	23	42
76.06	32.65	2008	5	29	4.1	23.4	22	30
81.06	29.42	2008	6	15	4.9	26.1	3	27
77.61	31.41	2008	8	15	3.8	21.2	19	36
77.77	30.07	2008	8	16	4.2	26.4	19	16
80.07	30.04	2008	8	19	4.3	19.1	10	54
80.38	30.24	2008	9	4	5	8.9	12	53
76.34	32.56	2008	9	14	4.2	12.8	22	11
77.39	31.57	2008	10	21	4.8	10.4	15	9
79.89	31.96	2008	12	31	4.2	41.9	15	46
79.25	30.57	2009	1	3	4	10	13	9
78.33	31.8	2009	1	9	4.3	12	12	40
80.73	28.98	2009	1	18	3.8	5	10	13
80.26	30.1	2009	1	30	3.8	16	23	52
76.49	32.51	2009	1	31	4.4	11.5	3	7
80.33	29.97	2009	2	14	3.8	10.4	16	27
80.45	32.46	2009	2	24	3.8	5	19	47
79.59	30.77	2009	2	25	4	15.5	4	4
79.96	30.88	2009	3	2	3.2	10	14	48
76.36	32.5	2009	3	12	3.9	10	16	21
76.63	32.38	2009	3	15	4	10	9	14

78.19	30.87	2009	3	18	3.9	11.2	11	23
80.43	30.38	2009	4	9	4.2	2.7	0	44
76.46	28.7	2009	5	4	3	10	19	43
79.32	30.59	2009	5	15	4.1	31.5	18	42
79.59	30.4	2009	5	20	3.8	15.5	19	43
80.44	30.38	2009	6	2	4.2	0.4	6	36
76.05	32.83	2009	6	4	4.3	17.1	13	50
77.83	29.58	2009	6	17	4	10.4	12	7
76.72	32.51	2009	7	17	4.9	42	11	7
75.65	32.76	2009	7	18	4	32.4	4	48
79.03	28.51	2009	7	21	4.2	5	3	14
77.54	31.67	2009	7	30	3.9	15	3	43
76.43	32.31	2009	8	7	3.8	14	11	25
80.07	29.81	2009	8	27	4	25.4	16	54
80.4	29.78	2009	9	19	4.3	15.8	18	20
79.03	30.83	2009	9	21	5	52.5	9	43
79.83	30.02	2009	10	3	4.9	24.5	5	20
77.72	31.36	2009	11	10	4	10	13	55
80.64	29.23	2009	12	6	4.3	35	21	49
80.28	30.41	2009	12	8	4.3	10.1	7	5
80.15	30.02	2009	12	15	3.8	18.5	23	12
80.17	30.09	2010	1	5	4.1	4.5	15	4
80.5	29.77	2010	1	11	4.4	13.7	5	15
76.85	32.4	2010	1	19	4	1	20	45
80.35	29.99	2010	1	26	4.3	12.1	6	51
80.07	29.99	2010	2	22	4.9	20.5	17	23
76.27	32.86	2010	3	10	3.9	10	17	5
76.04	31.61	2010	3	14	4.9	35	6	53
78.15	31.41	2010	3	16	3.4	8	22	44
76.1	32.75	2010	4	10	4.1	20	19	56
76.59	32.86	2010	4	10	4.2	15	12	26
80.71	30	2010	4	14	3.8	10	5	40
80.02	30.08	2010	5	1	4.8	49.6	22	36
76.48	32.14	2010	5	3	3.8	10	9	50
78.22	30.32	2010	5	3	4.3	24.8	17	15
77.86	31.2	2010	5	28	5	40.8	7	25
79.98	29.96	2010	5	31	3.9	10	11	37
80.25	31.39	2010	6	2	4.3	1.9	8	5
76.05	32.72	2010	6	21	4.1	8.3	8	42
80.46	29.91	2010	6	22	5.4	20.4	23	14
80.11	30.93	2010	7	5	3.8	35	21	23

80.67	31.16	2010	7	7	4.2	10	23	44
75.59	32.35	2010	7	8	4.1	10	19	6
77.55	31.75	2010	7	10	3.8	6.2	16	49
79.61	30.01	2010	7	10	4.7	6.6	3	16
80.71	31.32	2010	8	6	3.8	10	12	0
77.7	31.35	2010	8	13	4.3	10	17	11
76.61	32.51	2010	8	21	3.9	14	15	2
76.14	32.82	2010	8	29	3.9	28	18	31
74.98	31.47	2010	9	18	3.8	10	22	5
76.23	28.37	2010	11	29	2.4	22.5	9	2
80.56	29.71	2010	12	24	4	10	15	36
78.39	30.97	2011	1	26	3.8	10	20	47
76.6	31.82	2011	2	6	4.1	11	16	16
78.09	31.76	2011	2	9	3.8	17	4	7
81	29.49	2011	2	17	4.1	17	9	48
79.18	30.54	2011	3	14	4.3	24	9	1
80.73	29.63	2011	4	4	5.4	17.4	11	31
78.18	31	2011	4	8	3.9	5.7	21	18
81.17	29.73	2011	4	10	4	17	18	43
80.42	30.22	2011	5	4	4.9	23	20	57
76.23	32.49	2011	5	13	4.1	3.9	7	36
78.22	31.09	2011	5	13	4.1	9.9	14	40
76.49	28.08	2011	5	29	3.8	11.1	0	5
81.04	29.69	2011	6	15	4.2	17	0	59
79.32	30.55	2011	6	20	5.1	26.6	6	27
80.61	29.93	2011	6	23	4.4	23	22	13
76.69	32.74	2011	8	13	4.2	15	22	53
76.99	28.64	2011	8	23	2.9	10.6	20	14
76.35	31.32	2011	9	7	4.2	13	0	55
77.17	28.64	2011	9	7	4.3	15.8	17	58
80.54	29.99	2011	10	9	4	23	7	34
75.85	27.99	2011	10	12	4	28.1	10	27
77.27	31.35	2011	10	16	3.2	9	6	33
77.1	31.56	2011	10	26	4.2	25.3	16	17
80.07	30.92	2011	10	28	4	35	5	3
80.59	29.62	2011	11	3	4	19	19	37
80.37	30.2	2011	11	6	4.1	11	18	34
80.31	30.18	2012	1	9	3.7	23	10	41
80.47	30.26	2012	1	13	4.1	11	1	26
78.91	29.72	2012	1	16	4.1	5.2	5	1
76.14	32.73	2012	1	22	4.1	14	7	18

76.79	28.81	2012	1	28	4.1	16.3	23	24
78.3	30.94	2012	2	9	5.4	24.8	19	17
81.15	29.49	2012	2	26	4.2	17	22	56
81.01	29.61	2012	2	26	4.6	17	23	8
76.69	28.78	2012	3	5	5.3	11.5	7	41
78.21	32.11	2012	3	7	4.4	17	13	18
76.97	29.04	2012	3	12	3.9	10	22	7
77.13	31.25	2012	4	10	4.3	19.7	0	52
76.21	28.18	2012	5	2	3.8	10	23	12
76.32	32.4	2012	5	6	3.9	10	5	43
79.48	30.18	2012	5	10	4.2	35	22	0
79.56	32.83	2012	5	14	3.8	10	19	22
76.83	28.78	2012	5	15	3.3	8.1	21	56
76.75	28.87	2012	5	17	3.7	12.1	13	39
81.14	29.61	2012	5	17	4.2	5	3	31
76.64	28.57	2012	6	19	4.4	22.5	14	0
77.08	29.02	2012	6	22	3.8	15	2	44
80.24	31.13	2012	6	25	3.8	5	19	26
76.22	28.53	2012	7	2	3.6	10	10	7
80.6	29.85	2012	7	28	4.8	23	5	48
76.49	32.4	2012	10	2	4.9	14	8	34
76.25	32.72	2012	10	3	4.2	11.1	22	59
78.49	31.84	2012	10	8	5.1	19.3	17	46
77.74	32.2	2012	10	11	4	10	13	21
79.61	30.18	2012	10	26	3.8	10	4	10
76.29	32.37	2012	11	6	4.3	16	12	21
80.39	29.21	2012	11	14	3.8	5	17	58
76.65	28.66	2012	11	19	4.2	27.2	6	25
78.4	30.9	2012	11	27	4.7	10	12	15
76.06	27.44	2012	12	20	4.3	12	13	0
81.2	29.42	2013	1	2	5	25	17	42
80.47	30.1	2013	1	10	4.2	10	15	16
79.73	28.7	2013	1	17	3.4	20	16	50
80.68	29.84	2013	1	29	4.3	5	19	42
80.05	30.26	2013	1	30	3	10	21	30
76.59	28.84	2013	2	6	3.3	10.3	8	22
80.94	29.48	2013	2	7	4.1	10	1	8
79.88	31.15	2013	2	8	4.8	50	19	34
79.41	30.98	2013	2	11	4.8	10	14	9
78.27	30.97	2013	2	11	4.9	10	10	48
76.78	28.83	2013	3	6	2.9	10.2	10	9

80.42	29.65	2013	3	6	3.6	10	4	28
80.64	29.95	2013	3	24	3.2	10	0	17
79.96	29.88	2013	3	26	3.2	10	21	6
80.24	30.33	2013	3	27	4.3	227.9	18	51
79.17	30.88	2013	4	6	4.2	5	22	29
76.9	28.78	2013	4	10	4	5	20	9
80.72	29.42	2013	4	13	3.8	5	19	54
78.97	31.22	2013	4	16	3.9	20.2	12	50
80.23	29.75	2013	4	25	4.1	5	14	38
79.8	30.33	2013	5	11	4.1	5	22	15
76.25	32.75	2013	6	4	4	5	21	31
76.77	32.72	2013	6	4	5.2	10	17	34
79.43	31.5	2013	6	24	5	10	21	8
80.2	30.28	2013	6	27	4.3	5	6	20
78.3	32.69	2013	7	9	4.9	10	13	49
76.54	32.38	2013	7	13	4.8	25.5	17	49
76.3	31.55	2013	8	29	4.8	31	10	13
80.74	29.22	2013	9	18	4	5	8	16
79.17	27	2013	9	26	5.2	33	2	11
76.09	32.61	2013	10	14	3.8	5	23	46
76.2	31.32	2013	11	6	4.6	5	14	53
78.98	29.95	2013	11	13	4.3	5	23	33
78.93	32.88	2013	12	6	4.5	5	10	8
77.63	31.33	2013	12	17	4.2	5	14	45
78.08	31.56	2013	12	18	4.2	5	8	52
78.7	30.82	2013	12	25	4.3	5	2	56
79.2	30.5	2014	2	16	4	5	19	2
79.65	30.28	2014	2	17	4.1	5	0	30
76.15	29.94	2014	2	21	4.2	5	6	46
78.6	29.41	2014	4	14	3.8	5	19	43
79.62	30.41	2014	5	14	4	5	1	54
80.59	29.57	2014	5	14	4.2	5	19	3
77.52	31.59	2014	5	19	4.1	5	21	53
76.73	32.51	2014	6	17	4.8	17	17	31
79.83	29.99	2014	7	3	4.3	5	11	34
80.32	30.44	2014	7	6	4.5	36	14	48
81.24	29.44	2014	7	7	4.3	5	16	37
76.54	32.64	2014	7	12	4.2	5	15	27
75.12	32.65	2014	8	21	4.3	5	1	19
76.35	32.28	2014	8	21	5.2	5	8	11
79.93	29.89	2014	8	24	4.4	5	8	29

77.76	29.27	2014	9	4	4.2	5	11	31
79.28	29.92	2014	10	9	4	5	1	14
77.85	31.14	2014	10	14	4.1	5	11	16
75.93	32.72	2014	11	18	4.3	5	15	55
79.24	29.94	2014	12	6	4.3	5	4	27
80.7	29.27	2014	12	11	4	5	3	11
81.2	29.23	2014	12	16	4.1	5	18	43
80.93	31.35	2014	12	19	4	50.2	20	59
81.19	31.53	2014	12	22	4	85.2	6	42
80.63	29.28	2014	12	28	4.2	5	18	23
81.02	29.2	2015	1	22	4.4	5	3	42
80.72	29.54	2015	1	23	4	5	4	48
80.55	29.07	2015	1	26	3.8	5	11	7
80.46	31.3	2015	2	14	4.4	5	0	44
81.2	28.31	2015	2	22	4.1	5	11	2
79.47	30.32	2015	4	1	5	5	21	23
79.04	30.31	2015	6	3	4.3	5	11	28
80.48	29.32	2015	6	23	3.9	5	20	33
79.13	30.35	2015	7	18	4.3	5	23	48
80.89	30.14	2015	7	26	4.1	5	16	59
80.7	30.5	2015	8	5	4.2	8	19	16
80.37	30	2015	9	29	4.9	35	9	27
80.66	32.97	2015	9	30	3.2	6	22	0
76.97	31.6	2015	10	8	4.6	36.04	1	4
78.73	31.37	2015	11	29	4.5	35	2	47
76.04	32.85	2016	2	4	4.7	58.67	7	10
81.13	29.56	2016	6	29	4.9	9.03	9	10
76.99	31.31	2016	8	1	4.9	35.06	13	38
77.71	31.47	2016	8	27	4.9	10	1	14
76.57	28.77	2016	9	10	4.5	10	15	27
76.7	28	2016	11	16	4.8	10	22	59
80.63	29.98	2016	12	1	5.5	31.96	16	52
79.16	30.65	2017	2	6	5.1	16.05	17	3
76.3	32.87	2017	5	20	4.6	35.36	5	48
76.78	28.97	2017	6	1	5	10	22	55
76.24	32.87	2017	8	16	4.8	44.78	3	26
81.16	29.39	2017	8	22	4.9	10	0	50
77.43	31.95	2017	10	27	4.5	14.96	2	37
79.16	30.63	2017	12	6	5.4	10	15	19

List of Publications

1. *Static & Dynamic Analysis of a Tailings Dam.* 2016. In Proceedings of 1st International Conference on Civil Engineering for Sustainable Development – Opportunities and Challenges, Guwahati, Assam. **15-21.**

2. *Estimation of Bedrock Depth for a Part of Garhwal Himalayas using Two Different Geophysical Techniques.* 2018. Geoscience Letters, **5(1), 1-9**.

3. *A Review of the Current Practice in Inclusion of Seismicity in Landslide Susceptibility Zonation: A Case Study for Indian Himalayas.* (1st revision) Himalayan Geology. Manuscript No. **MS#578-2018.**

4. *Landslide Susceptibility Zonation (LSZ) with Special Emphasis on Tectonic Features for Occurrence of Landslides in North-West Indian Himalaya.* Journal of Mountain Science. (2nd revision). Manuscript No. **18-5359.**

5. *Effect of Earthquake Generated Strong Ground Motion Scenarios in Landslide Hazard Zonation: A case study for Indian Himalaya.* Landslides (Manuscript submitted). **LASL-D-19-00308.**